

---

*Leibniz-Zentrum für Agrarlandschaftsforschung (ZALF) e. V.*

*Institut für Bodenlandschaftsforschung*

---

Einfluss der erosionsbedingten Pedogenese auf den Wasser-  
und Stoffhaushalt ackerbaulich genutzter Böden der  
Grundmoränenbodenlandschaft NO-Deutschlands -  
hydropedologische Untersuchungen mittels wägbarer  
Präzisionslysimeter

**Kumulative**

## **Dissertation**

**zur Erlangung des akademischen Grades**

**"doctor rerum naturalium"**

**(Dr. rer. nat.)**

**in der Wissenschaftsdisziplin**

**„Geoökologie“**

**eingereicht an der**

**Mathematisch-Naturwissenschaftlichen Fakultät**

**der Universität Potsdam**

**von**

**Marcus Herbrich**

**Potsdam, den 16.08.2017**



---

*Leibniz Centre for Agricultural Landscape Research (ZALF) e.V.*

*Institute of Soil Landscape Research*

---

Effects of erosion-affected soil evolution on water and dissolved carbon fluxes, soil hydraulic properties, and crop development of soils from a hummocky ground moraine landscape - hydro-pedological analysis using high precision weighing lysimeters

**Cumulative**

## **Thesis**

**submitted in fulfilment of the requirements**

**for the academic degree**

**"doctor rerum naturalium"**

**(Dr. rer. nat.)**

**in the scientific discipline**

**„Geoecology“**

**submitted at the**

**Mathematisch-Naturwissenschaftlichen Fakultät**

**University of Potsdam**

**by**

**Marcus Herbrich**

**Potsdam, den 16.08.2017**

Published online at the  
Institutional Repository of the University of Potsdam:  
URN urn:nbn:de:kobv:517-opus4-408561  
<http://nbn-resolving.de/urn:nbn:de:kobv:517-opus4-408561>

## Preface

This study was implemented in the lysimeter network SoilCan as a part of the TERENO (***TER**restrial **E**nvironmental **O**bservatories*) project. SoilCan primarily focuses on the soil water, carbon and nutrient balance using fully automated lysimeter systems. Within the framework of SoilCan, overall 132 high-precision lysimeters were installed at 14 experimental field sites across four TERENO-observatories which are located all over Germany.

The lysimeters were filled with undisturbed soil monoliths to quantify the components of the terrestrial water balance and to provide information on the transport of carbon, nitrogen and other nutrients. The aim of the SoilCan TERENO project is to receive long-term data series (>15 years) as a basis for analysis and forecast of the effect of climate and land-use changes on terrestrial ecosystems (soil-plant-atmosphere).

To investigate effects of the climate change on soil landscapes in Germany, monoliths for lysimeters were translocated from their original sites within or between the TERENO observatories. Thereby, contrasting climatic conditions (amongst others temperature and precipitation gradients) are mimicked for the transferred soils allowing predictions about the impact of climate change on terrestrial ecosystems.

## Abstract

In the arable soil landscape of hummocky ground moraines, an erosion-affected spatial differentiation of soils can be observed. Man-made erosion leads to soil profile modifications along slopes with changed solum thickness and modified properties of soil horizons due to water erosion in combination with tillage operations. Soil erosion creates, thereby, spatial patterns of soil properties (e.g., texture and organic matter content) and differences in crop development. However, little is known about the manner in which water fluxes are affected by soil-crop interactions depending on contrasting properties of differently-developed soil horizons and how water fluxes influence the carbon transport in an eroded landscape. To identify such feedbacks between erosion-induced soil profile modifications and the 1D-water and solute balance, high-precision weighing lysimeters equipped with a wide range of sensor technique were filled with undisturbed soil monoliths that differed in the degree of past soil erosion. Furthermore, lysimeter effluent concentrations were analyzed for dissolved carbon fractions in bi-weekly intervals.

The water balance components measured by high precision lysimeters varied from the most eroded to the less eroded monolith up to 83 % (deep drainage) primarily caused due to varying amounts of precipitation and evapotranspiration for a 3-years period. Here, interactions between crop development and contrasting rainfall interception by above ground biomass could explain differences in water balance components. Concentrations of dissolved carbon in soil water samples were relatively constant in time, suggesting carbon leaching was mainly affected by water fluxes in this observation period. For the lysimeter-based water balance analysis, a filtering scheme was developed considering temporal autocorrelation. The minute-based autocorrelation analysis of mass changes from lysimeter time series revealed characteristic autocorrelation lengths ranging from 23 to 76 minutes. Thereby, temporal autocorrelation provided an optimal approximation of precipitation quantities. However, the high temporal resolution in lysimeter time series is restricted by the lengths of autocorrelation.

Erosion-induced but also gradual changes in soil properties were reflected by dynamics of soil water retention properties in the lysimeter soils. Short-term and long-term hysteretic water retention data suggested seasonal wettability problems of soils increasingly limited rewetting of previously dried pore regions. Differences in water retention were assigned to soil tillage operations and the erosion history at different slope positions. The three-dimensional spatial pattern of soil types that result from erosional soil profile modifications were also reflected in differences of crop root development at different landscape positions. Contrasting root densities revealed positive relations of root and aboveground plant characteristics. Differences in the spatially-distributed root growth between different eroded

---

soil types provided indications that root development was affected by the erosion-induced soil evolution processes.

Overall, the current thesis corroborated the hypothesis that erosion-induced soil profile modifications affect the soil water balance, carbon leaching and soil hydraulic properties, but also the crop root system is influenced by erosion-induced spatial patterns of soil properties in the arable hummocky post glacial soil landscape. The results will help to improve model predictions of water and solute movement in arable soils and to understand interactions between soil erosion and carbon pathways regarding sink-or-source terms in landscapes.

## Kurzfassung

Hydropedologische Wechselwirkungen zwischen Wasserflüssen und erosionsbedingten Veränderungen im Profilaufbau ackerbaulich genutzter Böden treten insbesondere in der Jungmoränenlandschaft auf, die sich durch eine überwiegend flachwellige bis kuppige Topographie auszeichnet. Mit der dynamischen Veränderung von Bodenprofilen, wie etwa der veränderten Solumtiefe und Horizontabfolgen, sowie deren Verteilungen in der Landschaft gehen Veränderungen in den bodenhydraulischen Eigenschaften einher. Über deren Auswirkungen auf den Wasser- und Stoffhaushalt ist bislang nur wenig bekannt.

Im Rahmen dieser Dissertation wurden kontinuierliche Messungen aus vier Jahren (2011 bis 2014) unter Verwendung von wägbaren Lysimetern in der ackerbaulich genutzten Bodenlandschaft Nordostdeutschlands (Uckermark) erhoben. Dabei sollte die zentrale Frage, inwieweit die erosionsbedingte Pedogenese, in Wechselwirkung mit der pflanzenbaulichen Nutzung, den Wasser- und Kohlenstoffhaushalt beeinflusst, beantwortet werden. Ziel dieser Arbeit war es, 1D-Wasserflüsse und Austräge an gelöstem Kohlenstoff für unterschiedlich erodierte Bodenprofile zu quantifizieren. Damit einhergehend wurden Untersuchungen zu hydraulischen Bodeneigenschaften sowie möglichen Veränderungen im System Boden-Pflanze (Wurzeluntersuchungen) durchgeführt. Um derartige Veränderungen zwischen unterschiedlich erodierten Böden beschreiben zu können, wurden Bodenmonolithe in ungestörter Lagerung entnommen und in Lysimeteranlagen installiert. Zudem erfolgte eine Instrumentierung der einzelnen Lysimeter mit verschiedener Sensorik, u.a. um Wassergehalte und Matrixpotentiale zu messen. Für stoffhaushaltliche Untersuchungen wurden darüber hinaus Konzentrationen der gelösten Kohlenstofffraktion in der Bodenlösung in 14-tägigen Intervallen bestimmt.

Der Wasserhaushalt von sechs gering bis stark erodierten Parabraunerden unterschied sich im Hinblick auf die bilanzierten Wasserhaushaltskomponenten deutlich. Anhand dieser Ergebnisse liegt die Vermutung nahe, dass die dynamischen Veränderungen im Gefüge- und Profilaufbau (in Abhängigkeit von der Bodenerosion) einen Effekt auf die Wasserbilanzen aufweisen. Über die mehrjährige Messperiode von 2011 bis 2014 konnte für das mit einer stark erodierten Parabraunerde gefüllte Lysimeter ein circa 83 Prozent höherer Abfluss als für das Lysimeter mit einer wenig erodierten Parabraunerde gemessen werden. Somit variierte der Abfluss am unteren Rand in Abhängigkeit zum Erosionsgrad. Neben dem unterschiedlichen Abflussverhalten variierten die Bodenmonolithe innerhalb der Lysimeter ebenfalls in den Evapotranspirations- und Niederschlagsmengen, hervorgerufenen durch die Differenzierung in den Horizontabfolgen, -mächtigkeiten und deren Einfluss auf die bodenhydraulischen Eigenschaften in Abhängigkeit vom Pflanzenbewuchs. Aufgrund der homogen verteilten Stoffkonzentrationen des gelösten organischen und anorganischen



Kohlenstoffs am unteren Rand waren Kohlenstoffausträge maßgeblich von den Wasserflüssen abhängig. Als Grundlage der Lysimeter-basierten Wasserhaushaltsanalyse diente ein im Rahmen dieser Dissertation entwickeltes Auswertungsverfahren von kontinuierlichen Gewichtsänderungen unter Berücksichtigung der zeitlichen Autokorrelation. Um eine mögliche Periodizität in zeitlich hochaufgelösten Änderungen des Lysimeterwaagensystems zu ermitteln, fand eine Autokorrelationsfunktion in der Zeitreihenanalyse von vier saisonalen Messzeiträumen Anwendung. Die Ergebnisse der Arbeit deuten darauf hin, dass hochaufgelöste Lysimeterzeitreihen in einem Bereich von circa 30 min bis circa 60 min zeitlich autokorreliert sind. Die ermittelten Autokorrelationslängen bieten wiederum eine Möglichkeit zur Annäherung von (optimalen) Zeitintervallen für die Niederschlagsberechnung, basierend auf Änderungen in den Wiegedaten. Im Vergleich zu einem Kippwaagenregenschirm nahe der Lysimeterstation überstiegen die ermittelten Niederschlagsmengen der Lysimeter in Bodennähe die der in zwei Metern Höhe erfolgten Messung deutlich.

Zur Charakterisierung der zeitlichen (Hysterese), als auch räumlichen (erosionsbedingter Pedogenese) Veränderungen der bodenhydraulischen Eigenschaften der Lysimeterböden wurden kontinuierliche Datenreihen des Wassergehaltes und Matrixpotentials analysiert. Die daraus abgeleiteten Wasserretentionskurven wurden in 3 Messtiefen (10, 30, 50 cm) unter Feldbedingungen ausgewertet und mit Labormessungen von Bodenkernen verglichen. Sowohl zwischen den unterschiedlich erodierten Bodenprofilen als auch zwischen den Feld- und Labormessungen waren Unterschiede in den Wasserretentionseigenschaften ersichtlich. Innerhalb eines Jahres (eingeschränkte Benetzbarkeit) sowie zwischen den Jahren (Veränderung der Porenmatrix) zeigten die Ergebnisse zudem eine zeitliche Veränderung der Wasserretentionseigenschaften. Diese dynamische Variabilität der Wasserretention wiederum unterliegt der räumlichen Heterogenität von Bodeneigenschaften, wie Textur und Lagerungsdichte. Für die Interpretation der unterschiedlichen bodenhydraulischen Eigenschaften sowie im Hinblick auf Veränderungen im Wasserhaushalt von ackerbaulich genutzten Lysimetern spielt das System Boden-Pflanze eine bedeutende Rolle. Diesbezüglich wurden Biomasse- und Wurzeluntersuchungen an unterschiedlich erodierten Böden durchgeführt. Die erzielten Ergebnisse verdeutlichen, dass erosionsbedingte Veränderungen im Profilaufbau beziehungsweise Horizonteigenschaften die Wurzelentwicklung beeinflussen können. Zudem stehen die Durchwurzelungsraten an grundwasserbeeinflussten Senkenstandorten in enger Beziehung zum Grundwasserstand (insbesondere im Frühjahr). Die oberirdisch beobachteten Unterschiede in der Biomasse korrelierten stark mit den ermittelten Wurzel-dichten (Winterweizen), dies lässt vermuten, dass eine Abschätzung der Wurzelentwicklung mittels oberirdischer Biomasse möglich ist.

---

Zusammenfassend zeigen die Ergebnisse der vorliegenden Lysimeterstudie komplexe Wechselwirkungen zwischen dem pedogenetischen Zustand erodierter Böden und dem Wasserhaushalt, den bodenhydraulischen Eigenschaften sowie der Wurzelentwicklung angebaute Kulturen. Zudem leisten die ermittelten unterschiedlichen Austragsraten an gelöstem Kohlenstoff einen Beitrag zur Abschätzung der langfristigen, in die Tiefe fortschreitenden Entkalkung sowie zur Beantwortung der Fragestellung, ob ackerbaulich genutzte Böden eher als Quell- oder als Senkenterm für Kohlendioxid fungieren.

---

# Table of contents

Preface .....	1
Abstract.....	2
Kurzfassung .....	4
I General Introduction.....	11
1.1 Hummocky ground moraine landscape .....	12
1.2 Erosion-affected soil evolution in the hummocky soil landscape.....	13
1.3 Lysimeter application.....	14
1.4 Methodological design.....	16
1.4.1 TERENO SoilCan lysimeters .....	16
1.4.2 The experimental site and climate.....	17
1.4.3 Soils.....	19
1.5 Motivation and objectives .....	19
1.6 Thesis outline .....	21
II Autocorrelation analysis of high resolution weighing lysimeter time series as a basis for determination of precipitation .....	24
Abstract.....	25
2.1 Introduction .....	26
2.2 Materials and method.....	28
2.2.1 Study site and lysimeters .....	28
2.2.2 Analysis of lysimeter mass time series' .....	30
2.3. Results.....	39
2.3.1 Temporal autocorrelation .....	39
2.3.2 Daily precipitation using autocorrelation-based filtering.....	42
2.3.3 Daily evapotranspiration after autocorrelation-based filtering .....	45

---

2.4. Discussion.....	46
2.4.1 Possible explanations for temporal autocorrelation .....	46
2.4.2 Comparison between the lysimeter based precipitation and with rain gauge measurements .....	47
2.4.3 Filtering effect on evapotranspiration rates .....	49
2.5. Conclusions .....	51
Acknowledgements.....	52
References.....	52
III Water balance and leaching of dissolved organic and inorganic carbon of eroded Luvisols using high precision weighing lysimeters .....	56
Abstract.....	57
3.1 Introduction .....	58
3.2 Methods .....	61
3.2.1 Study site and lysimeter design .....	61
3.2.2 Physical and chemical soil properties .....	63
3.2.3 Cropping periods and biomass analyses.....	65
3.2.4 Water balance analyses.....	67
3.2.5 Dissolved organic and inorganic carbon.....	69
3.3 Results.....	71
3.3.1 Water balance components .....	71
3.3.2 Dissolved organic and inorganic carbon.....	76
3.3.3 Biomass production .....	78
3.4 Discussion.....	79
3.4.1 Drainage in relation to soil erosion history and intensity.....	79
3.4.2 Erosional effects on carbon concentrations and leaching.....	82
3.4.3 Effects of erosion induced soil profile modifications on biomass yield .....	86
3.5 Conclusions .....	87
Acknowledgements.....	88
References.....	89
Appendix.....	96

---

IV Scales of water retention dynamics observed in eroded Luvisols from arable postglacial soil landscape..... 101

*Abstract*..... 102

4.1. *Introduction* ..... 103

4.2. *Material and Methods*..... 105

    4.2.1 Site description, soils, and lysimeter experiment..... 105

4.3 *Results*..... 112

    4.3.1 Field and laboratory soil water retention ..... 112

    4.3.2 Drying periods and parameterization ..... 117

    4.3.3 Wetting periods and parameterization..... 121

4.4. *Discussion*..... 121

    4.4.1. Differences between laboratory and field water retention..... 121

    4.4.2 Water retention dynamics at daily, seasonal, and annual scales..... 123

    4.4.3 Intra-seasonal dynamics and effective porosity..... 125

4.5. *Conclusions* ..... 127

*Acknowledgements*..... 128

*References*..... 129

*Appendix*..... 133

V Root development of winter wheat in erosion-affected soils depending on the position in a hummocky ground moraine soil landscape..... 136

*Abstract*..... 137

5.1. *Introduction* ..... 138

5.2. *Material and Methods*..... 140

    5.2.1. Experimental design, above-ground biomass and soil characteristics..... 140

    5.2.2 Root image collection and minirhizotron installation..... 142

5.3. *Results*..... 145

    5.3.1 Root density and root length ..... 145

    5.3.2 Root length density and root biomass calculations..... 148

5.4. *Discussion*..... 151

    5.4.1 Root development at contrasting landscape positions..... 151

---

5.4.2 Root penetration depending on landscape position.....	152
5.4.3 Root biomass and root-to-shoot ratios at different landscape positions.....	154
5.5. <i>Conclusions</i> .....	155
<i>Acknowledgements</i> .....	156
<i>References</i> .....	156
VI General Discussion.....	161
6.1 <i>Main results and concluding remarks</i> .....	161
6.2 <i>Classification of study results regarding carbon leaching</i> .....	166
6.3 <i>Suggestions based on thesis results</i> .....	167
6.4 <i>Soil water balance simulations</i> .....	169
6.5 <i>Limitations</i> .....	171
6.6 <i>Outlook and suggestions for further research</i> .....	172
6.7 <i>Data access</i> .....	173
References .....	175
Acknowledgments .....	181
Curriculum vitae and publications.....	182
Conference contributions.....	184
Erklärung .....	185
Erklärung des Eigenanteils.....	186



Photo: C. Kappler

Aerial photograph of the arable hummocky soil landscape

## 1| General Introduction

Soil degradation in terms of soil erosion is an overall problem at global scales. It affects soil and water quality, short and long-term productivity of arable land, and emissions of radiatively active gases to the atmosphere (Lal, 2001). Processes of soil degradation are not only related to geo-ecological factors like lithology, topography, vegetation and climate, but also to anthropogenic activities, especially in regions with agricultural practices (Morgan, 2009). The agricultural expansion and its associated intensification of land use with tillage operations like ploughing caused a set of adverse effects on landscape. Under intensive agricultural use, soil landscapes represent a spatial continuum of differently eroded areas and continuous transitions of soil types reflecting an erosion-induced spatial differentiation of soils (Sommer et al., 2008). In general, this heterogeneity of soils and properties can be found in regions with extensive soil erosion such as the undulating, hilly loess regions or in the hummocky ground moraine soil landscapes.

## 1.1 Hummocky ground moraine landscape

The hummocky soil landscape was formed during the Pleistocene glacial retreat about 10.000 to 100.000 years ago. On the global scale, soils of hummocky moraine landscapes cover an area of approximately  $1.8 \times 10^6$  km<sup>2</sup> of the northern hemisphere and around fifty percent of this area are estimated to be actually or formerly used as arable land (Sommer et al., 2004).

In Germany, a periglacial corridor has disconnected the southern edge of the Scandinavian Ice Sheet from the northward limit of the Alpine glacier area during the last glacial maximum (see Fig. 1.1). Within the periglacial corridor, small isolated glaciated mountainous regions were formed such as the Harz or the Black Forest (Raab and Völkel, 2003).

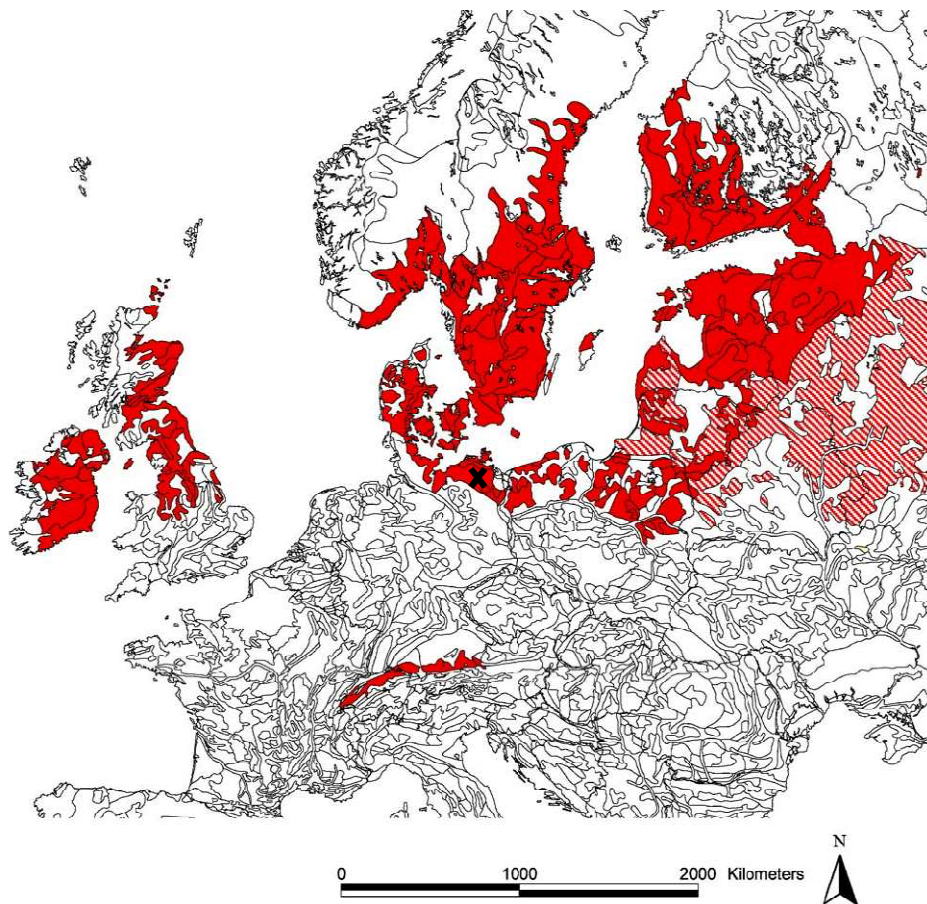


Figure 1.1: A soil map extract of Europe (Sommer et al., 2004 modified); Shaded areas represent the younger glacial drift areas with a undulating, hilly (hummocky) ground moraine terrain, while hatched areas are considered only in part; the symbol (X) shows the Uckermark study area in NE-Germany.



The topography of the hummocky soil landscape is characterized by a hilly ground moraine surface including knolls, plain plateaus, steep slopes and enclosed depression areas. In the undulating landscape of north-east Germany, surface water is typically accumulating in these topographic depressions (Kalettka et al., 2001). The small, shallow wetlands, so called kettle holes, cover a total area of about  $38 \times 10^3 \text{ km}^2$  of the hummocky landscape up to an amount of 150,000 to 300,000 of the small standing waters (Kalettka and Rudat, 2006). Interactions between kettle holes and aquifers are difficult to evaluate because of high landscape heterogeneity. Soil hydrological and geophysical investigations revealed that most kettle holes are unconnected water bodies and not related to any stream or groundwater (e.g., Gerke et al., 2010). Furthermore, strong short-term water level fluctuations can result in a complete desiccation and rewetting of the small standing waters during drying periods.

### *1.2 Erosion-affected soil evolution in the hummocky soil landscape*

For arable post glacial landscapes, the relationship between the topography and the distribution of soils has been recognized so far (e.g., Jenny, 1961; McCaig, 1985; Pennock, 2003). In north-east Germany, a three-dimensional continuum of soil types has been evolved that developed from glacial till as the parent material (Sommer et al., 2008). A typical catena (Fig. 1.2) shows non-eroded soils at plateaus and flat (mid-)slopes. Strongly eroded soils occurred at steep slopes and exposed hilltops. Colluvial, groundwater-influenced soils are found in the topographic depressions as a result from varying intensities of erosion and deposition due to water and tillage erosion.

Tillage erosion, i.e. the soil uplift and lateral movement during tillage operations (e.g., Van Oost et al., 2006) strongly affects convex landscape positions (Govers et al., 1999). During the ploughing process, soil material of the first 30 centimeter depths is captured and mixed. When the thickness of the plough (Ap-) horizon is reduced by the soil loss at the surface due to water and tillage erosion, soil material of deeper horizons will be incorporated into the Ap-horizon at the next tillage operations. The combined effect of the loss of surface soil and tillage operations (ploughing with deep-cutting plows) lead to a gradual truncation of soil profiles at convex slope positions with time (e.g., Kosmas et al., 2001). In this thesis, the process of the removal and incorporation of soil material due to plugging operations and water/tillage erosion leading to differently truncated soil profiles and colluvial deposition areas are termed 'erosion-induced soil evolution'.



*Figure 1.2: Typical catenary soil sequence of Calcaric Regosols (left) at exposed hilltops, more or less eroded Haplic Luvisols (three middle pictures) along the slopes and Colluvic Regosol (right) in closed depressions; red dashed lines represent the depths of C-horizons and solum, respectively; for the colluvial soil, the orange solid line shows the depth of the fossil A-horizon buried with eroded material. Photos: Institute of Soil Landscape Research, Leibniz Centre ZALF.*

Soil erosion rates by tillage operations are usually highest at convex terrain and slope positions while the largest soil removal by water erosion occurred at steep mid-slopes. The degree of soil erosion can be indicated by the depths of the C-horizon (equals the solum depth) relative to the soil surface (Fig. 1.2, cf. the reddish scatted line). Furthermore, the vertical sequence of soil horizons can be truncated by soil erosion (Gerke and Hierold, 2012). Here, soil erosion is evident by the absent clay eluviation horizon (E-horizon) or by the mixture of E- and Bt-horizons (cf. Fig. 1.2, second from the left). A disappearance of the eluvial zone results from the truncation of A- and the E-horizons in eroded soils.

### **1.3 Lysimeter application**

Lysimeters have been applied since the late 17<sup>th</sup> century to study hydrological related aspects such as the water movement through the soil profile (e.g., Titus and Mahendrapa, 1996). While first non-weighing lysimeters were often used to observe deep drainage by measuring differences in the water content with depth and time, lysimeters with a high

precision weighing system have been proposed to quantify the overall water balance (Young et al., 1996) including water fluxes at the upper and bottom lysimeter boundaries. Today, several weighing lysimeter systems including additional sensors and **Time Domain Reflectometry (TDR)** probes are in use for a variety of purposes (Meißner et al., 2010), such as CO<sub>2</sub> measurements, solute and water balance modeling or analysis of leaching rates of fertilizers.

High-precision weighing lysimeters (Unold and Fank, 2008) as introduced in this study (Fig. 1.3) are designed to determine even small amounts of precipitation manifested as rime, fog or dew by measuring small changes in water storage in a temporal resolution of one hour (e.g. Meissner et al., 2007).

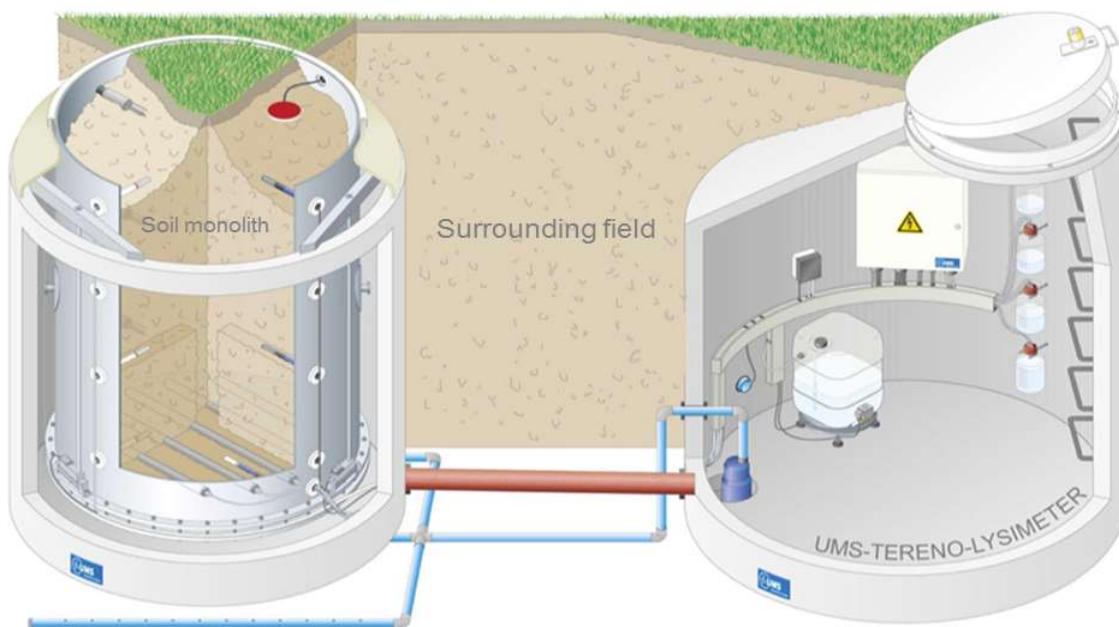


Figure 1.3: Construction of a TERENO-SoilCan lysimeter (left) embedded into the surrounding field, which includes an intact soil monolith with installed sensors (Pütz et al., 2016, modified). Each cylindrical lysimeter have a height of 1.5 m and diameter of 1.13 m. Sampling bottles and the seepage water tank are located in the service well (right).

Due to the high temporal resolution, recently developed lysimeter systems are accompanied by correlated data and noise. A pre- and post-processing of lysimeter time series is highly essential to assure long-term data quality (Marek et al., 2014). Reason are mechanical disturbances and vibrations, among others due to animals, tillage operations or wind (Nolz et al., 2013). To separate external sources of errors from the weighing time series, data smoothing was frequently used to remove the noise in high-resolution time-

series of lysimeters (e.g., Vaughan and Ayars, 2009; Vaughan et al., 2007). Schrader et al. (2013) demonstrated for synthetic data that water balance components are affected by the selection of smoothing windows, e.g. leading to a systematic misfit when sudden changes in the lysimeter weight occurred. While Peters et al. (2014) revealed an adaptive filtering solution, the so called 'Adaptive Window and Adaptive Threshold (AWAT) filter', Hannes et al. (2015) developed a non-adaptive filter scheme to reduce the impact of external errors and noise for high-resolution weighing time series.

## *1.4 Methodological design*

### *1.4.1 TERENO SoilCan lysimeters*

For the current study, weighing lysimeters with a soil surface area of 1.0 m<sup>2</sup> (1.5 m height; 1.13 m in diameter) were installed on ground surface level at the Experimental Field Station Dedelow (Fig. 1.4). To avoid oasis effects as far as possible all lysimeters were embedded within a larger field approx. 2.3 ha in size, which had the same crop sequence and was managed (spraying and fertilization) as similarly as possible to the lysimeters. Due to newly developed cutting techniques characterized by a reduced coat friction against the soil material, intact and undisturbed monoliths of four different soil types were installed into the TERENO SoilCan lysimeters without structural damages during the cutting process. The selection of these soil monoliths that were representative for the hummocky soil landscape was based on prior field studies (e.g., Deumlich et al., 2010).

Overall, 12 individual lysimeters were assembled in two separated hexagons. Each of them determined both the total mass and the leachate outflow at the bottom with an accuracy of 10 g or 0.01 mm water equivalent. Every lysimeter was equipped with different sensors and probes. Among others, MPS-1 matrix potential sensors (Decagon Devices Inc., Pullman, USA), TS-1 tensiometers (UMS, Munich, Germany) and time domain reflectometry probes TDR-100 (Campbell Scientific Ltd, Logan, USA) were inserted in 10, 30, and 50 cm depths in short distance of about 50 cm to each other. Pressure boundary conditions at the bottom of the lysimeters were controlled by reference matric potentials measured with tensiometers that were installed in the intact field soil next to the lysimeter tranches. Through the suction cup rake in 140 cm depth, either soil water can be extracted by suction and stored in the outflow storage tank, or water from the storage tank can be injected back into the lysimeter by applying pressure.



*Figure 1.4: Weighing lysimeter (UMS, Munich, Germany) during sensors installation process (right); suction cup rake (SIC40, UMS, Munich, Germany) at the lysimeter bottom (1.45 m depth) consisting of six porous tubes (left above) and glass bottle attached to the lysimeter tank (left below). Photos: Institute of Soil Landscape Research, Leibniz Centre ZALF.*

For analyses of dissolved carbon fluxes, soil solution was extracted from 0.3 m, 0.5 m, and 1.4 m soil depths with silicon carbide cups (SIC20, UMS GmbH, Munich, Germany) and stored in glass bottles. In terms of dissolved inorganic carbon, extracted soil solution was collected in headspace-free sampling bottles (SF1000; UMS GmbH, Munich, Germany) to avoid or at least minimize effects caused by degassing of carbon dioxide from the extracted soil solution (e.g., Kindler et al., 2011).

#### *1.4.2 The experimental site and climate*

The Experimental Field Station Dedelow (53°22'2.45"N, 13°48'10.91"W) of the Leibniz-Centre for Agricultural Landscape Research (ZALF) is located in the hummocky arable soil landscape near the city of Prenzlau, North-east Germany (Fig. 1.5). The altitude ranges from approx. 30 to 45 m (a.s.l.). Near-surface groundwater can be observed in small closed depressions (kettle holes).

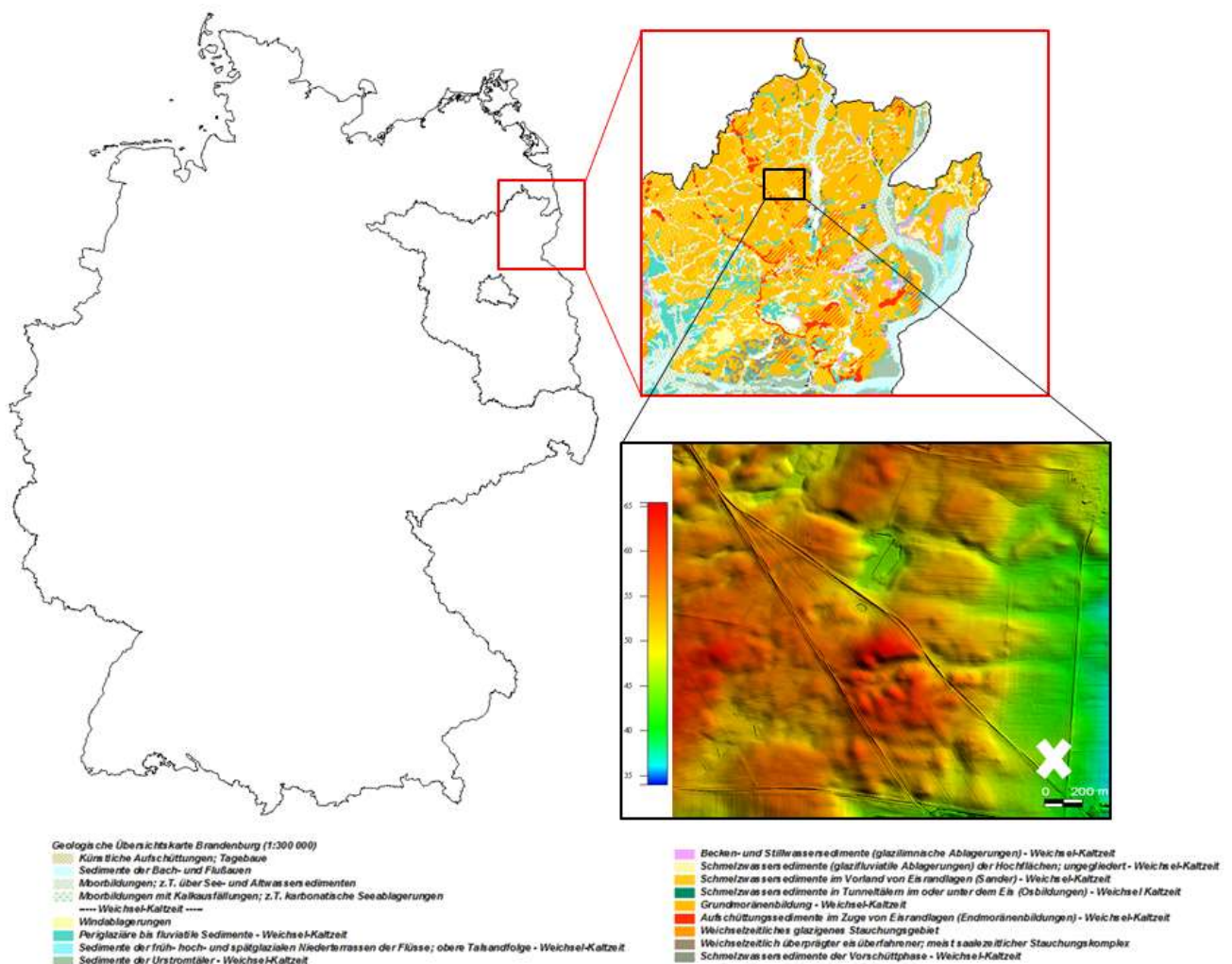


Figure 1.5: Location map of Germany (left) including the borders of Brandenburg and the soil map of the Uckermark region (enlarged view, right above). Digital terrain model (DGM1, 1 m grid) of the study area near Prenzlau (enlarged view, right below). The indicator (X) shows the lysimeter station at Dedelow. The license for use of the DGM1 was given by LGB Brandenburg, ©Geobasis-DE/LGB 2012.

The study site is located at the transition zone between oceanic and continental climate with an annual long-term precipitation of 485 mm, an annual long-term potential evapotranspiration of 633 mm and an annual long-term air temperature of 8.6°C. These values were reported in Rieckh et al. (2014) for a 20-years period (1992 – 2012). For the actual period (2011 – 2015), precipitation was 635 mm (2011), 538 mm (2012), 446 mm (2013), 561 mm (2014), 414 mm (2015) and the annual mean air temperature at 2 m above soil surface was 7.9°C (2012), 8.0°C (2013), 9.3°C (2014), 9.1°C (2015). In general, these meteorological data are indicating a sub-oceanic/sub-continental climate.

### 1.4.3 Soils

The present lysimeter study focuses on four characteristic erosion-affected soils developed from glacial till (cf. Fig. 1.2): (i) Haplic Luvisols with none or small erosional soil profile modifications, (ii) Haplic Luvisols with moderate to strong erosion and related profile modifications, extremely eroded Calcaric Regosol and depositional Anocolluvic Regosol (IUSS Working Group WRB, 2015).

The fully developed Haplic Luvisols (Ap-E-Bt-C) can be found in plateau positions, while more-or-less eroded Haplic Luvisols (Ap-(E/Bt)-Bt-C) starting from a flat upper- to a flat mid-slope, and Calcaric Regosols (Ap-C) typically developed in exposed landscape positions. The eroded topsoil material that accumulated in the topographic depressions and toe slopes formed Colluvic Regosols (cf. Fig. 1.5).

### 1.5 Motivation and objectives

The aim of this thesis was to identify feedbacks of erosion affected spatial differentiation of soil types on water balance, dissolved carbon fluxes, soil hydraulic properties and crop growth in a morainic arable soil landscape - a landscape of great global relevance (Sommer et al., 2008). Until now, it is largely unknown how water flow and solute transport are affected by erosion history, which created three-dimensional patterns of soil properties such as structure, texture and organic matter content or differences in crop development.

An important hot spot in recent research is the interface between pedosphere and hydrosphere, so called hydropedology, where pedogenetic features and the position of soils in the landscape setting are explored to understand interactive pedological and hydrological processes (e.g., Lin, 2010). The water movement and solute transport in heterogeneous landscapes has been linked to soil hydraulic properties that are changing over time and space (Lin, 2011). In arable soil landscapes such as those of the hummocky ground moraine, changes in soil hydraulic properties can also be associated with soil compaction and erosion processes (Alaoui et al., 2011). The pedogenetic structure, slope positions and depths of soil development were found to affect the soil hydraulic properties such as the soil hydraulic conductivity (e.g., West et al., 2008). Influences of the soil structure and texture on hydraulic properties are explained basically by hydraulic and hydromechanical effects of shearing forces and compaction processes on the water flow (Gebhardt et al., 2009, Horn et al., 1998). In the undulating, hummocky ground moraine landscape, water flow influenced by surface topography was found to be the main factor on the spatial variability of long-term soil water and solute balances (Woods et al., 2013).

Differences in soil hydraulic properties of the same diagnostic horizons depending on horizon thickness and soil structure have also been observed for erosional modified soil profiles in the arable hummocky ground moraine soil landscape of NE-Germany (Rieckh et al., 2012, Rieckh et al., 2015). However, these measurements of soil hydraulic properties on soil core samples in the laboratory did not reflect the spatial heterogeneity and temporal variability of soil properties under field conditions as reported for arable soils analyzed in the present study (i.e., bulk density, Gerke and Hierold, 2012) and elsewhere (e.g., Pachepsky et al., 2001). The 1D-modeling approach considering lab derived pedogenetic variations in soil horizons at the different hillslope positions (Rieckh et al., 2014) suggested interactions between erosion-induced modifications on the soil profile (truncation, soil accumulation), their soil properties, water fluxes, and leaching rates. Nevertheless, the (long-term) *in situ* water balance and solute transport in variably saturated soils remains still unclear. Furthermore, soil hydraulic properties under field conditions such as water retention properties may be hysteretic or changing in time due to changing soil properties, processes that were not considered yet. Taking a hillslope position-specific crop and root growth into account, water balance simulations of Gerke et al. (2016) revealed that crop-soil interactions induced by the erosion-induced soil evolution increased the spatial heterogeneity of water balance components and might also influence the rate of soil development. However, the assumed complex feedbacks of Gerke et al. (2016) between position-specific soil properties, soil moisture, and crop growth are still limited by a lack in data on the root dynamics in a morainic arable soil landscape. Here, hillslope position-specific data of root growths for the hummocky soil landscape would be a step forward.

To identify soil erosion feedbacks on water and dissolved carbon fluxes, crop and root growth, arable used lysimeters are an appropriate instrument for determining water balance components and carbon leaching at different depths. Recent lysimeter research primary focused on filter schemes and smoothing algorithms to reduce noise in the high resolution lysimeter time series (e.g., Hannes et al., 2015, Peters et al., 2014). Validity problems e.g., due to temporally auto-correlated data, however, were not considered although statistical uncertainties in time series analysis of hydrological data are well known, e.g., Kohyama et al. (2005) or Yue et al. (2002). In this context, an (auto)correlation analysis may identify repeating patterns in high resolution lysimeter data such as a presence of a periodic signal masked by data noise.

The central research question of this thesis - raised by the lack of knowledge - is: how soil evolution processes in connection with the crop and tillage management affect the soil water balance and, further, may have contrasting water fluxes an influence on leaching rates of the dissolved carbon fraction. In this way, it might be possible to relate the significance of the carbon export due to soil water fluxes with the gaseous export of organic and inorganic



carbon. The quantification of dissolved carbon losses also allows the estimation of decalcification processes within the soil profile and hence undergoing pedogenetic changes. Results of following thesis objectives and their interrelationship derived from the motivation as described above should lead to a better understanding of the interaction between the soil water balance, the carbon leaching potential and dynamics in soil-crop-system for the arable hummocky ground moraine landscape. The four study objectives of this thesis were:

1. i) to analyze temporal autocorrelation in high-resolution time-series of weighing changes for determining time-dependent time lags, ii) deriving optimal time intervals according to the determined autocorrelation lengths and iii) to provide an autocorrelation based filtering scheme for determination of precipitation from lysimeter time series.
2. i) to relate water balance components and crop yield with erosion-induced soil profile modifications and ii) to quantify leaching rates of dissolved organic and inorganic carbon for the differently eroded soils of the same diagnostic soil type (Haplic Luvisols).
3. i) to analyze soil hydraulic properties (water retention data) of characteristic soil horizons of differently eroded Luvisols using field data measured in high precision lysimeter soils, ii) to compare field and lab water retention data and iii) to identify complex field water retention dynamics at different time scales.
4. i) to determine the effect of an erosion-affected soil evolution, hence modifications of soil properties depth functions, on the root system and ii) evaluate the relationship of root growths to above-ground plant development in the hummocky soil landscape.

## ***1.6 Thesis outline***

The current doctoral thesis is conceptualized in a cumulative style in accordance with the guidelines for a cumulative PhD-thesis at University of Potsdam, Institute of Earth and Environmental Science. The thesis comprises four manuscripts that were accepted for publication or are under the revision process (manuscript #4), respectively, in peer-reviewed ISI-journals. The thesis ends with a synopsis chapter where results and findings will be discussed in a general context.

*Manuscript #1 - Autocorrelation analysis of high resolution weighing lysimeter time series as a basis for determination of precipitation*

*The manuscript deals with an autocorrelation analysis of lysimeter time series for determining precipitation. Minute-based time series of weighing changes were recorded by a lysimeter system consisting of six individual lysimeters. The objective was to analyze the temporal autocorrelation in the time series of weighing changes and to identify optimal time intervals for determining precipitation rates.*

Declaration of the contribution on publications

Marcus Herbrich performed the data analysis and calculations, reviewed the relevant literature, wrote the manuscript and created figures and tables. The co-author Horst H. Gerke participated in the interpretation of the results, provided valuable remarks on the discussion and revised the manuscript text.

Own contribution of Marcus Herbrich: 70 percent of the total manuscript

*Manuscript #2 - Water balance and leaching of dissolved organic and inorganic carbon of eroded Luvisols using high precision weighing lysimeters*

*The manuscript deals with an analysis and comparison of the water balance for differently-eroded lysimeter soils for a 3-years period. Water balance components, in particular deep drainage rates, and concentration measurements of dissolved carbon fractions at the lysimeter bottom were used to evaluate the carbon leaching potential of the arable hummocky ground moraine soil landscape.*

Declaration of the contribution on publications

Marcus Herbrich performed the data analysis and calculations, reviewed the relevant literature, wrote the manuscript and created figures and tables. The co-author Horst H. Gerke participated in the interpretation of the results, provided valuable remarks on the discussion and revised the manuscript text. The co-authors Michael Sommer and Oliver Bens provided useful advices and helped to improve the final manuscript by proofreading.

Own contribution of Marcus Herbrich: 70 percent of the total manuscript

*Manuscript #3 - Scales of Water Retention Dynamics Observed in Eroded Luvisols from Arable Postglacial Soil Landscape*

*The manuscript deals with hysteretic field-measured water retention data depending on changing soil properties and the erosion history which created spatial patterns of soil properties or differences in crop development. Drying and wetting water retention was identified in depths representing same soil horizons and compared to drying retention data obtained from soil cores.*

Declaration of the contribution on publications

Marcus Herbrich performed the data analysis and calculations, reviewed the relevant literature, wrote the manuscript and created figures and tables. The co-author Horst H. Gerke participated in the interpretation of the results, provided valuable remarks on the discussion and revised the manuscript text.

Own contribution of Marcus Herbrich: 70 percent of the total manuscript

*Manuscript #4 - Root development of winter wheat in erosion-affected soils depending on the position in a hummocky ground moraine soil landscape*

*The manuscript deals with erosion-induced changes in the root development of winter wheat depending on erosional soil profile modifications using the minirhizotron technique. Root density values and root lengths were measured for a non-eroded reference soil at the plateau, an extremely eroded soil at steep midslope and for a depositional soil at the footslope. Finally, the root length density and root biomass density were derived from the root density data and discussed for each landscape position.*

Declaration of the contribution on publications

Marcus Herbrich performed the data analysis and calculations, reviewed the relevant literature, wrote the manuscript and created figures and tables. The co-author Horst H. Gerke participated in the interpretation of the results, provided valuable remarks on the discussion and revised the manuscript text. The co-author Michael Sommer provided useful advices and helped to improve the final manuscript by proofreading.

Own contribution of Marcus Herbrich: 70 percent of the total manuscript

## 2| Autocorrelation analysis of high resolution weighing lysimeter time series as a basis for determination of precipitation

## *Abstract*

The determination of precipitation ( $P$ ) is still a challenge, but central for quantifying soil water and element balances. Time series' of mass changes ( $\Delta M$ ) from high precision weighing lysimeter may be used to estimate  $P$  if deep drainage rates are determined independently. High temporal resolution; however, is accompanied by problems such as correlated data and noise. The objective was to analyze the temporal autocorrelation (AC) in  $\Delta M$  time series' and to identify temporal resolutions for determining uncorrelated  $P$  rates. Minute-based time series' of  $\Delta M$  are analysed; the data have been recorded at the UMS Science Lysimeters that are located in Dedelow (northeast Germany) as part of the TERENO SoilCan lysimeter network. Periods in 2012 and 2013 were selected in which the wind speed was below  $6 \text{ ms}^{-1}$ . Data noise-correction was carried out by using a moving average before the  $\Delta M$  values cumulated over 60, 30, and 10 min intervals were compared. On a monthly basis, the temporal AC lengths for  $\Delta M$  were larger in spring (68 min), autumn (62 min), and winter (76 min) than in the summer (23 min). These AC lengths reflected mainly the effect of differences in  $P$ -rates and –duration between lower-intensity rainfall and shorter summer storms. The monthly sums of  $P$  based on the 60-min interval were up to 20 % lower than those obtained by using the 10-min intervals. For  $P$ -values obtained by summing up the  $\Delta M$  over periods shorter than the autocorrelation length, oscillated fluctuations in  $\Delta M$  did not cancel out within an interval. The temporal autocorrelation in the highly-resolved lysimeter data limited the evaluation of  $\Delta M$  time series. Compared to rain gauge data, the  $P$ -rates obtained from the weighing lysimeters were generally higher; however, this difference decreased when increasing the time interval for cumulating mass changes. Cumulated positive  $\Delta M$  values based on time intervals larger than the AC length (e.g., 60 min) provided an optimal approximation of the quantity of  $P$ , but on the expense of a loss in temporal resolution limited by the AC lengths. Smoothing could reduce noise in the original lysimeter data; however, not the validity problems that are related to the temporal AC.

## 2.1 Introduction

Quantification of the precipitation ( $P$ ) is of central interest for many hydro-pedological aspects, e.g. causing fluvial soil erosion (Nearing et al., 2005) or controlling the budget of dissolved carbon in soils (Kalbitz et al., 2000). Rain gauges installed at 1 m above a ground surface are used as a standard method to quantify precipitation; the data obtained with this method may be erroneous by up to 75 % for single  $P$ -events (Neff, 1978). These measurement errors of collecting  $P$  are mostly due to the deformation of the wind field above the rain gauge orifice (Sevruk et al., 1989), evaporation losses of collected rain water in the rain gauge container (Strangeways, 1996), wetting losses of rain water from the inner walls of gauge container and collector (Yang et al., 1999) and (out) splash of rain drops from the rain gauge funnel (Strangeways, 1996). For winter conditions including frost and snow, these errors can be even larger as compared to rain (Sevruk, 1996). Rain gauges are known to underestimate the total volume of rainfall events (Aldridge, 1976; Nespor and Sevruk, 1999); thereby creating problems in quantifying the correct water balance of soils (Fekete et al., 2004; Kampf and Burges, 2010).

Optimal conditions for  $P$ -measurements would require rain collection at the soil surface with micro topographic structure that is identical with that of the surrounding area (Mekonnen et al., 2015). In this context, lysimeters are able to match surrounding field conditions (Unold and Fank, 2008; Meißner et al., 2010) like the crop sequence or the micro topographic surface structures. Lysimeters with a high-precision weighing system (Unold and Fank, 2008) have been proposed to quantify precipitation in a high temporal resolution (Peters et al., 2014; Schrader et al., 2013). Even rime or dew was recorded by measuring small changes in water storage of lysimeter time series in a temporal resolution of one hour (Meissner et al., 2007; Xiao et al., 2009).

Time-series of mass changes from high precision lysimeter could be used to estimate  $P$ , if deep drainage rates are determined independently, on assuming that positive values of  $\Delta M$  represent  $P$  and negative values  $ET$ , respectively (e.g., Young et al., 1996). In this way lysimeter technology developed at a quality level to investigate hydrological aspects exceeding old-fashioned outdoor leaching tests (Meißner et al., 2010).

The more recently developed high precision weighing lysimeters can reach resolutions in determining the mass of 10 g, which equals 0.01 mm water equivalent, by a total weight of > 3000 kg depending on the measurement system (Unold and Fank, 2008). High temporal resolution, however, is accompanied by correlated data and noise. Multiple sources of errors can produce data noise when the resolution of lysimeter systems increased; mechanical disturbances and vibrations, among others due to animals, field work or wind (Nolz et al.,

2013) could be effected mass changes in the weighing signal by an absence of water fluxes at the soil-atmosphere interface. Therefore  $P$  based on high-resolution time-series' of lysimeter mass changes can be influenced by external errors resulting in an overlay of the weighing signal by a random component (weighing oscillation). Hence, the determination of  $P$  from lysimeter data needs an adequate processing of  $\Delta M$  time series.

To separate external errors in high-resolution time-series of lysimeters from the weighing signal of  $P$ , data smoothing is commonly used to remove the noise (e.g., *Vaughan et al., 2007; Vaughan and Ayars, 2009*). Smoothing functions were tested by *Nolz et al. (2013)* on a set of noisy lysimeter weighing data using a sigmoidal function for single days and a polynomial spline function for a longer time period with rainfall events to remove noise. The effects of smoothing and averaging on the accuracy of the estimated water fluxes are rarely discussed so far. On the basis of synthetic data *Schrader et al. (2013)* demonstrated that water balance components are affected by the selection of smoothing windows, e.g. leading to a systematic misfit when sudden changes in the lysimeter weight occurred. Recently, an adaptive filtering algorithm and a non-adaptive filter scheme to obtain temporal high-resolution lysimeter weighing data were developed (*Peters et al., 2014; Hannes et al., 2015*). *Peters et al. (2014)* presented the Adaptive Window and Adaptive Threshold (AWAT) filter using filtering parameters according to the signal strength, while *Hannes et al. (2015)* provided a processing scheme of five separately filtering steps: manual filter, threshold filter, median filter, smoothing filter and an oscillation threshold filter. In lysimeter studies of *Fank (2013)* and *Peters et al. (2014)*, differences in quantified precipitation calculated from lysimeter time series were reported depending on the length of time intervals over which high resolution data were integrated. In the AWAT filter scheme of *Peters et al. (2014)*, the length of the maximum allowed time window over which signal strength and data noise information are collected influenced the amount of estimated fluxes. Also, *Hannes et al. (2015)* reported for his synchro filter time interval depended filtering errors.

Despite these efforts of developing filtering approaches to determine water balance components like precipitation from high-resolution time-series of  $\Delta M$ , temporal autocorrelation in the weighing signal were not considered. However, precipitation performs typically in a non-random fashion, since significant autocorrelation appears in rainfall of periods of relatively short duration (e.g., *Kotz and Neumann, 1959; Matalas, 1963*). The temporal memory of rain fall events can be highly significant; the signal of autocorrelation in precipitation was observed to roughly follows an exponential decay (*Rakovec et al., 2012*). Therefore we hypothesized; the time series of lysimeter measurements also include autocorrelation induced by the momentum from mass changes of  $P$  among other factors buried in data noise. The autocorrelation, in turn, may create problems in the time series

analysis of the lysimeter data to determine  $P$ . In time series of ecological data autocorrelation is well known to underestimate the standard error and consequently the Type-I-error, defined as a rejection of a null hypothesis when it is true, is under- or overestimated which complicates the statistical testing of hypotheses in analysis (Legendre, 1993). For example, in hydrological time series analysis of streamflow events autocorrelation can increase the probability to detect significant trends where there are none (Yue et al., 2002). Besides filtering uncertainties, unfiltered influences on lysimeters and the natural heterogeneity in the precipitation (Hannes et al., 2015), temporal autocorrelation in time series' could be also a relevant factor for  $P$  calculations, but have not been considered for the time interval selection, analysis and evaluation; it was unknown how and to what extent the autocorrelation length affected the evaluation of precipitation data from high resolution lysimeter data.

The objectives of this study were (i) to analyze high-resolution time-series of weighing changes  $\Delta M$  on autocorrelation, (ii) to determine  $P$ -rates from lysimeter weighing data using an autocorrelation based filtering approach and (iii) to compare results of calculated precipitation with  $P$ -rates with other processing schemes (e.g., synchrofilter: Hannes et al., 2015) and rain gauge data from a weather station next to lysimeters for identical time periods. The autocorrelation analysis of high-resolution time-series' aimed at determining the length of temporally dependent time lags. Time series' of weighing data recorded by TERENO SoilCan lysimeters (Pütz et al., 2016) were analyzed for deriving the optimal time intervals according to temporal autocorrelation for determining  $P$ -rates.

## 2.2 Materials and method

### 2.2.1 Study site and lysimeters

The lysimeters were installed in 2010 at the Experimental Field Station Dedelow (53°22'2.45"N, 13°48'10.91"W, 35m a.s.l.) of the Leibniz-Centre for Agricultural Landscape Research (ZALF), located near the city Prenzlau, north-eastern Germany. The study areas is characterized by annual precipitation rates between 2000 and 2012 of 365 (minimum) to 760 mm·y<sup>-1</sup> (maximum) and by annual mean air temperatures that range from 7.0 to 9.6 °C (at 2 m above soil surface). The potential evapotranspiration is approximately 734 mm·y<sup>-1</sup>, which is 1.5-times the average annual precipitation of 489 mm y<sup>-1</sup> (snowfall included). Weather data were recorded directly at the ZALF station Dedelow (Verch, 2014). The data are publicly available under <http://open-research-data.ext.zalf.de>. The precipitation,  $P_{Stat}$ , at this station (FMA 86, Wilh.Lambrecht Company, Göttingen, Germany), was measured with a temporal



resolution of 10 min with an automated rain gauge (LB 15188, heated type, Wilh. Lambrecht Company, Göttingen); the sensitivity was 0.1 mm per tipping ( $\approx 2 \text{ cm}^3$ ).

The lysimeter system consists of a hexagon of six individual lysimeters of the type UMS Science-Lysimeter (Special Version) that are controlled from a central monitoring chamber (UMS GmbH, Munich, Germany, [http://www.ums-muc.de/en/lysimeter\\_systems.html](http://www.ums-muc.de/en/lysimeter_systems.html); *Unold and Fank*, 2008). Each cylindrical lysimeter with a surface area of about  $1 \text{ m}^2$  and a height of 1.5 m was filled with intact soil monoliths of more or less eroded Luvisols extracted from sites "Dedelow" and "Holzendorf". Both sites were located in a hummocky arable soil landscape developed from glacial till as the parent material (*Sommer et al.*, 2008). Soil monoliths were denoted as L\_1, L\_2, L\_3, L\_4, L\_5, and L\_6. The scales for lysimeter mass and outflow at the bottom are operating with an accuracy of 10 g, which is corresponding to 0.01 mm of water equivalent. The temporal resolution of the mass and outflow data was 1 min (i.e., as an average of the 10 sec measurements provided by the scale over the 1 min interval). At the bottom in about 140 cm depth, a silicon-carbide suction cup rake allows drainage of soil water or injection of effluent from the storage tank. This pump regulation (amount of water pumped in and out) is controlled by the applied suction provided by reference tensiometers. These tensiometers are installed in the undisturbed field next to the lysimeter station at the same soil depth (140 cm).

Lysimeters and the surrounding field of approximately 2.3 ha in size were uniformly cultivated with winter rye (*Secale cereal L.*) from January to May 2012, Sudan grass (*Sorghum sudanense*) from May to September 2012, triticale (*Triticosecale*) from October 2012 to March 2013. Biomass of crops ranged for winter rye between 25 to  $41 \text{ t}\cdot\text{ha}^{-1}$  and for Sudan grass between 48 to  $79 \text{ t}\cdot\text{ha}^{-1}$  (Table 2.1).

*Table 2.1: Above ground biomass yield (kg, fresh mass) harvested from the six 1 m<sup>2</sup>-sized lysimeters L\_1 to L\_6; the crop rotation consisted of winter rye (*Secale cereal L.*) from September 2011 to May 2012, Sudangrass (*Sorghum sudanense*) from May to September 2012, harvest date were May 9<sup>th</sup>, 2012 for winter rye and September 21<sup>th</sup>, 2012 for Sudangrass;  $k$  denotes the logistic growth coefficient of [Eq. 2]*

Lysimeter	Winter Rye	Sudangrass	Winter Rye	Sudangrass
	Biomass yield		coefficient $k$	
	/ kg	/ kg	/ -	/ -
L_1	2.5	5.7	0.053	0.021
L_3	2.9	8.1	0.042	0.025
L_5	2.5	7.9	0.048	0.016
L_2	3.3	4.8	0.035	0.023
L_4	4.1	5.2	0.053	0.016
L_6	3.7	5.4	0.038	0.022

Biomass of triticale was not determined because of negligibly-small plant growth. Soil tillage and fertilization (March 19<sup>th</sup>, 2012), harvesting (May 9<sup>th</sup>, 2012; September 21<sup>th</sup>, 2012), and seeding (May 15<sup>th</sup>, 2012) operations were carried out manually for the lysimeters and the surrounding area. Fresh above-ground biomass was gravimetrically determined with the scale QS16000B (Sartorius AG, Göttingen, Germany) for winter rye on May 9<sup>th</sup>, 2012 and for Sudangrass on September 21<sup>th</sup>, 2012.

### 2.2.2 Analysis of lysimeter mass time series'

The gross lysimeter mass,  $M_{Lys}$ (kg), consists of the soil monolith with the instrumentation and included the temporary crop and snow coverage as well as the interception of water by plant and crop residue surfaces. Mass changes resulting from the growth of plant biomass,  $M_{plant}$ , were subtracted to obtain a corrected total mass,  $M_{tot}$ , as:

$$M_{tot}(t) = M_{Lys} - M_{plant} \quad [2.1]$$

The biomass correction is an attempt to realistically distribute the effect of biomass increase on precipitation data over the vegetation period, which was based on measured crop biomass data at harvest (see above) and temporal estimates derived from a logistic growth function first for the above-ground biomass,  $M_{crop}$  (kg), which was adapted from the formulation used for estimating the leaf area index, LAI, (Rieckh et al., 2014) as:

## II Autocorrelation analysis of high resolution weighing lysimeter time series as a basis for determination of precipitation

$$M_{crop}(t) = \frac{M_i M_f}{M_i + (M_f - M_i) e^{-M_f k t}} \quad [2.2]$$

Where  $t$  is time (d),  $k$  is a logistic growth coefficient (-),  $M_i$  (kg) is initial biomass at the beginning of the growing season and  $M_f$  (kg) the final value of biomass at harvest. From these daily estimates of biomass, minute-based values were derived by a simple linear interpolation between each two daily biomass data. The mass changes due to biomass correction ranged between 0.2 and 13.2 g (60min)<sup>-1</sup> (Table 2.2). Coefficient  $k$  in Eq.2 was calibrated for each crop according to wet above-ground biomass data of each lysimeter measured at the two harvest times in 2012 (i.e., May and September). Values of  $k$  for the vegetation period ranged from 0.05 to 0.02 for the six lysimeters (Table 2.1).

*Table 2.2: The range of the minimal and maximal mass changes due to biomass production for months April and July in 2012. Values were derived from daily biomass data (linear interpolation within a day) of lysimeters L\_1-L\_6.*

Period		Biomass changes					
		L_1	L_2	L_3	L_4	L_5	L_6
month		/ g 60min <sup>-1</sup>					
April	Minimum	0.2	0.2	0.2	0.3	0.2	0.2
	Maximum	3.6	4.8	4.1	6.4	3.6	5.4
July	Minimum	1.4	1.2	1.9	1.3	1.9	1.3
	Maximum	8.9	7.3	13.2	8.0	12.8	8.4

The increase of root mass, representing the below ground biomass, was estimated from  $M_{crop}$  by assuming a shoot/root (s/r) ratio of 0.3 for Sudangrass (Ali et al., 2009; Promkhambutet et al., 2010) and 0.22 for winter rye (Bray, 1963). The sum of above- and below-ground biomass,  $M_{plant}$ , was considered for each lysimeter, as:

$$M_{plant} = M_{crop} + M_{crop} * \frac{s}{r} \quad [2.3]$$

The time series' of biomass-corrected total lysimeter mass,  $M_{tot}$  (kg) in Eq. 1, were treated in the following steps as, for example, for a period in July, 2012 (Fig. 2.1). Mass changes,  $\Delta M_{tot}$  (kg min<sup>-1</sup>), were calculated as the difference between two consecutive values (min) from  $M_{tot}$  (Fig. 2.1a). Outliers in (Fig. 2.1b)  $\Delta M_{tot}$  above a threshold were eliminated as proposed by Gebler et al. (2013) and Schrader et al. (2013). The threshold of 3.0 kg·min<sup>-1</sup>

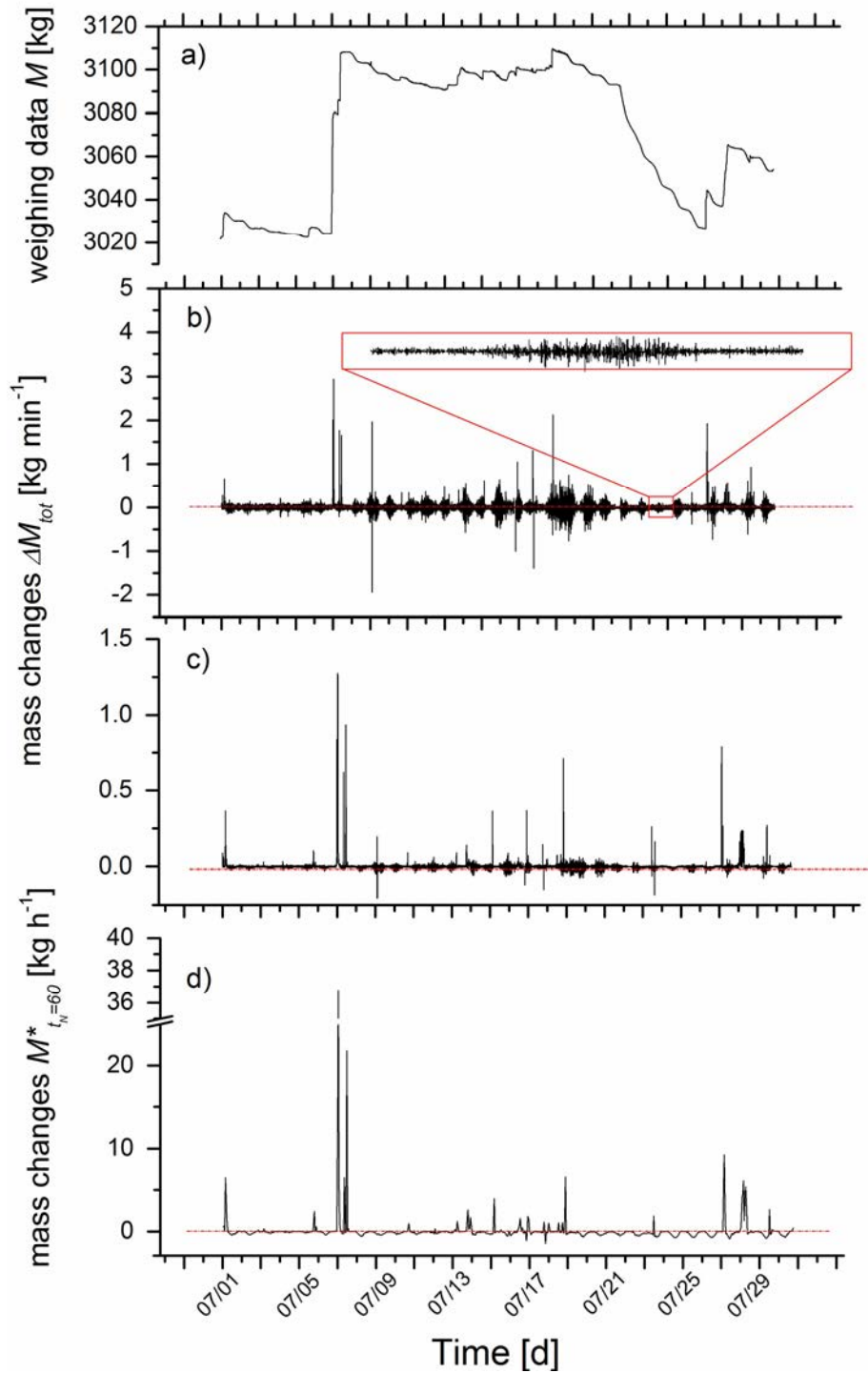


Figure 2.1: Examples of the data processing for lysimeter time series' weighing data of lysimeter L\_1 showing (a), the 1-minute data series of lysimeter mass; (b) the 1-minute based mass changes after seepage and biomass correction, the minute-based mass changes treated by a simple moving average,  $\Delta M^*$ , (c), and the mean hourly-based mass changes  $\Delta \overline{M}^*$ , (d) for the July 1 - 31 period in 2012 (period B in Figure 3). The small inlet in (b) is an enlarged view indicating the magnitude of noise in the data during a single day. Red dotted lines in a), b), and c) indicate the zero mass change level.

used here was based on the assumption that a mass increase larger than 3 kg within a single minute could only be caused by artificial manipulations of the lysimeters (e.g., soil tillage, animal activity) and not by precipitation. The maximum precipitation rate was about 2 mm·min<sup>-1</sup> (i.e., 2 kg min<sup>-1</sup> per lysimeter) observed at the agro-meteorological weather station in Dedelow between years 2000 and 2013 (i.e., 19.5 mm (10 min)<sup>-1</sup>). The increases of lysimeter mass and positive mass changes in  $\Delta M_{tot}$  (Fig. 2.2a and 2.2b) were highly concordant to  $P$  events determined by the rain gauge of the agro-meteorological weather station (Fig. 2.2c). The oscillations in the lysimeters weighing induced by severe wind (Fig. 2.2d) and the raindrop impact (Fig. 2.2c) resulted in an enhanced over- and undershooting of mass changes (2.2b). At rain and wind-free periods, the oscillations in the lysimeters weighing was reduced at a minimum.

At the lysimeter bottom in about 1.4 m depth, the mass of the drainage water,  $M_{drain}$ (kg) was separately measured in the same temporal resolution of one minute. The lysimeter mass change related only to water fluxes through the upper surface of the lysimeter was obtained as:

$$\Delta M(t) = (M_{tot} - M_{drain})_{t+1} - (M_{tot} - M_{drain})_t \quad [2.4]$$

Missing data resulting from technical problems (July 13<sup>th</sup> 2012 to July 24<sup>th</sup> 2012, lysimeter L\_5 leachate scale) was treated as “no data”; the gap in outflow data was associated with the last measured value as the fix lysimeter mass until the measurements continued were used for calculations (i.e., no interpolation of masses was carried out, because seepage water fluxes were unknown for this period). These complete time series’ of mass changes  $\Delta M(t)$  were then treated by a noise reduction procedure. *Schrader et al.* (2013) demonstrated for lysimeter weight measurements (minutely raw data) of similarly designed precision lysimeters that an increase of smoothing windows from 10 minutes (=11 data points) to 30 minutes (=31 data points) can create a systematic misfit when sudden changes in the lysimeter weight occurred (e.g.,  $P$  event). Here, noise reduction by data smoothing was carried out using a simple moving average (SMA) over a time window of  $n= 11$  min as,

$$\Delta M^*(t_{min}) = \frac{1}{n} \sum_{i=0}^{n-1} \Delta M_{t-i} \quad [2.5]$$

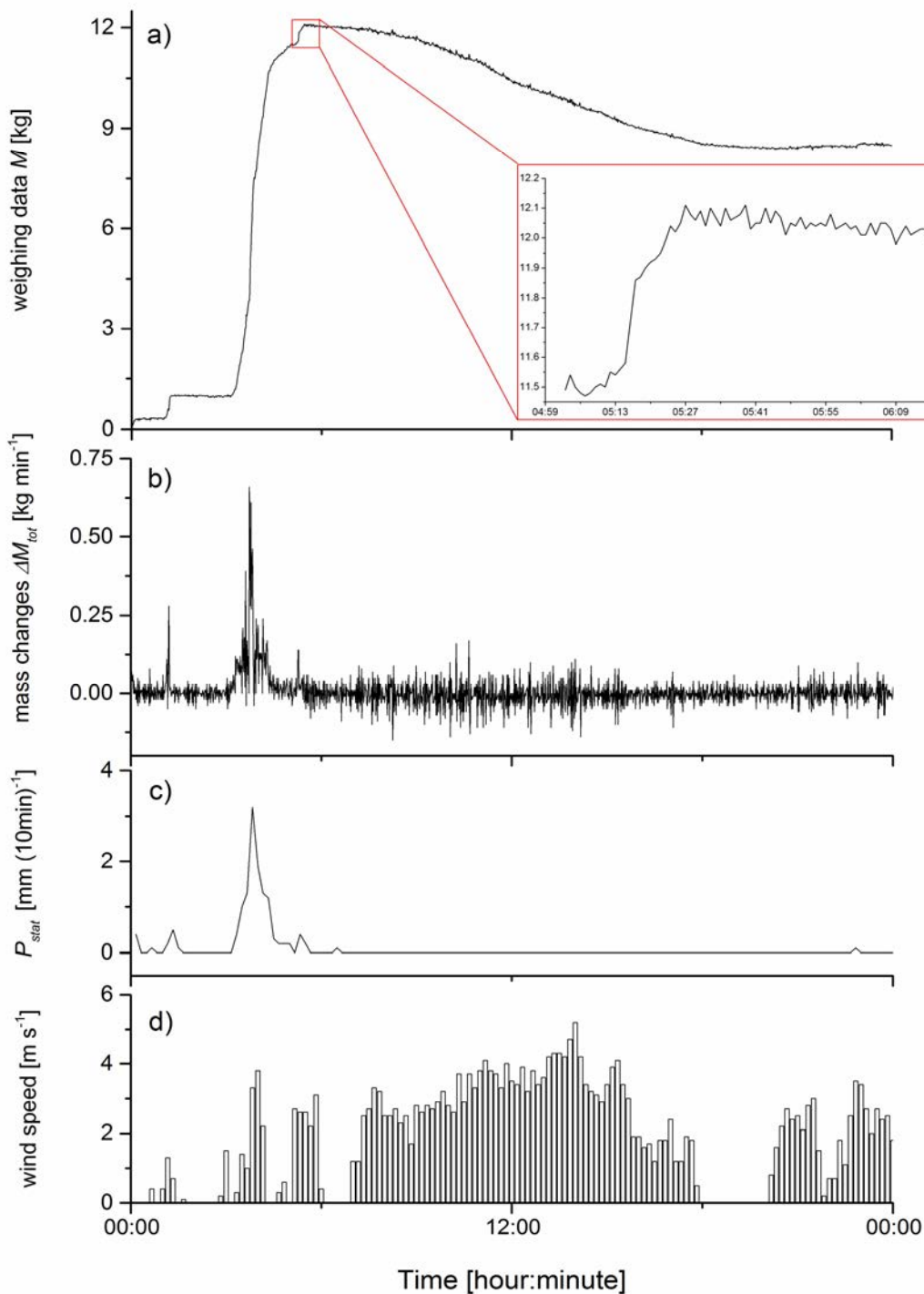


Figure 2.2: Illustration of lysimeter and weather station data for July 1st to July 2nd (24h) including precipitation events and wind fluctuations. The figure shows a) the 1-minute data series of lysimeter mass; (b) the 1-minute based mass changes after seepage and biomass correction; (c) the rain gauge data  $P_{Stat}$  (10 min) and (d) the wind speed values (10 min average) for that 24h period. The small inlet in a) is an enlarged view indicating the magnitude of noise in the data during a single precipitation event. The mass is here related to the reference of 3021.7 kg at the beginning July 1<sup>st</sup>, 2012

## II Autocorrelation analysis of high resolution weighing lysimeter time series as a basis for determination of precipitation

---

The smoothed  $\Delta M^*(t_{min})$  values ( $\text{kg min}^{-1}$ ) still at the 1-minute interval,  $t_{min}$ , (Fig. 2.1c) were used to calculate the mass changes cumulated over time intervals,  $t_N$ , as (Fig. 2.1d):

$$\overline{\Delta M^*(t_N)} = \sum_{t_{min}=1}^N \Delta M^*(t_{min}) \quad [2.6]$$

The length of the time intervals of  $t_N = 10, 30,$  and  $60$  min were selected according to the results of the autocorrelation analysis explained below.

A positive value of the sum of mass changes,  $\overline{\Delta M^*(t_N)}$  was assumed to represent an input into the lysimeter through all positive mass changes as precipitation (*Young et al., 1996*), condensation and interception, denoted as  $P_{Lys}$ . The latter was calculated as:

$$P_{Lys} = \sum_{i=0}^N \overline{\Delta M^*(t_N)} \text{ for } \Delta M^* > 0 \quad [2.7]$$

A negative value of  $\overline{\Delta M^*(t_N)}$ , a mass loss through evaporation,  $E_{Lys}$ , or transpiration,  $T_{Lys}$  was calculated as:

$$ET_{Lys} = \sum_{i=0}^N \overline{\Delta M^*(t_N)} \text{ for } \Delta M^* < 0 \quad [2.8]$$

for time intervals of  $t_N = 10, 30,$  and  $60$  min.

In addition to the autocorrelation based processing scheme, precipitation values for selected time periods were determined using the filtering scheme of *Hannes et al. (2015)*; so called synchro filter. The filtering of discrete events are based on three filter steps (manual filter, threshold filter, median filter) followed by the filtering of noise using a smoothing and oscillation threshold filter. The threshold for the maximum possible precipitation was set to  $3.0 \text{ kg}\cdot\text{min}^{-1}$ . The time window of the median and smoothing filter was set to 15 min as recommended; detailed information about the filtering procedure are given by *Hannes et al. (2015)*.

The calculation of the temporal autocorrelation coefficient at any point in the time series,  $r(h)$  as a function of the arbitrary time lag,  $h$ , was based on the 1-mininterval biomass corrected  $\Delta M$  data (see [Eq. 2.4]) using the AC function of the SPSS software package (IBM, Armonk, USA), which is given in the notation of this paper as:

$$r(h) = \frac{\sum_{i=1}^{n-h} (\Delta M_i - \overline{\Delta M})(\Delta M_{i+h} - \overline{\Delta M})}{\sum_{i=1}^n (\Delta M_{i+h} - \overline{\Delta M})^2} \quad [2.9]$$

where  $\overline{\Delta M}$  is the arithmetic average of the  $n$  observations, and  $\Delta M_i$  the  $i^{\text{th}}$  observation of time series ( $i= 1, \dots, n$ ). For the analysis, periods representing the four seasons in 2012 and 2013 were selected. These periods (i.e., spring (A), summer (B), autumn (C), and winter (D); Fig. 2.3) were characterized by low to moderate wind speeds ( $<6 \text{ m}\cdot\text{s}^{-1}$ ) according to *Nolz et al. (2013)*, which observed a non-linear relation between wind velocity and measuring accuracy of lysimeters.

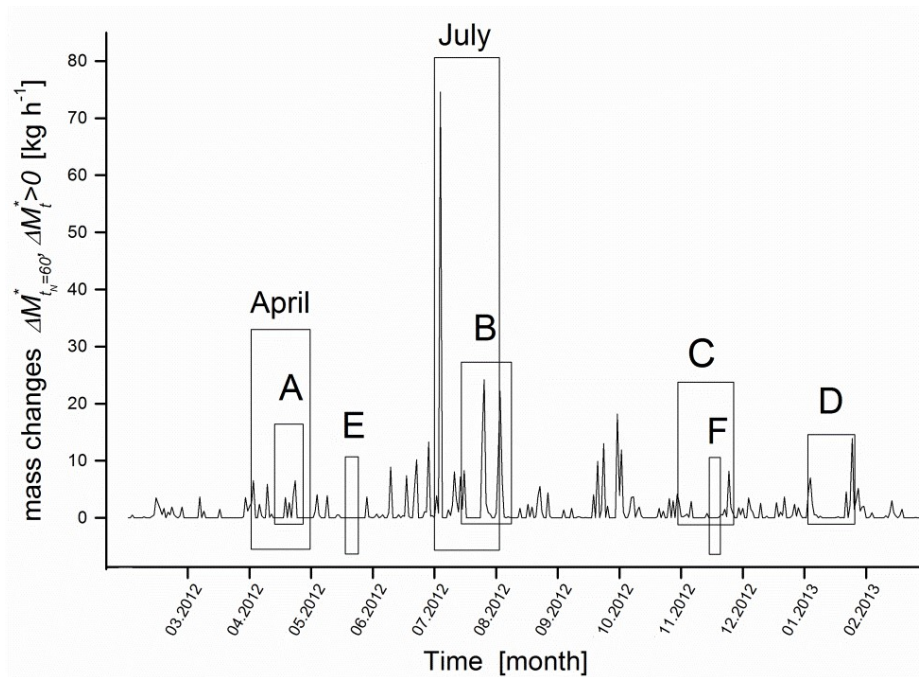


*Figure 2.3: Schematic of lysimeter mass changes time series for indicating the selected precipitation time periods with moderate wind speed values below  $6 \text{ m}\cdot\text{s}^{-1}$  used in the autocorrelation analysis. The periods were in spring (A, April 20<sup>th</sup> – April 26<sup>th</sup>, 2012), summer (B, July 22<sup>th</sup> - August 14<sup>th</sup>, 2012), autumn (C, November 1<sup>st</sup> - November 22<sup>th</sup>, 2012), and winter (D, January 14<sup>th</sup> - January 29<sup>th</sup>, 2013). In addition, two longer observation periods (April 2012; July 2012) and two periods without increases of the lysimeter weight by mass changes due to rainfall events (period E: May 18<sup>th</sup> - May 25<sup>th</sup>, 2012; period F: November 11<sup>th</sup> - November 18<sup>th</sup>, 2012) were included.*

At a higher wind velocity the accuracy of the sensitive weighing systems would be affected (reduced) and changes in the lysimeter mass due to disturbances, e.g. forces exerted by wind, and precipitation could be overlaid. In period D, times with solid precipitation (snowfall) were included.



## II Autocorrelation analysis of high resolution weighing lysimeter time series as a basis for determination of precipitation

Temporal autocorrelation coefficient,  $r$ , was transformed to a normalized AC coefficient,  $r^*$ , considering the maximum and minimum values of  $r$  as,

$$r^* = (r - r_{min}) / (r_{max} - r_{min}) \quad [2.10]$$

For the selected periods A to D, an exponential model was fitted to the resulting autocorrelation coefficient  $r^*(h)$  data using the software OriginLab Pro 8G (Northampton, USA):

$$r^*(h) = A e^{-\frac{h}{z}} + r_0^* \quad [2.11]$$

where the parameter  $A$  was the amplitude,  $z$  the decay constant, and  $r_0^*$  was defined as the offset. The distance over which autocorrelation occurred is given by the autocorrelation lengths  $\lambda$  defined by the time interval, where the autocorrelation function dropped below the significance level of  $p=(0.1)r^*$  for the first time, similar to a study of *Wolf* (1999). The drop of the autocorrelation function below the significance level  $p = 0.1$  was determined by the intersection point of  $P'$  at  $(0.1)r^*$  (Table 2.3).

*Table 2.3: Values of fitting parameter ( $r_0^*$ ,  $A$ ,  $z$ ) and intersection points ( $P'$  at  $p=(0.1)r^*$ ;  $L'$  at  $p = (e^{-1}) r^*$ ) from the exponential model of observation periods A to D. The intersection point  $P'$  denotes the AC length,  $\lambda$ , and  $L'$  the AC length,  $\lambda_D$ . The parameter  $a$  describes the ratio of the two AC lengths and  $R^2$  denotes the coefficient of determination. The root mean square error,  $RMSE$ , is of model fit to data points.*

Period	$P'$ / min	$L'$ / min	$a(\lambda)$ /-	$r_0^*$ /-	$A$ /-	$z$ /-	$R^2$ /-	$RSME$ /-
A	67.5	24.1	2.8	0.05	0.887	23.55	0.84	0.095
B	22.5	10.7	2.1	0*	1.28	8.59	0.98	0.035
C	62.2	13.9	4.4	0.09	0.716	14.75	0.87	0.063
D	76.2	20.3	3.8	0.09	0.871	17.79	0.91	0.065

\* the value of  $r_0^*$  was fixed as zero for the minimum of the exponential fitting parameter

Also, for exponentially decaying AC functions it is often been applied to determine length of autocorrelation as the intersection of  $L'$  at  $(e^{-1})r^*$  (Table 2.3) for a significant level (*Nielsen and Wendroth*, 2003). A length of AC for  $p=(e^{-1})r^*$  is called Debye-Length  $\lambda_D$ . To compare

autocorrelation lengths of both approaches, the intersection  $L'$  ( $\lambda_D$ ) are given as  $\lambda$  with the intersection  $P'$  and a factor of  $a$  (Table 2.3).

The 90 % prediction limits of  $r^*$ ,  $r_{PL}^*(h)$ , related to the exponential model fit [Eq. 2.11] were determined for the (expected) mean value of  $r^*$  at  $h = h_{predict}$  as:

$$r_{PL}^*(h) = \hat{r}^* \pm t_{\left(\frac{\alpha}{2}, n-1\right)} S_e \sqrt{1 + \frac{1}{n} + \frac{(h_{predict} - \bar{h})^2}{\sum_{i=1}^n (h_i - \bar{h})^2}} \quad [2.12]$$

where  $\bar{h}$  is the average of the time lags  $h$ ,  $S_e$  denotes the standard deviation,  $\alpha$  is the confidence level and  $t_{\left(\frac{\alpha}{2}, n-1\right)}$  denotes the  $100\left(\frac{\alpha}{2}\right)$  percentile of the student  $t$  distribution with  $n-1$  degrees of freedom. The upper and lower limit was denoted by + (plus) and – (minus), respectively. Prediction limits were calculated using software OriginLab Pro 8G (Northampton, USA).

To compare calculated precipitations  $P_{Stat}$  and  $P_{Lys}$ , analyses of the Euclidean distance ( $ED$ ) and the root mean square error ( $RMSE$ ) were calculated by using [Eq. 2.13] and [Eq. 2.14] as:

$$ED = \sqrt{\sum_{i=1}^n (P_{Stat_i} - P_{Lys_i})^2} \quad [2.13]$$

$$RMSE = \sqrt{\frac{\sum_{i=1}^n (P_{Stat_i} - P_{Lys_i})^2}{n}} \quad [2.14]$$

where  $n$  is the number of data considered for analyzing the similarity between the observed,  $P_{Stat}$ , and the calculated precipitation,  $P_{Lys}$ , for each variable  $i$ . A perfect match is indicated by a value of zero.

## 2.3. Results

### 2.3.1 Temporal autocorrelation

Lysimeter time series for selected precipitation time periods A to D (Fig. 2.3) were analyzed using the autocorrelation function [Eq. 2.9]. The results of AC analyses in Fig. 2.4 show that temporal autocorrelation in  $\Delta M$  time series of periods A to D for periods in spring (period A), summer (period B), autumn (period C), and winter (period D) was observed.

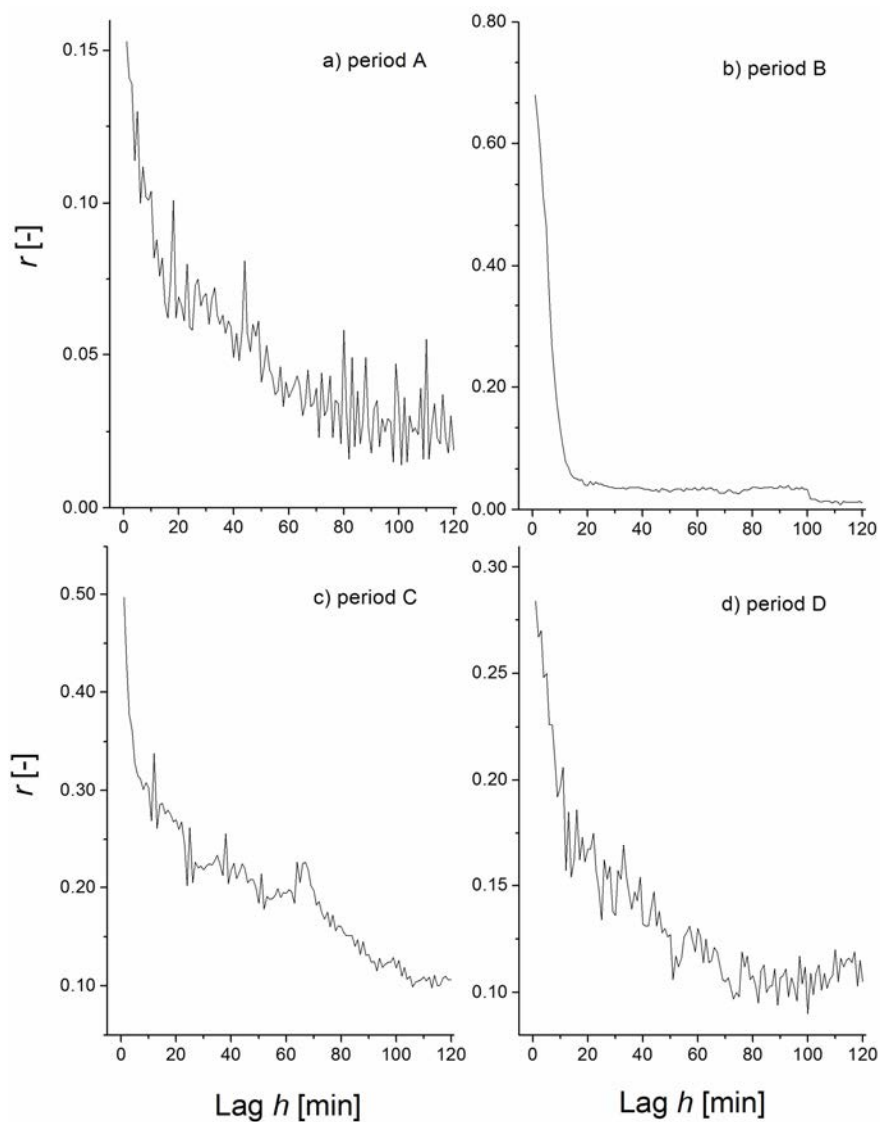


Figure 2.4: Autocorrelation coefficient,  $r$ , as function of time lag,  $h$ , from the analysis of lysimeter data sets (corrected mass changes,  $\Delta M$ ) for the minute-based time lags,  $h$ , over four selected time periods including precipitation events (Fig. 2.3) in spring (A), summer (B), autumn (C), and winter (D) expressed by the autocorrelation coefficient,  $r$ , Eq. 2.3.

## II Autocorrelation analysis of high resolution weighing lysimeter time series as a basis for determination of precipitation

---

Maximum values of the AC coefficient  $r$  ranged between 0.16 in April 2012 (Fig. 2.4a) and 0.68 in summer 2012 (Fig. 2.4b). Due to short but intensive rain events during the summer period (B) with a maximum rain intensity of  $P_{Stat} = 22.2 \text{ mm}\cdot\text{h}^{-1}$  (Table 2.4), a temporal autocorrelation of  $\Delta M$  was high at small time lags, dropped quickly and disappeared already at lags of 10 to 20 min (Fig. 2.4b).

*Table 2.4: Measured weather station data  $P_{Stat}$  (maximum rain intensity, total amount of rain) for the selected precipitation time periods used in the autocorrelation analysis of periods in spring (A, April), summer (B, July/August), autumn (C, November), winter (D, January) and for periods E (May) and F (November); time periods correspond to Figure 2.2.*

Period	max. rain intensity		total amount
	hourly / $\text{mm d}^{-1}$	daily / $\text{mm d}^{-1}$	/ mm
A	79.2	6.5	16.9
B	532.8	24.2	82.2
C	33.6	4.2	15.3
D	62.4	4.6	7.5
E	0	0	0
F	0	0	0

In contrast, temporal autocorrelation for periods A and C was lower at small time lags and dropped more delayed until the AC signal disappeared at time lags around 60 to 80 min. The temporal AC of  $\Delta M$  in spring (A) and autumn periods (C) was significant for larger time lags reflecting the longer-lasting rainfall events with small rain intensity compared to period B (c.f., Fig. 2.4 and Table 2.4). In general for high total  $P$ -amounts (period B) higher autocorrelation coefficients were observed compared to periods of rather low amounts of precipitation as in spring (period A) or as in the winter period, D (c.f., Fig. 2.4 and Table 2.4). In contrast to periods A to D, the periods E and F (Fig. 2.5a and 2.5b) did not include precipitation events. Here, the autocorrelation analysis of  $\Delta M$  time series of both periods revealed no drop for AC coefficients at small time lags as compared to the periods A to D. The signal of AC was more or less constant with time scattering around an average line of AC coefficients nearly zero (approx. 0.06 for period E and 0.08 for period F). Overall, the temporal autocorrelation in  $\Delta M$  time series was not affected by the correction of weighing data due to short term plant biomass changes; the AC coefficients varied between corrected and uncorrected time series' only at the fourth position after decimal point at a maximum for periods with highest plant biomass increases (July; data not shown).

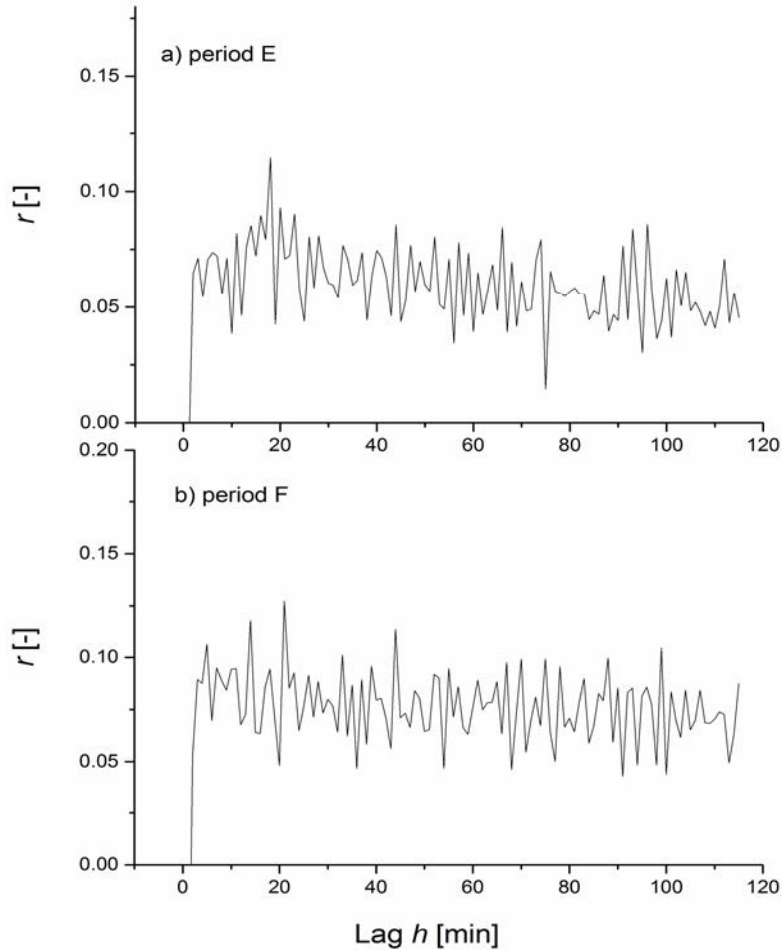


Figure 2.5: Autocorrelation coefficient,  $r$ , as function of time lag,  $h$ , from the analysis of lysimeter data sets (corrected mass changes,  $\Delta M$ ) for the minute-based time lags,  $h$ , over rain-free periods E and F (period E, solid curve; period F, dashed curve).

A transformation of  $r$  in normalized autocorrelation coefficients  $r^*$  was applied to compare AC results of the four seasons with respect of the autocorrelation lengths. Therefore, values of  $r$  for periods A to D was defined by  $r^* = +1$  for the maximum (total correlation) and values of  $r$  by  $r^* = 0$  for the minimum (no autocorrelation). The temporal autocorrelation in  $\Delta M$  time series was significant for approximately one hour (Fig. 2.6), except for periods characterized by summer storm events (period B). Determined autocorrelation lengths ranged between 22 and 76 minute-based time lags (Table 2.3). In contrast to A, C, and D, in period B including summer storms and precipitation rates of  $P_{Stat}$  up to  $22.2 \text{ mm}\cdot\text{h}^{-1}$  autocorrelation was observed well below 60 min-based time lags; the  $\lambda$  and  $a$  values were 22 lags and 2.1 (Table 2.3), respectively.

## II Autocorrelation analysis of high resolution weighing lysimeter time series as a basis for determination of precipitation

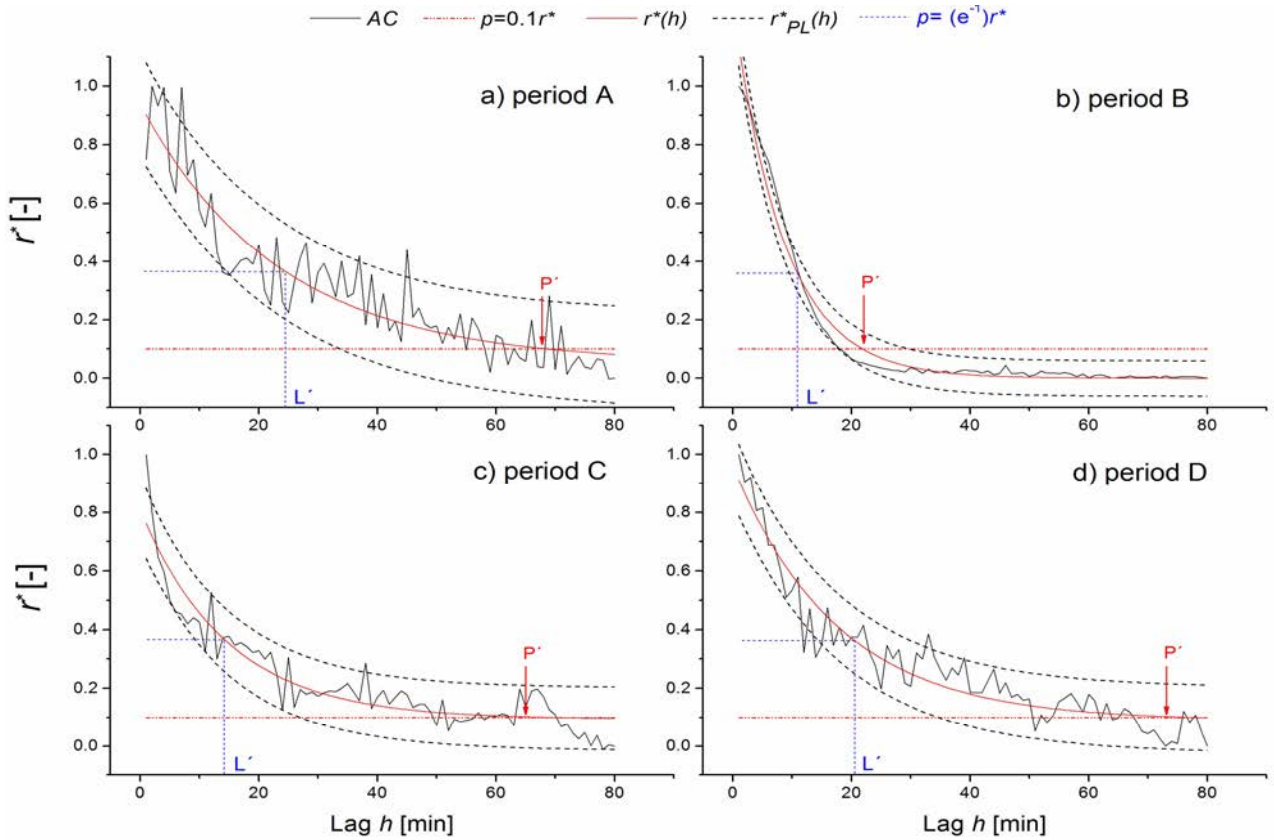


Figure 2.6: Temporal autocorrelation of lysimeter-derived precipitation data for selected time periods (Figure 2.2) in spring (A), Summer (B), autumn (C), and Winter (D); here in form of the normalized autocorrelation coefficient,  $r^*$ , as a function of the time lag  $h$  (min). The exponential fit  $r^*(h)$  [Eq. 2.11] (red curves) and the intersection point  $P'$  for  $p = (0.1)r^*$  were used to determine the range of autocorrelation length  $\lambda$ , and the intersection point  $L'$  to determine the range of the autocorrelation length  $\lambda_D$ ; black dashed lines denote the 90 % prediction limits,  $r^*_{pL}(h)$ .

### 2.3.2 Daily precipitation using autocorrelation-based filtering

Results of  $P$  calculations from  $\Delta M^*$  time series showed that precipitation increased or decreased depending on the selected time intervals over which high resolution lysimeter data was integrated (Table 2.5). For periods of April and July in 2012 (Fig. 2.3), monthly precipitation values calculated from 1-min time series' of  $\Delta M^*$  differed between time intervals up to 17 % for lysimeter data (Table 2.5). Precipitation obtained from time intervals of  $t_N = 60, 30,$  and  $10$  minutes varied between lysimeters  $L_1$  to  $L_6$  of about 1.7 to 5.6 % for April and of about 6.1 to 7.5 % for July. In general, values of  $P_{Lys}$  were smaller if calculated over a longer time interval (Table 2.5) because positive and negative fluctuations in  $\Delta M$  cancelled each other out. In particular short-ranged precipitation events ( $< 1 \text{ mm} \cdot \text{d}^{-1}$ ) of time intervals of  $t_N = 10$  min were

II Autocorrelation analysis of high resolution weighing lysimeter time series as a basis for determination of precipitation

*Table 2.5: Cumulative precipitation of  $\Delta M^*$  lysimeter time series  $P_{Lys}$  of two data sets (July 2012; April 2012) of six lysimeters  $L_1$  to  $L_6$  on the basis of daily mean values; mean values of  $P_{Lys}$  ( $L_1$ - $L_6$ ) and standard deviation (in parenthesis).  $\Delta P$  are the differences between the weather station (Dedelow) reference precipitation  $P_{Stat}$  (April, 38.7 mm; July, 169 mm) and lysimeter data based precipitation  $P_{Lys}$ .*

Period	Interval	$P_{Lys}$						Mean (SD)	$\Delta P$
		$L_1$	$L_2$	$L_3$	$L_4$	$L_5$	$L_6$		
/ month	/ min	/ mm month <sup>-1</sup>							
April	60	47.1	47.0	46.6	46.6	47.1	46.3	46.8 (0.3)	8.1
	30	49.1	49.4	48.8	48.6	49.2	48.4	48.9 (0.3)	10.2
	10	56.1	59.1	57.4	56.6	56.3	55.7	56.9 (1.1)	18.2
July	60	192.1	183.7	189.6	187.3	180.5*	184.2	186.2 (3.6)	17.2
	30	197.8	188.4	194.4	192.0	183.8*	192.8	191.5 (4.1)	22.5
	10	207.8	194.5	203.1	200.4	194.3*	202.4	200.4 (4.4)	31.4

\* Missing data resulting from technical problems of the leachate scale (July 13<sup>th</sup> 2012 to July 24<sup>th</sup> 2012)

cancelled out when data was integrated by a higher values of  $t_N$  (Fig. 2.7). Noise reduction by applying a moving average on the original data sets, did not remove all deviations between the cumulative  $P$ -values of the three time intervals (Table 2.5; Fig. 2.7), but reduced them to a lower level. The cumulative precipitation of  $\Delta M^*$  lysimeter time series' without biomass correction revealed a small increase in mean  $P$  values of about 0.4 mm (April) and 0.7 (July, Table 6).

*Table 2.6: Cumulative precipitation of  $\Delta M^*$  lysimeter time series  $P_{Lys}$  of two data sets (July 2012; April 2012) of six lysimeters  $L_1$  to  $L_6$  on the basis of daily mean values with and without biomass correction; mean values of  $P_{Lys}$  ( $L_1$ - $L_6$ ) and standard deviation (in parenthesis), the time interval  $t_N$  was 60 min.*

Period	Biomass correction	$P_{Lys}$						Mean (SD)
		$L_1$	$L_2$	$L_3$	$L_4$	$L_5$	$L_6$	
/ month		/ mm month <sup>-1</sup>						
April	yes	47.1	47.0	46.6	46.6	47.1	46.3	46.8 (0.3)
	no	47.4	47.4	47.0	47.1	47.4	46.7	47.2 (0.3)
July	yes	192.1	183.7	189.6	187.3	180.5	184.2	186.2 (3.6)
	no	192.7	184.3	190.6	188.0	180.7	184.9	186.9 (4.1)

## II Autocorrelation analysis of high resolution weighing lysimeter time series as a basis for determination of precipitation

The comparison of summed up precipitation values  $P_{Lys}$  and  $P_{Stat}$  showed that the time interval  $t_N = 60$  min reduced divergences in quantified  $P$  at a minimum; the deviations ranged from 9.9 to 17.3 % for the data set. The calculated sums of precipitation using 60 min time intervals from  $\Delta M^*$  lysimeter time series demonstrated differences in a range from 8.1 to 17.2 mm in comparison to the  $P_{Stat}$  measured with rain gauge measurements at monthly rates (Table 2.5). Results of the *ED* and *RMSE* analysis of time intervals of 60, 30, and 10 minutes confirmed the smallest deviations between the two precipitation measurements, for  $t_N = 60$  min, followed by  $t_N = 30$  min and  $t_N = 10$  min for periods of April and July (Table 2.7).

*Table 2.7: Euclidian distance (ED) and root mean square error (RMSE) of two data sets (July 2012; April 2012) between the reference precipitation ( $P_{Stat}$ ) and the lysimeter L\_1-L\_6 data based precipitation  $P_{Lys}$  on the basis of daily mean values; the higher the value of L\_1-L\_6 the greater the differences in the ED and RSME between  $P_{Stat}$  and  $P_{Lys}$*

Period	Interval	Lysimeters											
		L_1		L_2		L_3		L_4		L_5		L_6	
		ED	RMSE	ED	RMSE	ED	RMSE	ED	RMSE	ED	RMSE	ED	RMSE
/ month	/ min	/ mm											
April	60	3.5	0.3	3.5	0.3	3.2	0.3	2.5	0.3	3.6	0.3	3.4	0.3
	30	4.5	0.6	4.8	0.6	4.4	0.5	3.8	0.5	5.0	0.7	4.6	0.6
	10	9.9	3.1	12.0	4.4	10.4	3.4	9.9	3.3	11.1	3.9	10.2	3.3
July	60	11.8	5.0	8.9	2.7	12.3	5.0	13.0	5.4	13.1	5.1	8.6	2.4
	30	12.5	5.6	9.2	2.9	12.7	5.3	13.4	5.6	13.8	5.2	9.3	2.8
	10	18.6	12.6	13.3	6.1	16.5	9.2	16.9	9.2	19.5	9.5	16.1	8.2
April	60	2.8	0.3	2.7	0.3	2.7	0.3	2.9	0.3	2.6	0.2	2.6	0.2
	30	4.3	0.3	3.7	0.3	4.3	0.3	2.9	0.4	4.4	0.3	4.6	0.3
	10	5.4	0.6	5.2	0.6	5.1	0.6	5.2	0.6	5.5	0.6	5.3	0.5
July	60	12.0	4.8	9.0	2.7	11.9	4.7	12.6	4.9	12.7	5.1	8.6	2.5
	30	12.5	5.2	9.4	2.9	12.3	5.0	12.9	5.5	12.4	5.2	9.6	3.1
	10	13.3	5.9	10.1	3.4	12.9	5.5	13.3	5.9	12.8	5.4	10.5	3.7

The cumulative precipitation over the periods April and July from the two approaches used here,  $P_{Syncro}$  based on the processing scheme of *Hannes et al. (2015)* and  $P_{Lys}$ , differed in average between 0.1 mm and 2.6 mm, respectively (Table 2.8). These differences were in a single-digit percentage area of monthly mean values of about 0.2 % and 1.4 % based on differences in data processing. In correspondence to  $P_{Lys}$ , precipitation values using the filtering scheme of *Hannes et al. (2015)* showed larger differences to the reference precipitation  $P_{Stat}$  (Table 2.8). Similar to  $P_{Lys}$ , deviations in the precipitation values  $P_{Syncro}$  and  $P_{Stat}$  were 17.1 % for April and 11.1 % for July.



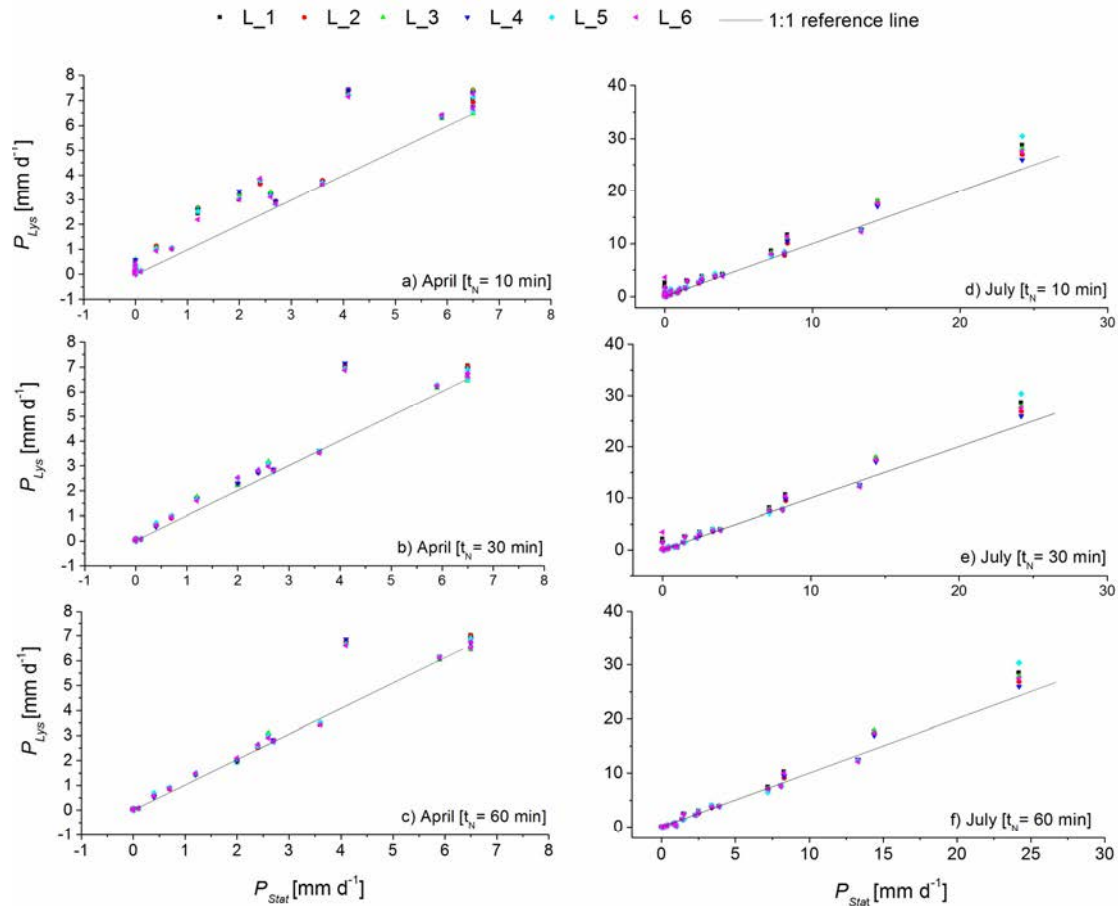


Figure 2.7: Comparison of daily rain gauge  $P_{Stat}$  data and daily  $P_{Lys}$  data (in  $\text{mm d}^{-1}$ ) based on three time intervals ( $t_N = 10, 30,$  and  $60$  min) according to the AC analysis for the periods of April (2012) and July (2012). Note that the scale of the precipitation axes for April (figures left) is different from the scale for July (figures at the right side).

### 2.3.3 Daily evapotranspiration after autocorrelation-based filtering

Similar to results of  $P$  calculations from  $\Delta M$  time series, evapotranspiration  $ET_{Lys}$  decreased if calculated over a longer time interval (Table 2.9). Values of  $ET_{Lys}$  of time intervals of  $t_N = 60, 30,$  and  $10$  min varied between lysimeters  $L_1$  to  $L_6$  from  $67.7$  to  $79.8 \text{ mm month}^{-1}$  for April and from  $126.9$  to  $141.3 \text{ mm month}^{-1}$  for July. The cumulative actual evapotranspiration determined from lysimeter data for  $t_N = 60$  min were lower for April and higher for July as compared to the reference evapotranspiration  $ET_0$  (April:  $71.9 \text{ mm}$ ; July:  $110.9 \text{ mm}$ ; cf. Table 2.9).

## II Autocorrelation analysis of high resolution weighing lysimeter time series as a basis for determination of precipitation

*Table 2.9: Cumulative evapotranspiration of  $\Delta M^*$  lysimeter time series  $ET_{Lys}$  of two data sets (April 2012; July 2012) of six lysimeters  $L_1$  to  $L_6$  on the basis of daily mean values; mean values of  $ET_{Lys}$  ( $L_1$ - $L_6$ ) and standard deviation (in parenthesis). The cultivated crops were winter rye (April) and Sudangrass (July). For comparison, the reference evapotranspiration  $ET_0$  was in the same time period 71.9 mm (April) and 110.9 mm (July).*

Period	Interval	$ET_{Lys}$						Mean (SD)
		$L_1$	$L_2$	$L_3$	$L_4$	$L_5$	$L_6$	
/ month	/ min	/ mm month <sup>-1</sup>						
April	60	68.9	73.3	68.2	74.6	66.5	66.5	69.7 (3.2)
	30	70.9	75.6	70.4	76.6	68.6	68.6	71.8 (3.2)
	10	78.0	84.4	79.0	85.5	75.7	75.9	79.8 (3.9)
July	60	124.5	113.8	133.3	118.6	147.3*	124.1	126.9 (10.9)
	30	130.2	118.4	138.2	123.2	150.8*	132.5	132.2 (10.5)
	10	140.5	124.8	147.2	131.8	161.3*	142.3	141.5 (11.5)

\* Missing data resulting from technical problems of the leachate scale (July 13<sup>th</sup> 2012 to July 24<sup>th</sup> 2012)

## 2.4. Discussion

### 2.4.1 Possible explanations for temporal autocorrelation

The AC analysis showed a similar decrease of autocorrelation coefficients in  $\Delta M$  time series' between periods A to D reflecting its recurring precipitation signal (Fig. 2.4). Temporal autocorrelation in time series' of lysimeter weighing data indicated temporal (seasonal occurrences) and intensity dependencies of the AC coefficients for precipitation events, respectively (periods A to D; Fig. 2.5). Results suggested that the AC lengths depend on the impact, but also on the temporal distribution of rain intensity and length of rain-free periods (Table 2.1). The hypothesized impact of  $P$  on induced autocorrelation in weighing data of lysimeters was based on reported temporal autocorrelation of precipitation time series of rain gauge measurements (Kotz and Neumann, 1959; Mirza et al. (1998) Kantelhardt et al. (2006). Thus, the temporal distribution of precipitation in lysimeter time series seemed to be not random (Fig. 2.4); the decrease of autocorrelation in Fig. 2.4 corresponds to the exponential decay of the AC coefficient for hourly rain gauge data reported by Rakovec et al. (2012). Time periods without changes in the lysimeter weight due to precipitation events supported this assumption; here, for rain-free periods no temporal autocorrelation could be found in lysimeter time series (cf. Fig. 2.5a and 2.5b). Only weighing time series' with mass changes induced by precipitation confirmed temporal autocorrelation in lysimeter data (Fig. 2.4 and 2.6) as reported for time series of rain gauges earlier (e.g., Kotz and Neumann,

1959). Results suggested when temporal autocorrelation occurred in lysimeter time series (cf. Fig. 2.4), the calculated  $P$  scattered stronger for periods with high  $AC$ -coefficients (cf., April and July; Fig. 2.7).

We applied lengths of autocorrelation for determining optimal time intervals for precipitation, however, temporally uncorrelated time intervals may be also an issue in other lysimeter related studies; e.g. filtering procedures (Peters et al., 2014, Hannes et al., 2015). Data noise removal in lysimeter time series would not replace observations of autocorrelation, because smoothing procedures only reduced data errors induced by e.g. vibrations due to wind even for moderate or low conditions and tillage management or lysimeter mass changes due to animals, not the autocorrelation in the lysimeter weighing data. Peters et al. (2014) reported that the AWAT-filter was influenced by the maximum window widths; the latter is defined as the time length over which signal strength and data noise was collected. Peters et al. (2014) observed lowest filtering errors and most reliable results for 31 to 61 minutes time intervals for the window width selection. This time window was in a range of our presented autocorrelation lengths determined for data of the four seasons. Analysis of autocorrelation could be a reproducible method to define window widths for the AWAT filter, which was previously derived by empirically analyzing benchmark events.

### *2.4.2 Comparison between the lysimeter based precipitation and with rain gauge measurements*

Results suggested that cumulative precipitation values based on lysimeter data were higher as compared to weather station reference precipitation for selected time periods; the reasons for the difference between lysimeter  $P_{Lys}$  and measured  $P_{Stat}$  values could be explainable by interception and wetting of rain drops from the collector walls (Yang et al., 1999) and the wind turbulences blowing the rain drops (or snowflakes) away from the rain gauge funnel of rain gauges installed at 1 m above the ground surface (Sevruk et al., 1989). Results suggested that short time intervals of < 30 min often overestimated  $P$ -values (cf. Fig. 2.7, Table 2.5), since differences in the cumulative precipitation increased with time intervals from  $\Delta M^*$  lysimeter time series from 8.1 to 18.2 mm and 17.2 to 31.4 mm in comparison to the  $P_{Stat}$  measured with rain gauge for monthly rates (cf.,  $P_{Lys}$  and  $P_{Stat}$ ; Table 2.5). The reason for the assumed overestimation of precipitation using lower time intervals was based on the separation process of positive ( $P$ ) and negative ( $ET$ ) mass changes (Eq. 2.7 and 2.8) as proposed by Young et al. (1996) and the weighing oscillations within the temporal autocorrelation; in the small time intervals shorter than the autocorrelation length, e.g. 10 min, the weighing oscillations (noise) producing short-term negative and positive mass

## II Autocorrelation analysis of high resolution weighing lysimeter time series as a basis for determination of precipitation

changes in  $\Delta M$  time series did not cancel out. Hannes et al. (2015) also observed for the synchro filter an overestimation of precipitation because of the noise error for small averaging timer intervals; averaging times below 20 min led to a strong increase of the noise error, while for higher averaging times the noise error decreased. Also, if the mass increases due to plant biomass would not be considered for agricultural used lysimeters, results suggested that  $P$ -values are slightly overestimated for a long-term period (Table 2.6); here, the biomass increase in weighing data represent an input into the lysimeter assumed as precipitation.

Compared to the total amount of precipitation, differences between lysimeter based  $P_{Lys}$  values ( $t_N=60$  min) and  $P_{Stat}$  of about 9.9 to 17.3 % were similar to those reported by Gebler et al. (2013), which found differences of about 13.6 % for monthly rates (May, 2012). In contrast, Fank (2013) observed smaller differences between lysimeter based  $P_{Lys}$  values and  $P_{Stat}$  of about 1.9 % for monthly rates (May, 2012); for the period from 2011, June to 2012, August precipitation values differed of about 2.2 %.

The variety of 0.6 to 1.5 % in cumulative mean precipitation between lysimeters L\_1 to L\_6, found here for April 2012 ( $46.8 \pm 0.3$  mm; Table 2.8) and July 2012 ( $187.4 \pm 2.9$  mm; Table 2.8), was similar to the variety of about 2 % between cumulative precipitation found by Hannes et al. (2015) for 18 lysimeters of the same building type.

*Table 2.8: Comparison of cumulative hourly precipitation using the processing scheme of Hannes et al. (2015;  $P_{Synchro}$ ) consisting of five separately filtering steps and the autocorrelation based processing scheme for  $P_{Lys}$  of two data sets (July 2012, 31 days; April 2012, 30 days);  $\Delta P$  are the differences between the weather station (Dedelow) reference precipitation  $P_{Stat}$  (April, 38.7 mm; July, 169 mm) and lysimeter data based precipitation  $P_{Synchro}$  and  $P_{Lys}$ .*

Period	Precipitation	Lysimeter						Mean (SD)	$\Delta P$
		L_1	L_2	L_3	L_4	L_5	L_6		
/month		/ mm month <sup>-1</sup>							
April	$P_{Lys}$	47.1	47.0	46.6	46.6	47.1	46.3	46.8 (0.3)	8.1
	$P_{Synchro}$	46.5	46.8	46.7	46.6	47.1	46.2	46.7 (0.3)	8
July	$P_{Lys}$	192.1	183.7	189.6	187.3	180.5*	184.2	187.4 (2.9)	18.6
	$P_{Synchro}$	193.6	186.9	192.9	189.3	196.7*	187.2	190.0 (2.8)	21.0

\* Missing data resulting from technical problems of the leachate scale (July 13<sup>th</sup> 2012 to July 24<sup>th</sup> 2012); not considered for mean value and  $\Delta P$  calculation

The author discussed differences in precipitation the different between lysimeters in the hexagon constructions by filtering uncertainties, unfiltered influences on the different lysimeters or the natural heterogeneity in the precipitation. Also, systematic deviations between the lysimeters L1-L6 can cause the variety in cumulative mean precipitation. These systematic deviations were among others differences in biomass production, which was supposed as the reason for residual deviations between lysimeters in quantified  $P_{Lys}$ . We assume that differences in biomass production was leading to differences in the mass and structure of the above-ground biomass, which in turn affected the interception of rainfall and led to increasing differences in measured precipitation between the lysimeters during the vegetation period. The interception losses of rainfall water by the above ground biomass was probably different between lysimeters L\_1 to L\_6 due to the contrasting surface of the plants (Muzylo et al., 2009) inferred by the different lysimeter biomass production (Table 2.1). However, deviations in  $P$  between the lysimeters were relatively small as compared to the total precipitation (Table 2.5) when using the proposed precipitation calculation procedure that considers the temporal autocorrelation of the high-resolution weighing lysimeter data.

### 2.4.3 Filtering effect on evapotranspiration rates

The separation of all positive mass changes as  $P_{Lys}$  and all negative mass changes as  $ET_{Lys}$  in the calculation process implied the assumption that no or only negligible amounts of evapotranspiration occurred during precipitation events. If times intervals of  $t_N = 60\text{min}$  were used, lengths of autocorrelation (Table 2.3) induced by mass changes in lysimeter weighing data due to precipitation suggested that only a short time period include both components:  $P_{Lys}$  and  $ET_{Lys}$  over one year. Hence, an underestimation of  $P_{Lys}$  due to negative mass changes of  $ET_{Lys}$  could only be expected for summer storm events with short and intensive precipitations of approx. 30 min. (cf. Figure 2.4). In that case, however, quantitative effects of  $ET_{Lys}$  on amounts of  $P_{Lys}$  were supposed as rather low, because the expected minute-based changes in lysimeter weighing data due to evapotranspiration was relatively small in comparison to mass increases of a single precipitation event; for the period B with the highest plant growth and a short temporal AC length, the maximal hourly  $ET$ -rates were  $1\text{ mm h}^{-1}$  ( $< 0.2\text{ mm (10min)}^{-1}$ ) – the average hourly  $ET$ -rates were only  $< 0.2\text{ mm h}^{-1}$  (data not shown).

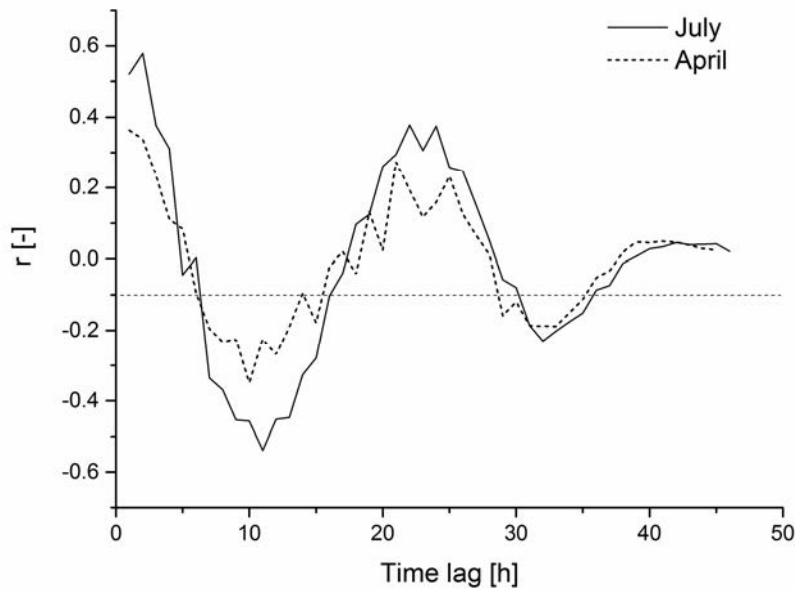


Figure 2.8: Autocorrelation coefficient,  $r$ , as function of time lag,  $h$ , from the analysis of lysimeter data sets (corrected mass changes,  $\Delta M$ ) for the hourly-based time lags,  $h$ , over two rain-free periods in April and July 2012. Each period comprises 2 days (48 h), starting from 12 pm (April: 8<sup>th</sup> to 10<sup>th</sup>; July: 19<sup>th</sup> to 21<sup>th</sup>).

The AC analysis of minute-based lysimeter time series revealed that autocorrelation did not appear in rain free periods where only mass changes due to evaporation and transpiration were assumed (Fig. 2.5). Though, the analysis of autocorrelation from hourly-based time lags of  $h$  (Fig. 2.8) indicated that  $\Delta M$  time series also include autocorrelation due to evapotranspiration, however, in a different temporal resolution as compared to precipitation events. Here, the autocorrelation coefficients in hourly-based  $\Delta M$  time series of the lysimeter reflected the diurnal cycles of  $ET_{Lys}$  between day and night.

Due to the separation of all positive mass changes as  $P$  and all negative mass changes as  $ET$  in the calculation process, the time interval selection of  $P_{Lys}$  and  $ET_{Lys}$  cannot be separated and calculations of the actual  $ET$  were applied in the same temporal resolution as the calculations for  $P$ -values. The differences in  $ET_{Lys}$  between the different lysimeter was comparatively higher (10.9 % for April; 14.6 % for July) as compared for precipitation values (Table 2.5). Here, differences in plant growth might be more important for  $ET$ -rates as compared to the assumed plant surface effect on amounts of  $P_{Lys}$ . The resulting standard deviation of about 4.8 % (April) and 7.8 % (July) of the total amount of  $ET_{Lys}$  for the two months were similar to the variability in  $ET$  (6.5 %) reported by Hannes *et al.* (2015).

## 2.5. Conclusions

High precision weighing lysimeters have been suggested as alternative technique for the measurement of precipitation. In this study, the temporal autocorrelation in the 1-min time-series' of lysimeter mass changes was analyzed. The lengths of temporal autocorrelation were tested as parameter to determine the minimal temporal resolution for the quantification of precipitation with precision weighing lysimeters.

The oscillations of the lysimeters mass changes induced by forces exerted by e.g. raindrops and/or wind disappeared because over- and undershooting of mass changes cancelled out. Results revealed that autocorrelation lengths varied according to the seasonal rainfall characteristics over one year. Our autocorrelation analysis suggested that during summer with a few storms followed by longer rain-free periods, oscillations with relatively large amplitudes are relatively short-lived. For the other seasons, autocorrelation characteristics reflected smaller rain intensities but more frequent and longer lasting rain events and shorter rain-free periods.

The cumulative values from time intervals larger than the AC length (e.g., 60 min) provide a most reliable approximation of the quantity of  $P$  on the expense of a reduced temporal resolution. Generally higher near-surface rainfall measured with weighing lysimeters as compared to rain gauge data confirmed results of previous lysimeter studies that showed the same direction in  $P$  differences between both measuring procedures.

The results suggested that the temporal resolution of precipitation data from the weighing lysimeters was restricted by the autocorrelation length of the underlying mass change time series'. The length of the correlated time period differed between the seasons and seemed to depend on the rainfall characteristics. A smoothing of the high resolution lysimeter data could reduce the noise in the original data; however, it could not remove validity problems caused by temporally auto-correlated data, nor could it suggest a "fictitiously" high temporal resolution of lysimeter-based data. The comparison of results obtained with and without smoothing (e.g., synchro-filter) suggested that both methods would approach the same amount of rainfall when increasing the integration time span. Thus, the techniques for lysimeter data noise removal should be complemented by a proper time series analysis.

## *Acknowledgements*

The study is a part of the TERENO-SoilCan project and supported by the infrastructure of the Terrestrial Environmental Observatory (TERENO-Northeast) of the Helmholtz Association ([http://teodoor.icg.kfa-juelich.de/observatories/GL\\_Observatory](http://teodoor.icg.kfa-juelich.de/observatories/GL_Observatory)). The TERENO-SoilCan lysimeters are operated by the Leibniz-Centre for Agricultural Landscape Research (ZALF) Müncheberg. The authors thank Jörg Haase and Gernot Verch from the Research Station Dedelow of the ZALF for providing biomass data and for maintenance and operation of the lysimeters.

## *References*

- Aldridge, R. (1976): The measurement of rainfall at ground level. *J. Hydrol.* 15, 35-40.
- Fank, J. (2013): Wasserbilanzauswertung aus Präzisionslysimeterdaten. 15. Gumpensteiner Lysimetertagung 2013, 85-92.
- Fekete, B. M., Vörösmarty, C. J., Roads, J. O., and Willmott, C. J. (2004): Uncertainties in precipitation and their impacts on runoff estimates. *J. Climate* 17, 294-304.
- Gebler, S., Hendricks-Franssen, H.-J., Pütz, T., Post, H., Schmid, H. P., and Vereecken, H. (2013): Simultaneous estimation of actual evapotranspiration and precipitation by weighable lysimeters and comparison with eddy covariance and rain gauge measurements. 15. Gumpensteiner Lysimetertagung 2013., 199-202.
- Hannes, M, Wollschläger, U, Schrader, F, Durner, W, Gebler, S, Pütz, T, Fank, J, Unold, G von, and Vogel, H-J (2015): High-resolution estimation of the water balance components from high-precision lysimeters. *Hydrol. Earth Syst. Sci. Discuss.* 12, 569-608.
- Kalbitz, K., Solinger, S., Park, J.W., Michalzik, B., and Matzner, E. (2000): Controls on the dynamics of dissolved organic matter in soils: A Review. *Soil Sci.* 165, 277-304.
- Kampf, Stephanie K, and Burges, Stephen J (2010): Quantifying the water balance in a planar hillslope plot: Effects of measurement errors on flow prediction. *J. Hydrol.* 380, 191-202.
- Kantelhardt, J. W., Koscielny-Bunde, E., Rybski, D., Braun, P., Bunde, A., and Havlin, S. (2006): Long-term persistence and multifractality of precipitation and river runoff records. *J. Geophys. Res. Atmos.* 111.
- Kotz, S., and Neumann, J. (1959): Autocorrelation in precipitation amounts. *J. Atmos. Sci.* 16, 683-686.



Legendre, P. (1993): Spatial autocorrelation: trouble or new paradigm? *Ecology* 74, 1659-1673.

Matalas, N. (1963): Autocorrelation of Rainfall and Streamflow Minimums. *Statistical studies in hydrology, Geological Survey. Professional Paper 434*, 14.

Meißner, R., Prasad, M.N.V., Du Laing, G., and Rinklebe, J. (2010): lysimeter application for measuring the water and solute fluxes with high precision. *Curr. Sci. India*. 99, 601.

Meissner, R., Seeger, J., Rupp, H., Seyfarth, M., and Borg, H. (2007): Measurement of dew, fog, and rime with a high-precision gravitation lysimeter. *J. Plant Nutr. Soil Sci.* 170, 335-344.

Mekonnen, GB, Matula, S, Doležal, F, and Fišák, J (2015): Adjustment to rainfall measurement undercatch with a tipping-bucket rain gauge using ground-level manual gauges. *Meteorol. Atmos. Phys.* 127, 241-256.

Mirza, MQ, Warrick, RA, Ericksen, NJ, and Kenny, GJ (1998): Trends and persistence in precipitation in the Ganges, Brahmaputra and Meghna river basins. *Hydrol. Sci. J.* 43, 845-858.

Muzylo, A, Llorens, P, Valente, F, Keizer, JJ, Domingo, F, and Gash, JHC (2009): A review of rainfall interception modelling. *J. Hydrol.* 370, 191-206.

Nearing, M.A., Jetten, V., Baffaut, C., Cerdan, O., Couturier, A., Hernandez, M., Le Bissonnais, Y., Nichols, M.H., Nunes, J.P., and Renschler, C.S. (2005): Modeling response of soil erosion and runoff to changes in precipitation and cover. *Catena* 61, 131-154.

Neff, E. (1978): How much rain does a rain gauge gauge. *Agric. Res.* 27, 213-220.

Nespor, V., and Sevruk, B. (1999): Estimation of wind-induced error of rainfall gauge measurements using a numerical simulation. *J. Atmos. Oceanic Technol.* 16, 450-464.

Nielsen, D. R., and Wendroth, O. (2003): *Spatial and temporal statistics: sampling field soils and their vegetation.* Catena Verlag, Reiskirchen, Germany. p. 398.

Nolz, R., Kammerer, G., and Cepuder, P. (2013): Improving interpretation of lysimeter weighing data *Bodenkultur [ZDB]* 64, 27-32.

Nolz, R., Kammerer, G., and Cepuder, P. (2013): Interpretation of lysimeter weighing data affected by wind. *J. Plant Nutr. Soil Sci.* 176, 200-208.

Peters, A. , Nehls, T., Schonsky, H., and Wessolek, G. (2014): Separating precipitation and evapotranspiration from noise - a new filter routine for high resolution lysimeter data. *Hydrol. Earth Syst. Sci. Discuss.* 18, 1189-1198.

Pütz, T., Kiese, R., Wollschläger, U., Groh, J., Rupp, H., Zacharias, S., Priesack, E., Gerke, H. H., Papen, H., Borg, E., Bens, O., Kaiser, K., Herbrich, M., Munch, J.-C., Sommer, M., Vanderborght, J., and Vereecken, H. (2016): TERENO-SOILCan a Lysimeter-Network in Germany Observing Soil Functions Influenced by Climate Change. *Environ. Earth Sci.*; in press.

Rakovec, O., Hazenberg, P., Torfs, P.J.J.F., Weerts, A.H., and Uijlenhoet, R. (2012): Generating spatial precipitation ensembles: impact of temporal correlation structure. *Hydrol. Earth Syst. Sci. Discuss.* 16, 3419-3434.

Rieckh, H., Gerke, H. H., and Sommer, M. (2014): Water and Dissolved Carbon Fluxes in an Eroding Soil Landscape Depending on Terrain Position Vadose Zone J. 13.

Schrader, F., Durner, W., Fank, J., Gebler, S., Pütz, T., Hannes, M., and Wollschläger, U. (2013): Estimating precipitation and actual evapotranspiration from precision lysimeter measurements. *Procedia Environ. Sci.* 19, 543-552.

Sevruk, B. (1996): Adjustment of tipping-bucket precipitation gauge measurements. *Atmos. Res.* 42, 237-246.

Sevruk, B., Hertig, J.-A., and Spiess, R. (1989): Wind field deformation above precipitation gauge orifices. *Int. Ass. Hydrol. Sci. Publ* 179, 65-70.

Sommer, M., Gerke, H. H., and Deumlich, D. (2008): Modelling soil landscape genesis - A "time split" approach for hummocky agricultural landscapes. *Geoderma* 145, 480-493.

Strangeways, I. C. (1996): Back to basics: The 'met. enclosure': Part 2(b) — Raingauges, their errors. *Weather* 51, 298-303.

Unold, G., and Fank, J. (2008): Modular Design of Field Lysimeters for Specific Application Needs. *Water Air Soil Pollut.* 8, 233-242.

Vaughan, P. J., and Ayars, J. E. (2009): Noise Reduction Methods for Weighing Lysimeters. *J. Irrig. Drain. Eng.* 135, 235-240.

Vaughan, P. J., Trout, T. J., and Ayars, J. E. (2007): A processing method for weighing lysimeter data and comparison to micrometeorological ETo predictions. *Agric. Water Manage.* 88, 141-146.

Verch, G. (2014): Weather Data, Dedelow, Germany, Leibniz-Zentrum für Agrarlandschaftsforschung (ZALF) e.V. - online available under [e.g. <http://dx.doi.org/10.4228/ZALF.2000.242>].

Wolf, F. (1999): Berechnung von Information und Komplexität in Zeitreihen - Analyse des Wasserhaushaltes von bewaldeten Einzugsgebieten. Dissertation, available under [<http://www.dr-frank-wolf.de/diss/dissde.pdf>], online 21.07.2014.

Xiao, H., Meissner, R., Seeger, J., Rupp, H., and Borg, H. (2009): Effect of vegetation type and growth stage on dewfall, determined with high precision weighing lysimeters at a site in northern Germany. *J. Hydrol.* 377, 43-49.

Yang, D. Q., Ishida, S., Goodison, B. E., and Gunther, T. (1999): Bias correction of daily precipitation measurements for Greenland. *J. Geophys. Res. Atmos.* 104, 6171-6181.

Young, M. H., Wierenga, P. J. , and Mancino, C. F. (1996): Large Weighing Lysimeters for Water Use and Deep Percolation Studies. *Soil Science* 7, 491-501.

Yue, S., Pilon, P., Phinney, B., and Cavadias, G. (2002): The influence of autocorrelation on the ability to detect trend in hydrological series. *Hydrol. Process.* 16, 1807-1829.

### 3| Water balance and leaching of dissolved organic and inorganic carbon of eroded Luvisols using high precision weighing lysimeters

## *Abstract*

Erosion can be observed in many arable soil landscapes such as those of the hummocky ground moraine. The topsoil removal by water erosion in combination with tillage operations (e.g., ploughing) is leading to truncated soil profiles along slopes with reduced solum thickness and modified properties of soil horizons. The objectives were to identify and quantify effects of erosion-induced soil modifications on the water balance and the leaching of dissolved organic and inorganic carbon (DOC, DIC), considering complex soil-crop interactions. The idea was to compare lysimeter-based water and solute balances of eroded Luvisols that differed in solum depth. The six high precision weighing lysimeters (1.0 m<sup>2</sup> surface, 1.5 m high; UMS Science-Lysimeter) had a resolution of 10 g (= 0.01 mm). The cylindrical steel rings of the lysimeters were filled with undisturbed soil monoliths from two fields. Lysimeter soils were cultivated with maize, winter rye, Sudangrass, triticale, alfalfa, and Persian clover during the observation period April 2011 to March 2014. Cumulative drainage of the six lysimeter soils ranged from 57 for the least to 104 mm y<sup>-1</sup> for the most eroded Luvisols; the differences of about 83 % indicated that the erosional profile modifications in combination with differences in crop development affected the water balance components. Soil-crop interactions depending on properties of differently-truncated soil profiles caused varying amounts of precipitation and evapotranspiration for the 3-years. Since lysimeter effluent concentrations of DOC (5 ± 0.5 mg·L<sup>-1</sup>) and DIC (62 ± 5 mg·L<sup>-1</sup>) were relatively constant in time, the DOC and DIC leaching was mainly controlled by the water fluxes. Thus, the leaching rates ranged from 0.3 (Luvisol) to 0.5 g m<sup>-2</sup>·yr<sup>-1</sup> (eroded Luvisol) for DOC and 3.3 (Luvisol) to 7.1 g m<sup>-2</sup>·yr<sup>-1</sup> (eroded Luvisol) for DIC. Because of the complex soil crop interactions, a clear relation between erosion-induced soil profile modification and the water balance and DOC and DIC leaching could not be identified. Nevertheless, when transferring lysimeter results to the arable soil landscape the erosion-induced modifications even within the same pedogenetic soil type should be considered.

### 3.1 Introduction

The water balance and its components are of fundamental interest because they affect the distribution of vegetation (Stephenson, 1990), crop yield (Ritchie, 1998) or carbon and nutrient releases (Bauhus and Barthel, 1995; Jandl et al., 2007). The relation between soils and their landscape position has been recognized for decades (e.g., Jenny, 1961; McCaig, 1985; Pennock, 2003). Spatial varying soil properties relative to their landscape position (e.g., Manning et al., 2001) can affect not only water balance components (Woods et al., 2013), but also the redistribution of solutes (Afyuni et al., 1994). The water and solute movement in heterogeneous landscapes depends on soil hydraulic properties that are subject to horizon specific pedological changes over time and space (Lin, 2011). This was observed for soil horizons of erosion-affected profiles of the hummocky landscape where soil hydraulic properties depended on erosion-induced soil profile modifications (Rieckh et al., 2012; 2014). Similarly, as a consequence of different tillage practices, soil hydraulic properties of pedogenetic identical soil horizons were not necessarily identical (e.g., Buczko et al., 2006). According to Woods et al. (2013), the components of the soil water balance in the hummocky landscape of southern Saskatchewan could significantly change due to the spatial heterogeneity of soils and thicknesses of soil horizons in different landscape positions.

The hummocky post glacial soil landscape is characterized by a three-dimensional continuum of soil types that developed from glacial till as the parent material (Sommer et al., 2008). Soils evolved that are taxonomically and functionally different basically due to varying intensities of erosion due to water and tillage (i.e., soil uplift and movement during tillage operations; Van Oost et al., 2006). Tillage erosion often occurs in combination with water erosion during surface runoff when soil gets lost from convexities and accumulates in concavities (Govers et al., 1999). Erosion rates by tillage operations are usually highest in shoulder and upper slopes while the largest soil removal by water erosion occurred in the mid to lower slope positions. During the tillage process, soil material of the first 0.3 m depths is captured and mixed. When the depth of the plough horizon (Ap) is reduced by the loss of surface soil due to water and tillage erosion, soil material of deeper horizons is incorporated into the Ap-horizon at the next tillage operations; The combined effect of the loss of surface soil and tillage operations (ploughing with deep-cutting plows) is leading to a gradual truncation of soil profiles at convex slope positions with time (e.g., Kosmas et al., 2001). In addition, the topsoil-incorporation of material from deeper horizons can influence soil hydraulic properties (Rieckh et al., 2012). Also the vertical sequence of soil horizons can be truncated by soil erosion (Gerke and Hierold, 2012) thus profile modifications are reflecting the history and intensity of soil erosion at a particular landscape position.

Soil types in the post glacial soil landscape are represented by fully developed Luvisols in plateau positions, more-or-less eroded Luvisols according to an erosion gradient starting from a flat upper- to a flat mid-slope, and Calcaric Regosols in expose landscape positions; and eroded topsoil material that accumulate in the topographic depressions and toe slopes formed Colluvic Regosols (Gerke et al., 2010). The relationships observed between landscape positions and soil properties such as soil horizon thickness and depth to carbonates (Manning et al., 2001) has been used to predict the magnitude of water and solute fluxes in the eroded, hummocky soil landscape (Thibodeau et al., 2007). Soils at upper slope positions tend to be less susceptible for leaching as compared to soils at lower slope positions (King et al., 1983). For truncated soil profiles Renger M. (1968) and Große and Renger (1974) observed differences in the infiltration and vertical downward water movement of rain water from topsoil to deeper soil horizons. Woods et al. (2013) identified the soil water fluxes at the upper boundary affected by the surface topography as the main factor responsible for the spatial and temporal variability of long-term soil water and solute fluxes. Also, the depth of the ground water level could be a main factor influencing the direction and magnitude of dissolved carbon fluxes of eroded soils in the hummocky soil landscape (Rieckh et al., 2014).

While meteorological studies tried to quantify the water vapor flux from the soil surface to the atmosphere (e.g., Baldocchi et al., 1996), a large number of soil-related studies aimed at quantifying the soil water balance by using a combination of modeling and measuring either in the field or by laboratory experiments (e.g., Gerke et al., 2016; Rieckh et al., 2014; Soldevilla-Martinez et al., 2014). For quantitative analyses, weighing lysimeters could provide highly resolved time series of mass changes (e.g., Unold and Fank, 2008). While in the past lysimeters were used for studying crop evapotranspiration, drainage, and recharge (e.g., Liu et al., 2002) and solute leaching (e.g., Meissner et al., 1995), the high temporal resolution of the present lysimeter technique enabled to determine individual water balance components, such as precipitation and evapotranspiration (Hannes et al., 2015; Peters et al., 2014) or even rime and dew (Meissner et al., 2007; Xiao et al., 2009), from lysimeter data when separately measuring mass changes and outflow.

The overall effect of erosion-induced soil profile modifications on the field and landscape scale water and dissolved carbon balances is widely unknown. This is due to methodological problems in the determination of the water fluxes and dissolved carbon leaching rates that are related to such relatively small pedological differences caused by profile modifications when considering the complexity involved, e.g. due to feedbacks between soil water movement, storage changes, and root water uptake. In this study, we assumed that changes in soil hydraulic properties caused by the erosion-induced truncation of soil profiles created

### III Water balance and leaching of dissolved organic and inorganic carbon of eroded Luvisols using high precision weighing lysimeters

---

differences in the water balance and leaching of dissolved organic (DOC) and inorganic carbon (DIC), which could possibly be quantified with data from high resolution weighing lysimeters filled with undisturbed soil monoliths of the same classified soil type (Luvisols).

The objectives were i) to analyze time series of lysimeter mass changes for more or less eroded Luvisols under arable use including biomass growth of cultivated crops, ii) to relate water balance components and agricultural crop yield with erosion-induced soil profile modifications, and iii) to quantify leaching rates of DIC/DOC for the differently eroded Luvisols. For this study, the data from six lysimeters were used that belonged to the Terrestrial Environmental Observatories (*TERENO*) project within the so called “SoilCan” framework (Pütz et al., 2016).



## 3.2 Methods

### 3.2.1 Study site and lysimeter design

The weighing lysimeters (1.5 m height; 1.13 m in diameter) with a soil surface area of 1.0 m<sup>2</sup> were installed on ground surface level at the Experimental Field Station Dedelow (53°22'2.45"N, 13°48'10.91"W) of the Leibniz-Centre for Agricultural Landscape Research (ZALF) located near the city of Prenzlau, North-east Germany. For the 20-years period (1992 – 2012) average annual values of rainfall (485 mm), potential evapotranspiration (633 mm), and air temperature (8.6 °C) were reported in Rieckh et al. (2014). For the actual period (2011 - 2014), precipitation was 635 mm (2011), 538 mm (2012), 446 mm (2013), 561 mm (2014) and the annual mean air temperature at 2 m above soil surface was 7.9°C (2012), 8.0°C (2013), 9.3°C (2014). The region was characterized by a potential evapotranspiration rate of 677 mm (2012), 690 mm (2013), 672 mm (2014, until October). Metrological data were recorded directly at the ZALF station Dedelow (Verch, 2014).

The lysimeter hexagon with six individual lysimeters (Unold and Fank, 2008) was constructed by the company UMS GmbH (Munich, Germany). Each cylindrical lysimeter had two scales with an accuracy of 10 g (or 0.01 mm), one for determining the lysimeter mass and the other for measuring the leachate outflow at the bottom. Instruments for measuring soil water content, matric potential, soil temperature and suction cups for soil water extraction were installed at 0.1 m, 0.3 m, 0.5 m and 1.4 m depths (Table 3.1). Pressure boundary conditions at the bottom of the lysimeters were controlled by reference matric potentials measured with tensiometers that were installed in the intact field soil next to the lysimeter hexagon. Through the suction cup rake in 140 cm depth, soil water could either be extracted by applying a suction and stored in the outflow storage tank or water from the storage tank could be injected back into the lysimeter by applying a pressure.

*Table 3.1: The instrumentation of the lysimeters with probes and sensors and installation depths [m].*

Parameter	Type	Units	Depth [m]
Tensiometer	TS-1	hPa	0.3 / 0.5/ 1.4
Matrix potential sensors	MPS-1	hPa	0.1
TDR probes	TDR 100	vol %	0.1 / 0.3 / 0.5
Temperature sensors	Thermistor	°C	0.3 / 0.5/ 1.4
Heat flux sensors	HFP1	W m <sup>-2</sup>	0.1
CO <sub>2</sub> gas sensors	MSH-P/CO2/NC	ppm	0.1
Suction cups	SIC20	ml h <sup>-1</sup>	0.1 / 0.3 / 0.5/ 1.4

### III Water balance and leaching of dissolved organic and inorganic carbon of eroded Luvisols using high precision weighing lysimeters

The soil types of the monoliths used in this study from two field sites Holzendorf (Hd) and Dedelow (Dd) were classified as Luvisols according to the FAO classification scheme world reference base for soil resources (IUSS, 2006). The Hd site was located about 2 km from the Dd experimental field site of the research station such that similar climatic conditions could be assumed for 2012 to 2014. However, the two fields differed in the previous soil tillage and crop management. The differently eroded Luvisols varied in soil depths to the carbonate-containing marly parent material (C-horizon) and the clay illuviation horizon (Bt); note that the E-horizon (clay eluviation) was absent at the more truncated soil profiles (Table 3.2).

*Table 3.2a: Soil characteristics of Haplic Luvisols Dd\_1-Hd\_6 from Dedelow (Dd) and Holzendorf (Hd); solum denotes the depths of the C-horizon; dry bulk density,  $\rho_b$ ; coarse particles, >2 mm; sand, 2.0 – 0.063 mm; silt, 0.063 – 0.002 mm; clay, <0.002 mm; saturated hydraulic conductivity,  $K_s$ ; soil organic carbon, SOC.*

soil	depth [m]	horizon [-]	solum [m]	$\rho_b$ [g·cm <sup>-3</sup> ]	$K_s$ [cm·d <sup>-1</sup> ]	>2 mm [g·kg <sup>-1</sup> ]	sand [g·kg <sup>-1</sup> ]	silt [g·kg <sup>-1</sup> ]	clay [g·kg <sup>-1</sup> ]	SOC [g·kg <sup>-1</sup> ]
Dd_1	0-0.3	Ap	-	1.53	443	24	538	305	157	7.5
	0.3-0.42	E+Bt	-	1.65	180	18	510	341	149	4.4
	0.42-0.8	Bt	-	1.52	278	41	507	299	194	3.5
	0.8-1.5	elCv	0.8	1.69	112	58	589	293	118	<0.1
Dd_3	0-0.35	Ap	-	1.48	244	37	475	374	147	7.5
	0.35-0.7	Bt	-	1.50	71	43	n.d.	n.d.	n.d.	n.d.
	0.70-1.15	elCv	0.7	1.51	63	19	n.d.	n.d.	n.d.	n.d.
Dd_5	0-0.3	Ap	-	1.57	617	34	468	395	158	7.5
	0.3-0.65	Bt	-	1.59	2657	27	n.d.	n.d.	n.d.	n.d.
	0.65-1.15	elCcv	0.65	1.69	20	35	n.d.	n.d.	n.d.	n.d.
Hd_2	0-0.28	Ap	-	1.66	455	40	501	395	104	7.8
	0.28-0.5	E	-	1.73	72	21	n.d.	n.d.	n.d.	n.d.
	0.5-0.8	Bt	-	1.62	15	16	n.d.	n.d.	n.d.	n.d.
	0.8-1.4	elCcv	0.8	1.74	216	29	n.d.	n.d.	n.d.	n.d.
Hd_4	0-0.3	Ap	-	1.58	95	24	576	313	111	7.4
	0.3-0.5	E+Bt	-	1.62	32	16	n.d.	n.d.	n.d.	n.d.
	0.5-0.78	Bt	-	1.66	334	25	n.d.	n.d.	n.d.	n.d.
	0.78-1.4	elCcv	0.78	1.74	108	35	n.d.	n.d.	n.d.	n.d.
Hd_6	0-0.29	Ap	-	1.60	540	24	622	312	66	6.2
	0.29-0.55	E	-	1.65	38	26	584	310	106	2.2
	0.55-0.85	Bt1	-	1.67	822	22	497	368	135	2.1
	0.85-1.15	Bt2	-	1.62	105	23	450	324	226	1.8
	1.15-1.5	elCcv	1.15	1.73	46	34	477	373	150	1.2

Overall six intact and undisturbed soil monoliths were extracted, three from each site. The soil monoliths of each field were taken closely to each other and the pedogenic horizons were continuously developed in lateral direction over that distance. All three are located within a horizontal distance of 15m (Hd) and 21m (Dd), respectively, and numbered as Dd\_1, Hd\_2, Dd\_3, Hd\_4, Dd\_5, and Hd\_6 and denoted by Dd\_1 – Hd\_6. The selection of the soil

monoliths that were representative for the hummocky soil landscape was based on prior field studies (Sommer et al., 2008; Deumlich et al., 2010). Additional information on the sampling locations can be found in Figure A1 and Tables A1 and A2 in the appendix.

*Table 3.2b: Soil characteristics of the Haplic Luvisols from Dedelow (Dd) and Holzendorf (Hd); mean values of the dry bulk density,  $\rho_b$ , and the saturated hydraulic conductivity,  $K_s$ , and the standard deviation in italic; number of replicates ( $n=3$ ) except for the E+Bt horizon of Dd ( $n=1$ ) and the Bt horizon of Hd ( $n=4$ ).*

soil	horizon [-]	$\rho_b$ [g·cm <sup>-3</sup> ]		$K_s$ [cm·d <sup>-1</sup> ]	
Dd_site	Ap	1.53	<i>0.04</i>	435	<i>154</i>
	E+Bt	1.65	-	180	-
	Bt	1.54	<i>0.04</i>	1002	<i>1174</i>
	eIC(c)v	1.63	<i>0.08</i>	65	<i>38</i>
Hd_site	Ap	1.61	<i>0.03</i>	363	<i>193</i>
	E/E+Bt	1.67	<i>0.05</i>	47	<i>18</i>
	Bt	1.64	<i>0.02</i>	319	<i>313</i>
	eICcv	1.74	<i>0.01</i>	123	<i>70</i>

### 3.2.2 Physical and chemical soil properties

Soil physical (Table 3.2) and chemical (Table 3.3) properties of the lysimeter monoliths Dd\_1-Hd\_6 were determined on disturbed soil samples and soil core samples of 100 cm<sup>3</sup> and 250 cm<sup>3</sup> taken from the excavated trench next to the monolith extraction area in October, 2010. The trench was sampled because the monoliths at each site were extracted next to each other and sampling was not possible inside the monoliths. For the subsoil horizons, we assumed that soil texture was not varying along the trenches at each site, thus the same textures were assumed in the three lysimeters of each site (Table 3.2). For the Ap horizons; however, due to the different erosional status of the peda, mixing of different portions of subsurface horizons into the Ap could be assumed. Therefore, textural properties were analyzed for all Ap horizons for Dd\_1-Hd\_6.

III Water balance and leaching of dissolved organic and inorganic carbon  
of eroded Luvisols using high precision weighing lysimeters

*Table 3.3: Soil chemical properties of the Ap horizon of lysimeters from sites Dedelow (Dd) and Holzendorf (Hd); contents of total nitrogen,  $N_t$ ; inorganic carbon,  $C_{CO_3}$ ; soil organic carbon, SOC; plant available phosphate  $P_{DL}$ , potassium  $K_{DL}$  and  $Mg_{CaCl_2}$ ; (DL: double lactate soluble, after 1:50 extraction for 2 hours with 0.02 M calcium lactate and 0.02 M HCl at pH 3.7); mean values of three replicates ( $n=3$ ) and standard deviations ( $\pm$ ).*

Lysimeter	$C_{CO_3}$ [g·kg <sup>-1</sup> ]	SOC [g·kg <sup>-1</sup> ]	$N_t$ [g·kg <sup>-1</sup> ]	pH <sub>CaCl<sub>2</sub></sub> [-]	$K_{DL}$ [mg·100·g <sup>-1</sup> ]	$P_{DL}$ [mg·100g <sup>-1</sup> ]	$Mg_{CaCl_2}$ [mg·100g <sup>-1</sup> ]
Dd_1_3_5	0.1 ± 0.02	7.2 ± 0.03	0.9 ± 0.0	6.5 ± 0.13	13.5 ± 1.9	7.2 ± 0.52	10.0 ± 0.21
Hd_2_4_6	0.1 ± 0.0	6.9 ± 0.72	0.9 ± 0.0	5.1 ± 0.37	4.7 ± 1.01	1.6 ± 0.14	6.6 ± 0.63

Soil texture was determined on disturbed soil samples taken from each horizon at the same trench as the core samples. Mixed samples were sieved to pass a 2-mm sieve. The sand and coarse silt particle-size fractions were determined by wet sieving (DIN-ISO:11464, 2006) after removal of soil organic matter using H<sub>2</sub>O<sub>2</sub>. The particles sizes <0.063 mm were analyzed with the pipette-method according to Köhn (DIN-ISO:11277, 2002; modified see HBU, 2005: 5.1.1.1a). The texture analyses were carried out at the Central Ecological Laboratory of the University of Sustainable Development (HNE) in Eberswalde (located 50 km northeast of Berlin).

Soil bulk density,  $\rho_b$ , was determined on 100 cm<sup>2</sup> soil core samples by drying at 105°C for >24 hours (Blake and Hartge, 1986). Soil organic carbon (SOC) was obtained by subtracting the amount of inorganic carbon ( $C_{CO_3}$ ) from that of the total carbon ( $C_t$ ). The content of  $C_{CO_3}$  was analyzed with an analytical gas-chromatographic procedure using H<sub>3</sub>PO<sub>4</sub>. For determining  $C_t$ , the soil samples were combusted at 1250 °C via an oxygen stream and the oxidized products determined with an elemental analyzer (DIN-ISO:10694, 1996). Plant available nutrients (Table 3.3)  $P_{DL}$  and  $K_{DL}$  (subscript DL denotes “Double-Lactat”, calcium lactate soluble), and  $Mg_{CaCl_2}$  (calcium chloride soluble) were determined using an adsorption photometer AT200 (Beckman-Coulter, Olympus) and an Atomic Absorption Spectrometer AAS-iCE3300 (Thermo-Fisher-Scientific; Waltham, USA), respectively. The saturated hydraulic conductivity,  $K_s$ , was determined with a laboratory permeameter (Eijkelkamp, Giesbeek, The Netherlands) using 250 cm<sup>3</sup> the constant pressure head method (Klute and Dirksen, 1986).

### 3.2.3 Cropping periods and biomass analyses

Lysimeters were embedded within a larger field approx. 2.3 ha in size, which had the same crop sequence and was managed (spraying and fertilization) as similarly as possible to the lysimeters. The soil tillage operations were carried out manually each year. The fertilizer applications for 2011 – 2014 are listed in the appendix (Table A2). The lysimeters were first cropped with maize (*Zea Mayze L.*), then with winter rye (*Secale cereal L.*), Sudangrass (*Sorghum sudanense*), triticale (*Triticosecale*), alfalfa (*Medicago sativa*) and with Persian clover (*Trifolium resupinatum*) (Table A3 in the appendix). Fresh biomass yields were determined for main crops (maize, Sudangrass, winter rye, alfalfa; Table 3.4), while winter cover crops Triticale and Persian clover were not considered due to the negligibly small biomasses.

The crop biomass development was calculated on a daily basis with a logistics growth function using planting and harvesting data including wet biomass of each lysimeter for each year and cropping season as:

$$Biomass(t) = \frac{M_i * M_f}{M_i + (M_f - M_i)e^{(-M_f kt)}} \quad [3.1]$$

where  $t$  is time (d),  $k$  is a logistic growth coefficient (-),  $M_i$  is initial biomass [kg] at the beginning of the growing season and  $M_f$  (kg) the final value of biomass at harvest. From the daily estimates, the minute-based values of above ground biomass  $M_a$  were obtained by a linear interpolation, in which the estimates of  $Biomass(t = \text{day})$  were assumed to represent the values of  $M_a(t = \text{min})$  at the end of the day (i.e., time 24:00). The coefficient  $k$  in Eq. 3.1 was calibrated for each crop according to wet above ground biomass data,  $M_f$  and  $M_i$ , of each lysimeter measured at the two harvest times each year (i.e., May and Sept). Fresh above-ground biomass was gravimetrically determined with the scale QS16000B (Sartorius AG, Göttingen, Germany) for maize, winter rye, Sudangrass and alfalfa at harvest (Table A3). The dry mass was determined after drying at 60°C for >24h according to Jörg Haase from the ZALF- Experimental Station Dedelow (personal communication, March, 23<sup>th</sup>, 2014).

III Water balance and leaching of dissolved organic and inorganic carbon  
of eroded Luvisols using high precision weighing lysimeters

Table 3.4: Fresh biomass yield [kg] harvested from the six 1 m<sup>2</sup>-sized lysimeters; the crop rotation consisted of maize (*Zea Mays*, L.) grown from April to October 2011, winter rye (*Secale cereal* L.) from September 2011 to May 2012), Sudangrass (*Sorghum sudanense*) from May to September 2012, triticale (*xTriticosecale*) from October 2012 to March 2013, alfalfa (*Medicago sativa* L.) from March to November 2013; water use efficiency (WUE, [kg m<sup>-3</sup>]), calculated for fresh mass (FM) and dry mass (DM), standard deviation in parenthesis; letters a and b indicate significant differences between mean biomass of Dd and Hd site.

Lysimeter		Maize <sup>†</sup> kg	Winter Rye <sup>†</sup> kg	Sudangrass <sup>†</sup> kg	Alfalfa <sup>†</sup> kg	Total mass <sup>†</sup> kg
Biomass yield	Dd_1	8.1	2.5	5.7	2.7	19.0
	Dd_3	8.6	2.9	8.1	2.9	22.5
	Dd_5	7.5	2.5	7.9	2.5	20.4
	Hd_2	6.0	3.3	4.8	1.9	16.0
	Hd_4	5.9	4.1	5.2	2.6	17.6
	Hd_6	6.3	3.7	5.4	2.7	18.1
	Mean (SD) Dd	8.1 <sup>a</sup> (0.4)	2.6 <sup>a</sup> (0.2)	7.2 <sup>a</sup> (1.1)	2.7 <sup>a</sup> (0.2)	20.6 <sup>a</sup> (1.4)
	Mean (SD) Hd	6.1 <sup>b</sup> (0.2)	3.7 <sup>b</sup> (0.3)	5.1 <sup>b</sup> (0.3)	2.4 <sup>a</sup> (0.4)	17.3 <sup>b</sup> (0.9)
	Total mean	7.1 (0.1)	3.2 (0.6)	6.2 (1.3)	2.6 (0.3)	19.0 (1.7)
WUE <sub>FM</sub> / WUE <sub>DM</sub>	Dd_1	14.6 / 6.7	11.5 / 2.2	13.8 / 4.4	6.8 / 1.7	-
	Dd_3	16.1 / 6.4	12.7 / 2.3	18.0 / 5.6	6.4 / 1.6	-
	Dd_5	15.1 / 6.1	11.8 / 2.0	17.1 / 5.2	6.1 / 1.6	-
	Hd_2	12.0 / 4.7	14.2 / 2.5	12.6 / 3.4	5.3 / 1.3	-
	Hd_4	12.1 / 4.6	16.9 / 3.0	14.3 / 4.6	6.2 / 1.6	-
	Hd_6	12.3 / 5.2	17.4 / 2.8	12.6 / 4.1	7.1 / 1.8	-
	Mean Dd	15.3 / 6.4	12.0 / 2.2	16.3 / 5.1	6.4 / 1.6	-
	Mean Hd	12.1 / 4.8	16.1 / 2.8	13.2 / 4.0	6.2 / 1.6	-
	Total mean	13.7 / 5.6	14.1 / 2.5	14.7 / 4.6	6.3 / 1.6	-

For lysimeters Dd\_1-Hd\_6, the values of  $k$  ranged from 0.123 (alfalfa) to 0.011 (maize). The mass increase of the plant roots, representing the below ground biomass,  $M_b$ , was estimated from  $M_a$  by assuming a shoot/root ratio of 0.25 for maize (Amos and Walters, 2006; Kuchenbuch et al., 2008), 0.5 for alfalfa (Bray, 1963), 0.3 for Sudangrass (Ali et al., 2009; Promkhambut et al., 2010), and 0.22 for winter rye (Bray, 1963). For each lysimeter, the minute-based sum of above- and below-ground biomass was considered as  $M_{plant} = M_a + M_b$ . The crop biomass was not considered for quantification of lysimeter mass changes for triticale in 2012 and Persian clover in 2014, because of negligibly-small plant growth.

The water use efficiency,  $WUE$  (Eq. 3.2), a ratio of *Biomass* with accumulation to consumed water, expressed as the total aboveground crop biomass to the rate of evapotranspiration (Sinclair et al., 1984), was calculated for each vegetation period as,

$$WUE_l = \frac{M_{a,l}}{ETa_{crop}} \quad [3.2]$$

where  $M_{a,l}$  is the biomass at harvest time with subscript  $l$  for either fresh (FM) or dry (DM) matter, and  $ETa_{crop}$  is the actual evapotranspiration [mm] during the growing season of each crop.

The linear correlation between two variables was measured using the Pearson correlation coefficient,  $R$ ; a value +1 denotes a positive correlation and -1 a negative correlation. The coefficient  $R$  was calculated by using Excel software (Microsoft, Remond, USA).

### 3.2.4 Water balance analyses

Components of the lysimeter water balance could be determined directly from the mass balance equation (Meißner et al., 2010, modified) describing the temporal changes in soil water storage,  $\Delta S$  [mm] and snow cover,  $\Delta SC(t)$  [mm], which is here not separately analysed, as a function of fluxes at the upper and lower boundaries, as:

as:

$$P - ET_a - D = \Delta SC(t) + \Delta S(t) \quad [3.3]$$

with the precipitation,  $P$ , [mm], deep drainage,  $D = D_{out} - D_{in}$  of seepage water injected at the lysimeter bottom,  $D_{in}$ , or water outflow from the lysimeter  $D_{out}$  [mm] and the actual evapotranspiration,  $ET_a$  [mm], which included also the interception loss,  $I$ , from plant and crop residue surfaces that could not be separated from the weighing signal here. The  $D_{in}$  denoted the water influx in the lysimeter soil from the storage tank during upward water movement. The weighing signal (i.e., kg water mass) related to the 1-m<sup>2</sup> lysimeter could be represented in the unit L·m<sup>-2</sup> or mm of water. The term  $\Delta SC$  represented a snow cover. At the present location, snow crusts were formed after self-compaction of the snow. The crust-induced shear forces at the lysimeter surface are a common problem for lysimeter operations during winter (Unold and Fank, 2008). The snow crusts lead to a disregarding of mass changes (e.g., due to new snowfalls) ensuring more or less constant scale values despite new precipitation; later when snow crusts disaggregate, only a single integrated signal of mass changes could be recorded in weighing data for the total snow crust period, which displayed in a sudden rise or fall in the weighing records. The mass change was either positive due to rain- or snowfall or negative due to snow drift. For such periods in 2011 -

2014, a combination of weighing records of lysimeter Dd\_1 and weather station records were used. In most cases, lysimeter Dd\_1 served as a reference for all other lysimeters (2012, December 11<sup>th</sup>; 2013, March 10<sup>th</sup>, 19<sup>th</sup> to 22<sup>th</sup>, 26<sup>th</sup> to 27<sup>th</sup>), because the snow crusting effects were comparably rare in weighing data of Dd\_1 as compared to the other lysimeters; which was caused perhaps by small topography differences between the lysimeters along the hexagon. However, when the weighing records of lysimeter Dd\_1 were also occasionally affected by snow crusts (2012, December 12<sup>th</sup> to 14<sup>th</sup>; 2013, March 23<sup>th</sup> to 25<sup>th</sup>), reference values for precipitation  $P_{Stat}$  were used from a frost-protected (heated) rain gauge of the weather station (FMA 86, Wilh. Lambrecht Company, Göttingen) with an accuracy of 0.1 mm recorded every 10 min.

Rates of  $P_{Lys}$  (Eq. 3.4) and  $ET_a$  (Eq. 3.5) were determined from lysimeter data by corrected mass changes  $\overline{\Delta M_{Lys}}$  for each time step  $i$ . A positive value of  $\overline{\Delta M_{Lys}}$  was assumed to represent mass increase through precipitation as suggested by Young et al. (1996), and *vice versa*, a negative value of  $\overline{\Delta M_{Lys}}$  a mass decrease through evaporation or transpiration. The values of  $P_{Lys}$  and  $ET_a$  of each lysimeter were calculated as cumulative lysimeter mass change for defined times,  $t_N$ , as,

$$P_{Lys} = \sum_{i=0}^N \overline{\Delta M_{Lys}(t_N)} \text{ for } \Delta M^* > 0 \quad [3.4]$$

$$ET_a = \sum_{i=0}^N \overline{\Delta M_{Lys}(t_N)} \text{ for } \Delta M^* < 0 \quad [3.5]$$

The time interval  $t_N = 60$  minutes was used, to consider the autocorrelation lengths of minute-based lysimeter mass time series'. The reference evapotranspiration,  $ET_0$ , was estimated on a daily basis using the FAO Penman-Monteith equation (Eq. 3.6) assuming a hypothetical reference crop height of 0.12 m, a fixed surface resistance of  $70 \text{ s m}^{-1}$  and a constant albedo of 0.23 (Allen et al., 1998),

$$ET_0 = \frac{0.408 s (R_n - G) + \gamma \frac{900}{T+273} v (e_s - e_a)}{s + \gamma (1 + 0.34 v)} \quad [3.6]$$

where  $s$  is the slope of the vapour pressure curve [ $\text{kPa } ^\circ\text{C}^{-1}$ ],  $R_n$  the net radiation at the plant surface [ $\text{MJ m}^{-2} \text{ day}^{-1}$ ],  $\gamma$  is the psychrometric constant [ $\text{kPa } ^\circ\text{C}^{-1}$ ],  $T$  is the mean daily air temperature at 2 m height [ $^\circ\text{C}$ ],  $e_s$  is saturation and  $e_a$  actual vapour pressure [ $\text{kPa}$ ],  $v$  is the wind speed at 2 m height [ $\text{m s}^{-1}$ ] and  $G$  is the soil heat flux density [ $\text{MJ m}^{-2} \text{ day}^{-1}$ ].



### 3.2.5 Dissolved organic and inorganic carbon

Dissolved organic (DOC) and dissolved inorganic (DIC) carbon was determined in soil solution extracted from 0.3 m, 0.5 m, and 1.4 m soil depths (Table 3.1) with SiC silicon carbide cups (SIC20, UMS GmbH, Munich, Germany). These cups had a pore size of approx. 2  $\mu\text{m}$  and a bubbling pressure point at approximately 90 kPa. The dimension of each SIC cup was 20 mm in diameter across a length of up to 60 mm. DIC was determined from soil solution sampled with a headspace-free instrumentation (SF1000 sampling bottles; UMS GmbH, Munich, Germany) to avoid or at least minimize effects caused by degassing of  $\text{CO}_2$  from the extracted soil solution (e.g., Kindler et al. (2011)). Degassing could occur because the atmospheric partial pressure of  $\text{CO}_2$  was usually much lower than that of the soil air. Soil solutions were extracted by applying a continuous suction of 250 hPa using the vacuum controller VS-pro (UMS GmbH, Munich, Germany). A two-week soil solution sampling period was selected depending on the usefulness of the amount of collected soil water volume for the analyses. The sampling interval was enlarged if the extracted volume of water was not sufficient (< 10 ml) for analyzing DOC and DIC.

DOC and DIC concentrations in the soil water samples,  $c$  [ $\text{mg L}^{-1}$ ], were analyzed with a TOC-VCPH analyser with TN-module (Shimadzu Solution for Science, Columbia, Maryland, USA) similar to DIN-EN-1484 (1997). For the DOC measurement, the residual inorganic carbon fractions were removed initially by acidification to  $\text{pH} < 2.5$  by using a hydrochloric acid solution (HCl). The DIC free samples were then oxidized at 680  $^\circ\text{C}$  and  $\text{CO}_2$  released from the organic carbon fraction was determined using the LECO RC612 (Leco Instruments GmbH, Germany). Soil solution samples for DIC analysis were mixed with 25%  $\text{H}_3\text{PO}_4$  and incoming  $\text{CO}_2$  gas was detected by infrared radiation (LECO RC612) in analogy to the measurement of DOC.

For each soil solution sampling interval,  $\Delta t$ , of mostly  $N=14$  days, the leaching rates,  $J$ , of DOC and DIC were calculated (Rieckh et al., 2014) as:

$$J_j(t) = \frac{c_j(t) \sum_{i=1}^{N_j} D_i(t)}{1000} \quad [3.7]$$

where  $J_j$  [ $\text{g m}^{-2} (\text{Nd})^{-1}$ ] is the DOC and DIC flux rate during the  $j$ th sampling interval  $\Delta t$ , and  $D_i = D_{\text{out}} - D_{\text{in}}$  is net daily drainage rate [ $\text{mm d}^{-1}$ ] at the bottom of the lysimeter for the  $i$ th day, cumulated over the days,  $N_j$ .

In some cases, soil solution was not sufficient for carrying out the chemical analyses and gaps in the time series' of concentration data appeared. To close the gaps for the leaching calculations, the last measured value of dissolved carbon concentrations was used until the

first new measured concentration value ended the gap. Calculation procedure for  $J$  was applied to the whole 3-years period except for April to Oct 2011 and July to Oct 2013. In 2011, soil solution could not be extracted from suction cups. Instead, solution was sampled from the lysimeter tank in bi-weekly average intervals. For these periods, the missing lysimeter drainage concentration per interval  $j$ ,  $c_j$ , which caused the changes in the tank concentrations between  $c_{t-1}$  and  $c_t$ , was calculated from the differences in tank concentration between two measurements as:

$$c_j = \frac{c_t * M_{T_t} - c_{t-1} * M_{T_{t-1}}}{M_{T_t} - M_{T_{t-1}}} \quad [3.8]$$

where  $M_{T_t}$  and  $c_t$  are the mass of the water in the outflow tank and DOC or DIC concentration at time  $t$ , respectively;  $M_{T_{t-1}}$  and  $c_{t-1}$  are the respective tank mass and DOC or DIC concentrations at the previous sampling time  $t-1$ .

In 2013, water was injected or pumped into the lysimeter at the bottom of the lysimeters during the vegetation period from July to October to compensate for upward water movement from the subsoil that was eliminated in the lysimeters but took place in the intact soils of the surrounding field. Since in this period only tap water was available after the soil water from the storage tank was emptied, tap water concentrations were used for calculating the solute concentration  $c$  in [Eq. 3.6].

### 3.3 Results

At study sites Dd and Hd, the Luvisols varied in degree of past soil erosion (Table 3.2). The degree of erosion of each soil monolith in the lysimeters Dd\_1-Hd\_6 was indicated by the distance of the C-horizon to the soil surface, the vertical sequence of soil horizons and the thickness of the Bt-horizon. For the eroded Luvisols (Dd\_3), the solum of the truncated profile had a thickness of about 0.65 m, while the solum of the moderately (Hd\_2) and slightly eroded (Hd\_6) Luvisols were 0.8 m and 1.15 m thick, respectively. The erosional truncation of the vertical sequence of soil horizons of eroded profiles was evident by the absent clay eluviation horizon (E-horizon) or by the mixture of E- and Bt-horizon. Also, the thickness of the Bt-horizon ranged from 0.3 to 0.6 m depending on erosion history at the particular slope positions of the soil monoliths.

#### 3.3.1 Water balance components

The water balance of Luvisols calculated by lysimeter time series revealed differences in the weather conditions between the 3-years period (Fig. 3.1). From 2011 to 2013, the mean ratio of annual precipitation to annual evapotranspiration ( $P_{Lys}/ET_a$ ) decreased from  $1.12 \pm 0.05$  (2011) to  $1.03 \pm 0.03$  (2012) and  $0.88 \pm 0.04$  (2013). Especially for 2013, the period of June to October was dominated by water losses from the lysimeters due to ET and relatively low amounts of precipitation for that region (cf. annual precipitation from rain gauge data, section 2.1).

Precipitation rates derived by lysimeter time series' and weather station varied between 15 and 21 % from of 2011 to 2014 (Table 3.5). The determination coefficients ( $R^2=0.98$ ) of both data sets showed that precipitation values derived from lysimeter time series' and weather station data were similarly distributed in time. The cumulative precipitation of lysimeters Dd\_1-Hd\_6 amounted to (mean) 1991 mm  $\pm$  (standard deviation) 56 mm from 2011 to 2014 (Table 3.5). Higher values of cumulative precipitation were observed for Dd soils (Dd\_1,3,5;  $P_{Lys} = 2037$  mm; Hd\_2,4,6;  $P_{Lys} = 1946$  mm). In periods with heavy rainfalls (summer storm events), deviations in measured precipitation between Dd\_1-Hd\_6 of up to 34 mm per day (July, 29<sup>th</sup> in 2011; Dd\_1 = 103 mm, Hd\_6 = 69 mm, not shown) were observed.

Evapotranspiration rates calculated by FAO-Penman-Monteith (Eq. 3.6) as reference and the  $ET_a$  determined by the lysimeters differed by 94 mm yr<sup>-1</sup> at maximum (Table 3.5).  $ET_a$  was highest from April to September for each of the years (Fig. 3.1). Differences in  $ET_a$  between Luvisol lysimeters Dd\_1-Hd\_6 were up to 204 mm in total for the 3-years period from 2011 to 2014 (Table 3.5). The cumulative drainage at the bottom differed for Luvisols Dd\_1-Hd\_6 along the erosion gradient up to 142 mm per 3-years (Fig. 3.2). Drainage was higher for the

more eroded soils (cf. Table 3.5, Dd\_3: 312 mm) as compared to the less eroded Luvisols (Hd\_6: 170 mm). The variation in  $D_{out}$  was 3-times higher for soils of site Hd (63 %) versus Dd (18 %). In 2012, water started to flow into the lysimeter at the bottom by the suction cup rake (Fig. 3.2, period D). Note that water injection at the lysimeter bottom allowed “simulating” or imitating an upward water movement in the lysimeter from soil layers below 1.5 m as in the neighboring intact soil. After the start of water injection, the curves of  $D_{out}$  (solid lines in Fig. 3.2) and of combined drainage and injection  $D_{in}+D_{out}$  (dashed lines in Fig. 3.2) started to deviate. The upward fluxes ranged between 169 mm (Dd\_3) and 33 mm (Hd\_2) (Table 3.5).

III Water balance and leaching of dissolved organic and inorganic carbon  
of eroded Luvisols using high precision weighing lysimeters

*Table 3.5: Water balance components of soils Dd\_1-Hd\_6 for the 3-years period of April 1<sup>st</sup>, 2011 to March 31<sup>th</sup>, 2014. The symbol  $P_{Lys}$  [mm]; denotes precipitation measured with lysimeters and  $P_{Stat}$  [mm] is precipitation measured with rain gauge at the weather station;  $D_{out}$  [mm] is deep drainage [mm];  $D_{in}$  [mm] is water injected at the lysimeter bottom via suction cup rake;  $ET_a$  is actual evapotranspiration [mm], and  $\Delta S$  is the soil water storage change (i.e.,  $\Delta S = P_{Lys} - ET_a - D_{out} + D_{in}$ ) [mm]; the relative fractions F1 to F3 [%] of  $P_{Stat}$  to  $P_{Lys}$  (F1),  $D_{out}$  to  $P_{Lys}$  (F2) and  $ET_a$  to  $(P_{Lys} + D_{in})$  (F3).*

Soil	Year	$P_{Stat}$ [mm]	$ET_0$ [mm]	$P_{Lys}$ [mm]	F1 [%]	$D_{out}$ [mm]	F2 [%]	$D_{in}$ [mm]	$ET_a$ [mm]	F3 [%]	$\Delta S$ [mm]
Dd_1	2011	580.7	647.6	711	82	123.7	17	0	649.4	91	-62.1
	2012	537.6	663.8	690.3	78	54.8	8	31.9	644.2	89	23.2
	2013	446.4	674.9	544.7	82	81.5	15	79.5	632.4	101	-89.7
	2014	75	135.6	79.1	95	3.3	4	0	50.8	64	25.0
	sum	1640	2122	2025	84	263	13	111	1977	93	-104
Dd_3	2011	580.7	647.6	698.8	83	160.7	23	0	622.6	89	-84.5
	2012	537.6	663.8	696.4	77	61.6	9	49.1	699.2	94	-15.3
	2013	446.4	674.9	560.9	80	86	15	119.2	695.7	102	-101.6
	2014	75	135.6	82.5	91	3.3	4	0	53.8	65	25.4
	sum	1640	2122	2039	83	312	15	168	2071	94	-176
Dd_5	2011	580.7	647.6	686.2	85	150.1	22	0	584.8	85	-48.7
	2012	537.6	663.8	704.3	76	66.6 <sup>†</sup>	9	44	706.7	94	-25.0
	2013	446.4	674.9	556.3	80	64.3	12	60.9	636.3	103	-83.4
	2014	75	135.6	87	86	6.8	8	0	56.4	65	24.2
	sum	1640	2122	2034	82	288	14	105	1984	93	-133
Hd_2	2011	580.7	647.6	651.9	89	90.2	14	0	596.1	91	-34.4
	2012	537.6	663.8	663.6	81	62.3	9	10.5	634.9	94	-23.1
	2013	446.4	674.9	545.7	82	58.4	11	22.3	580.7	102	-71.1
	2014	75	135.6	77.1	97	7.6	10	0	59.2	77	10.3
	sum	1640	2122	1938	87	219	11	33	1871	95	-118
Hd_4	2011	580.7	647.6	680.1	85	103.2	15	0	582	86	-5.1
	2012	537.6	663.8	675.6	80	75.3	11	11.2	634.2	92	-22.7
	2013	446.4	674.9	567	79	95.2	17	27.3	646.2	109	-147.1
	2014	75	135.6	81.1	92	3.3	4	0	63.2	78	14.6
	sum	1640	2122	2004	84	277	14	39	1926	94	-160
Hd_6	2011	580.7	647.6	618.5	94	86.2	14	0	593	96	-60.7
	2012	537.6	663.8	661.8	81	49.2	7	23.8	658.5	96	-22.1
	2013	446.4	674.9	542.8	82	34.4	6	34.1	594.6	103	-52.1
	2014	75	135.6	75.9	99	0.1	0	0	56.8	75	19.0
	sum	1640	2122	1899	89	170	9	58	1903	97	-116

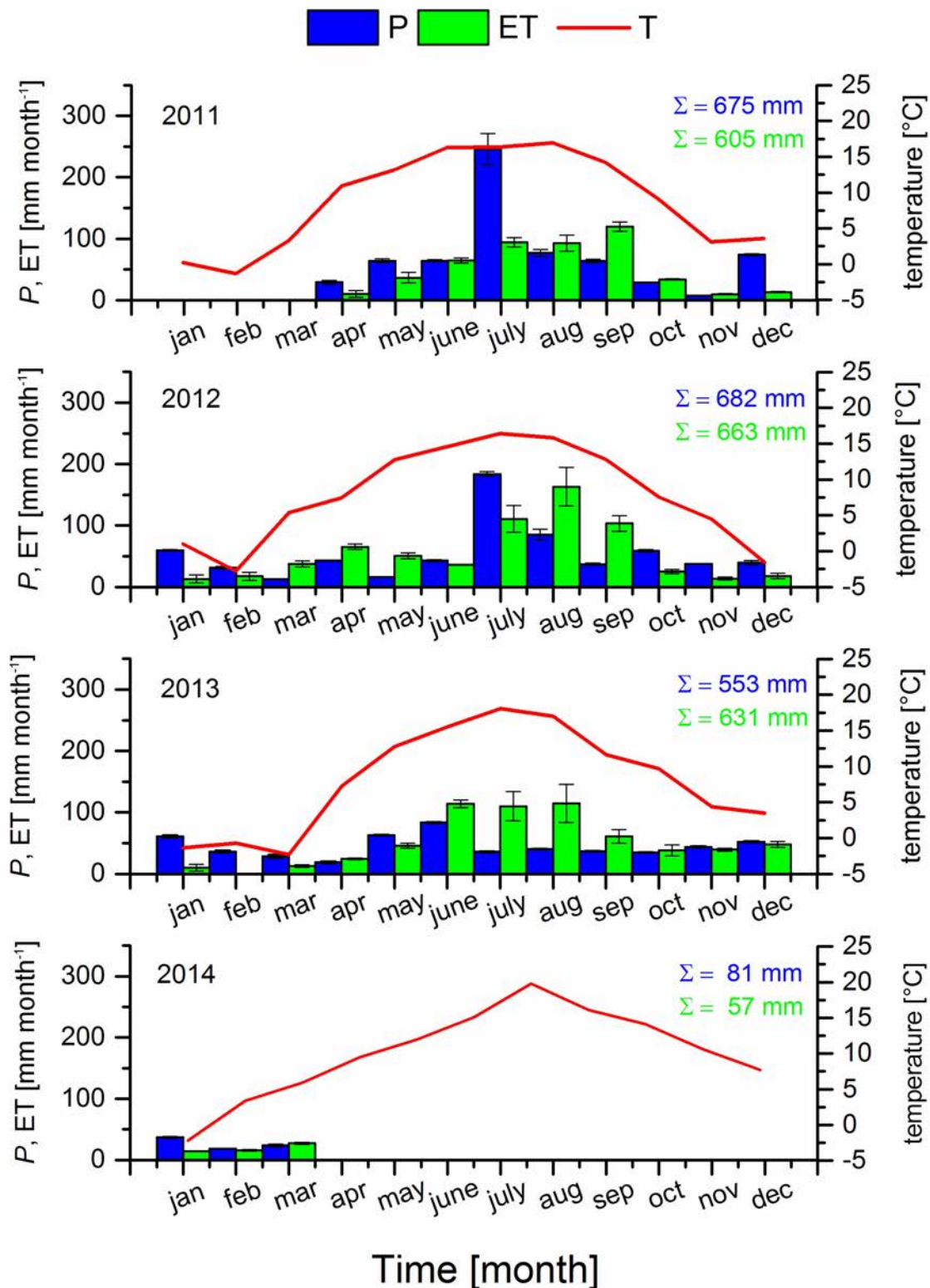


Figure 3.1: Mean values and standard deviation (whisker) of precipitation (P), evapotranspiration (ET) measured by lysimeters Dd\_1-Hd\_6 in 2011, 2012, 2013, and 2014; the air temperature (T) in 2 m above soil surface.

III Water balance and leaching of dissolved organic and inorganic carbon of eroded Luvisols using high precision weighing lysimeters

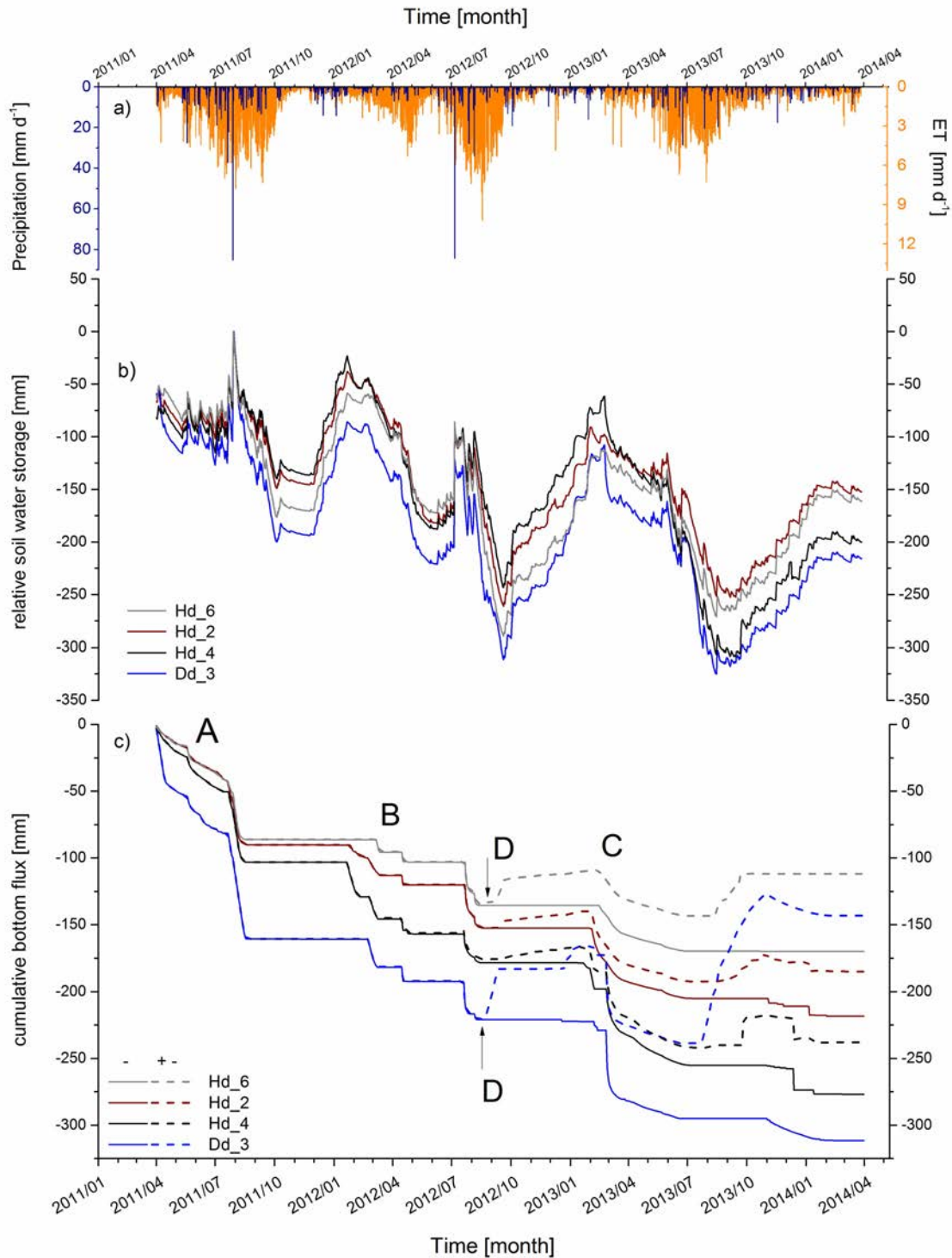


Figure 3.2: Water balance components of four lysimeters with differently eroded soils from Hd and Dd over the period of 3-years for 2011, April to 2014, March; a) precipitation [mm] and evapotranspiration [mm], b) the soil water storage changes [mm] and c) the cumulative seepage water flux [mm] (+ cumulative drainage, +/- cumulative water fluxes of drainage and injection by suction cup rake at the bottom); Note: lysimeter Dd\_1 and Dd\_3 with profiles similar to Dd\_3 were not considered here (see Table 3.5).

### 3.3.2 Dissolved organic and inorganic carbon

Dissolved organic carbon concentrations of soils Dd\_1-Hd\_6 decreased significantly with increasing soil depths (Fig. 3.3). For Ap-horizons three times higher mean concentrations of DOC (Dd site: 13 mg·L<sup>-1</sup>; Hd site: 19 mg·L<sup>-1</sup>) were observed as for Cc-horizons in 1.4 m depth (Dd site: 4 mg·L<sup>-1</sup>; Hd site: 5 mg·L<sup>-1</sup>), but the range of DOC concentrations was smaller for Cc horizons as compared to top soil concentrations. In contrast to DOC, dissolved inorganic carbon was conversely distributed across soil profiles (Fig. 3.4).

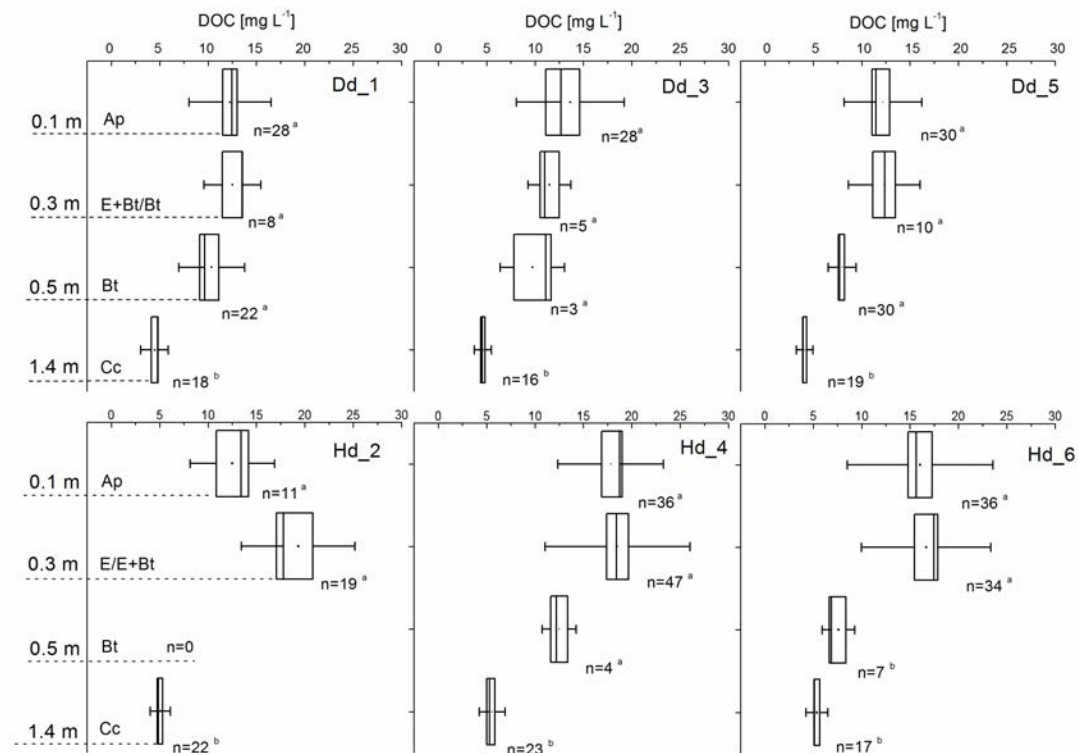


Figure 3.3: Dissolved organic carbon (DOC) concentrations [mg·L<sup>-1</sup>] of soils Dd\_1-Hd\_6 in different depths [cm] from 2011 to 2014; arithmetic mean (plot); standard deviation (whisker); standard error (box); median (line); Note: Significances a-b describes the ANOVA within the soil profile of each lysimeter, while k-l denote the significances between soil horizons (depth 0.1, 0.3, 0.5, 1.4 m); Note that the depth axes are not continuous and cut between 0.5 and 1.4 m.



### III Water balance and leaching of dissolved organic and inorganic carbon of eroded Luvisols using high precision weighing lysimeters

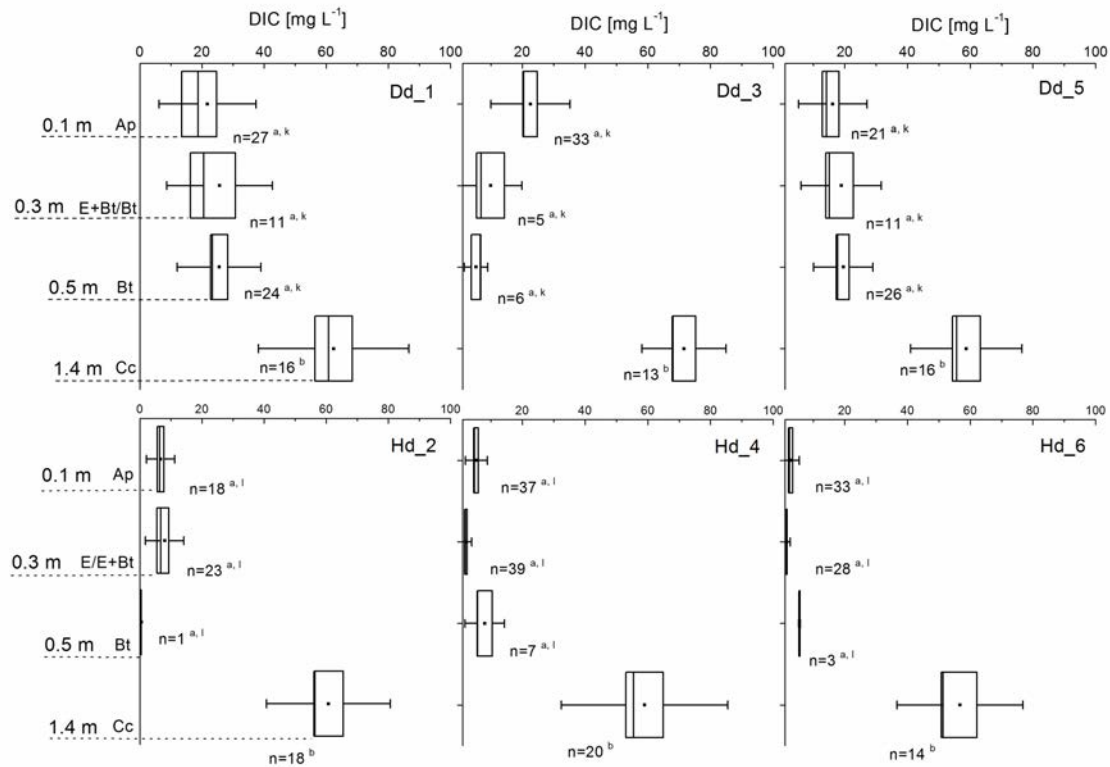


Figure 3.4: Dissolved inorganic carbon (DIC) concentrations [ $\text{mg}\cdot\text{L}^{-1}$ ] of soils Dd\_1-Hd\_6 in different depths [cm] from 2011 to 2014; arithmetic mean (plot); standard deviation (whisker); standard error (box); median (line); Note: Significances a-b describes the ANOVA within the soil profile of each lysimeter, while k-l denote the significances between soil horizons (depth 0.1, 0.3, 0.5, 1.4 m); Note that the depth -axes are not continuous and cut between 0.5 and 1.4 m).

Highest DIC concentrations could be found in 1.4 m for all six lysimeters and concentrations decreased significantly towards the top soil concentrations. The leaching was about  $0.8 - 1.4 \text{ g}\cdot\text{m}^{-2}$  for DOC and about  $9.7 - 21.2 \text{ g}\cdot\text{m}^{-2}$  for DIC for the period from 2011 to 2014. Thus, the annual DOC leaching ranged approximately between  $0.3$  to  $0.5 \text{ g DOC m}^{-2}\cdot\text{yr}^{-1}$  and the mean annual DIC leaching rate ranged between  $3.0$  and  $7.0 \text{ g DIC m}^{-2}\cdot\text{yr}^{-1}$ . The temporal changes and patterns in dissolved carbon were similar between sites Dd and Hd (Fig. 3.5). During summer periods, DIC concentrations increased, while for the rest of the year, DIC concentrations were found scattered around a level slightly over  $3 \text{ mg}\cdot\text{L}^{-1}$  (Hd site) and  $10 \text{ mg}\cdot\text{L}^{-1}$  (Dd site). For DOC, concentration peaks were observed for summer and winter periods, but, as for DIC, clear seasonal changes in DOC could not be identified.

### III Water balance and leaching of dissolved organic and inorganic carbon of eroded Luvisols using high precision weighing lysimeters

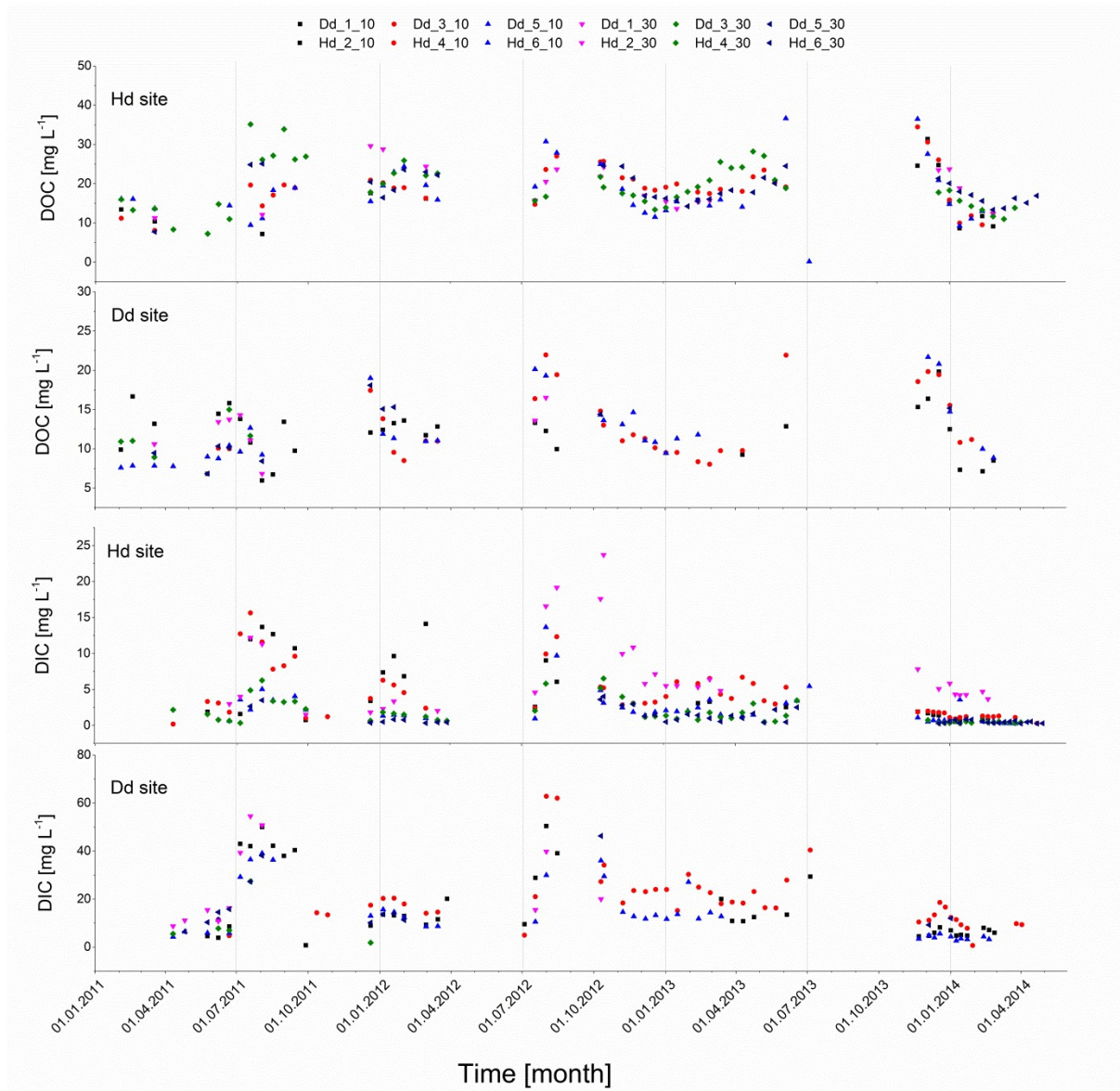


Figure 3.5: Time series' of dissolved organic (DOC) and inorganic carbon (DIC) concentrations [mg·L<sup>-1</sup>] sampled in bi-weekly intervals from lysimeters Dd\_1-Hd\_6 during the period from 2011 to 2014 at soil depths 0.1, 0.3, and 0.5 m; data gaps (e.g., 2<sup>nd</sup> half of 2013) represent relatively dry periods with no soil water extraction by suction cups.

#### 3.3.3 Biomass production

Fresh biomass production of the crops for the six lysimeters ranged from (maximal) 16.0 kg m<sup>-2</sup> (Hd\_2) to 22.5 kg m<sup>-2</sup> (Dd\_3) in sum over the 3-years period (Table 3.4). The crop yield of maize and Sudangrass was significantly higher for Dd soils in 2011 and 2012 as compared to Hd soils (Dd: 8.1 kg and 7.2 kg; Hd: 6.1 kg and 5.1 kg). Smaller differences were observed for averaged yields of fresh biomass for alfalfa in 2013 (Dd: 2.7 kg; Hd: 2.4 kg). On the contrary, biomass of Hd\_2, Hd\_4 and Hd\_6 for winter rye exceeded those

biomasses observed for soils Dd\_1, Dd\_3 and Dd\_5 (Dd: 2.6 kg; Hd: 3.7 kg). The ratio of dry matter to fresh biomass at harvest ranged between 17.5 % (winter rye, shoot biomass), 25.6 % (alfalfa), 30.9 % (Sudan grass), and 40.9 % (maize). Vegetation was correlated with the amount of  $P_{Lys}$  during the season ( $R_{maize}=0.72$ ;  $R_{sudan}= 0.70$ ,  $R_{alfalfa}= -0.09$ ) and  $ET_a$  for the cropping period ( $R_{maize}=0.87$ ;  $R_{sudan}= 0.62$ ;  $R_{alfalfa}=0.76$ ), with the exception of alfalfa, which was uncorrelated to precipitation data. The averaged water use efficiency of fresh ( $WUE_{FM}$ ) and dry ( $WUE_{DM}$ ) matter of crops (Table 3.4) was about 13.7 (FM) and 5.6 (DM)  $kg \cdot m^{-3}$  for maize, 14.7 and 4.6  $kg \cdot m^{-3}$  for Sudangrass, 14.1 and 2.5  $kg \cdot m^{-3}$  for rye, as well as 6.3 and 1.6  $kg \cdot m^{-3}$  for alfalfa.

### 3.4 Discussion

#### 3.4.1 Drainage in relation to soil erosion history and intensity

The variations in drainage of Luvisols Dd\_1-Hd\_6 of nearly 83 % for the 3-years period (cf., Dd\_3 and Hd\_6; Fig. 3.2) could be explained by erosional soil profile modifications manifested in contrasting distances of C- and Bt-horizons to the soil surface (cf. Table 3.2). Eroded Luvisols located on gentle slopes were characterized by Bt-horizons near the soil surface (depths of 0.3 m to 0.5 m) which has comparatively high hydraulic conductivities up to  $K_s >2600 \text{ cm} \cdot \text{d}^{-1}$  caused by the presence of continuous inter-aggregate pores and macropores, while less eroded Luvisols have instead of Bt- compacted E-horizons (Table 3.2) at the same depths. The  $K_s$  values of the Bt horizons varied in a wide range (cf. Dd\_3 and Dd\_5, Table 3.2) depending on sampling position, which could be explained for instance, with the influence of open-ended macro- or inter-aggregate pores in soil samples (Mohanty et al., 1994). Similar hydraulic conductivity values and variations of Bt- and compacted E-horizons of differently eroded Luvisol soil profiles were also reported by Rieckh et al. (2012).

Due to the enhanced swelling and shrinking (caused by its high clay content, e.g., Bronswijk, 1988) and the intensive root penetration near soil surface (modifications on soil structure; e.g. fractures, cracks; Angers and Caron, 1998), differences in depths and the thickness of aggregated Bt horizons may led to a diverse infiltration of seepage water via elongated macropores (Kodesova et al., 2009) from upper into lower soil horizons (Tsuboyama et al., 1994) between soils Dd\_1-Hd\_6. For the studied soils, the presence of well-developed polyhedral, angular blocky aggregates in the Bt-horizons was observed (Wilfried Hierold, Leibniz-Centre for Agricultural Landscape Research (ZALF), Müncheberg, personal communication, 2016). The network of larger pores in the aggregated Bt-horizons may also provide preferential flow paths for rapid infiltration during storms (Kodesova et al., 2009).

Renger M. (1968) observed for truncated soil profiles that the capillary rise especially between E- and Bt-horizon was reduced, which improved the vertical downward water movement of infiltrated rain water from topsoil to deeper soil horizons. Therefore, effects of erosional soil profile truncation might have led to less soil water in horizons near the soil surface and available for root water uptake or evaporation losses. For truncated Ap-Bt-soils in comparison to Ap-E-Bt-soils, Grosse (1964) reported that evaporation rates were lower because of earlier dewatered first centimeter soil depths and the reduced capillary delivery of soil water from deeper soil regions. In that way the partitioning of infiltrated rain water among evapotranspiration and drainage would be different for more or less eroded Luvisols (cf., Table 3.5); the ratio of drained soil water to precipitation was the lowest for Luvisols (Hd\_6: 9 %) and the highest for eroded Luvisols (Dd\_3: 15 %). Also, the relation of lysimeter water input ( $D_{in} + P_{Lys}$ ) to the evaporated and transpired soil water ( $ET_a$ ), was comparatively high for complete Luvisols (Hd\_6: 97 %) as compared to eroded Luvisols (Dd\_5: 93 %). Therefore, Luvisols with a smaller soil profile truncation were more strongly affected by water losses at the top of the lysimeter (evapotranspiration) in relation to their water drainage at the bottom (cf. water balance model illustration in Fig. 3.7).

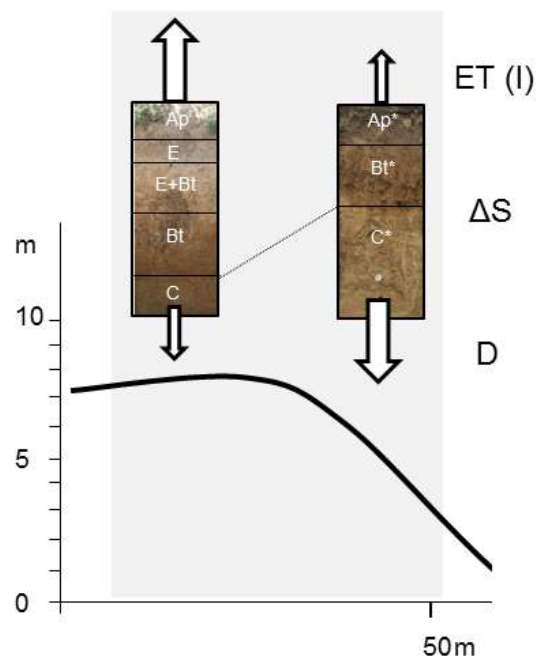


Figure 3.7: A sketch of illustrating the hypothesized effect of erosion-induced relatively large (right) and small (left) soil profile truncation on soil water balance components; the arrows represent the fluxes across the upper and lower boundaries such as evapotranspiration (ET) including interception loss (I) and drainage (D);  $\Delta S$  denotes changes in soil water storage; soil horizon symbols marked with an asterisk indicate erosion-induced modifications of soil properties; the line between the two soil profiles connects the surface of the C-horizons indicating reduced (solum depth).

Higher amounts of drained soil water of e.g., Dd\_3 and Hd\_6 especially from April to July in each year (period A, B and C; Fig. 3.2) could be explained by differences in the soil hydraulic properties (soil water tension) after the winter period. Große and Renger (1974) observed differences in the direction of the soil water movement between the less eroded Luvisol (Ap-E-Bt- horizons) and the more eroded Luvisol (truncated Ap-Bt- horizons) profile during an irrigation experiment; while the hydraulic gradient in the truncated profile indicated downward movement, water flow was still directed upwards in the uneroded Luvisol. These authors explain the differences by initial soil moisture differences before the experiment that had established during the winter period due to surface runoff on the less eroded Luvisol. The latter tended to more siltation and surface crust formation which reduced the water infiltration as compared to the truncated profile where the topsoil was less crusted. Similar differences in the direction of the soil water movement at the bottom of the lysimeters could be observed for lysimeter soils e.g. Hd\_6 (Luvisol) and Dd\_3 (eroded Luvisol). The differences in the outflow rates in the early spring (January to April, 2011-14) indicate a more downward movement of water of eroded Luvisols as compared to Luvisols in each year (drainage ratio of Hd\_6 to Dd\_3: 0.29 for 2011; 0.53 for 2012; 0.42 for 2013; 0.01 for 2014; not shown) under similar precipitation conditions (Dd\_3: 440 mm; Hd\_6: 422 mm, not shown).

However, the overall magnitude of the differences between the lysimeters was affected by the differences in precipitation between lysimeters (Table 3.5); Dd\_3 received 132 mm more precipitation than Hd\_6 in the 3-years period 2011-2014. The variability of  $P_{Lys}$  was suggested by differences in biomass production between the lysimeters (Table 3.4). The influence of plant biomass or above ground plant structure and crop growth was probably the reason for differences in  $P_{Lys}$  as given in particular for the summer period (e.g., for maize in July of 2011;  $35 \text{ mm}\cdot\text{d}^{-1}$ ; cf. Fig. 3.1). The differences in the mass and structure of the above-ground biomass affected the interception of rainfall and led to increasing differences in measured precipitation between the lysimeters during the vegetation period. The explanation is supported by the fact that strong differences in  $P_{Lys}$  were observed for vegetation periods 2011 and 2012 with the largest biomasses (cf., Table 3.4). In periods where crops reached their maximum growth and plant tissue surface area (July and August),  $P_{Lys}$  differed most strongly (e.g., July, 29<sup>th</sup> in 2011, 34 mm between Dd\_1-Hd\_6, not shown). The interception of rainfall water by the above ground biomass then depended on the structure of the plants (Muzylo et al., 2009). The plant specific surface areas probably affected the variability in  $P$  quantification with lysimeters during the vegetation period.

### *3.4.2 Erosional effects on carbon concentrations and leaching*

Dissolved organic carbon concentrations for soils Dd\_1-Hd\_6 decreased significantly from Ap to C-horizons after DOC passed the clay-enriched Bt-horizon (Fig. 3.3, Table 3.2). The decrease of DOC concentrations in the soil solution probably reflected DOC sorption in clayey soil material of Bt-horizons (Kalbitz et al., 2000) due to an increase in soil specific surfaces and mineral sorption sites with the increased content of clay minerals (Macht et al., 2011). Relatively similar concentrations at the lysimeter effluent (DOC  $\sim 5 \text{ mg}\cdot\text{L}^{-1}$ ) at 1.4 m depth suggested that the reduction of the DOC due to sorption seems to be independent of the thickness and location of the Bt horizons of the lysimeters soils here. DOC concentrations (Fig. 3.3) were similar to those reported by Kindler et al. (2011) and Walmsley et al. (2011) for cropland ranging from about  $4 \text{ mg}\cdot\text{L}^{-1}$  to  $17 \text{ mg}\cdot\text{L}^{-1}$  (0.4 m depth) and  $4 \text{ mg}\cdot\text{L}^{-1}$  to  $5 \text{ mg}\cdot\text{L}^{-1}$  (0.5 m depth, conventionally tilled), respectively. Mertens et al. (2007) observed for Luvisols from glacial till similar mean concentrations of DOC of about  $17 \text{ mg}\cdot\text{L}^{-1}$  (0.4 m depth) and  $9 \text{ mg}\cdot\text{L}^{-1}$  (1.2 m depth) as compared to DOC concentrations of Dd\_-Hd\_6 (Fig. 3.3), but under bare soil condition. Also, mean DOC concentrations in Luvisols ( $7 \text{ mg}\cdot\text{L}^{-1}$ , 2.0 m depth) and eroded Luvisol ( $6 \text{ mg}\cdot\text{L}^{-1}$ , 1.6 m depth) reported by Rieckh et al. (2014) for 2010 to 2012 were in line with those of Dd\_1-Hd\_6 (Fig. 3.3). In contrast to Kalbitz et al. (2000) and Buckingham et al. (2008), we could not observe clear seasonal changes on concentrations of dissolved organic carbon induced by hydrological or climatic conditions creating a DOC pattern over one year. For instance, higher DOC concentrations during summer could be induced by biological activity drivers and depending on soil temperature and soil moisture (Dawson and Smith, 2007).

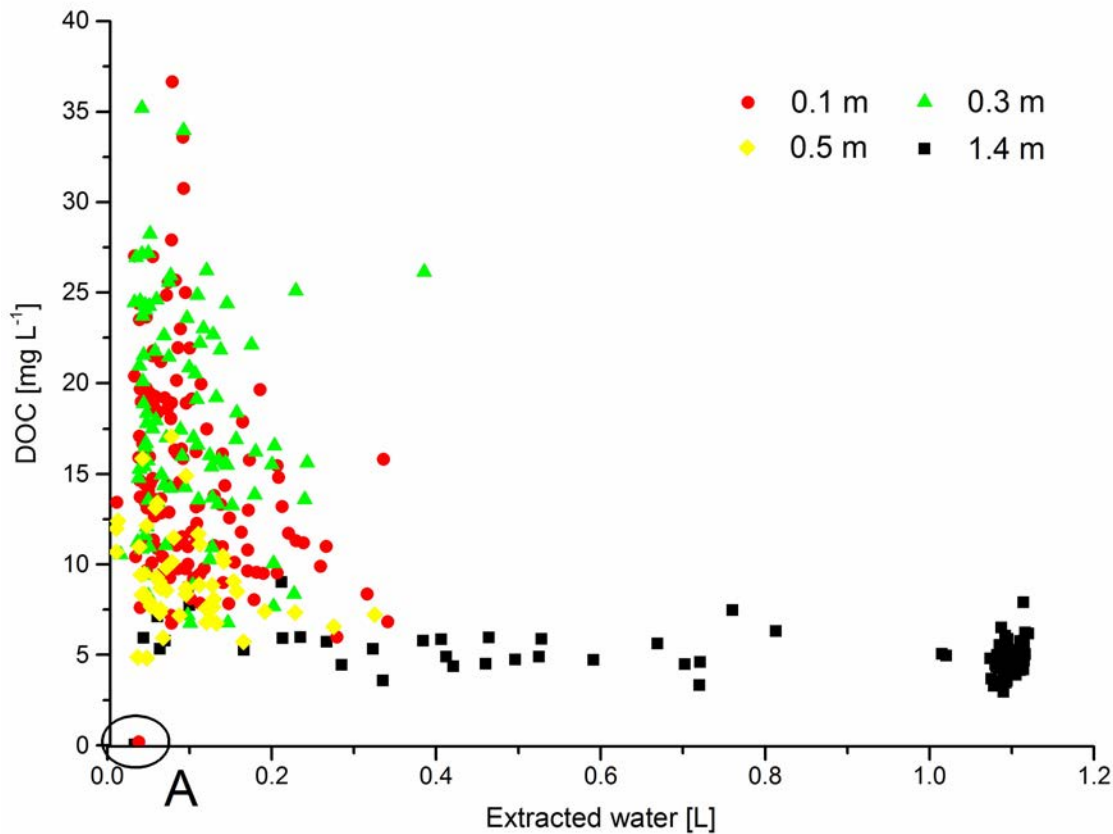


Figure 3.6: Relationship between observed concentrations of dissolved organic carbon (DOC) [mg·L<sup>-1</sup>] and amount of water [L] extracted by suction cups discontinuously sampled in bi-weekly intervals over a period of 2011, April to 2014, March (number of data points for soil depths were 134 for 10 cm, 93 for 30 cm, 51 for 50 cm, 98 for 140 cm). Mark A denotes very small concentrations in the soil solution. Further explanations are given in the text.

Indeed, highest values of DOC of soils Hd\_1-Dd\_6 for each year were analyzed during the summer period, but high DOC concentrations were also observed for winter months such as December 2013 (Fig. 3.5). These concentration peaks of DOC during the frost period with low biological activity could be explained by a lysis of freeze-damaged soil organisms (Soulides and Allison, 1961), disruption of microbial tissues by freeze (Kalbitz et al., 2000) or by the mortality of fine roots (Tierney et al., 2001).

The contact time over which soil water can dissolve organic carbon from the soil matrix was apparently important for the concentrations of dissolved carbon (Mertens et al., 2007). When assuming that a large volume of extracted soil water reflected a short contact time with the soil matrix, less time was available for desorption and/or dissolution processes of organic carbon causing a lower DOC concentration in the soil solution as compared to a lower volume of water extraction and a slower water percolation, respectively (Fig. 3.6). Negative

relationships ( $R = -0.5$ ) between DOC concentrations and extracted water volumes of the four soil depths underline the idea that low DOC concentrations arose with a large volume of extracted water and *vice versa*. Mertens et al. (2007) explained these inverse relationship of water velocity and DOC concentrations in the soil solution by kinetic processes having a limited net production rate. DOC concentrations  $<1 \text{ mg}\cdot\text{L}^{-1}$  (Fig. 3.6, remark A, July 2013) over a short period in summer could be explained by the decomposition of organic carbon by high microbiological activity in the soil water. The latter was inferred from concentrations peaks of  $\text{CO}_2$  in soil air during the summer period in combination with soil temperature increases (cf. Fig. A2 in the appendix, period A). The extraction of dissolved compounds (DOC) from the Bt horizons may also be affected by the suction cup position (i.e., a placement in macropores instead of the soil matrix) and, consequently, the influx into the suction cups by water from the coarser pores would be relatively higher.

In contrast to DOC, dissolved inorganic carbon concentrations for soils Dd\_1-Hd\_6 increased significantly from plough to C-horizons (Fig. 3.4). DIC was in lower concentration for topsoil horizons due to an eluviation of inorganic carbon by the downward movement of water through the soil profile. Slightly higher concentrations of Dd soils in 1.4 m soil depth (cf. Fig. 3.4, especially Dd\_3) could be explained by the truncation of soil profiles and the smaller distance of Cc-horizons to the soil surface.

The seasonal distribution of DIC concentration over one year (Fig. 3.5) was visible in concentration peaks of DIC (up to  $80 \text{ mg}\cdot\text{L}^{-1}$ ) during the summer period. The carbon peaks can be explained by the close relationship of DIC solubility and  $\text{CO}_2$  concentrations (Walmsley et al., 2011; cf. Fig. A2 in the appendix, periods B and C). The range of subsoil DIC concentrations (cf. Fig. 3.5) were in line with reported DIC concentrations of Kindler et al. (2011) with  $28 - 83 \text{ mg}\cdot\text{L}^{-1}$  for croplands. Rieckh et al. (2014) reported for Luvisols very similar mean concentrations of DIC ( $60 \text{ mg}\cdot\text{L}^{-1}$ ) at a depth of 1.2 m (cf. Fig. 3.4).



III Water balance and leaching of dissolved organic and inorganic carbon  
of eroded Luvisols using high precision weighing lysimeters

*Table 3.6: Cumulative leaching rates of dissolved organic (DOC) and inorganic (DIC) carbon [g m<sup>-2</sup>] for study sites Dd and Hd over the period of 2011, April to 2014, March; “in” denotes positive fluxes into the lysimeter; “out” denotes negative fluxes or output.*

		DOC [g m <sup>-2</sup> ]		DIC [g m <sup>-2</sup> ]	
		in	out	in	out
Dd_1	2011	0.00	0.55	0.0	7.7‡
	2012	0.12	0.12	2.0	4.1
	2013	0.17	0.33	0.1 <sup>†</sup>	4.6
	2014	0.0	0.01	0.0	0.4
	total	0.28	1.01	2.1	16.8
Dd_3	2011	0.00	0.64	0.0	11.4‡
	2012	0.14	0.37	3.1	4.6
	2013	0.30	0.33	1.4 <sup>†</sup>	4.9
	2014	0.0	0.01	0.0	0.2
	total	0.44	1.35	4.5	21.2
Dd_5	2011	0.00	0.59	0.0	8.8‡
	2012	0.12	0.32 <sup>††</sup>	3.2	3.7
	2013	0.14	0.21	1.0 <sup>†</sup>	3.8
	2014	0.0	0.03	0.0	0.2
	total	0.26	1.15 <sup>††</sup>	4.3	16.5
Hd_2	2011	0.00	0.35	0.00	5.5‡
	2012	0.11	0.36	0.71	3.8
	2013	0.05	0.23	0.18 <sup>†</sup>	3.2
	2014	0.0	0.05	0.0	0.5
	total	0.16	0.99	0.9	13.0
Hd_4	2011	0.00	0.44	0.00	6.2‡
	2012	0.04	0.49	0.66	3.7
	2013	0.06	0.39	0.13 <sup>†</sup>	4.1
	2014	0.0	0.03	0.0	0.2
	total	0.11	1.35	0.8	14.1
Hd_6	2011	0.00	0.31	0.00	4.9‡
	2012	0.06	0.28	1.27	3.0
	2013	0.08	0.17	0.13 <sup>†</sup>	1.8
	2014	0.0	0.0	0.0	0.0
	total	0.14	0.75	1.4	9.7

Leaching of DOC and DIC was affected by the erosional soil profile modifications (Table 3.6); here, leaching between Dd\_1-Hd\_6 differed due to contrasting seepage water fluxes (Fig. 3.2) rather than by concentration heterogeneities of dissolved carbon at the bottom (Figs. 3.3 and 3.4). Similar concentrations of DIC and DOC in 1.4 m soil depths, but contrasting cumulative soil water fluxes at same depths may be responsible for the varying dissolved carbon exports of soils Dd\_1-Hd\_6. Mean DOC exports (0.3 - 0.5 g DOC m<sup>-2</sup>.yr<sup>-1</sup>; Table 3.6)

of more-or-less eroded Luvisols were lower as compared to those reported by Kindler et al. (2011) with  $4.8 \pm 1.3 \text{ g DOC m}^{-2}\cdot\text{yr}^{-1}$  and Walmsley et al. (2011) with  $3.0 \pm 1.3 \text{ g DOC m}^{-2}\cdot\text{yr}^{-1}$  for arable soils. The offset between observed (Table 6) and the reported DOC leaching was properly affected by carbon concentration decreases of Luvisols Dd\_1-Hd\_6 due to DOC sorption mechanisms of the clayey Bt-horizons and the use of DOC concentrations at 1.4 m soil depth for leaching calculations, while Kindler et al. (2011) and Walmsley et al. (2011) used topsoil concentrations of DOC (0.4 – 0.5 m depths). A study of Brye et al. (2001) underlined the hypotheses of leaching differences due to differences in DOC concentrations by a lower leaching of DOC of about  $1.2 - 1.4 \text{ g}\cdot\text{m}^{-2}\cdot\text{yr}^{-1}$  for similar depths (1.2 m) of a loess soils over glacial till (Argiudoll) with tillage management, but without the concentration effect of the clayey Bt-horizons on DOC. For Luvisols of the hummocky soil landscape, leaching of dissolved carbon using a combination of modeling water fluxes (HYDRUS 1D) and field concentration measurements (Rieckh et al., 2014) was between 0.7 and 0.8  $\text{g DOC m}^{-2}\cdot\text{yr}^{-1}$  for a 3-years period (2010-2012); the comparison with DOC exports of Dd\_1-Hd\_6 (0.3 - 0.5  $\text{g DOC m}^{-2}\cdot\text{yr}^{-1}$ ; Table 3.6) revealed smaller leaching rates of DOC using the combined approach of Rieckh et al. (2014).

#### *3.4.3 Effects of erosion induced soil profile modifications on biomass yield*

The significant differences in biomass production (Table 3.4) between eroded (Dd site) and less eroded soils (Hd site) implied that not only differently eroded soil types can affect contrasting biomass yield (e.g. Moulin et al., 1994, Jowkin and Schoenau, 1998), but also erosion-induced modifications with a single soil type; here differently truncated Luvisols Dd\_1-Hd\_6. The solum depths, the location of Bt-horizon and the presence of the eluvial soil horizon (E) seemed to significantly reduce biomass yield of main crops, maize and Sudangrass (Table 3.4). For these plants with shallow root, structured clayey soil material of Bt-horizons in the rooting zone significantly improved biomass yields of eroded soils (Dd site) against less eroded soils (Hd site); also the clay content in plough horizons of eroded site Dd (e.g., Dd\_1:  $157 \text{ g}\cdot\text{kg}^{-1}$ ) was higher (> 200 %) as compared to site Hd (e.g., Hd\_1:  $66 \text{ g}\cdot\text{kg}^{-1}$ ) leading to an increase in the stability of soil structure. A higher biomass yield for among others for sugar beet and field bean was also observed for truncated soil profiles of Luvisols developed from loess (Grosse, 1964). Grosse (1964) suggested that differences in the structural properties of truncated Ap-Bt-soils (polyhedral structure) against Ap-E-Bt-soil profiles (platy structure) were the reason for a different biomass production; the contrasting structural properties, in turn, affected the water infiltration, the soil water movement and the aeration of soils. Deep rooting plants such as alfalfa compensating unfavourable effects of soil structure on biomasses (Table 3.4, Dd: 2.7 kg; Hd: 2.4 kg) by extracting water from the additional rooted soil volume. Thereby it seemed that alfalfa was less (non-significant)

affected by topsoil characteristics (0 – 0.5 m) comparing maize and Sudangrass. The comparison of biomass yield between Dd and Hd soils using only the effect of erosion-induced profile modifications on plant growth, however, is limited because of the different nutrient supply of Dd\_1-Hd\_6 (Table 3.3).

The contrasting yields of winter rye (Table 3.4) compared to main crops (cf., seeding and harvest times; section 2.3) can be explained by the fact that for the winter and spring period (low air temperatures; Fig. A2 in the appendix, low ET and high precipitation values; Fig. 3.1) rather wet soil conditions may have reduced the water stress effects in the phase of growing for winter rye from October to April. Interestingly for winter wheat in 2014/2015, we found similar results in biomasses as observed for the main crops (Dd site: 3.0 kg, Hd site: 2.5 kg; data not shown). This variation in biomass development especially for cereals of differently truncated Luvisols on cereals were in line with results of Grosse (1964), who also observed smaller biomass yields of winter rye for eroded soils compared to less eroded soils, but higher yields for winter wheat for truncated soils.

Results of the water use efficiency corresponded to those observed for harvested crop biomass (Table 3.4). Both, water use efficiency of fresh and dry matter revealed that crops in eroded positions produced a higher biomass for main crops during the vegetation season in relation to their water consumption (e.g., for fresh material of maize in 2011; Dd:  $15.3 \pm 0.7$  kg m<sup>-3</sup>; Hd:  $12.1 \pm 0.2$  kg m<sup>-3</sup>). In addition to differences in soil properties, the effect of the soil fertility on biomass development could be influenced by the water use efficiencies (cf. Table A2). The inverse situation of winter rye as compared to WUE of main crops with higher water use efficiencies for site Hd reflected differences in biomass production (cf., Table 3.4).

### *3.5 Conclusions*

In this study, the effects of erosional truncation of Luvisol profiles derived from glacial till on drainage and leaching were analyzed using high precision lysimeters. Time series of mass changes from the six lysimeters revealed that water balance components differed strongly between more or less truncated Luvisols. The results suggested that for erosion-affected arable soils, the water and solute balance depended on soil properties and soil-crop interactions that could be associated on erosion history at the particular slope positions of the soil monoliths. The increased drainage of eroded Luvisols suggested that the downward water movement in the soil profile increased from less to more eroded soils represented by less to more truncated soil profiles, respectively; this fact, however, was caused by a larger precipitation received by the truncated soils, which was possibly resulting from interactions between crop development and more rainfall interception by above ground biomass. Crop

yields confirmed a tendency of an increased biomass production of eroded soils (Ap-B-C) compared to less eroded soils (Ap-E-B-C); although the effect of erosional truncation of Luvisol profiles on biomass yield was derived from two different sites here with a different nutrient supply. Similar DOC and DIC concentrations in the effluent from the bottom of all Luvisol lysimeters and highest dissolved carbon leaching at eroded soils implied that leaching of DOC/DIC was in magnitude and direction controlled by the water drainage flux rates.

Results of differently eroded Luvisols suggested for the arable hummocky morainic soil landscapes that not only the distributed soil types but also erosion-induced modifications of horizons within a single soil type should be considered when trying to quantify the landscape scale water balance and the leaching of dissolved carbon fractions. For dissolved carbon leaching simulations in the hummocky landscape, future efforts to quantify DIC and DOC exports should among other processes focus on the improved spatial representation of the soil water fluxes and the interaction with root and crop development.

#### *Acknowledgements*

The study is a part of the TERENO-SoilCan project and supported by infrastructure of the Terrestrial Environmental Observatory TERENO-Northeast of the Helmholtz Association ([http://teodoor.icg.kfa-juelich.de/observatories/GL\\_Observatory?set\\_language=en](http://teodoor.icg.kfa-juelich.de/observatories/GL_Observatory?set_language=en)). The first author thanks the GFZ, German Research Centre for Geosciences Potsdam for financial support. The TERENO-SoilCan lysimeters are operated by the Leibniz-Centre for Agricultural Landscape Research (ZALF) Müncheberg. The authors thank Wilfried Hierold (soil classification) and Ute Moritz (data preparation) from the Institute of Soil Landscape Research, Jörg Haase and Gernot Verch from the research station Dedelow of the ZALF as well as Kristina Holz and her team from the Central Laboratory of the ZALF (chemical soil and solution analyses). We further thank the Central Ecological Laboratory of the University of Sustainable Development (HNE) in Eberswalde for texture analyses.

## References

- Afyuni, M. M., Cassel, D. K., and Robarge, W. P., 1994, Lateral and vertical bromide ion-transport in a piedmont landscape: *Soil Science Society of America Journal*, v. 58, no. 3, p. 967-974.
- Ali, M. A., Amjad, A., Shahid, N., Zulkiffal, M., and Shiraz, A., 2009, Morpho-physiological criteria for drought tolerance in sorghum (*Sorghum bicolor*) at seedling and post-anthesis stages: *International Journal of Agriculture and Biology*, v. 11, no. 6, p. 674-680.
- Allen, R. G., Pereira, L. S., Raes, D., and Smith, M., 1998, Crop evapotranspiration: Guidelines for computing crop water requirements: United Nations Food and Agriculture Organization, Irrigation and Drainage Paper 56, p. 300.
- Amos, B., and Walters, D. T., 2006, Maize Root Biomass and Net Rhizodeposited Carbon: *Soil Science Society of America Journal*, v. 70, no. 5, p. 1489.
- Angers, D. A., and Caron, J., 1998, Plant-induced changes in soil structure: Processes and feedbacks: *Biogeochemistry*, v. 42, no. 1-2, p. 55-72.
- Baldocchi, D., Valentini, R., Running, S., Oechel, W., and Dahlman, R., 1996, Strategies for measuring and modelling carbon dioxide and water vapour fluxes over terrestrial ecosystems: *Global Change Biology*, v. 2, no. 3, p. 159-168.
- Bauhus, J., and Barthel, R., 1995, Mechanisms for carbon and nutrient release and retention in beech forest gaps, *Nutrient Uptake and Cycling in Forest Ecosystems*, Springer, p. 585-592.
- Blake, G. R., and Hartge, K. H., 1986, Bulk density, In: *Methods of Soil Analysis. Part 1. Physical and mineralogical methods*, Madison, Wisconsin, American Society of Agronomy, p. 363 - 375.
- Bray, J. R., 1963, Root production and the estimation of net productivity: *Canadian Journal of Botany*, v. 41, no. 1, p. 65-72.
- Bronswijk, J. J. B., 1988, Effect of swelling and shrinkage on the calculation of water balance and water transport in clay soils: *Agricultural Water Management*, v. 14, no. 1-4, p. 185-193.
- Brye, K. R., Norman, J. M., Bundy, L. G., and Gower, S. T., 2001, Nitrogen and carbon leaching in agroecosystems and their role in denitrification potential: *Journal of Environmental Quality*, v. 30, no. 1, p. 58-70.
- Buckingham, S., Tipping, E., and Hamilton-Taylor, J., 2008, Concentrations and fluxes of dissolved organic carbon in UK topsoils: *Sci Total Environ*, v. 407, no. 1, p. 460-470.

Buczko, U., Bens, O., and Hüttl, R., 2006, Tillage effects on hydraulic properties and macroporosity in silty and sandy soils: *Soil Science Society of America Journal*, v. 70, no. 6, p. 1998-2007.

Dawson, J. J. C., and Smith, P., 2007, Carbon losses from soil and its consequences for land-use management: *Science of the Total Environment*, v. 382, no. 2-3, p. 165-190.

Deumlich, D., Schmidt, R., and Sommer, M., 2010, A multiscale soil-landform relationship in the glacial-drift area based on digital terrain analysis and soil attributes: *Journal of Plant Nutrition and Soil Science*, v. 173, no. 6, p. 843-851.

DIN-EN-1484, 1997, Wasseranalytik - Anleitungen zur Bestimmung des gesamten organischen Kohlenstoffs (TOC) und des gelösten organischen Kohlenstoffs (DOC); Deutsche Fassung EN 1484-1997.

DIN-ISO:10694, 1996, Soil quality - Determination of organic and total carbon after dry combustion (elementary analysis), DIN Deutsches Institut für Normen: Beuth Verlag.

DIN-ISO:11277, 2002, Soil quality - Determination of particle size distribution in mineral soil material - Method by sieving and sedimentation, DIN Deutsches Institut für Normen: Beuth Verlag.

DIN-ISO:11464, 2006, Soil quality - Pretreatment of samples for physico-chemical analyses, DIN Deutsches Institut für Normen: Beuth Verlag.

Gerke, H. H., and Hierold, W., 2012, Vertical bulk density distribution in C-horizons from marley till as indicator for erosion history in a hummocky post-glacial soil landscape: *Soil and Tillage Research*, v. 125, p. 116-122.

Gerke, H. H., Koszinski, S., Kalettka, T., and Sommer, M., 2010, Structures and hydrologic function of soil landscapes with kettle holes using an integrated hydro-pedological approach: *Journal of Hydrology*, v. 393, no. 1-2, p. 123-132.

Gerke, H. H., Rieckh, H., and Sommer, M., 2016, Interactions between crop, water, and dissolved organic and inorganic carbon in a hummocky landscape with erosion-affected pedogenesis: *Soil and Tillage Research*, v. 156, p. 230-240.

Govers, G., Lobb, D. A., and Quine, T. A., 1999, Tillage erosion and translocation: emergence of a new paradigm in soil erosion research: *Soil & Tillage Research*, v. 51, no. 167, p. 174.

Grosse, B., 1964, Die Ertragsfähigkeit stark erodierter Parabraunerden aus Löss im gemäßigten Klima, *Transactions of the 8th international congress of soil science*, Bucharest, Romania, v. 2, p. 729-735.

Große, B., and Renger, M., 1974, Untersuchungen über die Erodierbarkeit einer tiefgepflügten Parabraunerde aus Löß in Hanglage mit Hilfe der künstlichen Beregnung: *Journal of Plant Nutrition and Soil Science*, v. 137, p. 86-94.

Hannes, M., Wollschläger, U., Schrader, F., Durner, W., Gebler, S., Pütz, T., Fank, J., Unold, G. v., and Vogel, H.-J., 2015, High-resolution estimation of the water balance components from high-precision lysimeters: *Hydrol. Earth Syst. Sci. Discuss.*, v. 12, no. 1, p. 569-608.

HBU, 2005, *Handbuch der Bodenkunde*; Hans-Peter Blume, Berthold Deller, Klaus Furtmann, Reimar Leschber, Andreas Paetz, Berndt-Michael Wilke (Hrsg.), Wiley-VCH, Weinheim.

IUSS, 2006, *World reference base for soil resources 2006.: World Soil Resources Reports No. 103*. FAO, Rome.

Jandl, R., Vesterdal, L., Olsson, M., Bens, O., Badeck, F., and Rock, J., 2007, Carbon sequestration and forest management: *CAB Reviews: Perspectives in Agriculture, Veterinary Science, Nutrition and Natural Resources*, v. 2, no. 017.

Jenny, H., 1961, Derivation of state factor equations of soils and ecosystems: *Soil Sci Soc Amer Proc*, v. 25, no. (5), p. 385-388.

Jowkin, V., and Schoenau, J., 1998, Impact of tillage and landscape position on nitrogen availability and yield of spring wheat in the Brown soil zone in southwestern Saskatchewan: *Canadian Journal of Soil Science*, v. 78, no. 3, p. 563-572.

Kalbitz, K., Solinger, S., Park, J. W., Michalzik, B., and Matzner, E., 2000, Controls on the dynamics of dissolved organic matter in soils: A Review: *Soil Sci.*, v. 165, no. 4, p. 277-304.

Kindler, R., Siemens, J. A. N., Kaiser, K., Walmsley, D. C., Bernhofer, C., Buchmann, N., Cellier, P., Eugster, W., Gleixner, G., Grünwald, T., Heim, A., Ibrom, A., Jones, S. K., Jones, M., Klumpp, K., Kutsch, W., Larsen, K. S., Lehuger, S., Loubet, B., McKenzie, R., Moors, E., Osborne, B., Pilegaard, K. I. M., Reibmann, C., Saunders, M., Schmidt, M. W. I., Schrumpf, M., Seyfferth, J., Skiba, U. T. E., Soussana, J.-F., Sutton, M. A., Tefs, C., Vowinckel, B., Zeeman, M. J., and Kaupenjohann, M., 2011, Dissolved carbon leaching from soil is a crucial component of the net ecosystem carbon balance: *Global Change Biology*, v. 17, no. 2, p. 1167-1185.

Klute, A., and Dirksen, C., 1986, *Hydraulic conductivity and diffusivity: laboratory methods*, Madison, Wisconsin, American Society of Agronomy, Inc., *Methods of soil analysis. Part 1. Physical and mineralogical methods*, 687-734 p.:

Kodesova, R., Vignozzi, N., Rohoskova, M., Hajkova, T., Kocarek, M., Pagliai, M., Kozak, J., and Simunek, J., 2009, Impact of varying soil structure on transport processes in different diagnostic horizons of three soil types: *Journal of Contaminant Hydrology*, v. 104, no. 1-4, p. 107-125.

Kosmas, C., Gerontidis, S., Marathianou, M., Detsis, B., Zafiriou, T., Muysen, W. N., Govers, G., Quine, T., and Vanoost, K., 2001, The effects of tillage displaced soil on soil properties and wheat biomass: *Soil and Tillage Research*, v. 58, no. 1, p. 31-44.

Kuchenbuch, R. O., Gerke, H. H., and Buczko, U., 2008, Spatial distribution of maize roots by complete 3D soil monolith sampling: *Plant and Soil*, v. 315, no. 1-2, p. 297-314.

Lin, H., 2011, Three Principles of Soil Change and Pedogenesis in Time and Space: *Soil Science Society of America Journal*, v. 75, no. 6, p. 2049-2070.

Liu, C. M., Zhang, X. Y., and Zhang, Y. Q., 2002, Determination of daily evaporation and evapotranspiration of winter wheat and maize by large-scale weighing lysimeter and micro-lysimeter: *Agricultural and Forest Meteorology*, v. 111, no. 2, p. 109-120.

Macht, F., Eusterhues, K., Pronk, G. J., and Totsche, K. U., 2011, Specific surface area of clay minerals: Comparison between atomic force microscopy measurements and bulk-gas (N<sub>2</sub>) and -liquid (EGME) adsorption methods: *Applied Clay Science*, v. 53, no. 1, p. 20-26.

Manning, G., Fuller, L. G., Eilers, R. G., and Florinsky, I., 2001, Topographic influence on the variability of soil properties within an undulating Manitoba landscape: *Canadian Journal of Soil Science*, v. 81, no. 3, p. 439-447.

McCaig, M., 1985, Soil properties and subsurface hydrology: In K.S. Richards, R.R. Arnet and S. Ellis (eds): *Geomorphology and soils*, p. 121-140.

Meißner, R., Prasad, M. N. V., Du Laing, G., and Rinklebe, J., 2010, lysimeter application for measuring the water and solute fluxes with high precision: *Curr. Sci. India.*, v. 99, no. 5, p. 601.

Meissner, R., Rupp, H., Seeger, J., and Schonert, P., 1995, Influence of mineral fertilizers and different soil types on nutrient leaching: Results of lysimeter studies in East Germany: *Land Degradation & Development*, v. 6, no. 3 p. 163-170.

Meissner, R., Seeger, J., Rupp, H., Seyfarth, M., and Borg, H., 2007, Measurement of dew, fog, and rime with a high-precision gravitation lysimeter: *J. Plant Nutr. Soil Sci.*, v. 170, no. 3, p. 335-344.

Mertens, J., Vanderborght, J., Kasteel, R., Putz, T., Merckx, R., Feyen, J., and Smolders, E., 2007, Dissolved organic carbon fluxes under bare soil: *Journal of Environmental Quality*, v. 36, no. 2, p. 597-606.



Mohanty, B., Kanwar, R. S., and Everts, C., 1994, Comparison of saturated hydraulic conductivity measurement methods for a glacial-till soil: *Soil Science Society of America Journal*, v. 58, no. 3, p. 672-677.

Moulin, A., Anderson, D., and Mellinger, M., 1994, Spatial variability of wheat yield, soil properties and erosion in hummocky terrain: *Canadian journal of soil science*, v. 74, no. 2, p. 219-228.

Muzylo, A., Llorens, P., Valente, F., Keizer, J., Domingo, F., and Gash, J., 2009, A review of rainfall interception modelling: *J. Hydrol.*, v. 370, no. 1, p. 191-206.

Pennock, D. J., 2003, Terrain attributes, landform segmentation, and soil redistribution: *Soil & Tillage Research*, v. 69, no. 1-2, p. 15-26.

Peters, A., Nehls, T., Schonsky, H., and Wessolek, G., 2014, Separating precipitation and evapotranspiration from noise - a new filter routine for high resolution lysimeter data: *Hydrol. Earth Syst. Sci. Discuss.*, v. 18, p. 1189 -1198.

Promkhambut, A., Younger, A., Polthanee, A., and Akkasaeng, C., 2010, Morphological and Physiological Responses of Sorghum (*Sorghum bicolor* L. Moench) to Waterlogging: *Asian Journal of Plant Sciences*, v. 9, no. 4, p. 183-193.

Pütz, T., Kiese, R., Wollschläger, U., Groh, J., Rupp, H., Zacharias, S., Priesack, E., Gerke, H. H., Papen, H., Borg, E., Bens, O., Kaiser, K., Herbrich, M., Munch, J.-C., Sommer, M., Vanderborght, J., and Vereecken, H., 2016, TERENO-SOILCan a Lysimeter-Network in Germany Observing Soil Functions Influenced by Climate Change: *Environ. Earth Sci.*; in press.

Renger M., 1968, Verbesserung der physikalischen Eigenschaften von Parabraunerden aus Löss durch Tiefumbruch. - *Kali-Briefe* 9, Fachgeb.1, p. 1-8.

Rieckh, H., Gerke, H. H., and Sommer, M., 2012, Hydraulic properties of characteristic horizons depending on relief position and structure in a hummocky glacial soil landscape: *Soil and Tillage Research*, v. 125, p. 123-131.

Rieckh, H., Gerke, H. H., and Sommer, M., 2014, Water and Dissolved Carbon Fluxes in an Eroding Soil Landscape Depending on Terrain Position *Vadose Zone J.*, v. 13, no. 7.

Ritchie, J., 1998, *Soil water balance and plant water stress, Understanding options for agricultural production*, Springer, p. 41-54.

Sinclair, T. R., Tanner, C. B., and Bennett, J. M., 1984, water use efficiency in crop production *Bioscience*, v. 34, no. 1, p. 36-40.

Soldevilla-Martinez, M., Quemada, M., Lopez-Urrea, R., Munoz-Carpena, R., and Lizaso, J. I., 2014, Soil water balance: Comparing two simulation models of different levels of complexity with lysimeter observations: *Agricultural Water Management*, v. 139, p. 53-63.

Sommer, M., Gerke, H. H., and Deumlich, D., 2008, Modelling soil landscape genesis - A "time split" approach for hummocky agricultural landscapes: *Geoderma*, v. 145, no. 3-4, p. 480-493.

Soulides, D. A., and Allison, F. E., 1961, Effect of drying and freezing soils on carbon dioxide production, available mineral nutrients, aggregation, and bacterial population: *Soil Sci*, v. 91, no. (5), p. 291-298.

Stephenson, N. L., 1990, Climatic control of vegetation distribution: the role of the water balance: *American Naturalist*, p. 649-670.

Thibodeau, J., Fuller, L., and Chanasyk, D., 2007, Determination of solute leaching potential within a hummocky agricultural landscape: *Canadian Journal of Soil Science*, v. 87, no. 5, p. 541-549.

Tierney, G. L., Fahey, T. J., Groffman, P. M., Hardy, J. P., Fitzhugh, R. D., and Driscoll, C. T., 2001, Soil freezing alters fine root dynamics in a northern hardwood forest: *Biogeochemistry*, v. 56, no. 2, p. 175-190.

Tsuboyama, Y., Sidle, R. C., Noguchi, S., and Hosoda, I., 1994, Flow and solute transport through the soil matrix and macropores of a hillslope segment: *Water Resources Research*, v. 30, no. 4, p. 879-890.

Unold, G., and Fank, J., 2008, Modular Design of Field Lysimeters for Specific Application Needs: *Water Air Soil Pollut.*, v. 8, no. 2, p. 233-242.

Van Oost, K., Govers, G., De Alba, S., and Quine, T., 2006, Tillage erosion: a review of controlling factors and implications for soil quality: *Progress in Physical Geography*, v. 30, no. 4, p. 443-466.

Verch, G., 2014, Weather Data, Dedelow, Germany, Leibniz-Zentrum für Agrarlandschaftsforschung (ZALF) e.V. - online available under [e.g. <http://dx.doi.org/10.4228/ZALF.2000.242>].

Walmsley, D. C., Siemens, J., Kindler, R., Kirwan, L., Kaiser, K., Saunders, M., Kaupenjohann, M., and Osborne, B. A., 2011, Dissolved carbon leaching from an Irish cropland soil is increased by reduced tillage and cover cropping: *Agriculture Ecosystems & Environment*, v. 142, no. 3-4, p. 393-402.

### III Water balance and leaching of dissolved organic and inorganic carbon of eroded Luvisols using high precision weighing lysimeters

---

Woods, S. A., Dyck, M. F., and Kachanoski, R. G., 2013, Spatial and temporal variability of soil horizons and long-term solute transport under semi-arid conditions: *Canadian Journal of Soil Science*, v. 93, no. 2, p. 173-191.

Xiao, H., Meissner, R., Seeger, J., Rupp, H., and Borg, H., 2009, Effect of vegetation type and growth stage on dewfall, determined with high precision weighing lysimeters at a site in northern Germany: *J. Hydrol.*, v. 377, no. 1-2, p. 43-49.

Young, M. H., Wierenga, P. J., and Mancino, C. F., 1996, Large Weighing Lysimeters for Water Use and Deep Percolation Studies: *Soil Science* v. 7, no. 161, p. 491-501.

## Appendix

*Table A1: Terrain attributes of sampling locations Dedelow (Dd) and Holzendorf (Hd): geographic coordinate, slope, curvature and the topographic position index (TPI) of each location. TPI were calculated as proposed by Weis (2001) using ArcView GIS with the TPI extension package (Jenness Enterprises, Flagstaff, USA); Table corresponds to Figure A1 in the appendix.*

Soil	Geographic coordinates		Elevation [m a.s.]	Slope [%]	Curvature [°m <sup>-1</sup> ]	TPI [-]
	X	Y				
Dd_1	3420334.96	5913845.63	43.84	1.77	0.2	5
Dd_3	3420334.58	5913835.73	43.63	0.65	-4.9	5
Dd_5	3420334.20	5913824.93	43.59	2.37	-0.9	5
Hd_2	3419216.00	5915140.00	57.24	0.79	1.0	7
Hd_4	3419212.90	5915133.16	57.19	0.64	0.7	7
Hd_6	3419219.14	5915146.78	57.25	1.60	-0.7	7

III Water balance and leaching of dissolved organic and inorganic carbon  
of eroded Luvisols using high precision weighing lysimeters

Table A2: Mineral fertilizers [ $\text{kg}\cdot\text{ha}^{-1}$ ] applied at the lysimeter soils from Dedelow (Dd) and Holzendorf (Hd) during the period 2011 to 2014: Kieserit - 25% MgO and 20% S, ESTA Kieserit<sup>®</sup> granulated, K+S Kali GmbH, Kassel, Germany; KAS - calcium ammonium nitrate with approximately 74%  $\text{NH}_4\text{NO}_3$  and 26%  $\text{CaCO}_3$ ; Granukal - 80 %  $\text{CaCO}_3$  and 5 %  $\text{MgCO}_3$ , Vereinigte Kreidewerke Dammann KG, Granukal<sup>®</sup>, Söhlde, Germany.

Year	Month	Dd	Hd
2011	April	KAS, 160 $\text{kg}\cdot\text{ha}^{-1}$	KAS, 160 $\text{kg}\cdot\text{ha}^{-1}$
	May	Kieserit, 100 $\text{kg}\cdot\text{ha}^{-1}$	Kieserit, 100 $\text{kg}\cdot\text{ha}^{-1}$
2012	March	$\text{P}_2\text{O}_5$ , 110 $\text{kg}\cdot\text{ha}^{-1}$ $\text{K}_2\text{O}$ , 180 $\text{kg}\cdot\text{ha}^{-1}$	$\text{P}_2\text{O}_5$ , 110 $\text{kg}\cdot\text{ha}^{-1}$ $\text{K}_2\text{O}$ , 180 $\text{kg}\cdot\text{ha}^{-1}$
	October	Granukal, 1000 $\text{kg}\cdot\text{ha}^{-1}$	Granukal, 3000 $\text{kg}\cdot\text{ha}^{-1}$
2013	March	$\text{P}_2\text{O}_5$ , 110 $\text{kg}\cdot\text{ha}^{-1}$	$\text{P}_2\text{O}_5$ , 110 $\text{kg}\cdot\text{ha}^{-1}$
2014		-	-

III Water balance and leaching of dissolved organic and inorganic carbon  
of eroded Luvisols using high precision weighing lysimeters

Table A3: Times of sowing and harvesting from the six 1 m<sup>2</sup>-sized lysimeters Dd\_ 1 to Hd\_6 for crop rotation during the period from April 2011 to September 2014.

	Maize	Winter Rye	Sudangrass	Triticale	Alfalfa	Persian Clover
Sowing	Apr 26 <sup>th</sup> , 2011	Oct 4 <sup>th</sup> , 2011	May 15 <sup>th</sup> , 2012	Oct 19 <sup>th</sup> , 2012	Mar 19 <sup>th</sup> , 2013	Mar 4 <sup>th</sup> , 2014
Harvesting	Oct 4 <sup>th</sup> , 2011	May 9 <sup>th</sup> , 2012	Sept 21 <sup>th</sup> , 2012	Mar 19 <sup>th</sup> , 2013	Aug 23 <sup>th</sup> , 2013	Sept 19 <sup>th</sup> , 2014

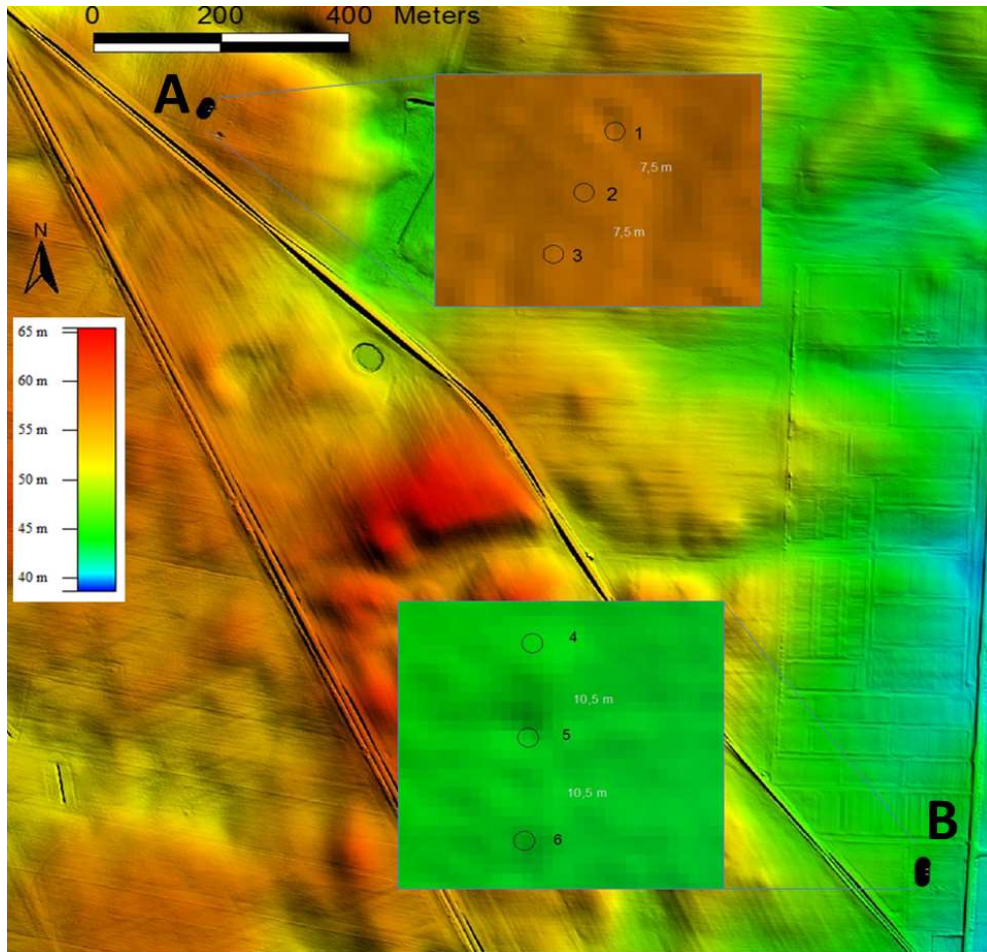


Figure A1: Digital terrain model (DGM1, 1 m grid) of the study sites Holzendorf (A) and Dedelow (B) near the town of Prenzlau (Northeast Germany), with locations of the soil pits (1-6) of monoliths Dd\_1 to Hd\_6; the distance (m) between soil monoliths Hd\_2 (1), Hd\_4 (2) and Hd\_6 (3) as well as Dd\_1 (4), Dd\_3 (5) and Dd\_5 (6) (enlarged view, small inlet); the terrain attributes of each study site are given in Table A1. The license for use of the DGM1 was given by LGB Brandenburg, ©Geobasis-DE/LGB 2012.

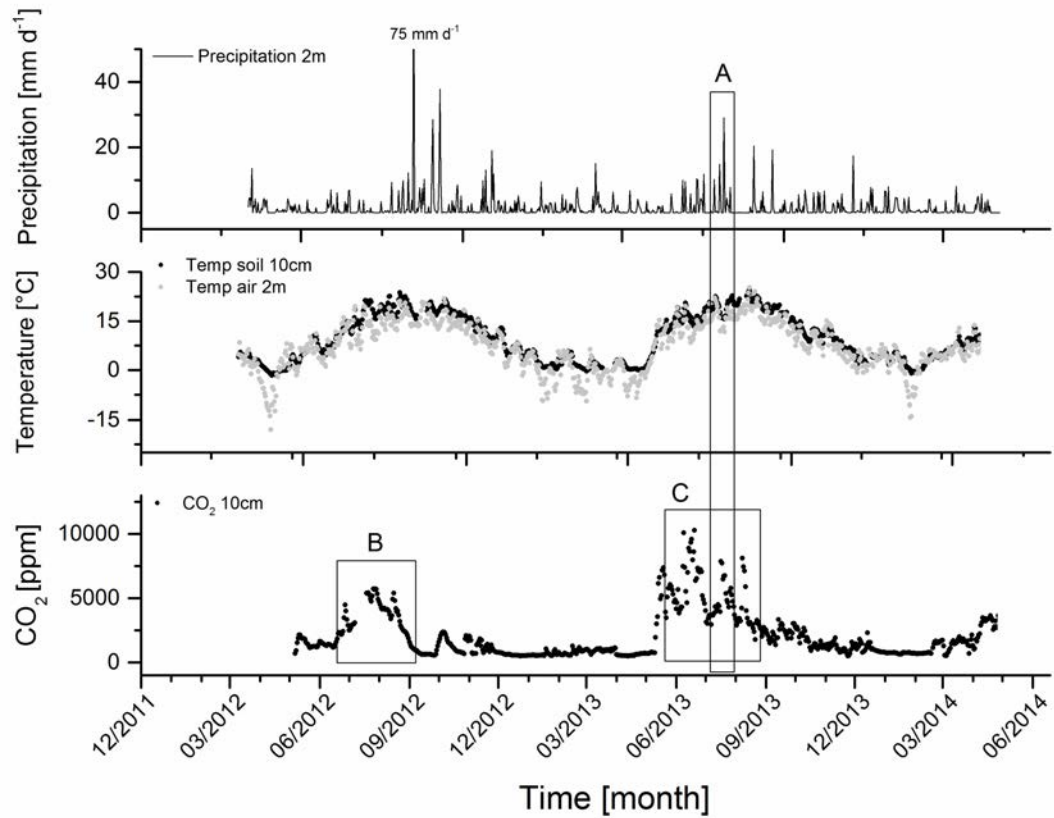


Figure A2: Daily means of air temperatures and precipitation in 2 m height and soil temperatures in 10 cm soil depth, as well as carbon dioxide (CO<sub>2</sub>) in 10 cm soil depth for a period of January 1<sup>st</sup>, 2012 to April 30<sup>th</sup>, 2014 including technical problems after a storm event from 15.10.2014.



## 4| Scales of water retention dynamics observed in eroded Luvisols from arable postglacial soil landscape

## *Abstract*

Soil water retention is frequently described by unique main drying curves measured in the laboratory on intact soil cores. In the field, however, soil pore structure is changing due to swelling and shrinkage, wetting and drying or tillage operations. For erosion-affected arable soils characterized by truncated profiles or due to soil management, water retention dynamics could be even more complex. The objective of this study was to separate shorter-term hysteretic from longer-term seasonal dynamics in field-measured water retention data of eroded Luvisols. Soil water content and matric potential data was from tensiometers and TDR sensors installed at 10, 30, and 50 cm depths of six lysimeter soil monoliths from two sites. For three years (2012-2014), individual drying and wetting periods were identified and fitted with separate parameters of the van Genuchten (VG) retention function. The results confirmed that drying water retention curves were generally steeper than those obtained in the laboratory. Steepness increased and fitted VG parameter values of saturated water content decreased during each season indicating that re-wetting rates successively declined after each intra-seasonal dry/wet cycle. Nevertheless, drying water retention curves returned to a similar level in each spring except for soils of monoliths transferred from a neighboring field where drying water retention tended to increase slightly. Results suggested that water retention dynamics of eroded Luvisols in arable landscapes was affected by continual incorporation of subsoil material in the Ap horizons and crop management practices in addition to hysteresis and seasonal dynamics. The disentangling of dry/wet cycles from time series' of soil water content and matric potential monitored in high temporal resolution was found useful for identifying the processes that were responsible for water retention dynamics and could eventually help improving flow and transport models.

#### 4.1. Introduction

The soil water retention curve (SWRC) describes the constitutive relationship between the water energy potential of the soil water and the amount of water in variably-saturated soils. The SWRC can be determined in the laboratory from soil core samples and in the field by simultaneous measurements of soil water content and suction *in-situ*, and indirectly by using inverse modeling (e.g., Vrugt et al., 2008) or derived from basic soil properties using hydraulic pedotransfer functions (e.g., Pachepsky et al., 2001; Rawls et al., 2003). Differences between laboratory and field measured SWRCs have long been observed (e.g., Flühler et al., 1976); these differences were explained, for instance, by an inadequate representation of larger pores and an easier soil air displacement by water in the laboratory than in the field (e.g., Basile et al., 2003) or by deviations in the soil properties between laboratory and field reflecting the spatial variability of soils (e.g., Morgan et al., 2001; Pachepsky et al., 2001), and by dynamic changes of the soil structure (e.g., Haynes and Naidu, 1998; Horn, 2004; Bronick and Lal, 2005) and the soil hydraulic properties during the year (e.g., Jirků et al., 2013).

The SWRC derived from smaller-scale soil core samples was often found to be insufficient for describing water dynamics at the larger spatial scale of the pedon (e.g., Mertens et al., 2005). Thus, inverse modeling techniques have been proposed that estimate soil hydraulic parameters by optimizing the fit of model predictions to measured field data (e.g., Vrugt et al., 2008). The inverse estimation of soil hydraulic parameters requires information on fluxes at the upper and lower boundaries that can especially be provided by high-resolution weighing lysimeters (e.g., Herbrich and Gerke, 2016; Herbrich et al., 2017). The conditions can be even better determined if lysimeters are equipped with soil water content and matric suction sensors such as in the case of the TERENO (TERrestrial ENVIRONMENTAL Observatories) SoilCan lysimeters (Pütz et al., 2016). The lysimeters are providing data for determining SWRCs used for a better understanding of temporal changes of soil hydraulic properties (e.g., Alletto et al., 2015) when modeling water flow in arable soils.

Water retention dynamics could be related to tillage effects (e.g., Strudley et al., 2008); intra-seasonal changes of soil water retention due to swelling and shrinkage, wetting and drying, tillage or changes in management (e.g., Jirků et al., 2013; Wang et al., 2015; Sandin et al., 2017) could cause the formation of new pores or aggregates and the closing or modification of existing pores by crop roots (Wang et al., 2015). For an intensively cultivated post-glacial landscape as exemplified in the present study, the water retention dynamics could be more complex because of erosion-induced pedogenetic modifications. Such erosion effects were characterized by truncated soil profiles that are experiencing tillage-induced incorporation of subsoil material in the topsoil together with a reduction in the thickness up to

a complete extinction of subsoil horizons (e.g., Van Oost et al., 2006; Rieckh et al., 2012). Arable post glacial soil landscape were characterized by more-or-less eroded soil profiles at steep slopes, exposed hilltops and plateau positions and by colluvial soils in the topographic depressions (Deumlich et al., 2010; Gerke et al., 2010). Rieckh et al. (2012) reported differences in soil drying water retention curves depending on soil structural and pedologic modifications of diagnostic horizon located at various landscape positions. The soil profile truncation was assumed to correspond with the erosion by tillage and water, manifested by the absence of some diagnostic horizon and a reduced thickness of the clay-illuviation (Bt) horizon. Herbrich et al. (2017) observed widely scattered paired values of suction and volumetric water content in eroded Luvisols that deviated from retention curves of soil cores measured in the laboratory. These differences could hardly be explained by a spatial heterogeneity of texture and bulk density (e.g., Gerke and Hierold, 2012).

Other explanations for differences between laboratory and field water retention dynamics may be related to seasonal changes in the wettability as frequently observed for coarser-textured soils (e.g., Doerr et al., 2000) and its temperature dependency (Bachmann et al., 2002; Schneider and Goss, 2011). Soil water repellency was reported to establish during dry conditions in summer and breaking down under moist conditions during winter months (e.g., Täumer et al., 2006; Rye and Smettem, 2015) such that in each spring, drying starts from an initially relatively moist and wettable soil state. However, seasonal changes in soil hydraulic properties may also occur more gradually during the year depending on the drying and wetting history, when assuming that changes in the soil water retention are linked to wettability restrictions. Lourenço et al. (2015) reported similar mechanisms during the dewatering of soil cores although only for sand-clay mixtures. Under field conditions, the suctions of the drying and wetting scanning branches of the SWRC at the same water content can vary by a factor of two or more depending on the dry-wet history (e.g., Canone et al., 2008). Thus, for the main wetting and drying curves a factor of two was suggested, which was sometimes used as default value in numerical models of soil water flow. The modeling of hysteretic water retention was tested in field studies (e.g., Basile et al., 2003; Canone et al., 2008); however, these models were not able to fully reproduce the dynamic behavior of water retention data under *in-situ* conditions (Hannes et al., 2016). Thus, Hannes et al. (2016) suggested grouping observed water retention dynamics in three categories; the hydraulic nonequilibrium, the quasi-nonequilibrium situation, and the soil structure dynamics. These concepts could still need more information on the relations of categories to relevant processes in the field and additional pedological factors that affected soil properties, e.g., manifested in erosion history; for instance, textural changes and profile truncation resulting from tillage erosion.

In this study, we examined the time series' of pairs of suction and water content data measured in characteristic soil horizons of eroded Haplic Luvisol monoliths of high precision weighing lysimeters based on the identification of individual drying and wetting events. The objective was to identify the regular patterns in the water retention non-equilibrium of such field soils and to distinguish between the retention dynamics at daily, seasonal, and annual time scales. The comparison between laboratory soil core and field water retention data and the parameterization of temporal changes in the hysteretic VG water retention function was used to discuss possible effects of soil management, seasonal wettability restrictions, and the soil changes following the erosion history on water retention dynamics of the eroded Luvisol soil monoliths.

## **4.2. Material and Methods**

### **4.2.1 Site description, soils, and lysimeter experiment**

The lysimeter measurements were carried out at the Experimental Field Station Dedelow (53°22'2.45"N, 13°48'10.91"W) of the Leibniz-Centre for Agricultural Landscape Research (ZALF) near Prenzlau in Northeast Germany. The Exp. Station Dedelow is located in the post-glacial hummocky arable soil landscape (50 - 60 m a.s.l.) of the Uckermark region. For the past 20-years period (1992 – 2012), average annual values of rainfall (485 mm), potential evapotranspiration (633 mm), and annual mean air temperature (8.6 °C) were reported in Rieckh et al. (2014). For the actual period (2012 - 2014), annual precipitation rates were 538 mm (2012), 446 mm (2013), and 561 mm (2014), and the annual mean air temperatures in 2 m above soil surface were 7.9°C (2012), 8.0°C (2013), and 9.3°C (2014). The potential evapotranspiration rates were 677 mm (2012), 690 mm (2013), and 862 mm (2014). Weather data were recorded directly at the ZALF station in Dedelow (Verch, 2014).

For the six cylindrical lysimeters, intact soil monoliths with a surface area of 1 m<sup>2</sup> and a height of 1.5 m were extracted in October 2010 from the experimental field in Dedelow (Dd) and a conventionally managed field near the village of Holzendorf (Hd), about 2 km from Dedelow. The lysimeters, three from each site, were arranged around a central below-ground service access pit, in alternating sequence (i.e., Dd\_1, Hd\_2, Dd\_3, Hd\_4, Dd\_5, Hd\_6) according to standard TERENO SoilCan lysimeter design (Pütz et al., 2016). Note that this notation was used to combine the origin of the soils with its specific position in the particular lysimeter arrangement (c.f., Herbrich et al., 2017).

All soils were Haplic Luvisols that differed mainly with respect to the location and thickness of the diagnostic horizons below the plow layer (Ap-horizon). Criteria of sampling were typical

IV Scales of water retention dynamics observed in roded Luvisols from  
arable postglacial soil landscape

arable soil at a mid-slope position. The extraction was as close as possible (about 3 m apart) to each monolith along a row to remain in the area of the same soil type. The depths to the carbonate-containing marl as the soil parent material (eICv- and eICcv-horizons; FAO scheme, IUSS Working Group WRB, 2015) varied between 65 cm for soil monolith Dd\_3 and 115 cm for Hd\_6 (Table 4.1). The E-horizon, characterized by clay eluviation was absent for Dd\_3 and Dd\_5, relatively shallow for Dd\_1 and Hd\_4, and most developed for Hd\_2 and Hd\_6; the thickness of the Bt-horizon was between 30 cm (Hd\_2) and 60 cm (Hd\_6). These data (Table 4.1) reflected differences in the history of erosion-induced soil profile truncation, typically occurring at up- and mid-slope landscape positions; soils at Dd site were generally more truncated than those at Hd site.

*Table 4.1: Physical and chemical soil characteristics of six Luvisols of lysimeters from Dedelow (Dd) and Holzendorf (Hd); soil bulk density,  $\rho_b$ , and porosity,  $\varepsilon$ , 250 cm<sup>-3</sup> core sample; >2 mm, (gravel); sand (2.0 – 0.063 mm); silt (0.063 – 0.002 mm); clay (<0.002 mm); SOC, soil organic carbon; pHCaCl<sub>2</sub>; plant available phosphate, PDL, potassium, KDL, and magnesium MgCaCl<sub>2</sub> (DL: double lactate soluble, after 1:50 extraction for 2 hours with 0.02 M calcium lactate and 0.02 M HCl at pH 3.7).*

Soil	Horizon	Depth [cm]	$\rho_b$ [g·cm <sup>-3</sup> ]	$\varepsilon$ [cm <sup>3</sup> cm <sup>-3</sup> ]	>2 mm	sand	silt	clay	SOC	pH <sub>CaCl<sub>2</sub></sub>	KDL	P <sub>DL</sub>	Mg <sub>CaCl<sub>2</sub></sub>
					-----	[g·kg <sup>-1</sup> ]	-----			[-]	-----	[mg·100g <sup>-1</sup> ]	-----
Dd_1	Ap	0-30	1.53	0.42	24	538	305	157	7.5	6.4	11.1	7.1	10.1
	E+Bt	30-42	1.65	0.38	18	510	341	149	4.4	6.5	4.8	2.9	8.1
	Bt	42-80	1.52	0.43	41	507	299	194	3.5	7.0	4.9	1.4	4.2
	eICv	80-150	1.69	0.36	58	589	293	118	0.0	7.8	2.9	0.5	1.2
Dd_3	Ap	0-35	1.48	0.44	37	475	374	147	7.5	6.4	14.4	6.8	10.0
	Bt	35-70	1.50	0.43	43	n.d.	n.d.	n.d.	n.d.	n.d.	n.d.	n.d.	n.d.
	eICv	70-150	1.51	0.43	19	n.d.	n.d.	n.d.	n.d.	n.d.	n.d.	n.d.	n.d.
Dd_5	Ap	0-30	1.57	0.41	34	468	395	158	7.2	6.5	15.7	8.1	10.5
	Bt	30-65	1.59	0.40	27	n.d.	n.d.	n.d.	n.d.	n.d.	n.d.	n.d.	n.d.
	eICcv1	65-150	1.69	0.36	35	n.d.	n.d.	n.d.	n.d.	n.d.	n.d.	n.d.	n.d.
Hd_2	Ap	0-28	1.66	0.37	40	501	395	104	7.8	5.6	6.2	1.8	7.3
	E	28-50	1.73	0.35	21	n.d.	n.d.	n.d.	n.d.	n.d.	n.d.	n.d.	n.d.
	Bt	50-80	1.62	0.39	16	n.d.	n.d.	n.d.	n.d.	n.d.	n.d.	n.d.	n.d.
	eICcv	80-150	1.74	0.34	29	n.d.	n.d.	n.d.	n.d.	n.d.	n.d.	n.d.	n.d.
Hd_4	Ap	0-30	1.58	0.40	24	576	313	111	7.4	5.1	4.5	1.5	6.8
	E+Bt	30-50	1.62	0.39	16	n.d.	n.d.	n.d.	n.d.	n.d.	n.d.	n.d.	n.d.
	Bt	50-78	1.66	0.37	25	n.d.	n.d.	n.d.	n.d.	n.d.	n.d.	n.d.	n.d.
	eICcv	78-150	1.74	0.34	35	n.d.	n.d.	n.d.	n.d.	n.d.	n.d.	n.d.	n.d.
Hd_6	Ap	0-29	1.60	0.40	24	622	312	66	6.2	4.7	3.8	1.5	5.8
	E	29-55	1.65	0.38	26	584	310	106	2.2	6.1	3.3	1.0	7.0
	Bt 1	55-80	1.67	0.37	22	497	368	135	2.1	6.5	5.1	0.6	6.0
	Bt 2	80-115	1.62	0.39	23	450	324	226	1.9	7.1	5.2	1.7	4.9
	eICcv	115-150	1.73	0.35	34	477	373	15.0	1.2	7.4	3.4	0.2	3.1

Assembly and instrumentation of the lysimeter system was by UMS GmbH (Munich, Germany). In each lysimeter, MPS-1 matrix potential sensors (Decagon Devices Inc.,

Pullman, USA) were installed at 10 cm and TS-1 tensiometers (UMS, Munich, Germany) at 30 and 50 cm depth. Time domain reflectometry probes TDR-100 (Campbell Scientific Ltd, Logan, USA) for measuring the volumetric water content,  $\theta$ , ( $\text{cm}^3 \text{cm}^{-3}$ ) were inserted at 10, 30, and 50 cm depths in short distance to the MPS-1 and TS-1 sensors. In most lysimeter soils, these three depths represented the Ap-, E- or E-Bt, and Bt- horizons, respectively (Table 4.1). In the plow layer (10 cm depth), TDR 100 and MPS\_1 probes with a 60 mm long and 24 mm diameter ceramic cup were installed from the surface so that they could be removed during soil cultivation. In the subsoil, installation was horizontally from the side. Data were recorded in 10-min intervals using DT 80 data loggers (UMS GmbH, Munich, Germany). For frost protection, the water reservoir inside the ceramic cup of TS-1 tensiometers was automatically emptying and refilling the water reservoir inside the ceramic cup depending on a critical soil temperature of  $+2^\circ\text{C}$ . For the present study, all data of the period from January 1<sup>st</sup>, 2012 to December 31<sup>th</sup>, 2014 were analyzed (see Herbrich et al., 2016 for access to data).

The MPS-1 sensors (10 cm depth) measured the soil water suction in a range between 150 and 3500 hPa, while the TS-1 sensors (30 and 50 cm depths) recorded suction values below about 850 hPa. The individual drying or wetting events were identified from the time series' of  $\theta$ - and  $\psi$ -values simply by considering the precipitation data: (i) Wetting was assumed for identified continuous pairs of  $\theta$ - and  $\psi$ -values at or shortly after a precipitation event; (ii) drying was noted during periods without rain and infiltration. The original 10-min data were then combined to hourly mean values. From the hourly data of three years (2012-2014), all wetting and drying periods were selected that could be clearly identified.

Laboratory soil water retention data were obtained from  $250 \text{ cm}^3$  intact soil cores (diameter: 80 mm; height: 50 mm) with the evaporation method using the HYPROP technique with an extended suction range (Schindler et al., 2010); the measurements were carried out by UMS GmbH (Munich, Germany). These soil cores were sampled in two replicates per horizon in vertical direction from the undisturbed soil trench wall next to the pit of the extracted soil monoliths on the same sampling date. Criterion for soil core sampling was to characterize specific soil horizons not a specific soil depth. Thus, the core sample depths (i.e., referring to center of a horizon) did not always match with that of the tensiometer and TDR sensor installations (10, 30, and 50 cm). In the HYPROP procedure, soil water retention data was calculated from the water loss during evaporation and the mean values of two mini-tensiometer in the suction range between 1 and 22000 hPa and analyzed (see section 2.2) with the HYPROP data evaluation software package (UMS GmbH, Munich, Germany).

For each lysimeter and soil horizon, disturbed soil material and  $100 \text{ cm}^3$  soil cores (diameter: 50 mm; height: 50 mm) in two replicates were sampled near the locations of the

250 cm<sup>3</sup> core sampling along the same trench on the same sampling date in October 2010. The mixed samples were air-dried, sieved to pass 2 mm, and used for texture and soil chemical analyses. Soil bulk density,  $\rho_b$  (g cm<sup>-3</sup>), was gravimetrically determined on the 100 cm<sup>3</sup> soil cores after oven-drying at 105 °C for >24 hours. The porosity,  $\varepsilon$ , of the soil (cm<sup>3</sup> cm<sup>-3</sup>) was calculated as:

$$\varepsilon = 1 - \frac{\rho_b}{\rho_s} \quad [4.1]$$

where  $\rho_s$  is the particle density (g cm<sup>-3</sup>); here a value of  $\rho_s = 2.64$  g cm<sup>-3</sup> for quartz was assumed. Information on physical and chemical soil properties and crop and soil management was reported in Herbrich et al. (2017) until March 2014. In the period beginning April 2014, Persian clover (*Trifolium resupinatum* L.) and then winter wheat (*Triticum aestivum* L.) were cultivated.

#### 4.2.2 Water retention model and parameter estimation

The well-known unimodal water retention function of van Genuchten (VG) was applied to describe the field and laboratory water retention data as:

$$\theta(\psi) = \theta_r + \frac{\theta_s - \theta_r}{(1 + \alpha\psi^n)^{1 - \frac{1}{n}}} \quad [4.2]$$

where  $\theta_s$  is the saturated and  $\theta_r$  the residual water content parameter (cm<sup>3</sup> cm<sup>-3</sup>),  $\alpha$  (cm<sup>-1</sup>) and  $n$  are empirical parameters and the suction,  $\psi$  (hPa, here in the unit of (1/0.981=1.0194) cm water column), is restricted to positive values ( $0 < \psi < \infty$ ). For characteristic soil horizons (Ap, E, E+Bt, and Bt) of the eroded Luvisols, the VG parameters in Eq. 2 were optimized by fitting the retention function to field and laboratory data using the non-linear optimization routine of the program RETC (van Genuchten et al., 1991) version 6.02 from 2009 ([www.pc-progress.com](http://www.pc-progress.com)).

The laboratory hydraulic parameters (Table 4.2) obtained with HYPROP from data of the 250 cm<sup>3</sup> core samples (see above) were used as initial estimates for the optimization of the field water retention. Parameterization was carried out in the following steps:

1. The VG parameters  $\theta_s$ ,  $n$ , and  $\alpha$  were first estimated for each of the six lysimeter soils and the three depths (10, 30, and 50 cm) using data of the **initial drying (ID)** periods; values of  $\theta_r$  were fixed to those obtained with HYPROP on soil cores to reduce the number of parameters to be fitted. With “initial drying”, we defined the first consistent drying period in each spring of 2012-2014 starting at relatively high soil water contents (Table 4.2). Missing water content data prevented the identification of ID periods for 30 and 50 cm depth in 2013.



IV Scales of water retention dynamics observed in roded Luvisols from  
arable postglacial soil landscape

2. For selected drying periods in 2013 and 2014 (Tables A1 and A2), the VG parameters  $\theta_s$  and  $\alpha$  were fitted to **intra-seasonal drying** retention data for 10 and 30 cm depth (Dd\_1) and 10 cm depth (Hd\_6) (Table 4.3); the values of  $\theta_r$  and  $n$  were fixed to those of the ID curves obtained in Step 1. By fixing the  $n$ -value, a constant relative pore size distribution was assumed and the intra-seasonal dynamic was described by varying the effectively wettable porosities ( $\theta_s$ ) and the air-entry values ( $h_a$ , the inverse of parameter  $\alpha$ ).

*Table 4.2: Fitted parameters of the van Genuchten soil water retention model ( $\theta_s, \theta_r, \alpha, n$ ) and “air-entry suction” value,  $h_a$ , for lysimeter soils Dd\_1- Hd\_6 for HYPROP-fitted lab-measured soil core (Lab) and RETC-fitted field-measured (Field) initial drying water retention data (2012 to 2014); the goodness of fit to water retention data is indicated by the sum of squared deviations (SSQ) for RETC-fitted parameters and root mean squared error (RMSE) for HYPROP-fitted parameters.*

	Lab							Field						
	Depth [cm]	Soil horizon	$\theta_s$ [cm <sup>3</sup> cm <sup>-3</sup> ]	$\theta_r$ [cm <sup>-3</sup> ]	$\alpha$ [cm <sup>-1</sup> ]	$h_a$ [cm]	$n$ [-]	RMSE	$\theta_s$ [cm <sup>3</sup> cm <sup>-3</sup> ]	$\theta_r$ [cm <sup>-3</sup> ]	$\alpha$ [cm <sup>-1</sup> ]	$h_a$ [cm]	$n$ [-]	SSQ
Dd_1	10	Ap	0.419	0.02	0.035	28.6	1.305	0.005	0.236	0.02	0.003	333.3	1.276	0.002
	30	E+Bt	0.364	0.01	0.025	40.0	1.297	0.003	0.294	0.01	0.012	83.3	1.147	0.02
	50	Bt	0.377	0.04	0.073	13.7	1.269	0.004	0.297	0.04	0.012	83.3	1.18	0.03
Dd_3	10	Ap	0.43	0.0	0.051	19.6	1.263	0.006	0.292	0.0	0.006	166.7	1.248	0.003
	30	Bt	0.432	0.0	0.052	19.2	1.225	0.007	0.28	0.0	0.024	41.7	1.15	0.01
	50	Bt	0.432	0.0	0.052	19.2	1.225	0.007	0.312	0.0	0.051	19.6	1.118	0.01
Dd_5	10	Ap	0.38	0.0	0.048	20.8	1.248	0.004	0.258	0.0	0.005	200	1.204	0.01
	30	Bt	0.382	0.0	0.050	20.0	1.231	0.005	0.306	0.0	0.034	294	1.146	0.02
	50	Bt	0.382	0.0	0.050	20.0	1.231	0.005	0.302	0.0	0.011	90.9	1.221	0.008
Hd_2	10	Ap	0.37	0.0	0.011	90.9	1.321	0.009	0.271	0.0	0.003	333.3	1.264	0.01
	30	E	0.353	0.01	0.013	76.9	1.286	0.002	0.278	0.01	0.015	66.7	1.148	0.02
	50	Bt	0.388	0.01	0.017	58.8	1.226	0.004	0.336	0.01	0.019	52.6	1.097	0.01
Hd_4	10	Ap	0.384	0.0	0.028	35.7	1.301	0.004	0.223	0.0	0.007	142.9	1.214	0.01
	30	E+Bt	0.376	0.03	0.026	38.5	1.353	0.002	0.286	0.03	0.011	90.9	1.207	0.02
	50	Bt	0.376	0.01	0.022	45.5	1.246	0.002	0.296	0.01	0.016	62.5	1.177	0.03
Hd_6	10	Ap	0.41	0.0	0.066	15.2	1.269	0.005	0.32	0.0	0.008	125.0	1.245	0.02
	30	E	0.355	0.01	0.029	34.5	1.285	0.004	0.287	0.01	0.026	38.5	1.135	0.02
	50	Bt	0.364	0.0	0.035	28.6	1.197	0.002	0.323	0.0	0.075	13.3	1.153	0.01

3. For selected wetting periods in 2014 (Tables A1 and A2), the VG parameters  $\theta_s$ ,  $\theta_r$ , and  $\alpha$  were fitted to **intra-seasonal wetting** retention data from Dd\_1 and Hd\_6 at 10 cm depths (Table 4.4); here, the VG parameters of the ID curves from Step 1 were used as initial estimates and the ID  $n$ -values were fixed.

4. For each Ap-horizon of the six lysimeter soils, **maximum drying (MD)** periods were identified as drying periods starting from the largest observed soil water content in a year (Table A3). The VG parameters  $\theta_s$  and  $\alpha$  were fitted to MD retention data. For each of the Dd lysimeters, the data for all three years could be fitted with a single MD curve. For Hd, separate MD curves were fitted to data of each year (Table 4.5). A zero  $\theta_r$  -value was assumed to simplify inter-annual comparisons; the  $n$ -value for all Dd soils was fixed to that of Dd\_1 from Step 1, and the  $n$ -value for Hd soils was fixed to that of Hd\_6 from Step 1 (Table 4.2). For all soils, values of  $\theta_s$  were fitted to MD data of 2012 (using  $\theta_s$  of ID as initial estimates) and then kept fixed for the two following years. For the 30 cm depth, MD retention data sets could only be identified for Hd\_6 soil; the fitting was as described for the 10 cm depth except that  $n$  was fixed to a value of 1.295 from MD in 2012.

*Table 4.3: Parameters of the van Genuchten (VG) soil water retention function ( $\theta_s, \theta_r, \alpha$ , and  $n$ ) fitted to intra-seasonal drying retention data of lysimeter soils Dd\_1 and Hd\_6 from 10 cm depth (Ap horizon) and 30 cm (E+Bt horizon) for 2013 and 2014; VG parameters correspond to graphs in Figs. 7 and 8; the goodness of fit to water retention data is indicated by the sum of squares (SSQ); the drying periods correspond to numbers 8-11 (2013) and 11-14 (2014) for Dd\_1 in 10 cm and 30 cm depths in Table A1 and 9,11-13 (2013) and 25 (2014) for Hd\_6 in Table A2 in the Appendix.*

Lysimeter & depth	Drying Period	Date	$\theta_s^\dagger$ [cm <sup>3</sup> cm <sup>-3</sup> ]	$\theta_r$ [cm <sup>3</sup> cm <sup>-3</sup> ]	$\alpha$ [cm <sup>-1</sup> ]	$n^\dagger$ [-]	SSQ
Dd_1 10 cm	D1	07/07-07/12	0.236	0.017	0.0032	1.276	0.0020
	D2	08/24-08/31	0.144	0.017	0.0005	1.276	0.0030
	D3	09/28-10/04	0.181	0.017	0.0011	1.276	0.0010
	D4	07/31-08/04	0.151	0.017	0.0004	1.276	0.0001
Dd_1 30 cm	D1	04/19-05/23	0.304	0.018	0.040	1.114	0.0047
	D2	08/06-08/14	0.233	0.018	0.012	1.114	0.0065
	D3	08/24-09/01	0.258	0.018	0.017	1.114	0.0002
	D4	06/12-06/30	0.236	0.018	0.005	1.114	0.0002
Hd_6 10 cm	D1	06/03-06/10	0.290	0.0	0.0021	1.288	0.004
	D2	07/03-07/12	0.255	0.0	0.0012	1.288	0.0010
	D3	08/21-09/02	0.155	0.0	0.0007	1.288	0.0011
	D4	08/03-08/07	0.155	0.0	0.0005	1.288	0.0090
	D'14	06/17-06/30	0.212	0.0	0.0015	1.288	0.006

<sup>†</sup>values of  $\theta_r$  and  $n$  were fixed at those obtained from initial drying data (D1)

The goodness-of-fit for optimization of soil hydraulic parameters from a number ( $i = 1, \dots, N$ ) of lab-measured retention data was expressed by HYPROP in terms of the Root-Mean-Square-Error (RMSE):

$$\text{RMSE} = \sqrt{\frac{\sum_{i=1}^N (\theta_i^{\text{sim}} - \theta_i)^2}{N}} \quad [4.3]$$

for optimization of field water retention data (at times  $i = 1, \dots, N$ ) from drying or wetting cycles, the goodness-of-fit was expressed in the RETC-software in terms of the Sum of Squared deviations (SSQ):

$$\text{SSQ} = \sum_{i=1}^N (\theta_i^{\text{sim}} - \theta_i)^2 \quad [4.4]$$

where  $\theta_i$  is the observed water content and  $\theta^{\text{sim}}$  is the water content predicted by the optimized VG function; a direct comparison of field and laboratory data optimization was based on the RMSE.

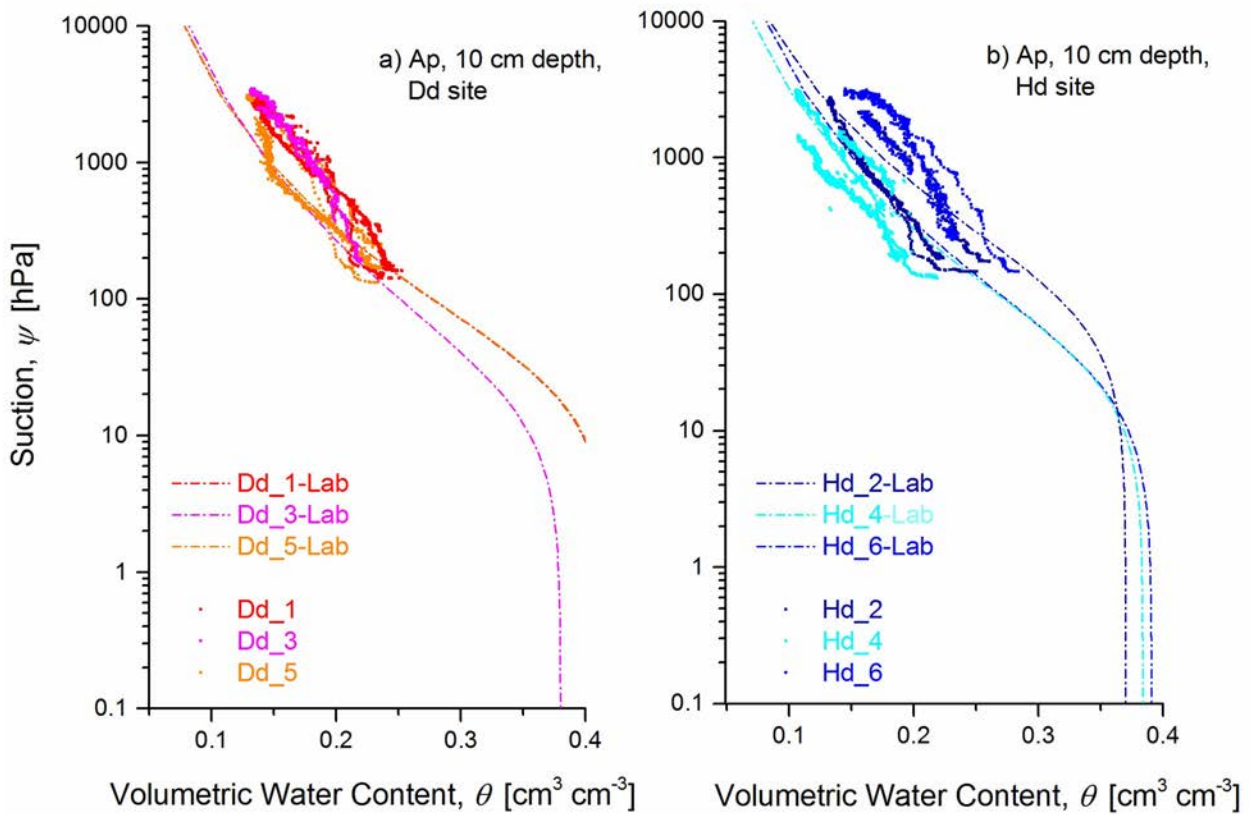


Figure 4.1: Comparison of soil water retention data of 10 cm depth (Ap-horizon) obtained by field measurements in lysimeters for soil monoliths a) from Dedelow site (Dd, left - reddish colored) and b) from Holzendorf site (Hd, right - bluish colored) for initial drying (ID) periods (April, 2012; June, 2013; April, 2014); dotted lines are lab retention data obtained using HYPROP for lysimeters Dd\_1, Hd\_2, Dd\_3, Hd\_4, Dd\_5, Hd\_6.

## 4.3 Results

### 4.3.1 Field and laboratory soil water retention

The laboratory drying water retention curves obtained from 250 cm<sup>3</sup> soil cores differed from the initial drying (ID) field water retention data with respect to slope and water contents in the observed suction ranges (Figs. 4.1 - 4.3). These differences were relatively small for 10 cm depth (Ap-horizon, Fig. 4.1) for both Hd and Dd soils; differences especially of the slopes were larger for the 30 cm (E- and E+Bt- horizons, Fig. 4.2) and the 50 cm depths (Bt-horizon, Fig. 4.3). The slopes of Ap-horizon ID retention data were relatively similar while the measured values of  $\theta$  varied in the three years and for the three lysimeters at the same suction (300 hPa) in a smaller range for Dd (i.e., 0.18 - 0.23 cm<sup>3</sup>cm<sup>-3</sup>, Fig. 4.1a) as compared to Hd (i.e., 0.15 - 0.27 cm<sup>3</sup>cm<sup>-3</sup>, Fig. 4.1b). The variations of ID retention data from 30 cm depth in the years 2012 and 2014 (E- and E/Bt-horizon); however, were smaller between the Hd soils (Fig. 4.2b) as compared to Dd soils (Fig. 4.2a) and those of the Ap-horizon. Note that each retention data point represented a pair of corresponding hourly mean suction and water content values.

*Table 4.4: Parameters of the van Genuchten (VG) hydraulic function, optimized to describe the observed retention data of wetting periods in 2014 that corresponding with no. 12, 14, 16, 21 in Table A1 and 19, 23, and 24 in Table A2 in 10 cm soil depth (Ap horizon); the VG parameters of the initial drying water retention (Table 4.4) were used as initial estimates; VG parameter  $n$  was fixed during the optimization, the SSQ-values show goodness of fit; VG parameters correspond with graphs in Figs. 11.*

Date		$\theta_s$	$\theta_r$	$\alpha$	$h_a$	$n^\dagger$	SSQ
		[cm <sup>3</sup> cm <sup>-3</sup> ]		[cm <sup>-1</sup> ]	[cm]	[-]	
Dd_1 10 cm	Dd-D1	0.23	0.0	0.0019	769.2	1.276	0.0018
	Dd-W1	0.2	0.125	0.021	714.6	1.276	0.0001
	Dd-W2	0.199	0.121	0.041	24.4	1.276	0.0001
	Dd-W3	0.151	0.059	0.0022	454.5	1.276	0.0004
	Dd-W4	0.204	0.113	0.0042	238.1	1.276	0.0002
Hd_6 10 cm	Hd-D1	0.29	0.0	0.0021	476.2	1.288	0.004
	Hd-W1	0.228	0.054	0.0039	256.4	1.288	0.0005
	Hd-W2	0.204	0.089	0.147	6.8	1.288	0.0002
	Hd-W3	0.116	0.1	0.068	14.5	1.288	0.0001

<sup>†</sup>values of  $n$  were fixed at those obtained from initial drying data (D1)

Strong seasonal dynamics in the field water retention was observed in all six lysimeter soils and in each of the 3-years (2012-2014): For the Ap-horizon of soils Dd\_1 (Fig. 4.4) and Hd\_6 (Fig. 4.5), for example, wetting and drying periods were indicated by numbers (i.e., Fig. 4.4: Dd\_1-Ap, numbers 4, 9, 10, 11, 16, and 18 refer to the drying and wetting periods listed in the Appendix Table A1; Fig. 4.5: Hd\_6-Ap, numbers 9, 11, 12, 15, 21, and 27 refer to those in Table A2). The field water retention data were widely scattered around the laboratory drying curves in the present suction range (Figs. 4.4 and 4.5). The water content values at a suction of about 1000 hPa for Dd\_1 ranged between 0.13 and 0.18  $\text{cm}^3\text{cm}^{-3}$  over the 3-years period (Fig. 4.4); the range was even larger for lower suction values ( $<1000$  hPa). For Hd\_6 (Fig. 4.5), water contents at a suction of 1000 hPa ranged between 0.13 and 0.24  $\text{cm}^3\text{cm}^{-3}$ .

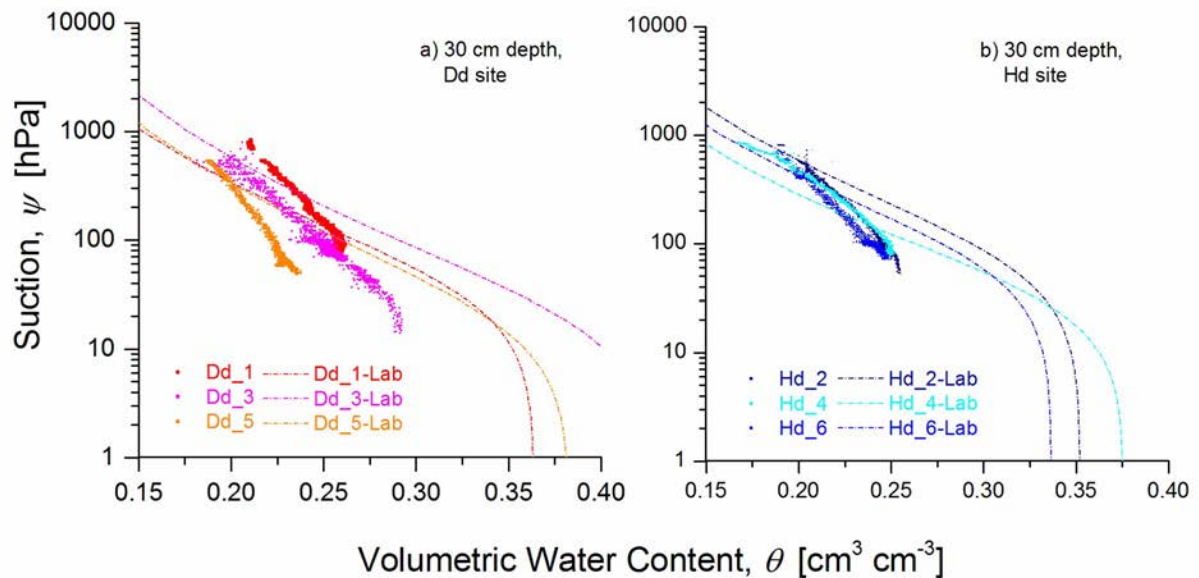


Figure 4.2: Comparison of soil water retention data of 30 cm depth (E-, Bt-horizon) obtained by field measurements in lysimeters for soil monoliths a) from Dedelow site (Dd, left - reddish colored) and b) from Holzendorf site (Hd, right - bluish colored) for initial drying periods (2012; 2014)\*; dotted lines are lab retention data obtained using HYPROP for lysimeters Dd\_1, Hd\_2, Dd\_3, Hd\_4, Dd\_5, Hd\_6. \*in 2013, the retention data did not allow to identify initial drying periods because of a lack of volumetric water contents using TDR probes.

At 30 cm depth (Fig. 4.6), the water content range at 300 hPa was about 0.20-0.26  $\text{cm}^3\text{cm}^{-3}$  for Dd\_1 (Fig. 4.6a) and about 0.12-0.24  $\text{cm}^3\text{cm}^{-3}$  for Hd\_6 (Fig. 4.6b). At 50 cm depth (not shown here), the scatter of the retention data was relatively narrow for Dd\_1 and again relatively large for Hd\_6.

The fitting of the VG model to field measured ID water retention data from lysimeters using RETC yielded mostly smaller values of  $\theta_s$  (0.22 to 0.34  $\text{cm}^3\text{cm}^{-3}$ ) and  $\alpha$  (0.002 to 0.075  $\text{cm}^{-1}$ ) as compared to those obtained with HYPROP ( $\theta_s$ : 0.35 to 0.43  $\text{cm}^3\text{cm}^{-3}$ ;  $\alpha$ : 0.011 to 0.073  $\text{cm}^{-1}$ ) (Table 4.2). For the E-horizon (30 cm) and the Bt-horizon (50 cm), steeper slopes in the field curves as compared to laboratory retention curves were reflected by mostly smaller values of VG-parameter  $n$  for the field curves (i.e.,  $n \approx 1.2$ ). The RMSE values (Table 4.2) indicating the goodness-of-fit were relatively small and in a similar range for laboratory and field curves.

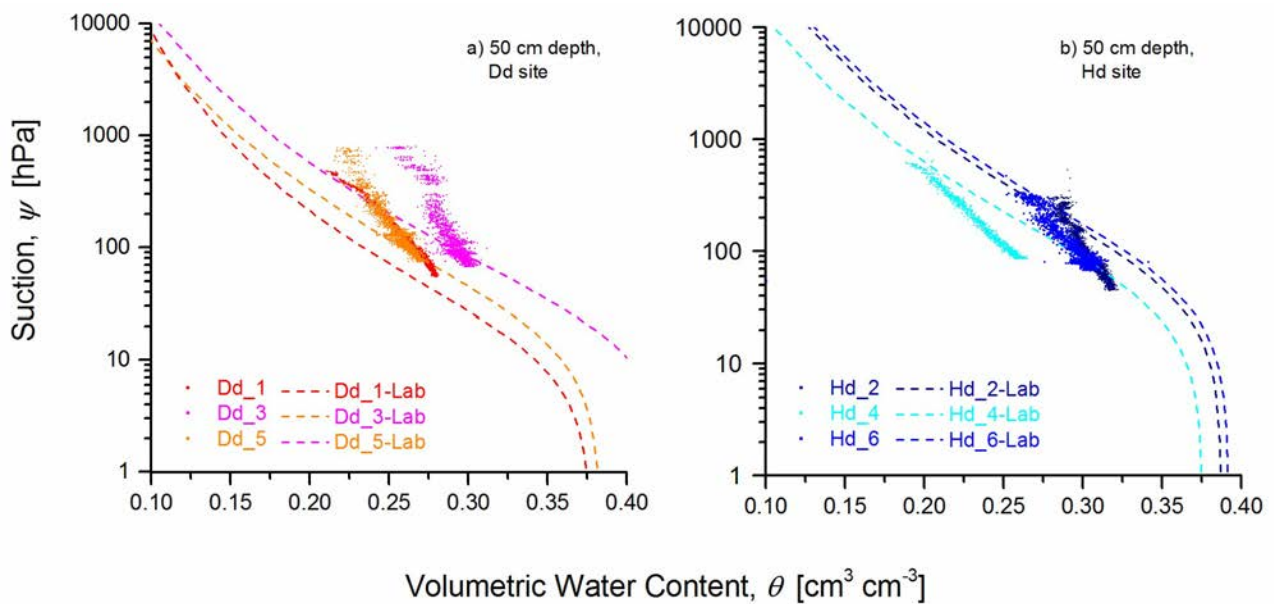


Figure 4.3: Comparison of soil water retention data of 50 cm depth (Bt-horizon) obtained by field measurements in lysimeters for soil monoliths a) from Dedelow site (Dd, left - reddish colored) and b) from Holzendorf site (Hd, right - bluish colored) for initial drying periods (2012; 2014)\*; dotted lines are lab retention data obtained using HYPROP for lysimeters Dd\_1, Hd\_2, Dd\_3, Hd\_4, Dd\_5, Hd\_6. \*in 2013, the retention data did not allow to identify initial drying periods because of a lack of volumetric water contents using TDR probes.

IV Scales of water retention dynamics observed in roded Luvisols from arable postglacial soil landscape

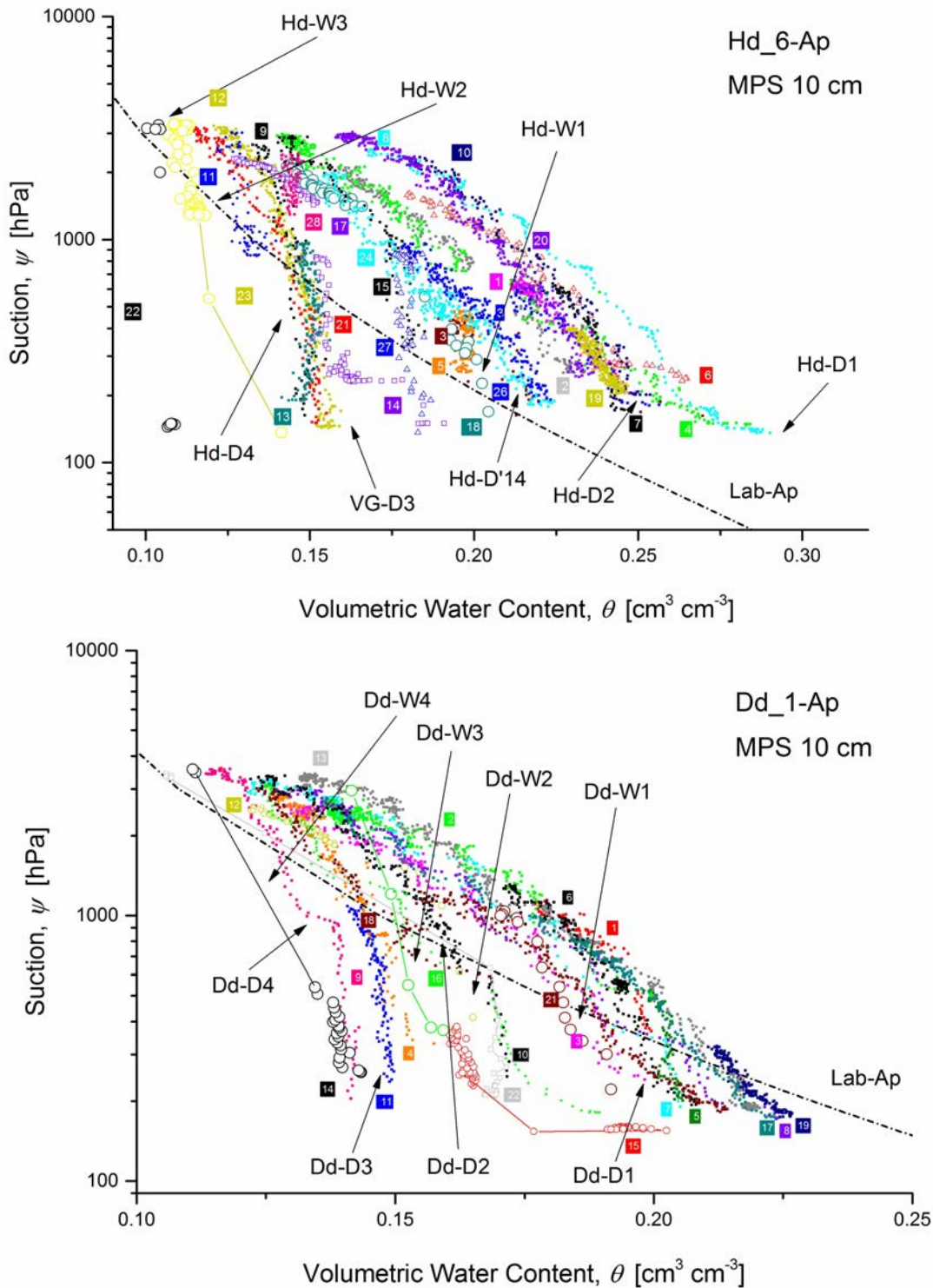
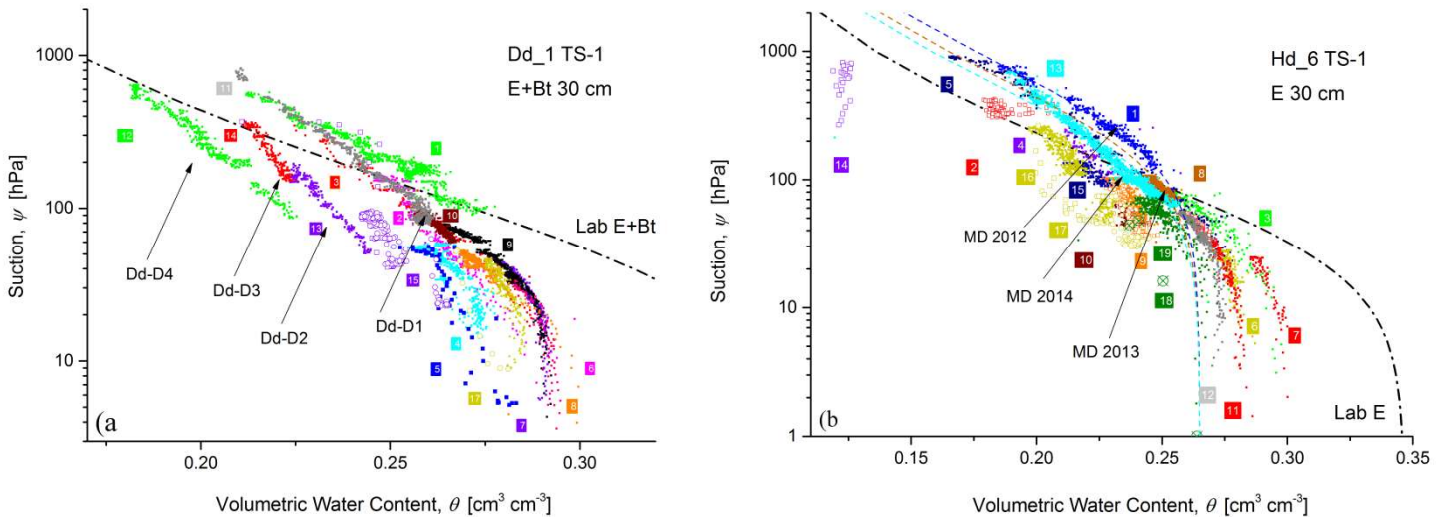


Figure 4.4 and 4.5: Soil water retention data of the 10 cm depth (Ap-horizon) of lysimeter Dd\_1/Hd\_6 for selected periods between January 1, 2012 to December 31, 2014; open squares indicate data points of wetting and solid squares that of drying periods; the dotted lines represent lab retention curves using HYPROP for core samples from Ap-horizon of Dd\_1/Hd\_6; VG-D1 to -D4 are selected drying periods corresponding to Fig. 7 and 8; numbers indicate the selected periods given in Appendix A1 and A2.

#### IV Scales of water retention dynamics observed in roded Luvisols from arable postglacial soil landscape

The data in Figs. 4.6 show that more drying (solid symbols) than wetting periods (open symbols) could be identified. Most of the drying retention data series' within a season tended to approach an increasingly steeper slope with similar shapes, while the wetting branches appeared mostly unconnected from the observed drying data. At the beginning of each subsequent drying period within a season, the drying started from a successively lower water content level. For example for Hd\_6 (Fig. 4.5; Table 4.3), the water contents at about 150 hPa were about  $0.13 \text{ cm}^3\text{cm}^{-3}$  smaller for drying period D4 (July 2013; about  $0.15 \text{ cm}^3\text{cm}^{-3}$ ) than for the earlier period D1 (June 2013; about  $0.28 \text{ cm}^3\text{cm}^{-3}$ ) at the beginning of the season. For the Dd\_1 soil, at 30 cm depth (Fig. 4.6a), the field water retention at about 100 hPa ranged from  $0.26 \text{ cm}^3\text{cm}^{-3}$  for drying period D1 (April 2013) to  $0.22 \text{ cm}^3\text{cm}^{-3}$  for D4 (Sept. 2013) and between  $0.20 \text{ cm}^3\text{cm}^{-3}$  for D1 (July 2013) to  $0.14 \text{ cm}^3\text{cm}^{-3}$  for D4 (Sept. 2013) at 10 cm depth (Fig. 4.4).



*Figure 4.6: Soil water retention data of the 30 cm depth (E, E+Bt-horizon) of lysimeter Dd\_1 a) and Hd\_6 for selected periods between January 1, 2012 to December 31, 2014; open squares indicate data points of wetting and solid squares that of drying periods; the dotted lines represent lab retention curves using HYPROP for core samples from Ap-horizon of Dd\_1 and Hd\_6; numbers indicate the selected periods given in Appendix A1 and A2.*

The data from Hd\_6 at 30 cm depth (Fig. 4.6b) were mostly scattered around a suction of 100 hPa and water contents of around  $0.25 \text{ cm}^3\text{cm}^{-3}$ ; some exceptional data points were related to wetting periods (no. 14 and no. 2 in Fig. 4.6b). At 50 cm depth, the field water retention data were even less scattered and relatively close to the laboratory drying curve for values  $>50 \text{ hPa}$  for Dd\_1 and  $>30 \text{ hPa}$  for Hd\_6 (data not shown). The variations in the water



## IV Scales of water retention dynamics observed in roded Luvisols from arable postglacial soil landscape

retention decreased with depth because of the smaller numbers and the reduced amplitudes of drying and wetting periods in the subsoil (Figs. 4.6) as compared to those at 10 cm depth (Figs. 4.4 and 4.5).

*Table 4.5: Parameters of the van Genuchten water retention model for the Ap-horizons (10 cm soil depth) fitted for maximum drying (MD) periods (no. 2, 7, and 13 of Dd\_1 in Table A1; no. 1, 9, and 21 of Hd\_6 in Table A2; Hd\_2-Dd\_5 periods see Table A3); lysimeters filled with soil monoliths from Dedelow (Dd) and Holzendorf (Hd); VG parameters are corresponding to graphs in Fig. 4.9 and Fig. 4.6b (no. 1, 8, and 13)*

Soil Depth	Year	Date (From – To)	$\theta_s$ [cm <sup>3</sup> cm <sup>-3</sup> ]	$\theta_r$ [cm <sup>3</sup> cm <sup>-3</sup> ]	$\alpha$ [cm <sup>-1</sup> ]	$n$ [-]	SSQ
Dd_1 10cm	2012	04/28 - 05/06	0.23	0.0	0.0019	1.276	0.018
	2013	06/05 - 06/11					
	2014	04/23 - 05/11					
Dd_3 10cm	2012	03/17 05/04	0.283	0.0	0.0040	1.276	0.024
	2013	05/21 05/26					
	2014	06/17 07/08					
Dd_5 10cm	2012	04/17 04/24	0.24	0.0	0.0021	1.276	0.097
	2013	10/21 10/31					
	2014	06/10 07/04					
Hd_2 10 cm	2012	04/16 - 05/03	0.272	0.0	0.0027	1.288	0.005
	2013	05/17 - 06/26	0.272	0.0	0.0055	1.288	0.015
	2014	06/15 - 07/12	0.272	0.0	0.0081	1.288	0.009
Hd_4 10 cm	2012	08/10 - 09/24	0.221	0.0	0.0028	1.288	0.014
	2013	06/05 - 06/18	0.221	0.0	0.0039	1.288	0.002
	2014	04/20 - 05/19	0.221	0.0	0.0068	1.288	0.019
Hd_6 10 cm	2012	04/17 - 04/24	0.290	0.0	0.0039	1.288	0.004
	2013	06/03 - 06/10	0.290	0.0	0.0021	1.288	0.016
	2014	04/25 - 05/11	0.290	0.0	0.0029	1.288	0.058
Hd_6 30 cm	2012	04/18 - 05/05	0.265	0.0	0.0035	1.295	0.002
	2013	04/13 - 05/13	0.265	0.0	0.0045	1.295	0.001
	2014	03/21 - 05/24	0.265	0.0	0.0053	1.295	0.008

### 4.3.2 Drying periods and parameterization

For the parameterization of the retention dynamics (Figs. 4.7 and 4.8), only the most characteristic drying events of the 2013 and 2014 vegetation periods were selected. These periods were indicated in Figs. 4-6 by arrows and with Dd-D2, -D3, -D4 (see no. 8 - 11 of Dd\_1-Ap in Table A1 and no. 9 –12 of Hd\_6-Ap in Table A2). In comparison with fitted parameters of initial drying curves (i.e., -D1), the values of  $\theta_s$  of the Ap-horizons (Table 4.3) for subsequent drying periods (i.e., -D2, -D3, -D4) decreased during the season (Figs. 4.7

and 4.8). Similar as of  $\theta_s$ , the fitted values of  $\alpha$  mostly decreased for subsequent drying periods for 10 cm (Hd and Dd) and 30 cm (Dd) depths (Table 4.3). Note that Dd\_1 and Hd\_6 represented the most contrasting soils with respect to erosion induced soil profile truncation. For the 30 cm depth, longer drying periods could mainly be identified in soil of Dd\_1. Here (Table 4.3), water retention decreased stepwise in terms of  $\theta_s$  by about  $0.06 \text{ cm}^3 \text{ cm}^{-3}$  from May to September 2013.

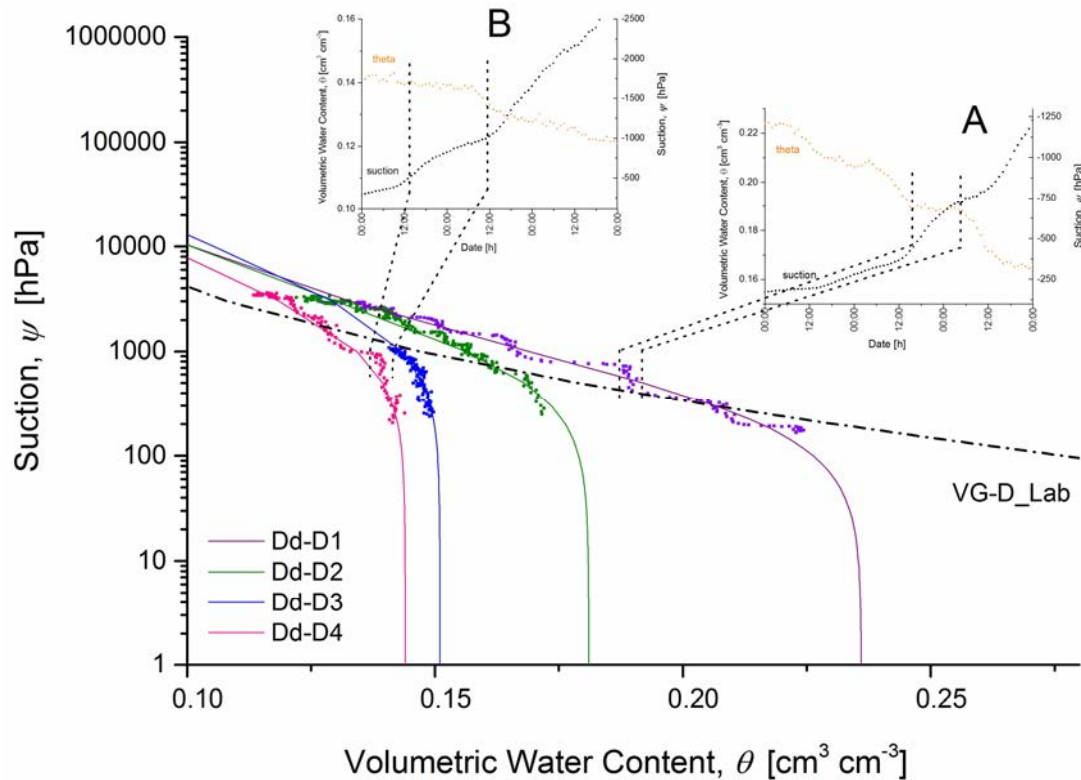


Figure 4.7: Fitted soil water retention curves and as compared to lysimeter-measured retention data for drying events of selected periods in 2013 for the 10 cm soil depth (Ap horizon) of Dd\_1 using the van Genuchten (1980) water retention model; selected periods are corresponding to numbers 8 to 11 in Appendix A1.

In the Ap-horizon, the retention data of the maximum drying (MD) periods were very similar for Dd soils but differed considerably for Hd soils between the 3 years (Fig. 4.9). Especially large differences in MD data were found for Hd\_2 and Hd\_4. Note that the VG retention curves for Hd soils were fitted separately to data from each year by assuming the same value of  $\theta_s$  for each soil (Table 4.5). In each year, the MD water retention returned to a relatively similar level (Fig. 4.9) for Dd soils despite the different crops (i.e., Sudan grass in 2012, Lucerne in 2013, Persian clover in 2014). For the Ap horizon of the HD\_2 and Hd\_4

soils, the highest water contents in the observation range (100 - 3500 hPa) were observed in 2012 and the fitted  $\alpha$ -values increased between 2012 and 2014 (Table 4.5) when keeping  $\theta_s$  and  $n$  fixed at values of 2012. A similar tendency of increasing MD  $\alpha$ -values between 2012 and 2014 was observed for the 30 cm soil depth (E horizon) of lysimeter Hd\_6 (Table 4.5).

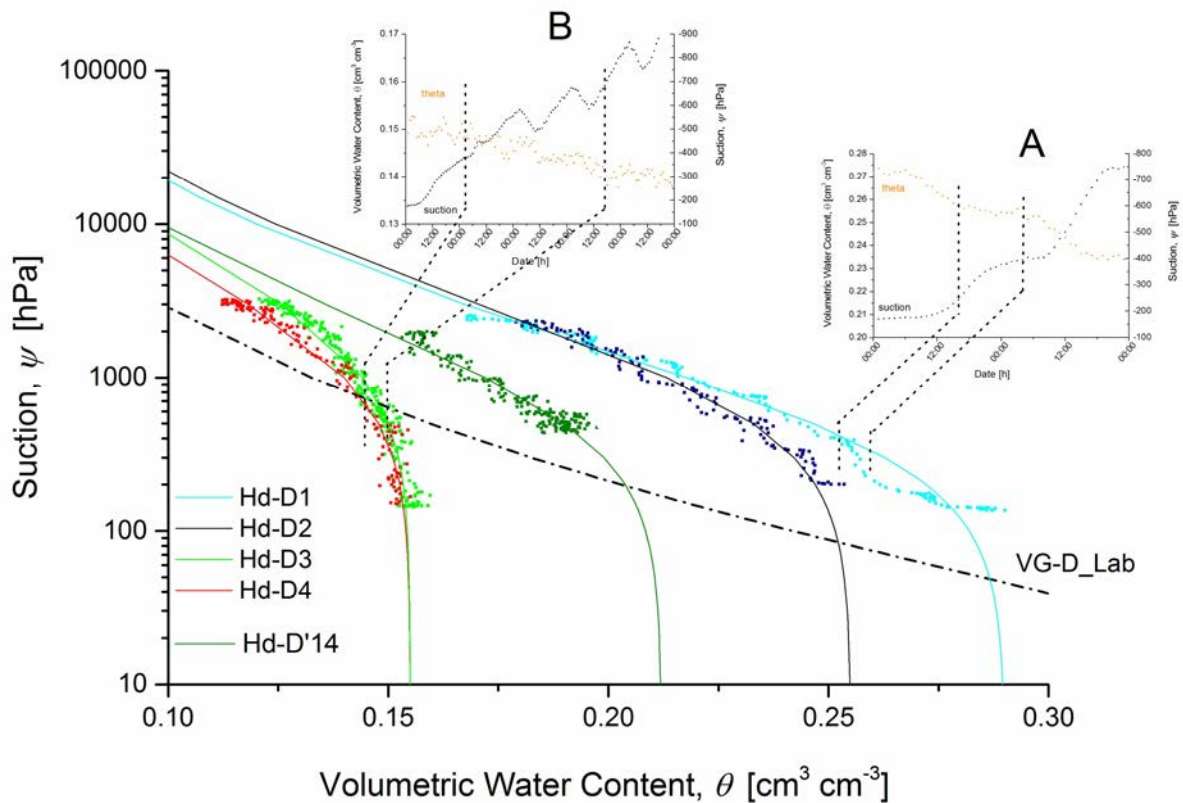


Figure 4.8: Fitted soil water retention curves and as compared to lysimeter-measured retention data for drying events of selected periods in 2013 for the 10 cm soil depth (Ap horizon) of Hd\_6 using the van Genuchten (1980) water retention model; selected periods are corresponding to numbers 9, 11 to 13, 25 in Appendix A2.

IV Scales of water retention dynamics observed in roded Luvisols from arable postglacial soil landscape

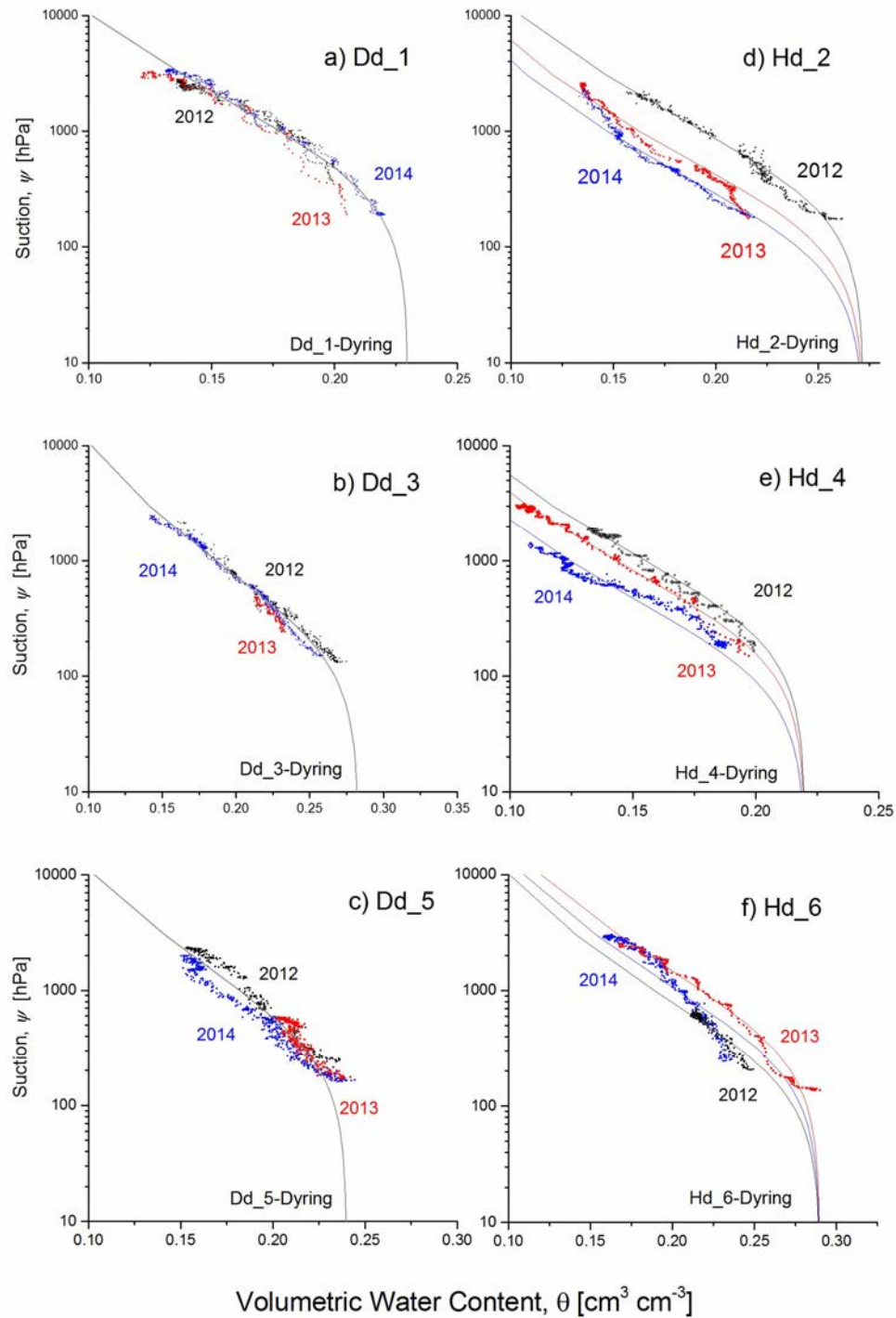


Figure 4.9: Soil water retention data of lysimeters filled with soil monoliths from Dedelow (Dd) and Holzendorf (Hd) for a) Dd\_1, d) Hd\_2, b) Dd\_3, e) Hd\_4, c) Dd\_5, f) Hd\_6 for years 2012, 2013 and 2014 for selected drying periods with highest values of the volumetric water content for a given suction obtained for each year (e.g. 2012, Jan to Dec); selected periods of Dd\_1 and Hd\_6 are corresponding to numbers 2, 7, 13 and 1, 9, 26 in Appendix A1 and A2, respectively; selected periods of Dd\_3/5 and Hd\_2/4 are corresponding to Appendix A3.

### 4.3.3 Wetting periods and parameterization

Wetting periods in the soil water retention data (i.e., open symbols in Figs. 4.4 - 4.6) could also be identified from retention data of Dd and Hd soils (i.e., marked by arrows in Figs. 4.4 and 4.5), and were parameterized for selected periods indicated by W1 to W4 (Fig. 4.10). The most characteristic wetting events of the 2014 vegetation period were plotted together with the initial drying curve of Dd\_1 (Fig. 4.10a) and Hd\_6 (Fig. 4.10b). For both Ap horizons of Dd and Hd soils, the data for the wetting periods -W1 to -W3 and -W4 seemed to follow a seasonal trend of decreasing water contents at the same suctions. For each period, the VG model was separately fitted to the wetting data assuming a fixed value of  $n$  obtained from the ID period in 2014 (Table 4.4). The fitting resulted in decreasing values of  $\theta_s$  (0.22-0.16  $\text{cm}^3\text{cm}^{-3}$  for Dd\_1; 0.29-0.12  $\text{cm}^3\text{cm}^{-3}$  for Hd\_6) and revealed a tendency of increasing values of  $\alpha$  for subsequent wetting periods and larger values as compared to drying (Table 4.4).

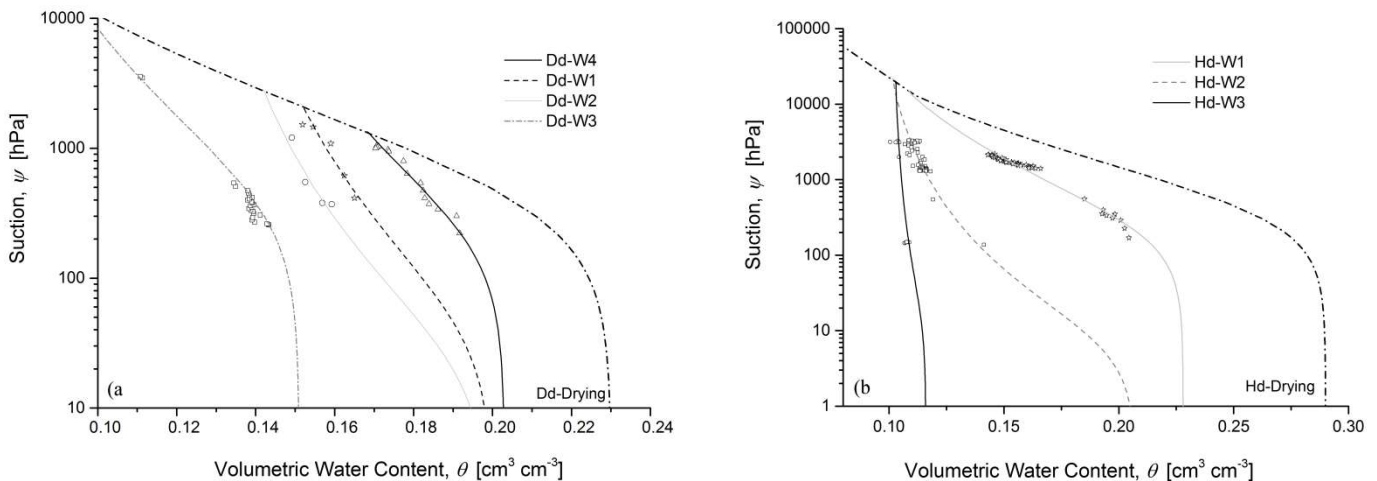


Figure 4.10: Fitted soil water retention curves of wetting events using retention data points in 10 cm depth (Ap-horizon) of lysimeter Dd\_1 a) and Hd\_6 b) for selected periods -W1 to -W4 between January 1, 2014 to December 31, 2014; Fig. corresponds to Table 4.4.

## 4.4. Discussion

### 4.4.1. Differences between laboratory and field water retention

Soil spatial variability at relatively small distances and erosion-effected soil profile modifications (e.g., truncation, topsoil modifications due to plowing) as reported for the bulk density (Gerke and Hierold, 2012) and soil hydraulic properties (Rieckh et al., 2012) could be

one explanation for differences in the soil water retention between laboratory and field data (e.g., Pachepsky et al., 2001; Basile et al., 2003), in combination with entrapped air effects in the field soil and bulk density alteration of laboratory samples (Morgan et al., 2001).

The soil profile truncation that resulted from the combined impact of water and tillage erosion along arable hillslopes (e.g., Van Oost et al., 2006) led to varying thicknesses of soil horizons (Table 4.1). These pedogenetic modifications could have changed textural and structural topsoil properties of the truncated Haplic Luvisol profiles (e.g., Deumlich et al., 2010) and formed the characteristic spatial patterns of soils in the arable hummocky soil landscape. Thus, differences in clay contents between 16 % for Dd\_1 and 7 % for Hd\_6 and differences in bulk densities between 1.4 and 1.7 g cm<sup>-3</sup> (Table 4.1) represented the range of small scale spatial variations within Ap-horizons of the eroded Luvisols in the six lysimeters. Here, the variability could have affected the field retention data since TDR and MPS-1 or tensiometer data did not refer exactly to the same soil volume; and it affected the laboratory-field comparison because soil cores could not be sampled in the lysimeter soil but in an adjacent soil trench. In the long-term, the incorporation of contrasting subsoil material from Bt- (more eroded Luvisols) and E-horizons (less eroded Luvisols) into the Ap-horizon during tillage led to increasing differences in soil texture and bulk density (Table 4.1) as another explanation for spatial differences in soil water retention of Dd\_1 to Hd\_6 (cf. Figs. 4.1 to 4.3) and hydraulic parameters (Table 4.2). Furthermore, the relatively larger differences in water retention data of Hd lysimeter soils as compared to those of Dd could be explained by an initially (in 2010) wider variations of the soil chemical properties (e.g., soil pH and soil organic carbon content) between for Hd than for Dd soils (Table A5). Changes in the soil pH could induce changes in soil structure (Bronick and Lal, 2005), for instance by influencing dispersion or flocculation of clay particles and thus soil aggregation (Haynes and Naidu, 1998) and water retention (e.g., Walker et al., 2005). Furthermore, an increase in soil pH could often result in increasing microbial activity and crop yields, and thereby contribute to increasing soil organic carbon contents and aggregation (Bronick and Lal, 2005).

In addition to effects of soil spatial heterogeneity, the temporal variability of soil properties in the field could have a major impact on soil water retention (e.g., Horn, 2004; Jirků et al., 2013; Sandin et al., 2017). In contrast, the laboratory water retention function represented only a single pore structural state at the time of sampling. Here, core sampling was carried out in autumn after crop harvest under relatively dry and mechanically stable soil conditions. At least within the suction range of the laboratory-field comparisons, it could be assumed that pore structural changes were probably smaller for core samples than for the field soil where the soil structure was affected by cultivation and other conditions.

Steeper slopes of field as compared to laboratory retention curves were already reported to occur especially in the suction range up to 100 hPa (Flühler et al., 1979). Larger water contents in core samples as compared to field soil were attributed to a more controlled displacement of air upon sample saturation under laboratory conditions (e.g., Basile et al., 2003). The field measured water contents at the same suctions were thus smaller as compared to those of the laboratory curves as indicated by the fitted  $\theta_s$ -values (Table 4.2). However, in the higher suction ranges, field  $\theta$ -values were often larger than those of the laboratory values (Figs. 4.1 to 4.6). This discrepancy could lead to contrasting predictions of field water retention by hysteresis models (e.g., Canone et al., 2008).

Nevertheless, the present differences between laboratory and field water retention curves could, at least partly, be explained with a hysteresis concept when assuming the effect of air entrapment. According to Basile et al. (2003), laboratory and field retention curves could belong to the same open hysteresis loop with similar  $n$ - and contrasting  $\alpha$ - and  $\theta_s$ - values. Then the field drying curves represented intermediate scanning branches and the laboratory water retention would more closely match the main drying curve. The present results were in agreement with this hysteretic framework, because the  $\alpha$ -values differed between laboratory and field and the  $\theta_s$ - values for scanning drying (Table 4.3) and wetting curves (Table 4.4) were smaller for the field than for the laboratory data; and as expected when assuming air entrapment, the values of  $n$  were relatively similar or almost identical for data from laboratory and field (Table 4.3). The values of  $\alpha$  (i.e., 0.0005-0.002 cm<sup>-1</sup> for drying (Hd\_6, Table 4.3) and 0.004-0.068 cm<sup>-1</sup> for wetting (Hd\_6, Table 4.5) were tending towards larger values. Differences in the steepness of the water retention between laboratory and field data (Figs. 4.2 to 4.3) reflected by values of  $\theta_s$  (Table 4.3) corresponded to such hysteresis framework.

#### 4.4.2 Water retention dynamics at daily, seasonal, and annual scales

Day and night cycles were explained as a local non-equilibrium effect of the recurring root water uptake by the crop (e.g., Šimůnek et al., 2001). Root water uptake during the day forced soil water suction to increase, which then tended to decrease during the night because of local soil water redistribution by water movement from more immobile regions, especially in structured soils. Since the TDR sensors captured a bulk soil water content, the local variations caused by non-equilibrium conditions could be reflected in changes of the soil water suction (i.e., A and B in Figs. 4.7 and 4.8). As a result of such time series', "waved" drying water retention data were obtained mainly during periods in early spring (e.g., Dd-D1 in Fig. 4.7). The limitation of daily cycles in water retention to early spring conditions indicated that the relatively moist and wettable soil provided a high continuity of the pore system for capillary water movement in the liquid phase, which later in the season could be

limited by air entrapment and repellency. The wavelike drying water retention data in Ap-horizons could alternatively be explained by an active translocation of water from relatively moist to dry soil regions by the plant root systems (e.g., Caldwell et al., 1998). Here, water that was extracted from the subsoil and uplifted usually during the day could be released by plant roots in the topsoil when transpiration is reduced during the night.

Note that in contrast to tensiometers, the MPS-1 sensors were known for a slower reaction due to a relatively low permeable ceramic plate and limitations by hysteresis and temperature sensitivity (e.g., Kammerer et al., 2014). Such sensor-related temporal shifts in the suctions recorded with MPS-1 could possibly explain an increase in the suction towards midnight (e.g., A and B, Fig. 4.7) and an additional waviness in the drying water retention (e.g., Dd-D4 in Fig. 4.7). For the seasonal and inter-annual comparisons, these retention data could be less critical, since MPS-1 sensor readings were found to be consistent in time and remained constant over longer periods (Malazian et al., 2011).

The intra-seasonal trend of a decrease in water retention with increasing numbers of drying and wetting cycles suggested that rewetting of previously dried pore regions was limited; this was observed in all lysimeter soils and depths and in all 3 seasons (Figs. 4.4 to 4.6). For water repellent soils, Täumer et al. (2006) observed a seasonal dynamics of the wettable soil area (i.e., acting as flow paths) upon soil drying that started from a maximum in spring and reached a minimum in the summer. Here, limitations in rewetting upon drying were reflected in decreasing  $\theta_s$ -values obtained from the parametrization of intra-seasonal drying periods (Table 4.4). Decreasing  $\theta_s$ -values could also be explained by entrapped air in isolated soil regions that restricted the hydraulic connectivity of the soil pores (c.f., Morgan et al., 2001). The starting point of rewetting cycles after drying was assumed to begin at successively smaller  $\theta_s$ -values. This hysteretic effect was probably caused by local water repellence of the soil organic matter (e.g., Doerr et al., 2000) that increased with the drying intensity (see below section 4.3). However, also a deposition of colloids in soil pores, the colloidal straining (e.g., Bradford and Torkzaban, 2008), could lead to decreasing  $\theta_s$ -values by blocking smaller soil pores. During the vegetation-free relatively cold and moist winter periods (Fig. A1), the seasonally modified soil water retention could be reset due to a breakdown of soil water repellence (e.g., Rye and Smettem, 2015), the displacement of soil air by water, and due to effects of frost and intensive soil moistening by infiltrating of water that was poor in electrolytes (e.g., Fig. 4.6a, drying-wetting periods 11-15). A reset could, however, also occur during longer wet periods in summer (e.g., Doerr et al., 2000), especially for the Ap-horizons (e.g., Fig. 4.4, drying-wetting periods 9, 10, 11, and 13).

Limitations in soil re-wetting could also be indicated by  $\alpha$ -values (Table 4.4) for wet-dry periods (e.g., Hd\_6 in 2013 for 10 cm depth, Fig. 4.8). With decreasing  $\alpha$ -values, water



retention was restricted to smaller soil pores, and vice versa, increasing intra-seasonal air entry values suggested that larger pores were excluded. Thus, the water retention curves revealed additional hysteresis effects due to dynamic restrictions in the effectively wettable fraction of pores.

For the Ap-horizon (10 cm depth), the inter-annual variation in soil water retention was small for all Dd soils but relatively large for the Hd soils (Fig. 4.9). These variations in the maximum drying retention data for the three years (2012-2014) could possibly be connected with the change in soil and crop management after the translocation of the Hd soil monoliths towards the Exp. Station Dedelow. Effects of changes in the cropping and fertilization regime on soil structure, bulk density, and porosity have been reported before (e.g., Strudley et al., 2008). Organic matter (e.g., Rawls et al., 2003) and soil pH (e.g., Walker et al., 2005) could be indicative for changes in the soil water retention. Here, the soil pH in 0-10 cm depth increased from values around 5 to 7 (Table A5) while the concentration of dissolved organic carbon in the soil solution at 10 cm depth increased for both soils (Table A4). Additional soil chemical measurements confirmed also an increase in plant available nutrients for Hd soils (not shown).

For wetting periods (Figs. 4.10a and 4.10b), the  $\alpha^w$ -values were larger as those of  $\alpha^d$  for drying (Table 4.5). The present ratios did not confirm the scaling relation of  $\alpha^w = 2\alpha^d$  for the maximum wetting and drying curves. The relation  $\alpha^w = 2\alpha^d$  was only observed for the first wetting scanning branch after the initial drying in the spring (e.g.,  $\alpha = 0.039$  for Hd-W1 in Fig. 4.10b, Table 4.4). Most  $\alpha^w$ -values of the intra-seasonal wetting events (e.g.,  $\alpha = 0.068$  for Hd-W3 in Fig. 4.10b, Table 4.5) were larger. In contrast to  $\theta_s$ -values, which followed an intra-seasonal trend of decreasing water contents for the same suction (cf., wetting periods -W1 to -W4, Table 4),  $\alpha$ -values of increased without an obvious trend.

#### 4.4.3 Intra-seasonal dynamics and effective porosity

The intra-seasonal dynamics of soil water retention in terms of VG  $\alpha$ - and  $\theta_s$ -values was assumed to reflect successive changes in the effectively wettable porosity with each wet-dry cycle (Figs. 4.7 to 4.9). Similar effects were hypothesized by Lourenço et al. (2015) who observed greater contact angles and smaller water retention characteristics for mineral mixtures with organic substances following drying and rewetting cycles. Moradi et al. (2012) identified organic particle coatings originating from root exudates, mucilage, and other polymeric organic substances of microbiological origin as a key for explaining a temporal water repellency of soils. Since carbon dioxide (CO<sub>2</sub>) gas production in soil could be related to the activity of roots and microorganisms, the peaks in measured CO<sub>2</sub> concentration in the soil air of lysimeter monoliths indicating increased root growth and soil biological activity

during the periods with pronounced water retention dynamics (Fig. 11). In particular, the CO<sub>2</sub> concentration peaks during summer and autumn periods (A and B in Fig. 4.11) corresponded with relatively large changes in soil water retention in terms of fitted VG  $\theta_s$ - and  $\alpha$ -values in 2013 and 2014 (Tables 4.3 to 4.5).

Increased water retention dynamics was mainly observed in periods with elevated soil temperatures (C and D in Fig. 4.11). The impact of elevated soil temperatures on intra-seasonal water retention dynamics could be explained by the temperature dependency of the liquid surface tension at the air-water interface thereby affecting the liquid-solid contact angles (Bachmann et al., 2002) and entrapped air bubbles (Morgan et al., 2001). This temperature dependence of the water retention could further increase with soil dryness (Schneider and Goss, 2011). The observed seasonal water retention dynamics could additionally be explained by an increasing coating of mineral particles by organic substances (e.g., Dekker et al., 1998) such as waxes that could migrate from plant residues on soil particle surfaces (Franco et al., 1995). Despite the present absence of experimental evidences for these explanations, the disentangling of the field data could provide ideas for better including the intra-seasonal dynamics of soil hydraulic properties in the simulation of the soil water flow (e.g., Alletto et al., 2015). Similarly, Hannes et al. (2016) stated that better model representations of the complex dynamics of soil water retention were needed that included a concept of hydraulic nonequilibrium, and temporal dynamics of soil structure that lead to changes in hydraulic properties. In this sense, long-term effects of soil erosion have to be considered: soil profile truncation and a continuous incorporation of subsoil material through plowing in the topsoil (or conversely the deposition of colluvium) may gradually change textural, structural, and soil chemical and biological properties.

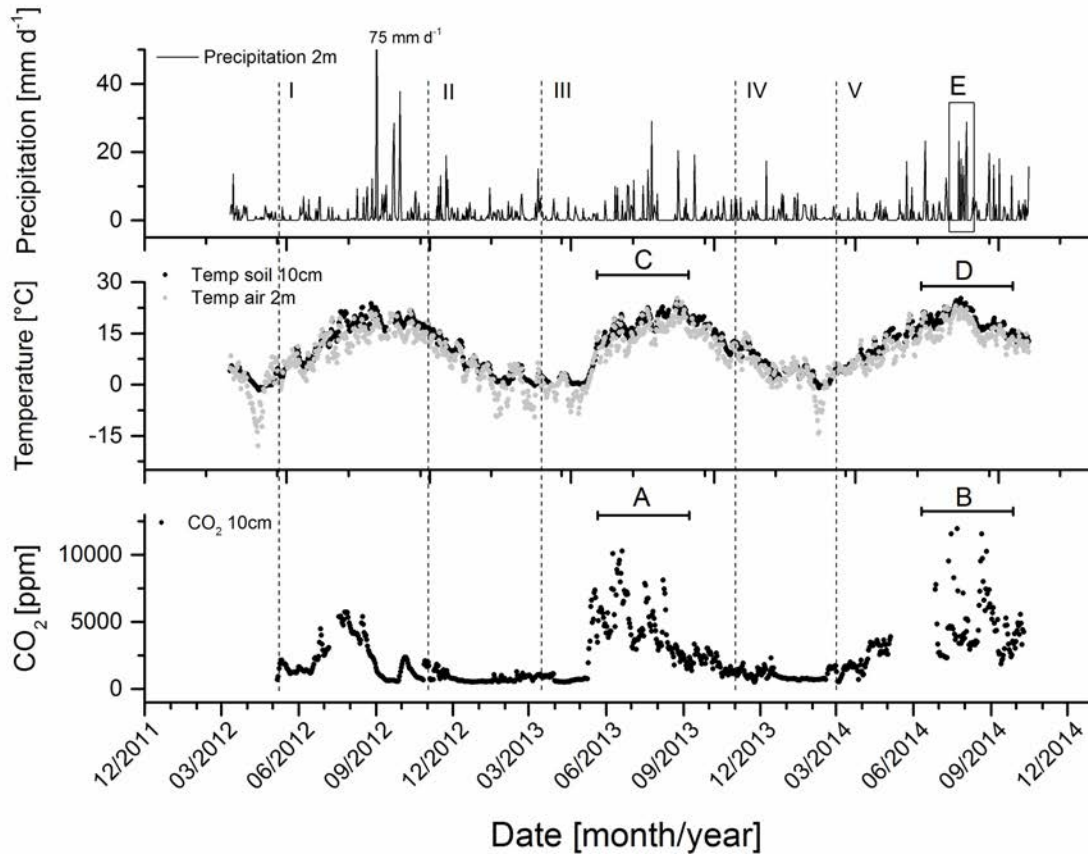


Fig. 4.11: Daily means of air temperatures and precipitation in 2 m height and soil temperatures at 10 cm soil depth, as well as carbon dioxide (CO<sub>2</sub>) at 10 cm soil depth for a period of January 1<sup>st</sup>, 2012 to December 31<sup>th</sup>, 2014 including technical problems after a storm event from October 15<sup>th</sup>, 2014; roman numbers I-V indicate crops cultivation (Sudangrass (*Sorghum sudanense*) from May to September 2012, triticale (*Triticosecale*) from October 2012 to March 2013, lucerne (*Medicago sativa* L.) from March to November 2013, Persian clover (*Trifolium resupinatum* L.) from March to September 2014).

#### 4.5. Conclusions

In this study, we analyzed the dynamics of soil water retention of eroded Haplic Luvisols over a 3-years period and compared field and laboratory data. Results confirmed that field drying retention curves were generally steeper than those obtained in the laboratory, basically because in the field, drying branches started at smaller water contents as compared to the laboratory. The scattered field water retention data suggested a non-unique, complex, and highly dynamic relation between suction and water content. The day and night fluctuations reflected mainly the formation of local non-equilibrium in suction between more and less mobile pore water regions in aggregated soils induced by root water uptake. Intra-seasonal dynamics revealed the combined effects of hysteresis (i.e., pore heterogeneity, air

entrapment), reductions in the effectively wettable porosity, and other temporal changes in the pore size distribution. Inter-annual dynamics, here by a single maximum drying water retention curve for each year, suggested that water retention properties of the Ap-horizon of translocated Hd soils gradual changed after the management-induced changes in soil chemical properties.

The results of the van Genuchten parameterization confirmed larger  $\alpha$ -values for wetting than for drying within hysteretic loops, however, the ratios were found to be variable and much larger than the ratio of 2 that was used in standard hysteretic models. Due to the successively decreasing  $\theta_s$ -values with each wet-dry cycle, the effective pore system for the water retention reflected in gradually steeper scanning drying curves tended towards that of a finer-textured soil. With respect to erosion-induced soil profile truncation and changes in the soil horizons, the differences in the water retention dynamics between the more (Dd\_1) and less (Hd\_6) eroded Luvisols, other than those related to texture and porosity, could not clearly be identified using the present methodical approach. The field water retention dynamics of the translocated lysimeter soils indicated a gradual shift in the soil hydraulic properties, which should be considered in addition to hysteretic and seasonal dynamics especially when dealing with soils of intensively cultivated and eroding landscapes.

### *Acknowledgements*

This study is part of the *TERENO-SoilCan* project and supported by the lysimeter infrastructure of the Terrestrial Environmental Observatory TERENO-Northeast of the Helmholtz Association ([http://teodoor.icg.kfa-juelich.de/observatories/GLObservatory?set\\_language=en](http://teodoor.icg.kfa-juelich.de/observatories/GLObservatory?set_language=en)). Financial support of the first author by the German Research Centre for Geosciences (GFZ), Potsdam, is gratefully acknowledged. The TERENO-SoilCan lysimeters are operated by the Leibniz-Centre for Agricultural Landscape Research (ZALF) Müncheberg. The authors thank Ute Moritz (data preparation) from the ZALF-Institute of Soil Landscape Research, as well as Jörg Haase and Gernot Verch (lysimeter maintenance) from the ZALF- Research Station Dedelow as well as Kristina Holz and the team from the Central Laboratory of the ZALF (chemical soil and solution analyses). We are also grateful to UMS GmbH (Munich, Germany) for carrying out the HYPROP measurements. We thank two anonymous reviewers for constructive comments and valuable suggestions for improving the manuscript.

## References

- Alletto, L., V. Pot, S. Giuliano, M. Costes, F. Perdrioux, and E. Justes. 2015. Temporal variation in soil physical properties improves the water dynamics modeling in a conventionally-tilled soil. *Geoderma* 243–244:18–28.
- Angers, D.A., and J. Caron. 1998. Plant-induced changes in soil structure: Processes and feedbacks. *Biogeochemistry* 42:55-72.
- Bachmann, J., R. Horton, S.A. Grant, and R.R. van der Ploeg. 2002. Temperature dependence of water retention curves for wettable and water-repellent soils. *Soil Sci. Soc. Am. J.* 66:44-52.
- Basile, A., G. Ciollaro, and A. Coppola. 2003. Hysteresis in soil water characteristics as a key to interpreting comparisons of laboratory and field measured hydraulic properties. *Water Resour. Res.* 39:1-12.
- Bradford, S.A., and S. Torkzaban. 2008. Colloid transport and retention in unsaturated porous media: A review of interface-, collector-, and pore-scale processes and models: *Vadose Zone J.* 7:667-681.
- Bronick, C. J., and R. Lal. 2005. Soil structure and management: a review: *Geoderma*, 124: 3-22.
- Caldwell, M. M., T. E., Dawson, and J. H. Richards. 1998. Hydraulic lift: consequences of water efflux from the roots of plants: *Oecologia*, 113: 151-161.
- Canone, D., S. Ferraris, G. Sander, and R. Haverkamp. 2008. Interpretation of water retention field measurements in relation to hysteresis phenomena. *Water Resour. Res.* 44:1-14.
- Dekker, L.W., C.J. Ritsema, K. Oostindie, and O.H. Boersma. 1998. Effect of drying temperature on the severity of soil water repellency. *Soil Sci.* 163:780-796.
- Deumlich, D., R. Schmidt, and M. Sommer. 2010. A multiscale soil-landform relationship in the glacial-drift area based on digital terrain analysis and soil attributes. *J. Plant Nutr. Soil Sci.* 173:843-851.
- Doerr, S., R. Shakesby, and R. Walsh. 2000. Soil water repellency: its causes characteristics and hydro-geomorphological significance. *Earth-Sci. Rev.* 51:33-65.
- Franco, C., M. Tate, and J. Oades. 1995. Studies on non-wetting sands. 1. The role of intrinsic particulate organic-matter in the development of water-repellency in non-wetting sands. *Soil Res.* 33:253-263.
- Flühler H., P. Germann, F. Richard, and J. Leuenberger, 1976. Determination of hydraulic parameters to estimate water movement and water storage in undisturbed soil. A comparison of field and laboratory methods. (In German with English abstract). *J. Plant Nutr. Soil Sci.* 3:329-342.

- Gerke, H.H., S. Koszinski, T. Kalettka, M. Sommer. 2010. Structures and hydrologic function of soil landscapes with kettle holes using an integrated hydropedological approach. *J. Hydrol.* 393:123-132.
- Gerke, H.H., and W. Hierold. 2012. Vertical bulk density distribution in C-horizons from marley till as indicator for erosion history in a hummocky post-glacial soil landscape. *Soil Tillage Res.* 125:116-122.
- Hannes, M., U. Wollschläger, T. Wöhling, and H.-J. Vogel. 2016. Revisiting hydraulic hysteresis based on long-term monitoring of hydraulic states in lysimeters. *Water Resour. Res.* 52:3847–3865.
- Haynes, R. J., and R. Naidu. 1998. Influence of lime, fertilizer and manure applications on soil organic matter content and soil physical conditions: a review: *Nutr. Cycl. Agroecosys.*, 51: 123-137.
- Herbrich, M., and H.H. Gerke. 2016. Autocorrelation analysis of high resolution weighing lysimeter time series as a basis for determination of precipitation. *J. Plant Nutr. Soil Sci.* 179:784–798.
- Herbrich, M., H.H. Gerke, M. Sommer, 2016. Matric potential and soil water content of differently eroded Luvisols using high precision weighing lysimeters. Leibniz-Zentrum für Agrarlandschaftsforschung (ZALF) e.V., doi:10.4228/ZALF.2015.291.
- Herbrich, M., H.H. Gerke, O. Bens, and M. Sommer. 2017. Water balance and leaching of dissolved organic and inorganic carbon of eroded Luvisols using high precision weighing lysimeters. *Soil Tillage Res.* 165:144-160.
- Horn, R. 2004. Time dependence of soil mechanical properties and pore functions for arable soils. *Soil Sci. Soc. Am. J.* 68:1131-1137.
- IUSS Working Group WRB. 2015. World Reference Base for Soil Resources 2014 (update 2015). International soil classification system for naming soils and creating legends for soil maps: World Soil Resources Reports No. 103. FAO. Rome.
- Jirků, V., R. Kodešová, A. Nikodem, M. Mühlhanslová, A. Žigová. 2013. Temporal variability of structure and hydraulic properties of topsoil of three soil types. *Geoderma* 204-205:43–58.
- Kammerer, G., R. Nolz, M. Rodny, and W. Loiskandl. 2014. Performance of Hydra Probe and MPS-1 soil water sensors in topsoil tested in lab and field. *J. Water Resource Prot.* 6:1207.
- Lourenço, S., N. Jones, C. Morley, S. Doerr, and R. Bryant. 2015. Hysteresis in the soil water retention of a sand–clay mixture with contact angles lower than ninety degrees. *Vadose Zone J.* 14:1-7.
- Malazian, A., P. Hartsough, T. Kamai, G. Campbell, D. Cobos, and J. Hopmans. 2011. Evaluation of MPS-1 soil water potential sensor. *J. Hydrol.* 402:126-134.

- Mertens, J., H. Madsen, M. Kristensen, D. Jacques, and J. Feyen. 2005. Sensitivity of soil parameters in unsaturated zone modelling and the relation between effective laboratory and in situ estimates. *Hydrol. Process.* 19:1611-1633.
- Moradi, A. B., A. Carminati, A. Lamparter, S.K. Woche, J. Bachmann, D. Vetterlein, H.-J. Vogel, and S.E. Oswald. 2012. Is the rhizosphere temporarily water repellent?. *Vadose Zone J.* 11.
- Morgan, K.T., L.R. Parsons, and T.A. Wheaton, 2001. Comparison of laboratory- and field-derived soil water retention curves for a fine sand soil using tensiometric, resistance and capacitance methods. *Plant and Soil*, 234: 153-157.
- Pachepsky, Y.A., W.J. Rawls, and D. Gimenez. 2001. Comparison of soil water retention at field and laboratory scales. *Soil Sci. Soc. Am. J.* 65: 460-462.
- Pütz, T., R. Kiese, U. Wollschläger, J. Groh, H. Rupp, S. Zacharias, E. Priesack, H.H. Gerke, H. Papen, E. Borg, O. Bens, K. Kaiser, M. Herbrich, J.-C. Munch, M. Sommer, J. Vanderborght, and H. Vereecken. 2016. TERENO-SOILCan a lysimeter-network in Germany observing soil functions influenced by climate change. *Environ. Earth Sci.* 75:1242. Doi: 10.1007/s12665-016-6031-5.
- Rawls, W.J., Y.A. Pachepsky, C. Ritchie, T.M. Sobecki, and H. Bloodworth. 2003. Effect of soil organic carbon on soil water retention. *Geoderma* 116:61-76.
- Rieckh, H., H.H. Gerke, and M. Sommer. 2012. Hydraulic properties of characteristic horizons depending on relief position and structure in a hummocky glacial soil landscape. *Soil Tillage Res.* 125:123-131.
- Rieckh, H., H.H. Gerke, J. Siemens, and M. Sommer. 2014. Water and dissolved carbon fluxes in an eroding soil landscape depending on terrain position. *Vadose Zone J.* 13(7).
- Rye, C., and K. Smettem. 2015. Seasonal and interannual variability of the effective flow cross-sectional area in a water-repellent soil. *Vadose Zone J.* 14.
- Sandin, M., J. Koestel, N. Jarvis, M. Larsbo. 2017. Post-tillage evolution of structural pore space and saturated and near-saturated hydraulic conductivity in a clay loam soil. *Soil Till. Res.* 165:161–168.
- Schindler, U., W. Durner, G. von Unold, L. Müller, and R. Wieland. 2010. The evaporation method: Extending the measurement range of soil hydraulic properties using the air-entry pressure of the ceramic cup. *J. Plant Nutr. Soil Sci.* 173:563-572.
- Schneider, M., and K.U. Goss. 2011. Temperature dependence of the water retention curve for dry soils. *Water Res. Res.* 47.
- Šimůnek, J., O. Wendroth, N. Wypler, and M.T. Van Genuchten. 2001. Non-equilibrium water flow characterized by means of upward infiltration experiments. *Eur. J. Soil Sci.* 52:13-24.

- Strudley, M.W., T.R. Green, and J.C. Ascough. 2008. Tillage effects on soil hydraulic properties in space and time: State of the science. *Soil Tillage Res.* 99:4-48.
- Täumer, K., H. Stoffregen, and G. Wessolek. 2006. Seasonal dynamics of preferential flow in a water repellent soil. *Vadose Zone J.* 5:405-411.
- van Genuchten, M.Th., F.J. Leij, and S.R. Yates. 1991. The RETC code for quantifying the hydraulic functions of unsaturated soils. Tech. Report. EPA/600/2-91/065. US Environ. Protect. Agency, Ada, Oklahoma, USA.
- Van Oost, K., G. Govers, S. De Alba, and T. Quine. 2006. Tillage erosion: a review of controlling factors and implications for soil quality. *Prog. Phys. Geogr.* 30:443-466.
- Verch, G. 2014. Weather Data. Dedelow. Germany. Leibniz-Zentrum für Agrarlandschaftsforschung (ZALF) e.V. - online available under [e.g. <http://dx.doi.org/10.4228/ZALF.2000.242>].
- Vrugt, J.A., P.H. Stauffer, T. Wohling, B.A. Robinson, and V.V. Vesselinov. 2008. Inverse modeling of subsurface flow and transport properties: A review with new developments: *Vadose Zone J.* 7:843-864.
- Walker, S.C., D. Gallipoli, and D.G. Toll. 2005. The effect of structure on the water retention of soil tested using different methods of suction measurement: *Advanced Experimental Unsaturated Soil Mechanics*. Balkema, London, pp. 33-39.
- Wang, H.-L., X.-Y. Tang, W. Zhang, S.-B. Song, and B.M. McKenzie. 2015. Within-year changes in hydraulic properties of a shallow Entisol in farmland and forestland. *Vadose Zone J.* 14. doi:10.2136/vzj2014.11.0163.



Appendix

Table A1. Numbered list of time periods (month/day) for the three soil horizons (Ap-, E-Bt-, Bt-horizons) of lysimeter Dd\_1, for which consistent pairs of TDR and MPS-1/tensiometer data could be identified in 2012, 2013, and 2014; these periods correspond with graphs in Fig. 4.4 (Ap-horizons, 10 cm depth), Fig. 4.6 (E+Bt-horizons, 30 cm depth); wetting periods are No. 12, 14, 16, 21, 22 for Ap-, No. 15, 16 for E+Bt-, and No. 5, 7, 10 for Bt-horizons.

	Dd_1; Ap			Dd_1; E+Bt			Dd_1; Bt		
	No.	From	To	No.	From	To	No.	From	To
2012	1	04/21	04/24	1	03/23	05/02	1	03/18	05/13
	2	04/28	05/06	2	07/07	07/19	2	07/17	07/19
	3	08/12	08/21	3	08/07	08/16	3	08/03	08/05
	4	08/29	09/07	4	10/12	10/24	4	08/06	08/22
	5	05/12	05/25	5	10/24	10/31	<b>5</b>	<b>10/29</b>	<b>11/14</b>
2013	6	05/06	05/09	6	01/10	01/14	6	01/10	01/19
	7	06/05	06/11						
	8	07/07	07/12						
	9	07/31	08/04						
	10	08/24	08/31						
	11	09/28	10/04						
2014	<b>12</b>	<b>02/02</b>	<b>02/10</b>	7	01/07	01/16	<b>7</b>	<b>01/07</b>	
	13	04/23	05/11	8	01/17	01/25	8	01/10	02/09
	<b>14</b>	<b>06/01</b>	<b>06/10</b>	9	02/14	03/16	9	03/04	06/04
	15	07/14	07/25	10	03/22	04/11	10	07/20	07/21
	<b>16</b>	<b>05/18</b>	<b>05/24</b>	11	04/19	05/23	11	08/01	08/02
	17	06/10	06/22	12	06/12	06/30	12	08/04	08/05
	18	07/05	07/13	13	08/06	08/14	13	08/06	09/02
	19	08/02	08/04	14	08/24	09/01	<b>14</b>	<b>09/15</b>	<b>09/15</b>
	20	08/04	08/17	15	<b>09/01</b>	<b>09/02</b>			
	<b>21</b>	<b>08/22</b>	<b>08/31</b>	16	<b>09/30</b>	<b>10/01</b>			
	<b>22</b>	<b>07/24</b>		17	10/01	10/09			

IV Scales of water retention dynamics observed in roded Luvisols from  
arable postglacial soil landscape

---

*Table A3. List of time periods (month/day) for the Ap-horizons of lysimeters Hd\_2, Dd\_3, Hd\_4, Dd\_5, for which consistent pairs of TDR and MPS-1/tensiometer data could be identified in 2012, 2013, and 2014; these periods correspond with graphs in Figs. 4.1 (ID; initial drying) and Fig. 4.9 (MD; maximum drying); only drying periods.*

	Year	Hd_2		Dd_3		Hd_4		Dd_5	
		From	To	From	To	From	To	From	To
MD	2012	04/16	05/03	03/17	04/04	08/10	08/26	04/17	04/24
				04/26	05/04	08/31	09/24		
	2013	05/17	06/26	05/21	05/26	06/05	06/18	10/21	10/31
	2014	06/15	07/12	06/17	07/08	04/20	05/19	06/10	07/04
ID	2012	04/16	05/03	04/26	05/04	04/27	05/04	04/17	04/24
	2013	06/04	06/17	06/05	06/17	06/04	06/15	06/05	06/18
	2014	04/20	05/18	04/22	05/18	04/22	05/18	04/24	05/18

Table A2. Numbered list of time periods (month/day) for the three soil horizons (Ap-, E-, Bt-horizons) of lysimeter Hd\_6, for which consistent pairs of TDR and MPS-1/tensiometer data could be identified in 2012, 2013, and 2014; these periods correspond with graphs in Fig. 4.5 (Ap, 10 cm depth), Fig. 4.6 (E, 30 cm depth); wetting periods are No. 6, 14, 16, 18, 21, 23, 24, 27 for Ap-, No. 2, 14, 17, 18 for E+Bt-, and No. 3, 5, 8 for Bt-horizons

	Hd_6-Ap			Hd_6-E			Hd_6-Bt		
	No.	From	To	No.	From	To	No.	From	To
2012	1	04/17	04/24	1	04/18	05/05	1	03/29	05/18
	2	04/26	05/05	<b>2</b>	<b>07/01</b>	<b>07/07</b>	2	07/07	07/19
	3	07/31	08/05	3	07/07	07/20	<b>3</b>	<b>08/01</b>	<b>08/06</b>
	4	07/31	08/05	4	07/31	08/06	4	08/06	08/20
	5	08/08	08/24	5	08/07	08/20	<b>5</b>	<b>10/26</b>	<b>12/04</b>
	<b>6</b>	<b>09/28</b>	<b>10/04</b>	6	11/30	12/06			
2013	7	03/29	04/02	7	01/10	01/13	6	03/02	03/15
	8	05/15	05/18	8	04/13	05/13	7	04/16	05/15
	9	06/03	06/10	9	10/15	11/06			
	10	06/21	06/25	10	10/05	10/15			
	11	07/03	07/12						
	12	08/03	08/07						
	13	08/21	09/02						
	<b>14</b>	<b>09/29</b>	<b>10/05</b>						
	15	10/10	10/13						
2014	<b>17</b>	<b>01/21</b>	<b>01/28</b>	11	01/07	01/25			
	<b>18</b>	<b>01/29</b>	<b>02/04</b>	12	02/14	03/01	<b>8</b>	<b>01/06</b>	<b>01/08</b>
	19	02/05	02/09	13	03/21	05/24	9	02/07	02/15
	20	03/27	04/06	<b>14</b>	<b>07/20</b>	<b>07/21</b>	10	02/20	06/16
	21	04/25	05/11	15	08/02	08/13	11	01/09	02/06
	22	05/20	05/24	16	08/18	09/07			
	<b>23</b>	<b>07/08</b>	<b>07/12</b>	<b>17</b>	<b>09/09</b>	<b>09/09</b>			
	<b>24</b>	<b>08/06</b>	<b>08/11</b>	<b>18</b>	<b>09/14</b>				
	25	06/17	06/30	19	09/14	09/30			
	26	08/20	08/30						
	<b>27</b>	<b>08/31</b>	<b>09/02</b>						
	28	05/26	05/28						

## 5| Root development of winter wheat in erosion- affected soils depending on the position in a hummocky ground moraine soil landscape

## *Abstract*

Agricultural soil landscapes of hummocky ground moraines are characterized by 3D spatial patterns of soil types that result from profile modifications due to the combined effect of water and tillage erosion. We hypothesize that crops reflect such soil landscape patterns by increased or reduced plant and root growth. Root development may depend on the thickness and vertical sequence of soil horizons as well as on the structural development state of these horizons at different landscape positions. The hypotheses were tested using field data of the root density (RD) and the root lengths (RL) of winter wheat using the minirhizotron technique. We compared data from plots at the CarboZALF-D site (NE Germany) representing a non-eroded reference soil profile (Albic Luvisol) at a plateau position, a strongly eroded profile at steep slope (Calcaric Regosol), and a depositional profile at the footslope (Anocolluvic Regosol). At each of these plots, three Plexiglas access tubes were installed down to approx. 1.5 m soil depth. The measurements were carried out during the vegetation period of winter wheat (September 2014 - August 2015) on six dates. The root length density (RLD) and the root biomass density were derived from RD values assuming a mean specific root length of  $100 \text{ m g}^{-1}$ . Values of RD and RLD were highest for the Anocolluvic Regosol and lowest for the Calcaric Regosol. The maximum root penetration depth was lower in the Anocolluvic Regosol because of a relatively high and fluctuating water table at this landscape position. Results revealed positive relations between below-ground (root) and above-ground crop parameters (i.e., leaf area index, plant height, biomass, and yield) for the three soil types. Root densities and root lengths in soils at the three landscape positions corroborated the hypothesis that the root system was reflecting erosion-induced soil profile modifications. Soil landscape position dependent root growth should be considered when attempting to quantify landscape scale water and element balances as well as agricultural productivity.

## 5.1. Introduction

The root system as the below-ground fraction of the vegetation is essential for crop development and water uptake but also an important factor for soil loss reduction in eroding soil landscapes (e.g., Gysels et al., 2005). Plant roots can affect soil hydraulic properties directly by the formation of biopores (e.g., Cresswell and Kirkegaard, 1995), the release of root exudates (e.g., Traoré et al., 2000) and by modifications on the soil pore structure (e.g., Kodešová et al., 2006) or more indirectly by changes on in-situ soil shrinkage rates (e.g., Mitchell and van Genuchten, 1992). In the arable hummocky soil landscape, soil development is affected by tillage and water erosion creating spatially-distributed patterns of soil types and properties that are closely related to landscape topography (Sommer et al., 2008). The plant growth can reflect soil landscape patterns by reduced or increased crop biomass, as reported for the wheat-cultivated hummocky moraine of central Saskatchewan, Canada (Moulin et al., 1994), topographically characterized by positive-vertical curvatures, such as knolls and steep slopes, and negative-vertical curvatures, such as topographic depressions. Relatively higher crop yields in topographic depressions as compared to slope positions can be attributed to accumulation of soil organic carbon and plant nutrients, especially nitrogen, potassium and phosphorous (Kaspar et al., 2004), together with water occasionally received by lateral surface and subsurface flow from eroded upper areas (e.g., Stone et al., 1985). In addition to these factors, a reduction of the soil thickness (i.e., solum depth) could also be associated with differences in the crop development of wheat (Moulin et al., 1994). These authors explained a negative correlation between solum depth and crop growth by a near-surface presence of relatively dense and massive, unstructured parent material with elevated carbonate contents.

While the above-ground crop development can be monitored directly or via remote sensing and other techniques (e.g., Migdall et al., 2009), the below-ground root development remains largely unknown. Effects of erosion-affected soil profile modifications (i.e., truncation and colluviation) on the root development of crops were discussed in only a few studies. Chirinda et al. (2014) observed effects of the topographic position on root biomass for winter wheat at shoulder and footslope positions. For spring wheat fields in the hummocky soil landscape of Saskatchewan, Canada, Slobodian et al. (2002) already tried to explain differences in the root biomass by elevation levels at convex shoulder and footslope positions. Root development and root distribution has been estimated for a model-based quantification of water fluxes in differently eroded soil profiles using a rooting depth data from a single location (e.g., Rieckh et al., 2014; Gerke et al., 2016). Nevertheless, information on root and root dynamics in erosion-affected soils at the different landscape positions remained limited. Similarly, the soil hydraulic properties of the horizons that control water and solute movement

could differ in space and time as a result of soil structural and pedogenic changes (e.g., Lin, 2011). Such differences were observed for erosion-affected soil horizons of the hummocky landscape and could be related to soil structure and horizon thicknesses (Rieckh et al., 2012). Soil structure was reported to affect plant growth via modification of the root distribution and thus the ability of soil water and nutrient uptake (e.g., Bronick and Lal, 2005). For the quantitative description of landscape-scale water and element balances of erosion-affected heterogeneous soil landscapes (e.g., Premke et al., 2016), the information on soil properties and crop and root development should be derived from soils at similar soil landscape positions (e.g., Ellerbrock et al., 2016; Aldana Jague et al., 2016).

In the widely-applied numerical simulation program HYDRUS (Šimůnek et al., 2008), the root distribution and the maximum root depth penetration have been proposed as parameters of the sink term for root water uptake of the Richards equation. Since spatially-distributed, landscape position-specific data on plant root dynamics was not available, the development and distribution of the root system was estimated for soil water balance simulations from observed above-ground plant characteristics including the leaf area index, LAI (Rieckh et al., 2014). Above-ground (LAI) and below-ground (maximum rooting depth) crop data was combined to estimate position-specific root model parameters (Gerke et al., 2016) for analyzing the effect of spatially-distributed root dynamics for erosion-affected soils at characteristic landscape positions. Still, the assumed complex feedbacks between position-specific soil properties, crop growth, and soil moisture patterns were lacking validation data on crop root dynamics.

We hypothesized that the crop root system dynamics reflected erosion-induced soil modifications and inter-related below- and above-ground crop biomass development most contrastingly at plateau, steep slope, and footslope positions. For monitoring the growth of plant roots, the in situ minirhizotron technique was proposed as a minimally-destructive method (e.g., Majdi, 1996). The ability to track the dynamics of root development of field crops was characterized as one of the advantages of using the minirhizotron technique (Johnson et al., 2001). However, the minirhizotron technique involved also disadvantages such as the inhibition of root growth in upper soil regions due to incomplete shielding from sunlight (Levan et al., 1987; De Ruijter et al., 1996) or the preferential root growths along the minirhizotron tube (Samson and Sinclair, 1994).

The objective of the present study was to better understand effects of soil properties and soil depth functions modified by erosion processes on root system dynamics and above ground plant development. Specific attention was given to the spatial and temporal differences in root growth between soils at contrasting landscape positions. Three steps were needed to achieve the objective: i) in-situ quantification of the winter wheat root density (RD)

dynamics with depth over a complete growing season (2014/15), ii) modelling the root lengths density (RLD) and position-specific root-to-shoot (R:S) biomass ratios and iii) identification of soil properties controlling differences in the growth of roots and also the above-ground plant biomass.

## 5.2. Material and Methods

### 5.2.1. Experimental design, above-ground biomass and soil characteristics

The minirhizotron measurements of the root development were carried out at an experimental field site denoted as “CarboZALF-D”, located near the city of Prenzlau in the hummocky arable soil landscape in Northeastern Germany at 53°23' N and 13°47'E (Fig. 5.1).

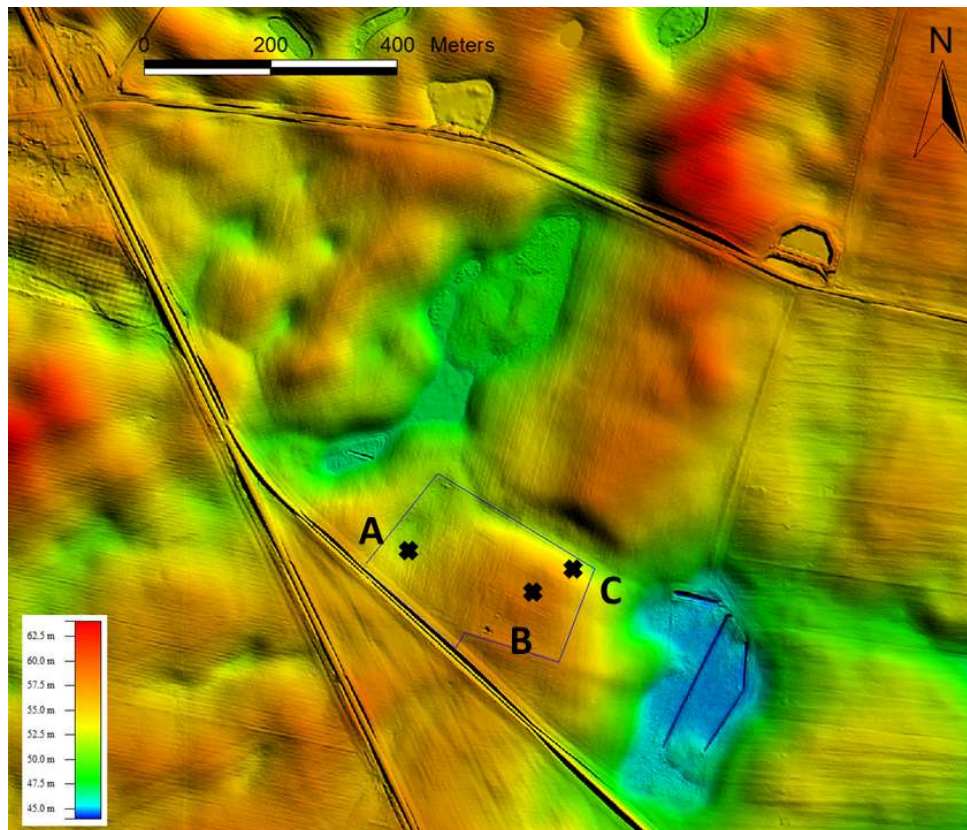


Figure 5.1: Digital terrain model (DGM1, 1 m grid) of the experimental field site denoted as “CarboZALF-D” (encircled by a thin blue line) located near the town of Prenzlau (Northeast Germany) in the hummocky soil landscape. Letters A, B, C indicate the location of the three characteristic soil profiles: A: RG-coa; B: LV-ab; C: RG-ca. The symbols [X] mark the sites where the minirhizotrons are installed (3 tubes at each site).

The DGM1 was licensed by LGB Brandenburg, ©Geobasis-DE/LGB 2012.



## V Root development of winter wheat in erosion-affected soils depending on the position in a hummocky ground moraine soil landscape

Three characteristic erosion-affected soil types that evolved from a glacial till ground moraine, classified here according to IUSS Working Group WRB (2015), were in the focus: Albic Luvisol (LV-ab) at plateau, Calcaric Regosol (RG-ca) at steep slope, and Anocolluvic Regosol (RG-coa) at footslope position where a fluctuating groundwater level was influencing the deeper subsoil (Table 5.1). Due to varying intensities of water and tillage erosion (i.e., mechanical soil movement during tillage operations), truncated (Ap-C) soil profiles have been formed at steep slopes (RG-ca), while relatively intact soil profiles (Ap-E-Bt-C) remained at plateau positions (LV-ab). The deposition of eroded soil material from slope positions formed the colluvial soils (RG-coa) at footslopes and nearby topographic depressions.

*Table 5.1: Characterization of the soil horizons of the three soil profiles: Anocolluvic Regosol (RG-coa), Albic Luvisol (Cutanic, Differentic) LV-ab-ct.df (in the text briefly denoted as LV-ab), and Calcaric Regosol (RG-ca), notation according to the FAO classification (IUSS-WRB, 2016); each replicate represents a separate borehole with a Plexiglas tube for minirhizotron measurements.*

Soil type	Replicate 1		Replicate 2		Replicate 3	
	Lower Depth / cm	Horizon	Lower Depth / cm	Horizon	Lower Depth / cm	Horizon
Anocolluvic Regosol RG-coa	30	Ap	30	Ap	30	Ap
	75	Ab	65	Ab1	85	Ab
	93	fAh	85	Ab2	120	fAh
	154	Btl	108	fAh	150	Btl
	200	Cl	158	Btl	200	Cl
		200	Cl			
Albic Luvisol (Cutanic, Differentic) LV-ab-ct.df	31	Ap	34	Ap	29	Ap
	50	Bt/E	50	Bt/E	37	E
	109	Bt	88	Bt1	61	Bt/E
	135	CBk	128	Bt2	100	Bt
	200	CB	180	CBk	130	CBk
		200	CB	200	CB	
Calcaric Regosol RG-ca	25	Ap	25	Ap	27	Ap
	85	CBk	80	CBk	83	CBk
	200	CB	160	CBkl	200	CBl
		200	CBk			

This study was related to the 2014 - 2015 growing season of winter wheat (*Triticum aestivum* L., Variety Julius), sown on September 19<sup>th</sup>, 2014 and harvested on August 14<sup>th</sup>, 2015. The growing period in 2014 ended on November 22<sup>th</sup> with the beginning of winter and re-started on March 28<sup>th</sup>, 2015. The start of the winter period was defined by five successive days with daily mean air temperatures of <5 °C; and vice versa, ended after five

## V Root development of winter wheat in erosion-affected soils depending on the position in a hummocky ground moraine soil landscape

successive days with air temperatures of  $>5$  °C. Annual precipitation was 561 mm in 2014 and 414 mm in 2015. The annual mean air temperatures at 2 m above the soil surface were 9.3°C (2014) and 9.1°C (2015). Compared to the 20-years average values (1992 – 2012) of 485 mm yr<sup>-1</sup> (mean annual precipitation) and 8.6 °C (annual mean air temperature), the year 2014 was wetter and 2015 drier, but both years were warmer (c.f., Rieckh et al., 2014).

*Table 5.2: Application rates of fertilizers and pesticides applied on the CarboZALF-D study site from September, 2014 to May, 2015 (Kieserit - 25% MgO and 20% S, ESTA Kieserit granulated; KAS - calcium ammonium nitrate with approximately 74% NH<sub>4</sub>NO<sub>3</sub> and 26% CaCO<sub>3</sub>; Baca Forte - 120 g L<sup>-1</sup> Flufenacet, 120 g L<sup>-1</sup> Flurtamone, 120 g L<sup>-1</sup> Diflufenican; Capalo - 62.5 g L<sup>-1</sup> Epoxiconazol, 200.0 g L<sup>-1</sup> Fenpropimorph, 75.0 g L<sup>-1</sup> Metrafenone; Urea - CH<sub>4</sub>N<sub>2</sub>O with approximately 46% N; Adexar - 62,5 g L<sup>-1</sup> Epoxiconazol, 62,5 g L<sup>-1</sup> Xemium).*

Date	Fertilizer/ pesticides	Application rates
24.09.2014	Bacara Forte	0.8 L·ha <sup>-1</sup>
23.03.2015	Kieserit	100 kg·ha <sup>-1</sup>
	KAS	80 kg N·ha <sup>-1</sup>
15.04.2015	Capalo	1.5 L·ha <sup>-1</sup>
22.04.2015	Urea	80 kg N·ha <sup>-1</sup>
11.05.2015	Adexar	1.5 L·ha <sup>-1</sup>

The above-ground crop parameters were determined from the wheat plants harvested at 1 m<sup>2</sup> subplots in 4 replicates. Fresh above-ground biomass (FM) was gravimetrically determined with the scale QS16000B (Sartorius AG, Göttingen, Germany). The dry mass (DM) was determined after drying at 60°C for  $>24$ h (Gudrun Buddrus, ZALF Experimental Station Dedelow, personal communication, December 7<sup>th</sup>, 2015). The LAI was measured with a SunScan probe SS1 (Delta-T Devices Ltd., Cambridge, UK). From September 2014 to May 2015, wheat plants at the CarboZALF-D experimental plots received several treatments with fertilizers and pesticides (see Table 5.2).

### 5.2.2 Root image collection and minirhizotron installation

The root density of winter wheat and its vertical distribution was determined from field-installed observation tubes by using the minirhizotron imaging system CI 600 (Root Imager CI 600; CID Inc., Camas, USA). The scanner-based technology produced 360 degree images of the tube–soil interface for the observation of root-soil interactions (e.g., Muñoz-Romero et al., 2012). The transparent acrylic minirhizotron tubes (1.8 m length with an

internal diameter of 70 mm) were vertically installed in three replicates at a distance of approximately 1 m and arranged parallel to the seed row direction at three plots (cf., Fig. 5.1: A, B, and C), each of them representing a defined landscape position with the respective soil type (Table 5.1).

The vertical installation of minirhizotron allowed obtaining information on root depth distribution down to soil depths of approx. 1.5 m. During measurements, the cylindrical tube–soil interface was subdivided over the whole soil profile into seven rectangular image increments of approx. 0.22 m × 0.19 m. The above-ground part of each tube was covered (airtight) with insulating tape to minimize light and moisture intrusion and heat exchange as recommended by Johnson et al. (2001). To ensure that the tubes were in close contact with the soil matrix, the minirhizotron bore holes were drilled with a soil corer of the same outer diameter as the tubes. The root growth of winter wheat plants was observed in the minirhizotron tubes on several crop development stages after germination on September 15<sup>th</sup>, 2014 (i.e., EC 00) as follows: tillering (EC22–October 28<sup>th</sup>, 2014; EC26–November 18<sup>th</sup>, 2014; EC28 – March, 10<sup>th</sup>, 2015), stem elongation (EC30–April 07<sup>th</sup>, 2015; EC33–April 29<sup>th</sup>, 2015), and during grain development at post-anthesis (EC71–June 22<sup>th</sup>, 2015). The phenological growth stages of wheat, denoted as Eucarpia code (EC), were selected according to the BBCH (Biologische Bundesanstalt, Bundessortenamt und Chemische Industrie) scale for cereals (Hack et al., 1992).

The images were processed with the software RootSnap! version 1.2.9.34 (CID Inc., Camas, USA) to optimize scanned images and monitor the root growth. The number of roots on the minirhizotron surface was counted by the procedure described in Upchurch and Ritchie (1983). Here, all roots and root branches were counted that intercepted the root image. The density of roots in ambient soil regions determined the number of root arrivals at the interface. This was in contrast to the procedure of Buckland et al. (1993), who considered only the first and the last contact points. Roots at a certain soil depth would not be considered for root density depths functions if they only were passing by the tube–soil interface images. In this study, we did not distinguish between living and dead roots.

The root density (i.e., root numbers per image area of 415 cm<sup>2</sup>) resulting from the minirhizotron images was converted to the equivalent root length density (RLD, km m<sup>-3</sup>) by using the model of Merrill and Upchurch (1994) as:

$$RLD = R_n \cdot C_{tube} \cdot 10 \quad [5.1]$$

## V Root development of winter wheat in erosion-affected soils depending on the position in a hummocky ground moraine soil landscape

---

where  $R_n$  is number of counted roots per square centimeter ( $\text{cm}^{-2}$ ) and  $C_{\text{tube}}$  is a theoretical, dimensionless conversion factor, which depends on the diameter of the minirhizotron tube. Here, a value of  $C_{\text{tube}}$  of 3.26 was used for the tube diameter of 70 mm (Merrill and Upchurch, 1994); a factor of 10 was included in Eq [5.1] to convert RLD values into SI units ( $\text{km m}^{-3}$ ).

To relate the above-ground with the below-ground biomass, the volumetric root biomass density, RBD ( $\text{g m}^{-3}$ ), was calculated based on the root biomass dry matter (Johnson et al., 2001) as:

$$RBD = \frac{RLD}{SRL * 1000} \quad [5.2]$$

where SRL is the wheat specific root length ( $\text{m g}^{-1}$ ) and RLD is the root length density [Eq. 5.1]. Here, mean RLD values of the 3 minirhizotron replicates of each soil type were used. An average SRL value of  $100 \text{ m g}^{-1}$  was assumed in [Eq. 5.2] for calculation of root biomass [Eq. 5.3] used for determining the root-to-shoot (R:S) ratio. This average SRL value was estimated from the range of SRL values for wheat reported in the literature (e.g.,  $17 - 24 \text{ m g}^{-1}$  (Meena et al., 2013),  $15 - 150 \text{ m g}^{-1}$  (Wang et al., 2014),  $90 - 120 \text{ m g}^{-1}$  (Paponov et al., 1999),  $150 \text{ m g}^{-1}$  (Wilhelm et al., 1982), and  $173 - 193 \text{ m g}^{-1}$  (Løes and Gahoonia, 2004)).

The root biomass, RB ( $\text{g m}^{-2}$ ), was calculated as the sum of RBD values [Eq. 5.2] of the  $n$  vertical sections of root scanner images RSI (m) as:

$$RB = \sum_{i=1}^n RBD_i * RSI_i \quad [5.3]$$

The daily rates of root penetration per temperature sum (RPT,  $\text{mm } ^\circ\text{C}^{-1} \text{ day}^{-1}$ ) were calculated following the approach of Barraclough and Leigh (1984) as the slope of regression lines of the accumulated average root depths (RP, mm) against the accumulated mean value of daily temperatures ( $T$ ,  $^\circ\text{C}$ ) using an air temperature of  $0^\circ\text{C}$  at least, for number of  $n$  days from the beginning of the crop vegetation as:

$$RPT = \sum_{i=1}^n \frac{RP_i}{T_i} \quad [5.4]$$

The linear correlation between two variables was determined using the Pearson correlation coefficient,  $r$ , calculated with Excel (Microsoft Office Professional Plus 2010, Redmond CA, USA).

### 5.3. Results

#### 5.3.1 Root density and root length

Differences in the above-ground (Table 5.3) and below-ground (Table 5.4) crop biomass were observed in the soils at the three landscape positions end of June 2015 at post-anthesis (EC 71): Most roots in terms of the root density (RD) were counted in the Anocolluvic Regosol (RG-coa) at footslope followed by the Albic Luvisol (LV-ab) at plateau and the Calcaric Regosol (RG-ca) at steep slope positions (Table 5.4).

*Table 5.3: Characterization of the above-ground vegetation: plant height, leaf area index (LAI), fresh biomass, and dry matter fraction (DM) at anthesis (EC 65), as well as the yield (total mass of fresh grain and straw) at harvest July 29-30, 2015; the phenological growth stage (BBCH-scale) of winter wheat (variety “Julius”) for the three plots at soil types RG-coa, LV-ab, and RG-ca was determined at anthesis (EC 65); mean values and standard deviations (in italic) from  $n = 3$  replicates SD is standard deviation of the plant height, biomass, yield ( $n=4$ ;  $n=2$  for Yield at LV-ab) and LAI ( $n_{RG-coa} = 5$ ,  $n_{RG-ca} = 18$ ,  $n_{LV-ab} = 15$ ). Winter wheat variety „Julius“*

Soil type	Plant height / cm		LAI / m <sup>2</sup> m <sup>-2</sup>		Fresh biomass / kg m <sup>-2</sup>		DM / %	Yield / kg m <sup>-2</sup>	
RG-coa	105	<i>5</i>	6.2	<i>0.1</i>	5.6	<i>0.1</i>	27	3.3	<i>0.3</i>
LV-ab	98	<i>2</i>	4.8	<i>0.4</i>	4.2	<i>0.1</i>	30	2.3	<i>0.04</i>
RG-ca	84	<i>6</i>	3.4	<i>0.3</i>	2.7	<i>0.3</i>	33	1.6	<i>0.4</i>

In comparison to the least erosion-affected reference soil at plateau position (i.e., Luvisol), the RD values were about 48 % higher at footslope and about 59 % lower at steep slope positions. While for the Anocolluvic Regosol, the root density was approximately 3.6-times higher as for the Calcaric Regosol, the above-ground biomass (Table 5.3) was only 2.1-times higher. The standard deviation of the root density between the three minirhizotron replicates of each soil type was highest for RG-coa and lowest for LV-ab (Table 5.4).

V Root development of winter wheat in erosion-affected soils depending on the position in a hummocky ground moraine soil landscape

Table 5.4: Root density (RD), root length density (RLD), root penetration depth (RP), daily mean root penetration rate per temperature sum (RPT), and a mean root penetration rate (Rate) of winter wheat at post-anthesis (EC 71, June 22, 2015) for the three different soil types RG-coa, LV-ab-ct.df, RG-ca; mean values and standard deviations (in *italic*) from  $n = 3$  replicates, except for RP at footslope position (RG-coa) where  $n = 2$ ; letters a, b, and c indicate statistically (ANOVA) significant differences ( $p < 0.001$ ) of RD and RLD between soil types.

Soil type	RD <i>/ roots m<sup>-2</sup></i>	RLD <i>/ km m<sup>-3</sup></i>	RP <i>/ mm</i>	RPT <i>/ mm °C<sup>-1</sup> day<sup>-1</sup></i>	Rate <i>/ mm day<sup>-1</sup></i>			
RG-coa	6422 <sup>a</sup>	1677	20.9 <sup>a</sup>	5.5	1325	100	0.83	5.0
LV-ab-ct.df	4333 <sup>b</sup>	269	14.1 <sup>b</sup>	0.8	1433	103	0.9	5.4
RG-ca	1763 <sup>c</sup>	321	5.7 <sup>c</sup>	1.1	1383	85	0.87	5.2

The above-ground plant characteristics (Table 5.3) of the winter wheat crop at anthesis (EC 65; June 8, 2015) was clearly dependent on soil type and landscape position and closely related to the root density, the latter determined two-weeks later at post-anthesis (EC 71; June 22, 2015). Fresh wheat biomass at EC 65 ( $r = 0.999$ ,  $n = 3$ ) and leaf area index (LAI,  $r = 0.998$ ,  $n = 3$ ) increased almost linearly with RD; while the harvested crop yield (i.e., grain and straw) increased non-linearly; the measured crop height was also positively related with RD (Fig. 5.2).

The temporal development of the rooting depths of the winter wheat crop (Fig. 5.3) showed largest deviations between soils at the three landscape positions during early growth stages in autumn 2014 (Fig. 5.3). During the 2014 vegetation period, the most rapid downward growth of wheat roots was observed for RG-coa where the winter wheat roots penetrated the upper 0.8 m of the soil. During spring 2015, the highest root penetration rates were observed in LV-ab, almost one month before the root penetration rate intensified also in RG-ca but not in RG-coa. At post-anthesis (EC 71, see last data points close to day 300 in Fig. 5.3), the rooting depth was greatest in LV-ab at plateau position and smallest for RG-coa. The root penetration depth was about 4% lower in the eroded RG-ca at steep slope and about 8 % lower in the RG-coa at the footslope as compared to the reference LV-ab soil (Table 5.4). The root depth penetration rate, averaged over the whole vegetation period, ranged from 5 to 5.4 mm day<sup>-1</sup> for the three soils; maximum mean root depths varied only between 1.33 and 1.43 m depth at the three landscape positions despite the large differences in root densities (Table 5.4).

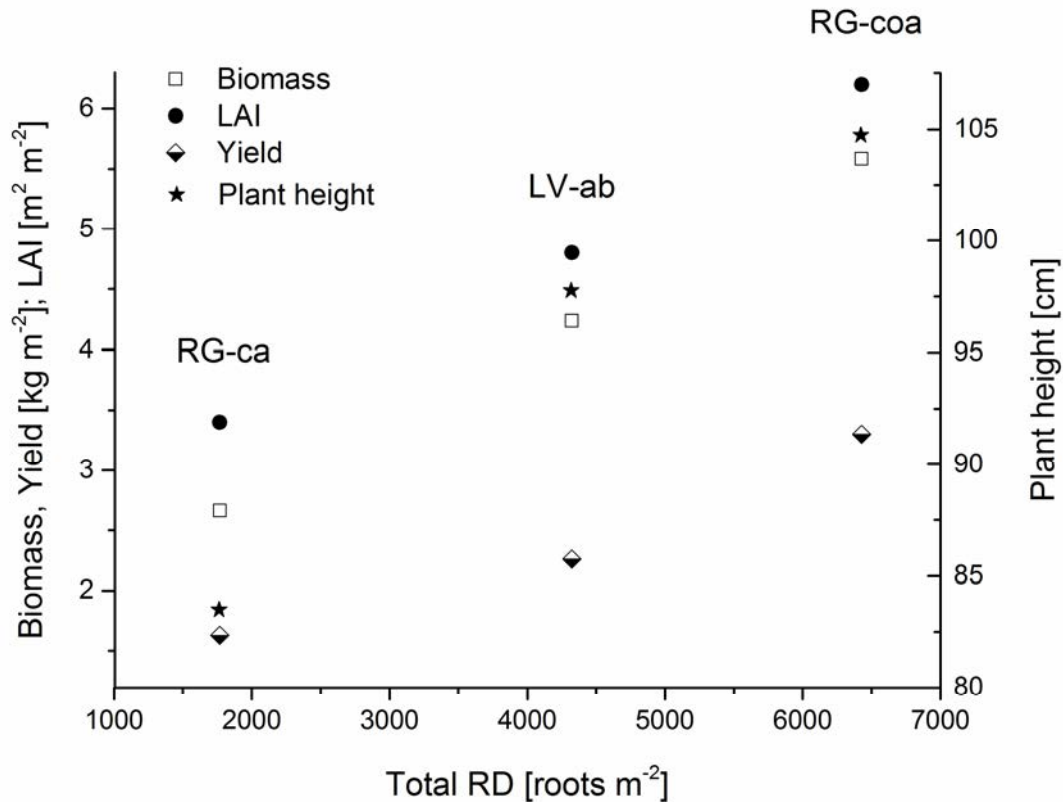


Figure 5.2: The relationship between the total root density (RD) and the above-ground plant biomass, crop yield, leaf area index (LAI), and plant height for winter wheat at the phenological growth stage EC 65 (anthesis, June 8, 2015) for the sites RG-ca (left), LV-ab (centre), and RG-coa (right); yield denotes the total grain and straw harvested end of July 2015.

The root penetration depth increased with cumulative daily air temperature (Fig. 5.4); increase was different for soils at the three landscape positions and almost linear for cumulative temperatures of about 500 - 1100 °C, up to the phenological growth stage of stem elongation (EC 33; April 29, 2015). Afterwards (>EC33), the observed root penetration depths remained almost unchanged. The daily rates of root penetration versus temperature sum (daily mean air temperatures) during the entire growing season of 284 days ranged between 0.83 and 0.9 mm °C<sup>-1</sup> day<sup>-1</sup> (Table 5.4).

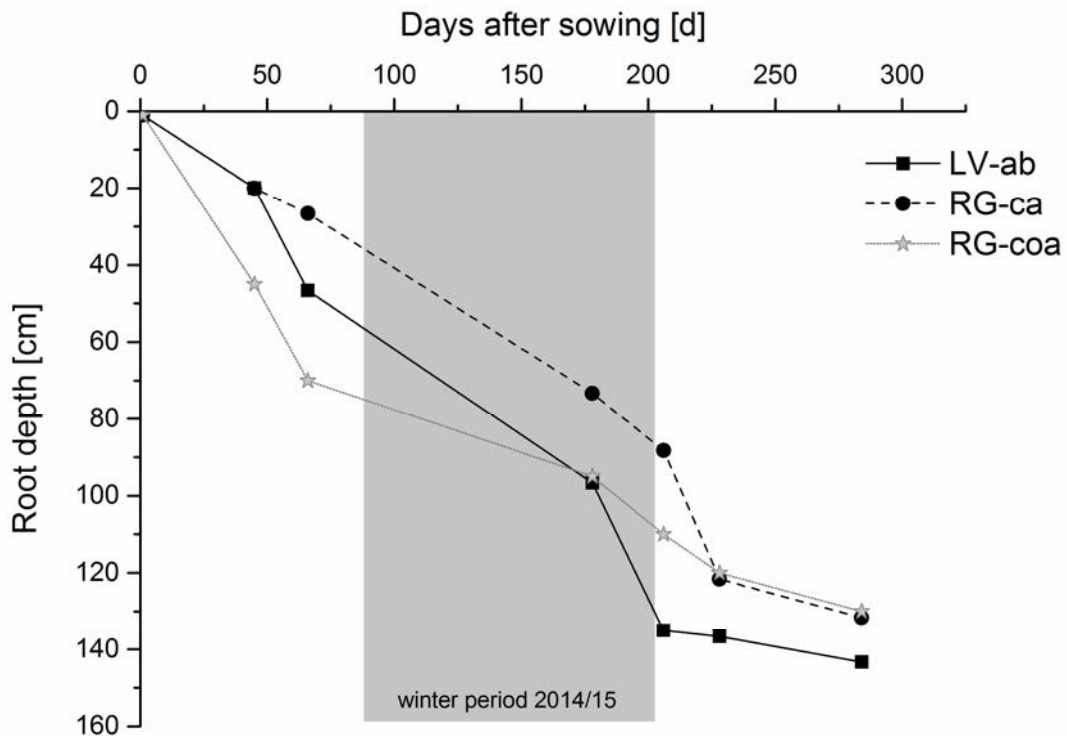


Figure 5.3: Mean values of the rooting depths of winter wheat for the soil types at three landscape positions: Albic Cutanic Luvisol (LV-ab), Calcaric Regosol (RG-ca) and Anocolluvic Regosol (RG-coa) from September 2014 to June 2015 (n=3), sowing date was September 19, 2014; winter period started on November 23, 2014 and ended on March 28, 2015.

### 5.3.2 Root length density and root biomass calculations

The total RLD values observed in the soils at the three landscape positions ranged from  $5.7 \text{ km m}^{-3}$  (RG-ca) to  $20.9 \text{ km m}^{-3}$  (RG-coa) at the phenological growth stage EC 71 (Table 5.4). The RLD values and the depth distribution for the three soils increased with crop development between November, 2014 and June, 2015 according to the observations at phenological stages EC 26, EC 33, and EC 71 (Figs. 5.5a-5i). For LV-ab (Fig. 5.5h), the vertical spatial patterns of RLD down to 1.5 m soil depth were relatively similar for the three minirhizotron replicates especially at the later stage EC 71; the RLD depth patterns differed considerably between replicates at lower values for RG-ca (Fig. 5.5g) as well as at higher values for RG-coa (Fig. 5.5i).



V Root development of winter wheat in erosion-affected soils depending on the position in a hummocky ground moraine soil landscape

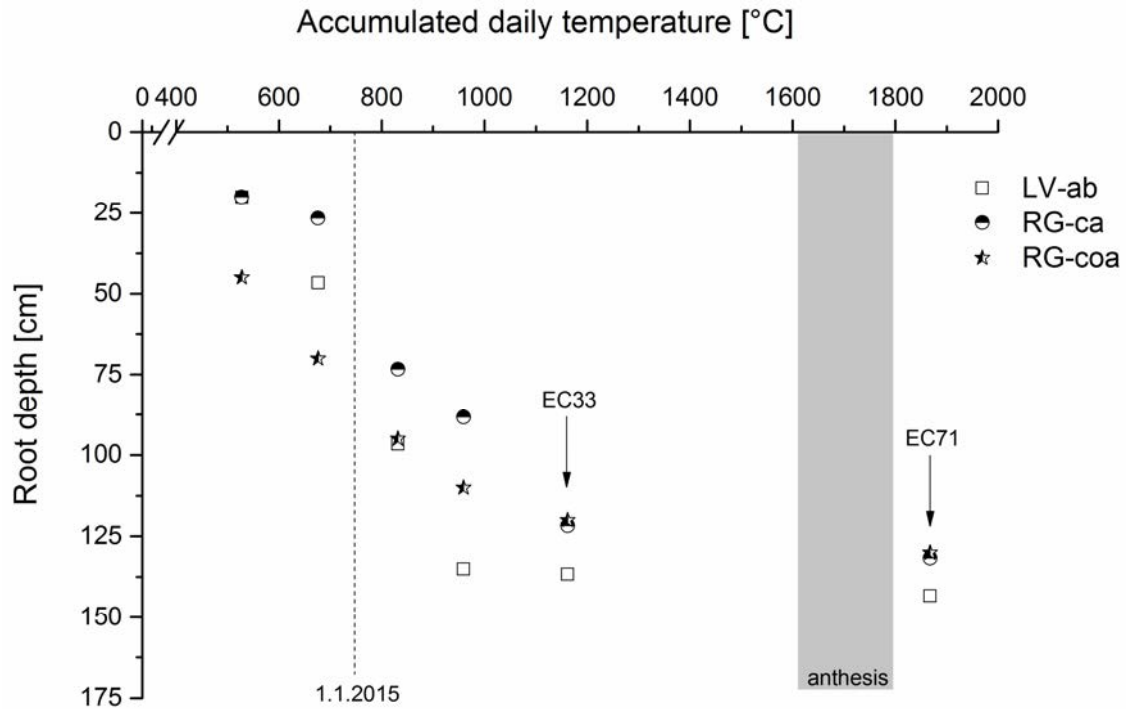


Figure 5.4: The relationship between the root penetration depth and the accumulated daily temperature beginning with the date of sowing for the three soil types: Albic Cutanic Luvisol (LV-ab), Calcaric Regosol (RG-ca), and Anocolluvic Regosol (RG-coa), from September 2014 to June 2015.

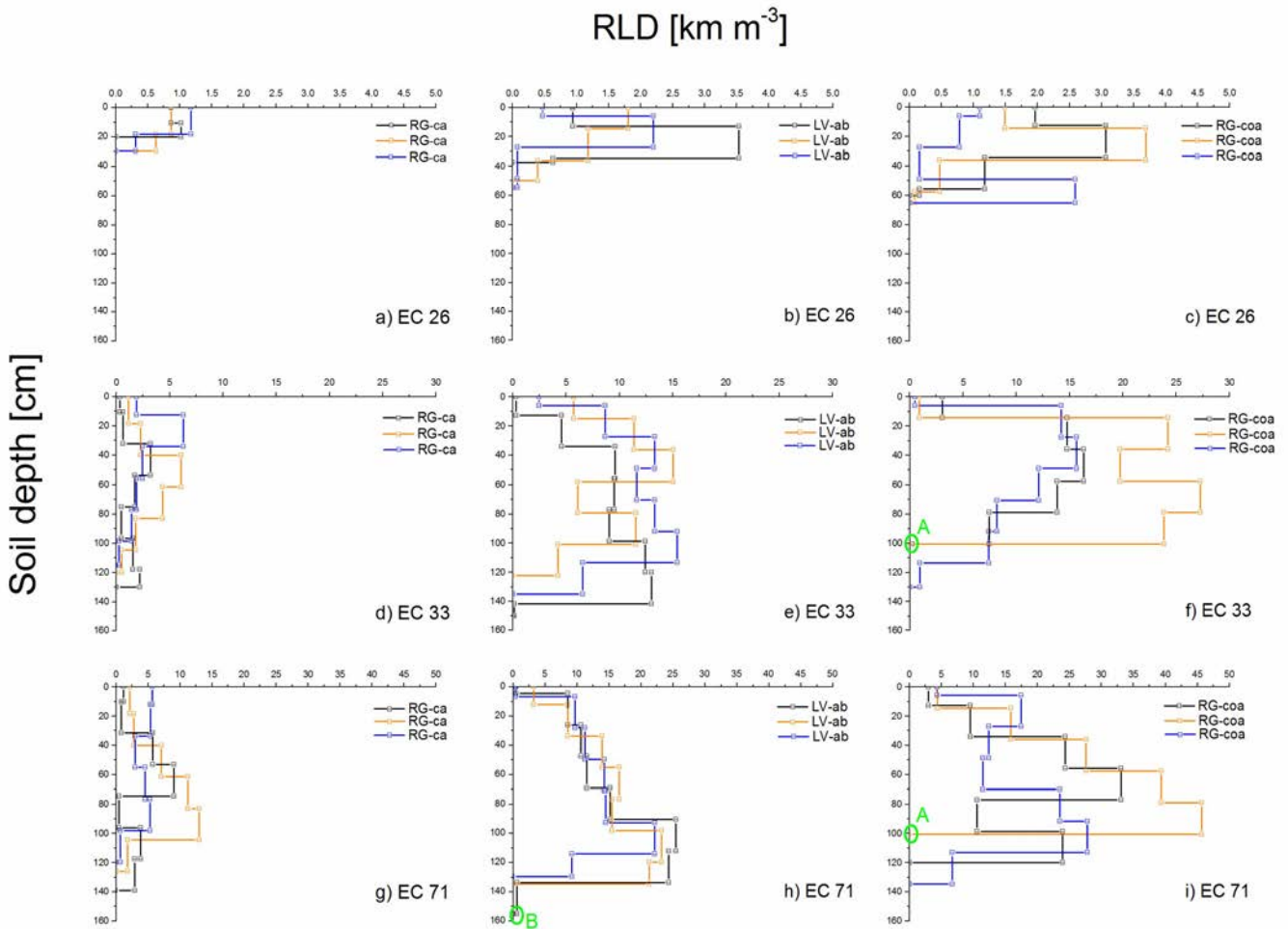
For the wheat crop at the phenological growth stage EC 26, the peak of RLD was in the upper 0.4 m soil depths for all soils (Figs. 5.5a-5c) while at stage EC 33, roots were more uniformly distributed along the depth for all soils without clear peaks (Figs. 5.5d-5f); at the later growing stage of EC 71, the RLD peak was located in 0.6 -0.8 m depth for footslope (RG-coa) and steep slope (RG-ca) positions, while for soils at the plateau (LV-ab), the maximal RLD values were in 0.9 - 1.3 m depth.

Table 5.5: The below ground biomass (Root) estimated at EC 71 (June 22, 2015), the above-ground biomass (Shoot) measured at EC 65 (June 8, 2015), and the mean root-to-shoot ratio (R:S) for the three soil types RG-coa, LV-ab, RG-ca; mean dry matter (DM) values and standard deviations (in italic> from  $n = 3$  replicates.

	Root		Shoot		R:S
	/ g DM m <sup>-2</sup>		/ g DM m <sup>-2</sup>		/ -
RG-coa	246	31	1486	50	0.17
LV-ab	198	16	1237	16	0.16
RG-ca	76	16	881	84	0.09

## V Root development of winter wheat in erosion-affected soils depending on the position in a hummocky ground moraine soil landscape

The calculated dry root biomass ranged from 76 to 246 g DM m<sup>-2</sup> for the three different soil types (Table 5.5); the dry matter values were highest for RG-coa (148 % of those of LV-ab) and lowest for RG-ca (41 % of LV-ab). The relations of the estimated (June 22, 2015) below-ground root biomass to the measured (June 8, 2015) above-ground shoot biomass (R:S ratios in Table 5.5) were relatively similar for RG-coa (0.17) and LV-ab (0.16) , and almost 50 % lower for RG-ca (0.09).



*Figure 5.5: Depth distribution of the root length density (RLD) for the winter wheat root system for three soil types: Albic Cutanic Luvisol (LV-ab), Calcaric Regosol (RG-ca), and Anocolluvic Regosol (RG-coa) at different stages of above-ground biomass development (EC 26, EC 33; EC71); green A marks the one Plexiglas access tube, which was blocked at 1 m depth and B indicates where roots possibly penetrated below the bottom of the access tube. Note that the scale of the root length density axes differed for each of the EC stages.*

## 5.4. Discussion

### 5.4.1 Root development at contrasting landscape positions

The minirhizotron measurement revealed hillslope position-specific RD values (Table 5.4) for soils at the three landscape positions: plateau (LV-ab), steep slope (RG-ca) and footslope (RG-coa). For the non-eroded reference soil at plateau, RD values indicated a higher root growth for winter wheat of up to 59 % as compared to the strongly eroded soil at steep slope with a truncated (Ap-C) profile. In turn, the colluvial soil at footslope revealed up to 48 % higher RD values as compared to the reference soil at plateau. The significant differences in the root density values ( $p < 0.001$ ) between the three soil types were reflected in contrasting total RLD values ranging from 5.7 to 20.9  $\text{km m}^{-3}$  at post-anthesis (Table 5.4), where the maximum root growth could be assumed (e.g., Liu et al., 2011). A relatively fast increase in the local root length densities (Fig. 5.5) up to values of  $>45 \text{ km m}^{-3}$  were in line with the range of RLD values reported for wheat plants elsewhere (e.g., Merrill et al., 2002: 25 to 36.1  $\text{km m}^{-3}$ ; Merrill et al., 1996: 38 to 53  $\text{km m}^{-3}$ ). The relatively small RLD values near the soil surface (Fig. 5.5) could perhaps be a result of artifacts introduced by the minirhizotron system causing root growth inhibition in the near-surface soil regions (De Ruijter et al., 1996). Despite the arrangements made to limit light intrusion into the minirhizotron tube, an incomplete shielding from sunlight could have led to reduced root densities in all topsoils (Levan et al., 1987). While the RLD values (Fig. 5.5) could have been underestimated for the first centimeter of the topsoil, RLD values were perhaps over-represented for larger depths by preferential root growths along the minirhizotron tube (c.f., Samson and Sinclair, 1994).

The peak in RLD values of LV-ab between 90 and 130 cm soil depth (Fig. 5.5h) at the phenological growth stage EC 71 could be explained by the abrupt change in soil properties at the interface between the clayey Bt- and the carbonate-containing CBk-horizon in 100 - 128 cm depth (cf., Table 5.1). The CBk-horizon consisting of marly glacial till with a high bulk density (Gerke and Hierold, 2012) could have probably impeded root growth and restricted root penetration due to the mechanical resistance (Unger and Kaspar, 1994). Likewise, in the heavily eroded RG-ca soil at an exposed landscape position where the C-horizon was located close to the soil surface (i.e., due to soil profile truncation), the root growth limitations indicated by RLD values of only about 5.7  $\text{km m}^{-3}$  (Table 5.4) were possibly caused by relatively high soil bulk density values in the CBk-horizon. Low RLD values were also caused indirectly by limited oxygen supply to roots as reported for compacted soils (e.g., Bengough and Mullins, 1990).

For eroded Stagnic Podzoluvisols developed on glacial till, Chirinda et al. (2014) also observed root growth restrictions in soils at steep slope positions where higher soil bulk

densities were found as compared to soils in topographic depressions. These authors suspected that root growth in soils at steep slopes was confined to shallower soil depths due to the higher bulk density of the subsoil, thus also impeding carbon accumulation at greater soil depths. The soil organic carbon depth functions of soils at footslope (RG-coa), plateau (LV-ab) and steep slope (RG-ca) positions (Rieckh et al., 2012) corroborated this hypothesis; here, organic carbon concentrations were reported to decrease with soil depth for RG-ca from  $4.7 \text{ g kg}^{-1}$  (topsoil) to  $0.3 \text{ g kg}^{-1}$  at 1.1 m depth while for RG-coa, the concentrations dropped from  $10.8 \text{ g kg}^{-1}$  in the topsoil to  $5.7 \text{ g kg}^{-1}$  at 1.2 m depth.

#### 5.4.2 Root penetration depending on landscape position

In contrast to the above-ground wheat plant development, roots continued to grow during winter 2014-2015 (Fig. 5.3). This was probably caused by relatively high soil temperatures during the cold season because only on 41 (RG-coa, LV-ab) and 32 (RG-ca) days from the total 128 days of the winter period, the soil temperatures in 0.2 m depth dropped below the critical temperature of  $+2^\circ\text{C}$  for root growth of wheat (Porter and Gawith, 1999) in the Ap-horizon of RG-ca, RG-coa, and LV-ab (Fig. 5.6).

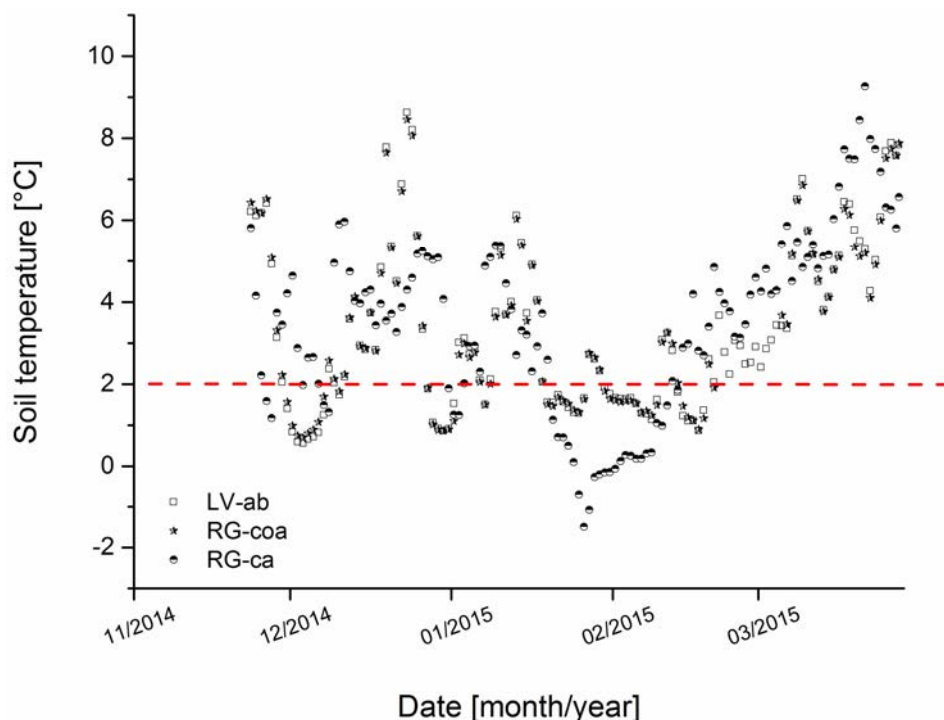
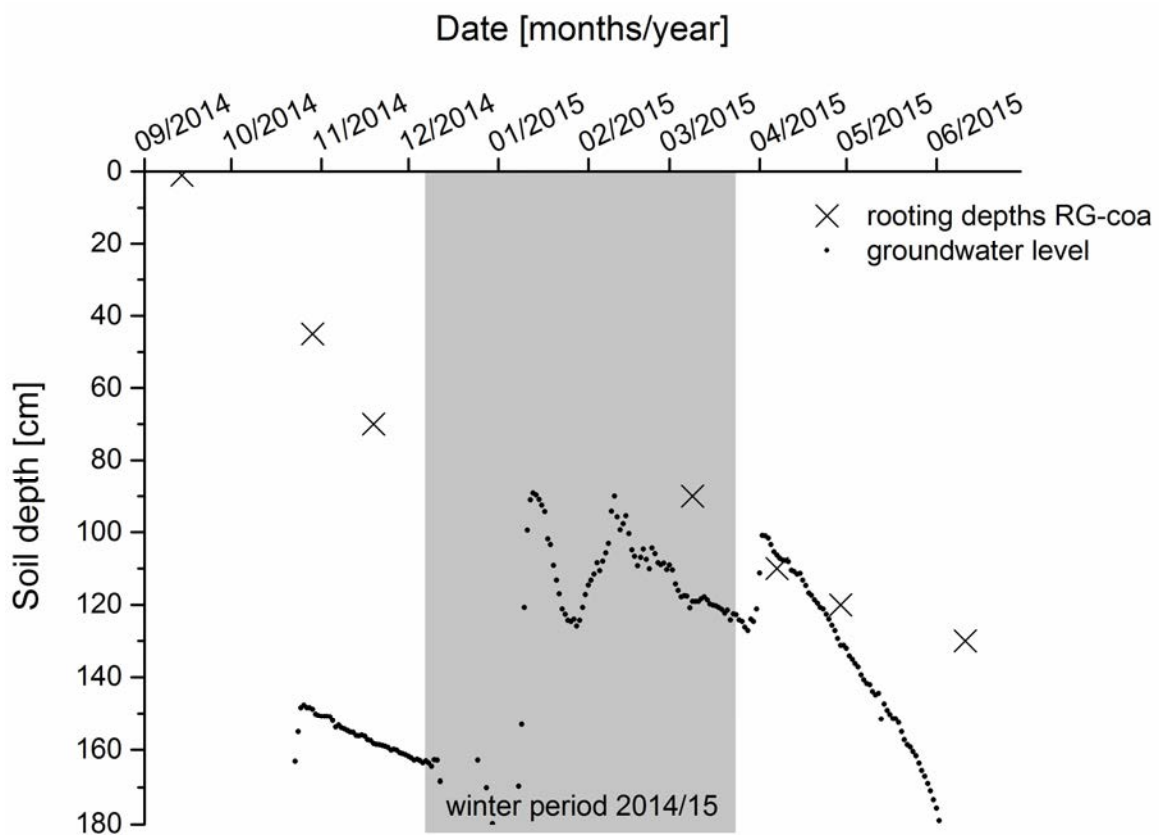


Figure 5.6: Daily mean temperatures in  $0.2 \text{ m}$  soil depth at the three landscape positions: footslope (RG-coa), plateau (LV-ab) and steep slope (RG-ca) for the winter period from November 22<sup>th</sup>, 2014 to March 28<sup>th</sup>, 2015; the red dotted line indicates the critical  $2^\circ\text{C}$  soil temperature threshold for the growth of wheat roots.

## V Root development of winter wheat in erosion-affected soils depending on the position in a hummocky ground moraine soil landscape

At greater depths ( $\geq 0.4$  m), soil temperatures did not drop below the critical value of  $+2^{\circ}\text{C}$  (data not shown). The smallest value of the root depth penetration for RG-coa could be explained by its landscape position. At the edge of a topographic depression, root penetration was affected and probably limited by the groundwater rise during the winter period (Fig. 5.7). For a similar landscape position at this experimental field, relatively high water tables ( $< 1$  m soil depth) were reported before (Gerke et al., 2016). The relatively high water saturation of the subsoil was likely unfavorable for the root growth; after a stagnation during the winter, root depth penetration seemed to followed the receding water table in the spring (Fig. 5.7), as similarly observed for wheat by Tripathi and Mishra (1986).



*Figure 5.7: The ground water table and the rooting depth development during the growing season of the winter wheat (September 2014 - June 2015) at the topographic depression of the experimental field site CarboZALF-D. The symbols [X] mark the mean rooting depths measured at the minirhizotron site RG-coa. The ground water table data was obtained from data of tensiometers that were located next to the minirhizotron tubes. The minirhizotron tubes were installed at an elevated position approx. 10 cm above that of the water table measurements, such that the water table was perhaps slightly deeper than indicated here as compared to the location of the root access tubes at the RG-coa profile.*

This position-dependent “water table effect” could also explain the observed deviations in the rates of downward root penetration between footslope (RG-coa), plateau (LV-ab), and steep slope (RG-ca) positions (Fig. 5.3) during the winter.

The almost linear relationship between root depths and cumulative daily temperatures for winter wheat of all soil types (Fig. 5.4) until the stem elongation stage corresponded with observations of Thorup-Kristensen et al. (2009), who reported a linear relationship for roots of wheat growing in Hapludalf soils. Rates of downward penetration of the wheat root system of LV-ab, RG-coa, and RG-ca determined here (Table 5.4) were close to the rates (0.6 - 0.9 mm °C<sup>-1</sup> d<sup>-1</sup>) found by Gregory and Eastham (1996) for a shallow “duplex soil” (Typic Natrixeralf); however, these rates were slightly lower than those (1.3 mm °C<sup>-1</sup> d<sup>-1</sup>) reported by Thorup-Kristensen et al. (2009). Considering the erosion history at each of the landscape positions at footslope (RG-coa), plateau (LV-ab) and steep slope (RG-ca), the erosion-induced modifications of the soil profile seemed to have only little impact on final downward penetration of the wheat roots at the end of the vegetation (Fig. 5.4). However, the development during the growth period (Fig. 5.3) indicated quite substantial differences in root dynamics between landscape positions mainly during autumn 2014 (crop establishment) and during the winter (i.e., water table effects), which eventually led to relatively large differences in crop yield (Table 5.3).

#### *5.4.3 Root biomass and root-to-shoot ratios at different landscape positions*

The root biomasses (Table 5.5) at RG-coa, LV-ab, and RG-ca (76 - 246 g DM m<sup>-2</sup>) were in a typical range reported for winter wheat by Chirinda et al. (2014) and Bolinder et al. (1997) of 93 - 121 g DM m<sup>-2</sup> and 251 - 386 g DM m<sup>-2</sup>. Higher root biomass at RG-coa as compared to RG-ca corresponded with results of Chirinda et al. (2014) and Slobodian et al. (2002) for wheat roots determined in soil cores at higher and lower elevated landscape positions in hummocky soil landscapes in Denmark (soils: Stagnic Podzoluvisol, Aric Anthrosol; 0 to 1 m depth) and in Canada (Chernozem in the Dark Brown soil zone; 0 to 1.8 m depth).

The calculated relationship between the below-ground and the above-ground biomass revealed typical R:S ratios (cf., Bolinder et al., 1997; 0.09 to 0.26) for winter wheat at post-anthesis of about 0.17 (RG-coa) and 0.16 (LV-ab), when assuming an average specific root length (SRL) value of 100 g m<sup>-2</sup> (Table 5.5). The much smaller R:S ratio for RG-ca of about 0.09 was probably caused by a combined effect of relatively small biomass (cf., Table 5.3) and highest dry matter content of the above ground biomass (Table 5.3); note that the plant stock of the winter wheat crop at RG-ca was relatively small (Gudrun Buddrus, ZALF Müncheberg, personal communication, 2015). However, such small R:S ratios of around 0.1 have also been reported for winter wheat after anthesis elsewhere (Barraclough and Leigh,

1984; loamy soils). For later crop development stages such as EC 71, a decrease in the ratio of root to shoot biomass with increasing phenological growth stages of wheat is well known (e.g., Siddique et al., 1990). The relatively similar R:S ratios at plateau and footslope position observed here (Table 5.5) were in line with R:S ratios reported by Chirinda et al. (2014) of about 0.12 for shoulder (Podzoluvisol) and 0.13 footslope (Anthrosol) positions.

Note that Gerke et al. (2016) simulated the hillslope position-specific water balance components by assuming that the root growth at different hillslope positions was proportional to observed LAI and a constant R:S relation. Considering the results of the biomass ratio (Table 5.5) and the strong correlations of root parameters to the LAI values (section 3.1), the recent assumptions in the model analysis of Gerke et al. (2016) were found to hold true except for the strongly eroded RG-ca profile. Therefore, cumulative differences in drainage and leaching between scenarios assuming position-specific crop growth at the most eroded hillslope position and the uniform crop growth scenario were probably larger as predicted in Gerke et al. (2016). The use of an adjusted R:S ratio for more-or-less colluviated and eroded soils could probably close this knowledge gap for many of the landscape positions – like the eroded Luvisol, which covers the largest aerial fraction in the hummocky soil landscape. However, more research is still needed to describe the dynamics of the interaction between gradually changing soil properties, seasonal changing soil moisture, and weather-dependent crop developments.

## 5.5. Conclusions

The root development of winter wheat (*Triticumaestivum* L.) was observed using the minirhizotron technique at three plots representing contrasting erosion-affected soils that occur in the hummocky post glacial soil landscape. Manifested by root density values, soils at extremely eroded steep slope position (RG-ca) seemed to impede the crop and root development of winter wheat in comparison to non-eroded Luvisol (LV-ab) located at plateau, while for the soils in topographic depressions, root growth appeared to be mostly enhanced unless not limited by the groundwater table.

These results corroborated the hypothesis that changes in the crop-soil interaction induced by soil profile modifications due to long-term soil erosion by tillage and water could be reflected also in the root growth of the wheat. At the colluvial soil (RG-coa), the depth penetration rate of roots indicated that the groundwater table fluctuations mainly in the topographic depression were controlling maximal root depths. The relationship between the above- and below-ground crop developments suggested that plant parameters could be used as indicator of root growth of winter wheat for major soils in the hummocky soil landscape.

However, only crops at the plateau and footslope positions seemed to establish a functional equilibrium in the root-to-shoot relation. Results confirmed that the field variability in the aboveground biomass could serve as a proxy for the variability in root biomass, but not for an approximation of R:S ratios in general. The stronger variation of root densities between soils as compared to crop yield indicated that erosion-induced landscape position-specific soil properties have a greater effect on below- than on above-ground plant development causing spatially variable R:S ratios. When simulating water fluxes and solute transport including crop uptake, the present results suggested that different water and solute balances when considering a position-specific belowground plant development as compared to assuming a uniform root development. The spatially according to the landscape position distributed root growth of winter wheat indicated that root development was affected by erosion-induced soil evolution. Still further improvements are needed to better analyze the relationships between the dynamic interactions of the crop and root system development and the erosion history at various landscape positions not only with respect to the hummocky soil landscape.

### *Acknowledgements*

The study was a part of the CarboZALF project of the Leibniz Centre for Agricultural Landscape Research (ZALF). The CarboZALF project was financially supported by the German Federal Ministry of Food, Agriculture and Consumer Protection (BMELV) and the Ministry of Environment, Health and Consumer (MLUV) of the State of Brandenburg. The authors thank Norbert Wypler (minirhizotron tube installation), Ingrid Onasch (LAI measurements), Wilfried Hierold (soil classification) and Lidia Völker (GIS application) from the ZALF-Institute of Soil Landscape Research and Gernot Verch (crop cultivation) and Gudrun Buddrus (plant data, biomass) from the Research Station Dedelow of the ZALF.

### *References*

Aldana Jague, E., Sommer, M., Saby, N. P.A., Cornelis, J.-T., Van Wesemael, B., Van Oost, K. (2016): High resolution characterization of the soil organic carbon depth profile in a soil landscape affected by erosion. *Soil Till. Res.* 156, 185-193.

Barraclough, P.B., Leigh, R.A. (1984): The growth and activity of winter wheat roots in the field: the effect of sowing date and soil type on root growth of high-yielding crops. *J. Agric. Sci.* 103, 59-74.

Bengough, A.G., Mullins, C.E. (1990): Mechanical impedance to root growth: a review of experimental techniques and root growth responses. *J. Soil Sci.* 41, 341-358.



Bolinder, M.A., Angers, D.A., Dubuc, J.P. (1997): Estimating shoot to root ratios and annual carbon inputs in soils for cereal crops. *Agric. Ecosyst. Environ.* 63, 61-66.

Bronick, C. J., Lal, R. (2005): Soil structure and management: a review. *Geoderma* 124, 3-22.

Buckland, S.T., Campbell, C.D., Mackie-Dawson, L.A., Horgan, G.W., Duff, E.I. (1993): A method for counting roots observed in minirhizotrons and their theoretical conversion to root length density. *Plant Soil* 153, 1-9.

Chirinda, N., Roncossek, S. D., Heckrath, G., Elsgaard, L., Thomsen, I. K., Olesen, J. E. (2014): Root and soil carbon distribution at shoulderslope and footslope positions of temperate toposequences cropped to winter wheat. *Catena* 123, 99-105.

Cresswell, H.P., Kirkegaard, J.A. (1995): Subsoil amelioration by plant-roots-the process and the evidence. *Soil Res.* 33, 221-239.

De Ruijter, F.J., Veen, B.W., Van Oijen, M. (1996): A comparison of soil core sampling and minirhizotrons to quantify root development of field-grown potatoes. *Plant Soil* 182, 301-312.

Ellerbrock, R. H., Gerke, H. H., Deumlich, D.(2016): Soil organic matter composition along a slope in an erosion-affected arable landscape in North East Germany. *Soil Till. Res.* 156, 209-218.

Gerke, H.H., Rieckh, H., Sommer, M. (2016): Interactions between crop, water, and dissolved organic and inorganic carbon in a hummocky landscape with erosion-affected pedogenesis. *Soil Till. Res.* 156, 230-240.

Gerke, H.H., Hierold, W. (2012): Vertical bulk density distribution in C-horizons from marley till as indicator for erosion history in a hummocky post-glacial soil landscape. *Soil Till. Res.* 125, 116-122.

Gregory, P.J., Eastham, J. (1996): Growth of shoots and roots, and interception of radiation by wheat and lupin crops on a shallow, duplex soil in response to time of sowing. *Crop Pasture Sci.* 47, 427-447.

Gyssels, G., Poesen, J., Bochet, E., Li, Y. (2005): Impact of plant roots on the resistance of soils to erosion by water: a review. *Prog.Phys.Geogr.* 29, 189-217.

Hack, H., Bleiholder, H., Buhr, L., Meier, U., Schnock-Fricke, U., Weber, E., Witzemberger, A. (1992): Einheitliche Codierung der phänologischen Entwicklungsstadien mono-und dikotyler pflanzen–Erweiterte BBCH-Skala, Allgemein. *Nachrichtenbl. Deut. Pflanzenschutzd* 44, 265-270.

IUSS Working Group WRB (2015): World Reference Base for Soil Resources 2014, update 2015, International soil classification system for naming soils and creating legends for soil maps. World Soil Resources Reports No. 103. FAO, Rome.

Johnson, M. G., Tingey, D. T., Phillips, D. L., Storm, M. J. (2001): Advancing fine root research with minirhizotrons. *Environ. Exp. Bot.* 45, 263-289.

Kaspar, Th. C., Pulido, D.J., Fenton, T.E., Colvin, T.S., Karlen, D.L., Jaynes, D.B., Meek, D.W. (2004): Relationship of corn and soybean yield to soil and terrain properties. *Agron. J.* 96, 700-709.

Kodešová, R.K., Vít, Ž.A., Šimůnek, J.(2006): Impact of plant roots and soil organisms on soil micromorphology and hydraulic properties. *Biologia* 61, 339-343.

Levan, M.A., Ycas, J.W., Hummel, J.W. (1987): Light leak effects on near-surface soybean rooting observed with minirhizotrons. *Minirhizotron Observation Tubes: methods and applications for measuring rhizosphere dynamics*, American Society of Agronomy, Inc., Crop Science Society of America, Inc., Soil Science Society of America, Inc., Madison, Wisconsin, USA, 89-98.

Lin, H. (2011): Three Principles of Soil Change and Pedogenesis in Time and Space. *Soil Sci. Soc. Am. J.* 75, 2049-2070.

Liu, L., Gan, Y., Bueckert, R., Van Rees, K.(2011): Rooting systems of oilseed and pulse crops I: Temporal growth patterns across the plant developmental periods. *Field Crops Res.* 122, 256-263.

Løes, A.-K., Gahoonia, T.S. (2004): Genetic variation in specific root length in Scandinavian wheat and barley accessions. *Euphytica* 137, 243-249.

Majdi, H. (1996): Root sampling methods-applications and limitations of the minirhizotron technique. *Plant Soil* 185, 255-258.

Meena, B.L., Singh, A.K., Phogat, B.S., Sharma, H.B. (2013): Effects of nutrient management and planting systems on root phenology and grain yield of wheat (*Triticum aestivum*). *Indian J Agric Sci* 83, 627-632.

Merrill, S.D., Black, A.L., Bauer, A. (1996): Conservation tillage affects root growth of dryland spring wheat under drought. *Soil Sci. Soc. Am. J.* 60, 575-583.

Merrill, S.D., Upchurch, D.R. (1994): Converting root numbers observed at minirhizotrons to equivalent root length density. *Soil Sci. Soc. Am. J.* 58, 1061-1067.

Merrill, S.D., Tanaka, D. L., Hanson, J.D. (2002): Root length growth of eight crop species in Haplustoll soils. *Soil Sci. Soc. Am. J.* 66, 913-923.

Migdall, S., Bach, H., Bobert, J., Wehrhan, M., Mauser, W. (2009): Inversion of a canopy reflectance model using hyperspectral imagery for monitoring wheat growth and estimating yield. *Precis. Agric.* 10, 508-524.

Mitchell, A.R., van Genuchten, M. Th. (1992): Shrinkage of bare and cultivated soil. *Soil Sci. Soc. Am. J.* 56, 1036-1042.

Moulin, A.P., Anderson, D.W., Mellinger, M. (1994): Spatial variability of wheat yield, soil properties and erosion in hummocky terrain. *Can. J. Soil Sci.* 74, 219-228.

Muñoz-Romero, V., López-Bellido, L., and López-Bellido, R. J. (2012) The effects of the tillage system on chickpea root growth. *Field Crops Res.*, 128, 76-81. Paponov, I.A., Lebedinskai, S., Koshkin, E.I. (1999): Growth analysis of solution culture-grown winter rye, wheat and triticale at different relative rates of nitrogen supply. *Ann. Bot.* 84, 467-473.

Porter, J. R., Gawith, M. (1999): Temperatures and the growth and development of wheat: a review. *Eur. J. Agron.* 10, 23-36.

Premke, K., Attermeyer, K., Augustin, J., Cabezas, A., Casper, P., Deumlich, D., Gelbrecht, J., Gerke, H. H., Gessler, A., Grossart, H.-P. (2016): The importance of landscape diversity for carbon fluxes at the landscape level: small-scale heterogeneity matters. *Wiley Interdiscip. Rev. Water* 4 601–617.

Rieckh, H., Gerke, H. H., Sommer, M. (2014): Water and Dissolved Carbon Fluxes in an Eroding Soil Landscape Depending on Terrain Position *Vadose Zone J.* 13.

Rieckh, H., Gerke, H. H., Sommer, M. (2012): Hydraulic properties of characteristic horizons depending on relief position and structure in a hummocky glacial soil landscape. *Soil Till. Res.* 125, 123-131.

Samson, B.K., Sinclair, T.R. (1994): Soil core and minirhizotron comparison for the determination of root length density. *Plant Soil* 161, 225-232.

Siddique, K.H.M., Belford, R.K., Tennant, D. (1990): Root: shoot ratios of old and modern, tall and semi-dwarf wheats in a Mediterranean environment. *Plant Soil* 121, 89-98.

Šimůnek, J., Sejna, M., Saito, H., Sakai, M., van Genuchten, M. Th. (2008): The HYDRUS-1D software package for simulating the one-dimensional movement of water, heat, and multiple solutes in variably-saturated media, Version 4.0x, Hydrus Series 3, Department of Environmental Sciences, University of California Riverside, Riverside, CA, USA. .

Slobodian, N., Van Rees, K., and Pennock, D. (2002): Cultivation-induced effects on belowground biomass and organic carbon. *Soil Sci. Soc. Am. J.* 66, 924-930.

Sommer, M., Gerke, H. H., Deumlich, D. (2008): Modelling soil landscape genesis - A "time split" approach for hummocky agricultural landscapes. *Geoderma* 145, 480-493.

---

Stone, J.R., Gilliam, J.W., Cassel, D.K., Daniels, R.B., Nelson, L.A., Kleiss, H.J. (1985): Effect of erosion and landscape position on the productivity of Piedmont soils. *Soil Sci. Soc. Am. J.* 49, 987-991.

Thorup-Kristensen, K., Cortasa, M. S., Loges, R. (2009): Winter wheat roots grow twice as deep as spring wheat roots, is this important for N uptake and N leaching losses? *Plant Soil* 322, 101-114.

Tingey, D.T., Phillips, D.L., Johnson, M. G. (2000): Elevated CO<sub>2</sub> and conifer roots: effects on growth, life span and turnover. *New Phytol.* 147, 87-103.

Traoré, O., Groleau-Renaud, V., Plantureux, S., Tubeileh, A., Boeuf-Tremblay, V. (2000): Effect of root mucilage and modelled root exudates on soil structure. *Eur. J. Soil Sci.* 51, 575-581.

Tripathi, R.P., Mishra, R.K. (1986): Wheat root growth and seasonal water use as affected by irrigation under shallow water table conditions. *Plant Soil* 92, 181-188.

Unger, P. W., Kaspar, Th. C. (1994): Soil compaction and root growth: a review. *Agron. J.* 86, 759-766.

Upchurch, D.R., Ritchie, J.T. (1983): Root observations using a video recording system in mini-rhizotrons. *Agron. J.* 75, 1009-1015.

Wang, B.J., Zhang, W., Ahanbieke, P., Gan, Y.W., Xu, W.L., Li, L.H., Christie, P., and Li, L. (2014): Interspecific interactions alter root length density, root diameter and specific root length in jujube/wheat agroforestry systems. *Agrofor. Syst.* 88, 835-850.

Wilhelm, W.W., Mielke, L.N., Fenster, C. R. (1982): Root development of winter wheat as related to tillage practice in western Nebraska. *Agron. J.* 74, 85-88.



Aerial photograph of the arable hummocky soil landscape

## 6| General Discussion

This thesis contributes to the general understanding of feedbacks of erosion affected spatial differentiation of soil types on the water balance, dissolved carbon fluxes, soil hydraulic properties and the root growth of crops in a morainic arable soil landscape. The following general discussion provides an overview of main findings and an integrative discussion, while a detailed illustration of thesis results is given within the individual chapters 2 to 5.

### *6.1 Main results and concluding remarks*

In Herbrich and Gerke (2016, chapter 2), the filtering scheme for lysimeter time series using time intervals larger than the recurrent temporal autocorrelation signal provides the basis for the calculation and comparison of water balance components between differently eroded Luvisols (chapter 3), respectively. The autocorrelation analysis of lysimeter time series revealed that temporal autocorrelation lengths varied according to the seasonal rainfall characteristics over one year. In general, correlated time lags were shortest for summer storm events and longest for winter periods including snow fall. The cumulative values of lysimeter mass changes from time intervals larger than the autocorrelation length

(e.g., 60 min) provided the most reliable approximation of the quantity of precipitation on the expense of a reduced temporal resolution.

Based on the autocorrelation filtering scheme, study results of Herbrich et al. (2017a) (chapter 3) identified changes in the water balance and dissolved carbon leaching as a result of the erosion-induced pedogenesis considering complex soil-crop interactions for lysimeter monoliths. The increased deep drainage of the truncated soils filled in lysimeters suggested that the downward water movement in the profile increased from less to more eroded soils. However, truncated profiles with reduced solum depths also received a larger amount of precipitation which was possibly resulting from interactions between the crop development and more rainfall interception by above ground biomass. Contrasting leaching rates of dissolved carbon between eroded and less eroded lysimeter monoliths suggested the dissolved carbon export in the hummocky soil landscape were mainly driven by seepage water fluxes rather than by heterogeneities of dissolved carbon concentration at the lysimeter bottom. In order to be able to infer differences in the water flow and carbon transport of lysimeters filled with truncated soil profiles that varied in solum thickness and the vertical profile sequence, information about the soil hydraulic properties and the soil water uptake by crops (root growth) were obtained in studies of Herbrich and Gerke (2017) (chapter 4) and Herbrich et al. (2017b) (chapter 5), respectively.

The observations of the TDR probes and matrix potential sensors installed into each lysimeter (chapter 4) allowed identifying individual drying and wetting cycles from field water retention data, which revealed complex dynamics at daily, seasonal, and inter-annual time scales. While short-term water retention dynamics reflected soil structural and wettability changes, long-term dynamics indicated modifications in tillage management and erosion history of each soil. Study results confirmed, thereby, the still occurring inconsistency between in situ field water retention and water retention data derived from soil core samples in the laboratory. In chapter 5, differences in the root growth between Haplic Luvisols, strong eroded Calcaric Regosols and depositional Colluvic Regosols reflected an inter-related landscape position-specific root development at contrasting terrain positions. Herbrich et al. (2017b) revealed that changes in the crop-soil interaction induced by soil profile modifications due to long-term soil erosion by tillage and water were not only distinguished for above-ground crop development but also for root growth of wheat plants.

The results of this thesis finally conclude that erosion-affected modifications of soil profiles affecting soil-crop interactions and soil properties should be considered for quantifications of landscape scale water balances and the leaching of dissolved carbon fractions. Especially in arable soils, hydraulic parameters represent non-equilibrium conditions in the suction-water content relations at different time scales reflected in changes of the van Genuchten

parameters – a parameter set to describe the soil-water-content-pressure-head relation and soil water retention curves, respectively. Therefore, not only erosional changes in soil horizon properties such as texture and porosity, but also hysteretic and seasonal dynamics in hydraulic properties during the vegetation period were shown to be important especially when dealing with soils of intensively cultivated, eroded landscapes. Changes in the crop-soil interaction due to long term soil erosion by tillage and water were reflected by the root growths of winter wheat; especially crops at exposed hilltops seemed to establish a dissimilar root-to-shoot functional equilibrium comparing crops at the plateau and toe slope positions. The correlation between the above- and below-ground crop biomass suggested that plant parameters can be used as indicator of root growth of winter wheat. However, the field variability in the aboveground biomass could not serve as a proxy for the variability in root biomass in general, because of the contrasting shoot-to-root-ratios for the different landscape positions. Finally, erosion-affected modifications on arable soil profiles including an alteration on root growth and soil water retention properties can be associated with differences in the water and carbon balance of differently eroded soils. Here, even a small differentiation of the soil profiles such as in the sequence of horizons or depths of solum results in large change of water balance components, in particular deep drainage, and hence carbon leaching.

Overall, the four articles within this thesis provide novel information on the hydro-pedological response of erosion induced profile modifications of soils from the hummocky post-glacial landscape. In the context of hydro-pedology, landscape positions and soil structural development were found to affect crop parameter and hydraulic properties of erosion induced soil horizons leading to heterogeneous distributed water and solute fluxes. Most study results (chapter 2 to 4), however, were derived by a rather small erosion gradient between differently eroded Haplic Luvisols. Hence, the benchmarked impacts of soil erosion on water balance components such as deep drainage should be regarded as a minimum impact only, considering the overall landscape erosion gradient. Study results of the water balance analysis from the second lysimeter hexagon (see Figs. 6.1a and 6.1b, not published yet) corroborated the hypothesis of Herbrich et al. (2017a, chapter 3) that rates of deep drainage increased with a stronger truncation of soil profiles. The positive cumulative water flux (drainage) at the lysimeter bottom increased from the Calcaric Regosols to the Haplic Luvisols strongly from 2014, April to 2016, December (Fig. 6.1a). For this almost 3-years-period, the lysimeter filled with the strong eroded Calcaric Regosol exceeded the cumulative outflow at the bottom of the Luvisols almost by the factor of 3. Similar to findings of Herbrich et al. (2017a), the partitioning of infiltrated rain water among drainage was different for more or less eroded profiles. The ratio of drained soil water to precipitation was much higher for

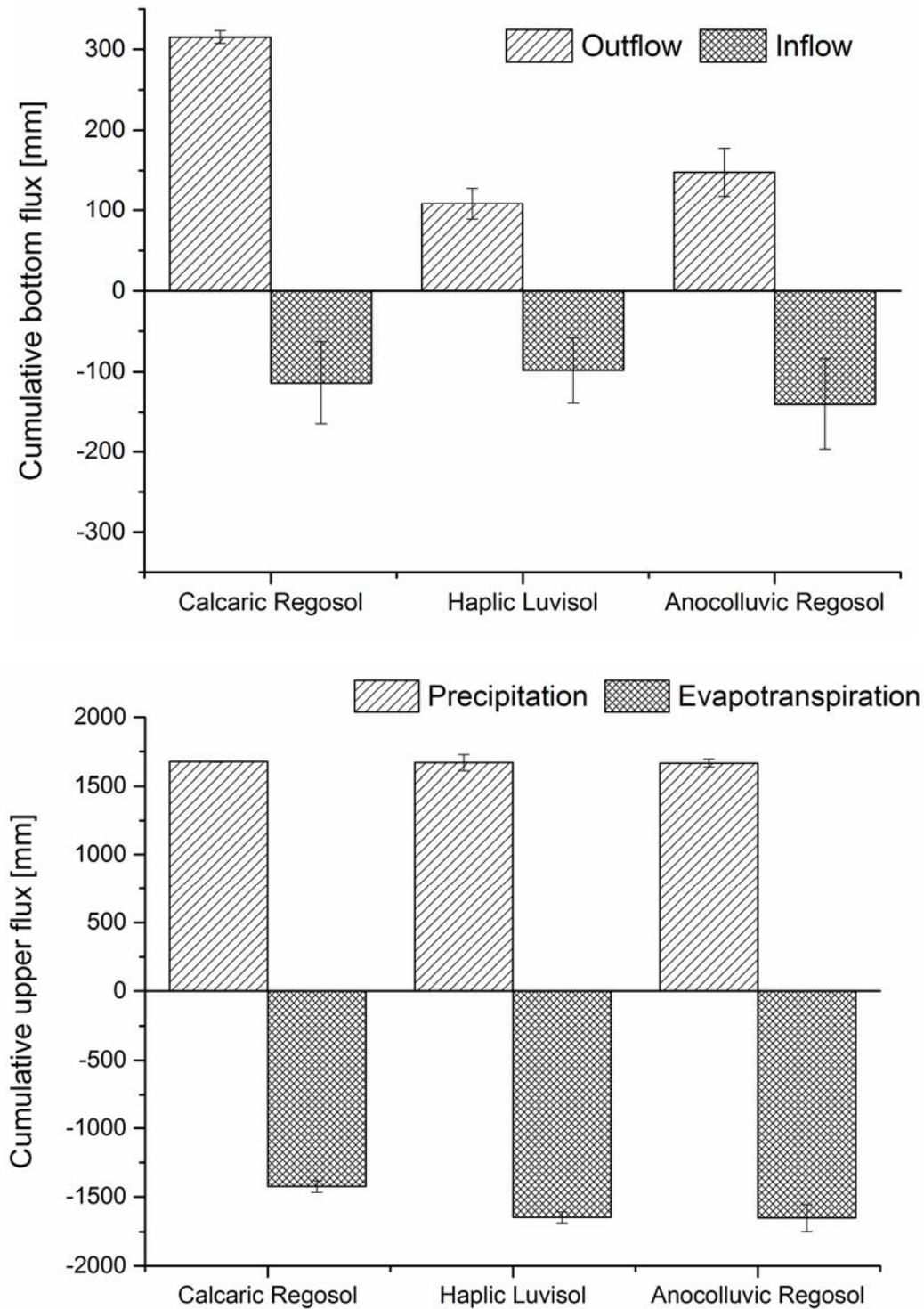
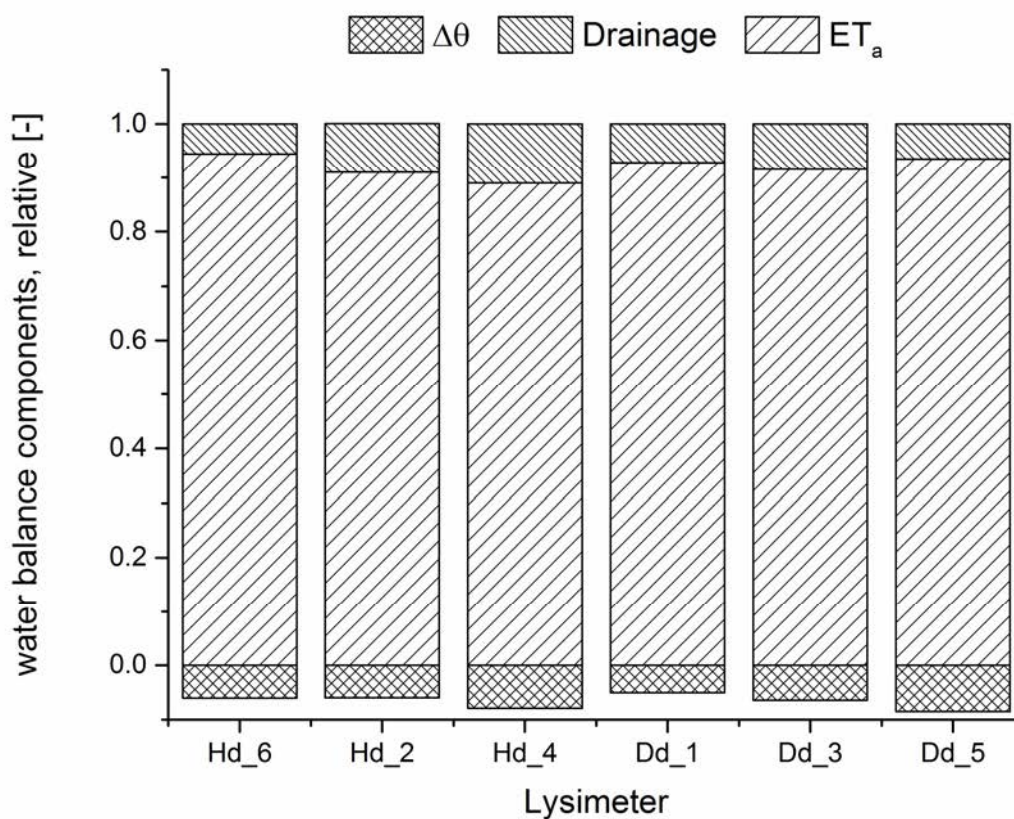


Figure 6.1a and 6b: Water balance components of 12 lysimeters with differently eroded Haplic Luvisols, strong eroded Calcaric Regosols and depositional Colluvic Regosols over the period of 3-years for 2014, April to 2016, December: a) cumulative bottom flux [mm] (above) and b) cumulative upper flux [mm] (below). The cumulative bottom flux was either positive (outflow) or negative (inflow) by the injection of water by suction cup rake at the bottom. The cumulative upper flux was either positive (precipitation) or negative (evapotranspiration).



the strong eroded soils located at steep slopes. Here, Calcaric Regosols revealed a drainage ratio of 0.19 while for Luvisols a value of 0.07 could be observed.

Therefore, the solum depths-drainage relation reported by Herbrich et al. (2017a, chapter 3) for Luvisols that varied in degree of past soil erosion seemed to be transferable to complete soil landscape inventory starting from Calcaric Regosols on exposed hilltops to less or non eroded Haplic Luvisols on plateau positions. However, erosion induced changes in drainage reported in Herbrich et al. (2017a) were not consistent between the two study sites Hd and Dd at all when considering the relative water balance components for the study period from 2011 to 2013 (Fig. 6.2).



*Fig. 6.2: Relative water balance components (drainage, evapotranspiration –  $ET_a$ , changes in soil water storage -  $\Delta\theta$ ) standardized to the amount of precipitation of each lysimeter from April, 2011 to March, 2013.*

Here, Hd lysimeter soils revealed a distinct relation between erosion-induced soil profile modification and the water balance drainage and evapotranspiration. Same holds true for monoliths taken from Dd site except that soil of Dd\_5 which had technical problems with the leachate scale during data collection. But, in general, the drainage/precipitation-ratio was smaller for the more eroded Dd soils, especially Dd\_3, in comparison to the less eroded soils

of Hd\_2 and Hd\_4. At this point more investigations are needed to explain such differences in water fluxes and deep drainage between more (Dd) and less (Hd) eroded monoliths and their dissolved carbon leaching potential - water balance simulations might be a helpful instrument giving reasons for the consistent drainage/precipitation-ratios within each study site and the inconsistent drainage/precipitation-ratios between Hd and Dd soils.

Furthermore, findings of Herbrich et al. (2017a) are evaluated for the 1-D water flow model from lysimeters only, and not for the specific positions of soils within the hillslope. From lysimeter derived study results, it can be suggested that percolation of rain waters will increase and groundwater storage are probably accelerated, respectively, if solum depths are truncated by soil erosion processes. This suggestion corresponds to field observations of Große and Renger (1974) during an irrigation experiment under early spring conditions. While the hydraulic gradient in the eroded (truncated) profile indicated downward movement, water flow was still directed upwards in the less eroded soil. These authors interpreted differences in the direction of the soil water movement between less and more eroded soil profiles (Luvisol) by contrasting initial soil moisture conditions that had established during the winter period before the irrigation experiment started. The differences in the drainage rates of the two lysimeter hexagons in the early spring from January to April (2014–2016) also indicate a more downward movement of soil water of the eroded soil profiles as compared to less or non-eroded profiles in each year. Here, the drainage ratios of Luvisols to the strong eroded Calcaric Regosols were 0.02 for 2014, 0.82 for 2015 and 0.25 for 2016 under similar precipitation conditions (RG-ca: 418 mm; LV-ab: 393 mm, data is not shown). In particular during vegetation periods, the generally lower soil water storage of the strong eroded Calcaric Regosols was reflected in the lowest amounts of evapotranspiration from 2014, April to 2016, December (Fig. 6.1b). In contrast to the study of Herbrich et al. (2017a, chapter 3), the amount of the cumulative precipitation was very similar for the three soil types for that period. Here, crops characterized by a small maximum height and surface such as winter wheat and Persian clover were probably the reason for homogeneous distributed precipitation as compared to Luvisols cultivated with rather tall crops (maize, sudangrass) during the growing seasons of 2010 to 2012.

## *6.2 Classification of study results regarding carbon leaching*

In the hummocky soil landscape, stocks of soil organic carbon varied strongly due to removal of carbon-rich soil material from eroding slope positions to colluvial depressions. The carbon pool in soil landscape under agricultural use can act as a sink or a source of carbon to the atmosphere (e.g., Doetterl, 2016). However, the carbon exchange between terrestrial ecosystems and the atmosphere is still rarely discussed. Results of the current lysimeter

study revealed annual rates of carbon leaching of about  $\sim 0.5 \text{ g C m}^{-2} \text{ yr}^{-1}$  (DOC) and  $\sim 5 \text{ g C m}^{-2} \text{ yr}^{-1}$  (DIC) for soils at plateau and shallow slope positions. Considering higher rates of drainage for the strong eroded soils at steep slopes by a factor of 3 (see section 6.1) and the close relation of soil water fluxes on carbon leaching (Herbrich et al, 2017a), it can be suggested that carbon exports were in a range of about  $\sim 1.5 \text{ g C m}^{-2} \text{ yr}^{-1}$  (DOC) and  $\sim 15 \text{ g C m}^{-2} \text{ yr}^{-1}$  (DIC) for the study period and landscape position, respectively. This magnitude of carbon leaching was more-or-less in the same range of values reported by Kindler et al. (2011; DOC:  $\sim 4 \text{ g C m}^{-2} \text{ yr}^{-1}$ , DIC:  $\sim 16 \text{ g C m}^{-2} \text{ yr}^{-1}$ ) and Walmsley et al. (2011) (DOC:  $\sim 3 \text{ g C m}^{-2} \text{ yr}^{-1}$ , DIC:  $\sim 15 \text{ g C m}^{-2} \text{ yr}^{-1}$ ) for arable soils, although dissolved organic carbon leaching was slightly lower as reported elsewhere. Also Rieckh et al. (2014) calculated similar carbon exports (DOC:  $\sim 1 \text{ g C m}^{-2} \text{ yr}^{-1}$ , DIC:  $\sim 8 \text{ g C m}^{-2} \text{ yr}^{-1}$ ) for strong eroded Calcaric Regosols using the combined approach of modeling water fluxes (HYDRUS 1D) and field concentration measurements.

Considering the whole carbon cycle of the postglacial soils at hummocky terrain, the revealed carbon export can be expected as rather small in comparison to the carbon sequestration of these soils postulated by field studies using automatic flow-through non-steady-state chamber measurements (e.g., Hoffmann et al. 2017). The reported annual mean erosion-induced carbon sequestration of about  $51 \text{ g C m}^{-2}$  seems to be exceeding that of the export of dissolved carbon fractions many times over for soils of the hummocky landscape. Moreover, the suggested carbon exports of about  $1.5 \text{ g C m}^{-2} \text{ yr}^{-1}$  (DOC) and  $\sim 15 \text{ g C m}^{-2} \text{ yr}^{-1}$  (DIC) ranged within the error margins ( $\sim 18 \text{ g C m}^{-2} \text{ yr}^{-1}$ ) of carbon budget measurements considering the  $\text{CO}_2$  exchange between soils and atmosphere (Hoffmann et al. 2017).

Nevertheless, the leaching potential of lysimeter soils indicated substantial differences in the solute export between landscape positions during each season, especially in spring and after storm events. These temporal exports, in turn, led to leaching hot spots and a relatively large potential effect on the carbon budget, which can mainly be observed during small-scale time frames.

### ***6.3 Suggestions based on thesis results***

Based on the Intergovernmental Panel on Climate Change report (IPPC, 2013), total precipitation and more intense rainfall events increased on average in the northern hemisphere and Europe, respectively, for the last decades. According to climate change scenarios in the IPCC report, further increases in extreme precipitation events can be expected. For regions of North and East Germany, a shift in the precipitation cycle is the

most likely scenario accordingly so that the probability of wet winter periods increased by a factor of five (e.g. Ministerium für Wirtschaft, Arbeit und Tourismus Mecklenburg-Vorpommern, 2010). In contrast, summer periods will be slightly drier, but characterized by more intense rainfall events.

Since rainfall characteristics have strong effects on soil erosion rates, erosion related climate change studies conclude that modifications in the amount and intensity of precipitation affect greater rates of soil erosion (e.g., Nearing et al., 2004; Mullan, 2013). The risk of soil erosion and related environmental consequences under climate change scenarios are apparent. Considering this thesis' results, the following conclusions can be drawn for the postglacial soil landscape under the forecasted changing climate conditions.

In Herbrich et al. (2017a) and in the discussion section above (see Figs. 6.1a and 6.1b) results illustrate that intense erosional modifications on soil profiles trend to result in larger rates of deep drainage. Considering that leaching of dissolved carbon fractions (DIC, DOC) were largely controlled by water fluxes, which corresponds with findings of e.g., Rieckh et al. (2014) and Don et al. (2008), thesis results suggest that decalcification processes may be fastest for strong eroded soil types as compared to the non-eroded profiles. The highest exports of DOC and especially DIC of the erosional truncated soil profiles of lysimeter soils indicate that the eroded soil profiles are undergoing rapid pedogenetic changes. The increased percolation and larger DIC leaching of truncated soils as compared to the less truncated ones may enhance the decalcification and weathering e.g., brunification, and lessivation of Bt-soil material in the transition zone of Bt-/C-horizons in Luvisols. Leaching of carbonates will further deepen the soil profile due to acidification and weathering processes of silicates and then decalcification may be followed by the formation of horizons with weathering characteristics. Therefore, the mismatch in drainage and carbon leaching rates will proceed to a differentiation of the vertical soil profile sequence between Luvisols and Regosols, but also between eroded and non eroded Luvisols.

In the future, the differentiation in the soil profile sequence and properties between differently erosional truncated soil profiles soils will probably increase due to higher rates of drainage and leaching, respectively, because of an alteration in the forecasted rainfall characteristics. Further, the characterization of soil horizon properties in Herbrich et al. (2017a, b), which are similar to findings of Gerke and Hierold (2012), showed spatial heterogeneity of bulk densities below the ploughing horizon. The E- and especially C-horizons of Luvisols can be strongly compacted into soils of the hummocky soil landscape. If the soil material of these horizons is dense enough to impede the infiltrated soil water for expanded periods of time, increased stagnic properties may result in soils at flat relief

positions such as plateaus due to forecasted increases in precipitation amounts during the winter months.

In addition to the water and carbon balance, changes in rainfall characteristics can be also associated with an alternation in the biomass production. In Herbrich et al. (2017a) and Herbrich et al. (2017b) results suggested that differences in crop growths depending on landscape position were driven by modifications in soil properties and differences in the soil moisture regime. Especially in summer periods reduced crop yields and crop development may be likely by taking climate change scenarios into consideration. The reported differences in plant stock and biomass production between steep slope and plateau positions (Herbrich et al., 2017b) will probably extend as a result of drying periods in summer which in turn lead to an enhanced soil removal at fallow areas during summer storm events.

Overall, thesis results suggest potential increases of carbon leaching and pedological differences between postglacial soil types for the upcoming decades, but results also suggest more research needs to be done to identify mechanism of the different drainage rates and carbon releases, respectively.

#### ***6.4 Soil water balance simulations***

To attain a better understanding of pedological processes between eroded and less eroded soil profiles leading to a divergence in the water and solute balance (Herbrich et al., 2017a), information about the water flow through the lysimeter monoliths is needed. Therefore, water balance simulations using program HYDRUS 1D (Simunek et al., 2005) were realized during this thesis (not published yet). The numerical modeling has been used to simulate specific water fluxes for each soil horizon for the undisturbed soil profiles of lysimeters of Dedelow and Holzendorf.

The water flow under variably-saturated conditions was described by the Richards equation with a uniform flow domain similar to the study of Rieckh et al. (2014). However, in this study the atmospheric upper boundary and the lower profile boundary conditions were set to the measured field data of the Hd and Dd lysimeters. Initially, the soil hydraulic functions of the van Genuchten-Mualem model were applied for parameterization using a parameter set of lab measurements (HYPROP) only. However, modeling attempts showed that the van Genuchten parameters derived by soil core measurements in the laboratory were not suitable to describe the hydraulic properties of lysimeter soils for a forward simulation under field conditions (not shown). To overcome this lack in parameterization, the unimodal water retention function of van Genuchten was used to describe the field water retention data (cf.

Herbrich and Gerke, 2017) and applied for the van Genuchten parameter set of this water balance simulations for topsoil regions (10, 30, 50 cm).

Modeling results using a combination of lab (50 – 150 cm soil depths) and field measurements (0 – 50 cm soil depths) to describe the hydraulic properties of monoliths ensured a much better match between field lysimeter and simulations of the volumetric water content (Fig. 6.3). However, results also revealed that simulations still were out of line with in situ data for certain time periods. Here, physical processes in the field water flow seem not to be properly described by the van Genuchten-Mualem model arising from occurring e.g., preferential flow paths (e.g. Gerke, 2006), soil hysteresis (e.g., Hannes et al., 2016) and/or seasonal dynamics in hydraulic properties (Herbrich and Gerke, 2017).

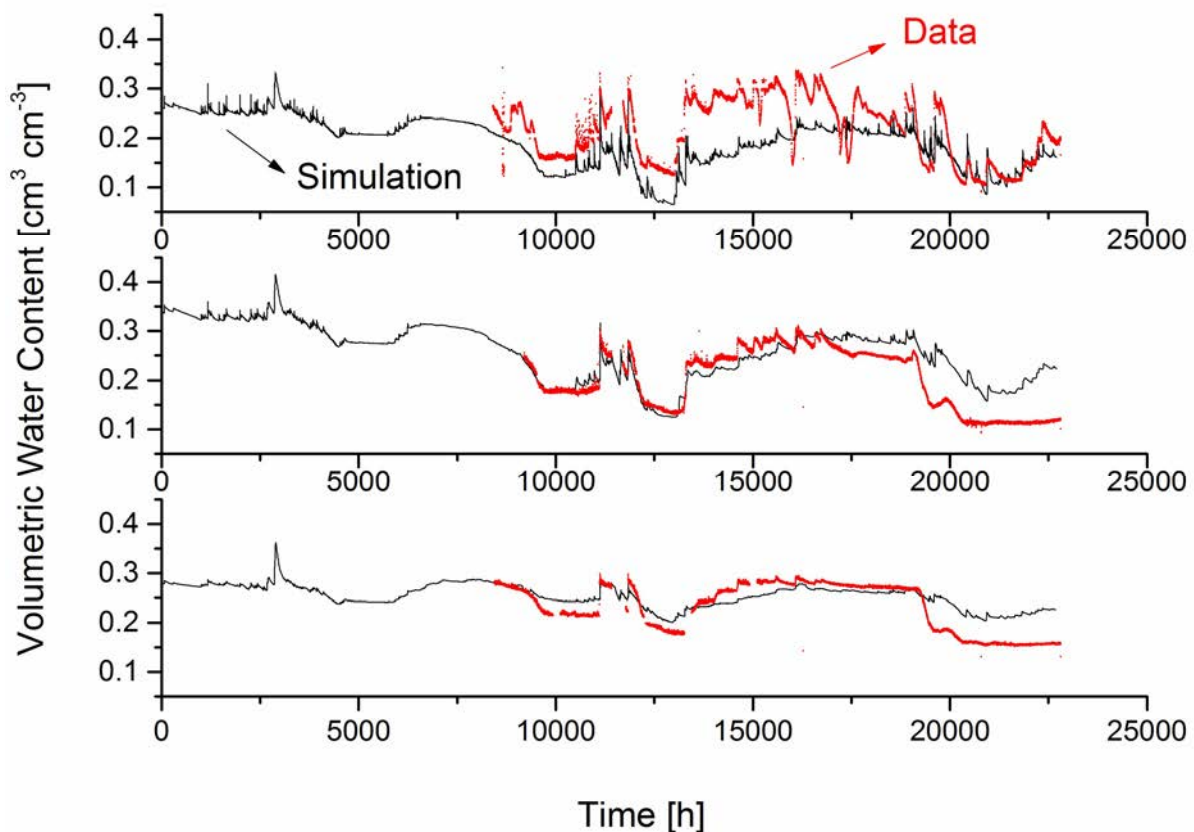


*Figure 6.3: Simulations of the soil water balance from April, 30th 2011 to Decemeber, 31th 2013 for three soil depths (10 cm – above; 30 cm – middle; 50 cm – below). Red data points belong to the volumetric water content of the field lysimeter filled with an eroded Luvisol (Dd\_1). The black line corresponds to the soil water simulations using HYDRUS 1D.*

In this context, first simulation results of this study demonstrated that the van Genuchten–Mualem model is limited for simulations of the water balance of lysimeters leading to

defective predictions of volumetric water content. A more complex dual-porosity or dual-permeability water flow model dealing with two interacting pore regions (inter-aggregate and intra-aggregate pores) would be promising to solve discrepancies between the forward simulation and field data of Dd and Hd soils. Otherwise, the provided lysimeter data from this thesis serves as the basis for an inverse modeling approach which would be a further instrument to solve the lack in the parameterization of soil hydraulic properties of the monoliths.

## 6.5 Limitations

The individual studies provide a comprehensive data set as basis for modeling of water fluxes and describing the landscape scale water and element balance in the hummocky post-glacial landscape, however, some limitations were included considering the methodology which was applied.

First, soil and atmospheric conditions for lysimeter applications were known to be more-or-less different to the surrounding area, so-called oasis effect. The oasis effect phenomenon is observed in different climates and environmental conditions (Gebler et al., 2015; Pochter et al., 2008; Wegehenkel and Gerke, 2013). Due to small differences in e.g., the heat and water exchange between monoliths and surrounding soils, a common characteristic of the oasis effect is that evapotranspiration rates are higher as compared to those from the field around the lysimeters. To avoid oasis effects, lysimeters in this study were embedded within a larger field (approx. 2.3 ha in size), which had the same crop sequence and was managed (spraying and fertilization) as similarly as possible to the lysimeters. So, differences between the “natural” in-situ conditions and lysimeters regarding the soil water and heat balance were minimized for that study. Further sources of errors could also have occurred in lysimeter measurements in terms of preferential flow paths at lysimeter walls based on an insufficient fit of soil monoliths inside the lysimeters (e.g., Corwin, 2000). However, state-of-the-art techniques for monolith extraction and lysimeter installation, respectively, were used in this study to minimize such bias in lysimeter data.

Second, for a water and carbon balance but also soil water retention analysis, the study was rather limited for an observation period of 3 years. A longer-lasting evaluation regarding the influence of the erosion-induced pedogenesis on water balance components, carbon leaching and soil hydraulic properties would be required for more ‘general’ conclusions.

Third, the TERENO SoilCan lysimeters used in the current study were not designed to measure lateral water flow, which would occur in the hill-slope specific positions of the monoliths. Therefore, thesis results of drainage differences and also carbon leaching

between the differently eroded soil types derived by the 1D-lysimeter water fluxes cannot be easily transferred to the hill-slope water balance including surface and subsurface runoff.

## *6.6 Outlook and suggestions for further research*

The research of soil erosion feedbacks on the crop development, soil hydraulic properties, and water and dissolved carbon fluxes highlighted in this thesis has raised a number of open questions that should be explored in future work.

The revealed contrasting water regime and carbon leaching potential for differently eroded lysimeter soils here is a first indication that water balance components and carbon releases were affected by an erosion-induced soil evolution. Further investigations are needed to analyze the relationships between water and carbon fluxes, respectively, and the erosion history at various landscape positions in the ground moraine soil landscape, especially for the second lysimeter hexagon including strong eroded and colluvial monoliths. Thesis studies mainly focused on rather small erosion-affected soil profile modifications of a single soil type in hummocky terrain due to water erosion and tillage operations; however, this erosion gradient between non-eroded (standard) and intensively eroded Haplic Luvisols reflects only a part of the overall soil landscape inventory. In a next step, detailed comparisons between the colluvial and the strong eroded soil types will allow an assessment of soil erosion effects on the water and solute balance within the overall erosion gradient that covers the hummocky soil landscape of NE-Germany. In particular, the second hexagon of the SoilCan lysimeters at the experimental research station in Dedelow is suited to provide information about the groundwater influence on soil water fluxes and therefore the landscape carbon balance. Longer lasting comparisons between soil types and lysimeter hexagons, respectively, in terms of weighing data, soil water concentration and sensor measurements would be preferable compared to the 3-years-periods in the current thesis. The provided autocorrelation based filtering approach (see chapter 2) could be the basis for further studies dealing with lysimeter time series.

A clear relation between erosion-induced soil profile modification and the water balance components such as deep drainage were not identified for differently eroded Luvisols in general; here, a dual-porosity, dual-permeability model or an inverse modeling approach might be helpful to explain differences in e.g., deep drainage of more-or-less eroded monoliths and their dissolved carbon leaching potential, and to simulate the (still unknown) water fluxes within the 'black box': lysimeter. The analyzed time series of the weighing lysimeters including water balance components for the period from 2011 to 2014 could provide initial and boundary conditions for such inverse modeling applications. Especially the



time dependency of the soil hydraulic parameters considering non-equilibrium conditions in the suction-water content relations at different time scales as discussed in chapter 4 should be considered for a better understanding of the hysteretic water flow in arable soils. In this context, improvements may be accomplished by adding additional sensors, especially in the top soil, to cover a wider suction range under unsaturated conditions. Further, the Bromid tracer experiment performed on lysimeter monoliths in 2013 (but still pending) could be used to examine the erosion-affected changes in the in-situ dispersion coefficients for modeling the solute transport by analyzing breakthrough curves of the Br-tracer between lysimeter monoliths.

Field measurements in chapter 3 revealed that concentration of dissolved organic carbon at the bottom of each lysimeter decreased to nearly the same baseline value for all lysimeter monoliths. The identification of such thresholds, in turn, gives the basis for linking the concentration decrease with the sorption of dissolved carbon on sorption sites of mineral surfaces in the clayey Bt-horizons that appears in every Haplic Luvisol. The study of Herbrich et al. (2017a) concluded that the reduction of dissolved organic carbon due to sorption seems to be independent and the occupancy of sorption sites on mineral surfaces with dissolved organic carbon is still incomplete. Further studies are needed for a better understanding of effects and mechanisms of organic coverage inducing quantitative and qualitative changes in the mineral surfaces for differently eroded soils – especially the transition areas between Bt- and C-horizons would be of particular interest.

Finally, the up-scaling of one-dimensional water fluxes and carbon transport from the lysimeter to e.g., the hill-slope scale is a challenge for the future research to solve issues that remain still unanswered in hill-slope hydrology; for instance, the identification of sinks and sources in the landscape carbon balance. The prepared data set of lysimeter measurements should be considered for simulations of the hill-slope water balance by the use of hydrological models working in complex terrain. In this context, lateral water flow paths such as surface and subsurface runoff would be of central interest so that conclusions can be drawn about the drainage and therefore hot spots of carbon exports in the eroded landscape. Dynamic interactions of the crop and root development and the erosion history at various landscape positions (Herbrich et al. 2017b, chapter 5) can provide useful information on soils along the overall erosion gradient in post-glacial hummocky soil landscapes.

## 6.7 Data access

The lysimeter data used for hydrological analysis are available under the public data repository of TEODOOR. This central data portal provides TERENO data for the general

public. The lysimeter data set of this study contains measurements of the lysimeter mass and the leachate outflow at the bottom for soil monoliths taken at different slope positions from the two field sites: Holzendorf (Hd) and Dedelow (Dd).

The water content and suction data used for the water retention analysis (Herbrich and Gerke, 2017) and measured with the MPS-1 matrix potential sensors (Decagon Devices Inc., Pullman, USA), TS-1 tensiometers (UMS, Munich, Germany) and time domain reflectometry probes TDR-100 (Campbell Scientific Ltd, Logan, USA) are published under Herbrich et al. (2017, doi:10.4228/ZALF.2015.291). This (raw) data set contains time series of the years 2012 to 2014.

---

## References

Alaoui, A., Lipiec, J., Gerke, H.H., 2011, A review of the changes in the soil pore system due to soil deformation: a hydrodynamic perspective: *Soil & Tillage Research* 115, 1–15.

Corwin, D. L., 2000, Evaluation of a simple lysimeter-design modification to minimize sidewall flow. *Journal of Contaminant Hydrology*, 42, 35-49.

Deumlich, D., Schmidt, R., and Sommer, M., 2010, A multiscale soil-landform relationship in the glacial-drift area based on digital terrain analysis and soil attributes: *Journal of Plant Nutrition and Soil Science*, 173, 843-851.

Doetterl, S., Berhe, A. A., Nadeu, E., Wang, Z., Sommer, M., & Fiener, P. 2016, Erosion, deposition and soil carbon: A review of process-level controls, experimental tools and models to address C cycling in dynamic landscapes. *Earth-Science Reviews*, 154, 102-122.

Don, A., and Schulze, E.-D., 2008, Controls on fluxes and export of dissolved organic carbon in grasslands with contrasting soil types. *Biogeochemistry* 91: 117-131.

Gebhardt, S., Fleige, H., and Horn, R., 2009, Effect of compaction on pore functions of soils in a Saalean moraine landscape in North Germany: *Journal of Plant Nutrition and Soil Science*, 172, 688-695.

Gebler, S., Hendricks Franssen, H. J., Pütz, T., Post, H., Schmidt, M., & Vereecken, H. , 2015, Actual evapotranspiration and precipitation measured by lysimeters: a comparison with eddy covariance and tipping bucket. *Hydrology and earth system sciences*, 19(5), 2145-2161.

Gerke, H. H., 2006, Preferential flow descriptions for structured soils. *Journal of Plant Nutrition and Soil Science*, 169(3), 382-400.

Gerke, H. H., and Hierold, W., 2012, Vertical bulk density distribution in C-horizons from marley till as indicator for erosion history in a hummocky post-glacial soil landscape: *Soil and Tillage Research*, 125, 116-122.

Gerke, H. H., Koszinski, S., Kalettka, T., and Sommer, M., 2010, Structures and hydrologic function of soil landscapes with kettle holes using an integrated hydropedological approach: *Journal of Hydrology*, 393, 123-132.

Gerke, H. H., Rieckh, H., and Sommer, M., 2016, Interactions between crop, water, and dissolved organic and inorganic carbon in a hummocky landscape with erosion-affected pedogenesis: *Soil and Tillage Research*, 156, 230-240.

Govers, G., Lobb, D. A., and Quine, T. A., 1999, Tillage erosion and translocation: emergence of a new paradigm in soil erosion research: *Soil & Tillage Research*, 51, 174.

Hannes, M., Wollschläger, U., Schrader, F., Durner, W., Gebler, S., Pütz, T., Fank, J., Unold, G., and Vogel, H.-J., 2015, High-resolution estimation of the water balance components from high-precision lysimeters: *Hydrol. Earth Syst. Sci. Discuss.*, 12, 569-608.

Hannes, M., Wollschläger, U., Wöhling, T., and Vogel, H. J., 2016, Revisiting hydraulic hysteresis based on long-term monitoring of hydraulic states in lysimeters: *Water Resour. Res.*, 52, 3847–3865.

Herbrich, M. and Gerke, H. H., 2016, Autocorrelation analysis of high resolution weighing lysimeter time series as a basis for determination of precipitation. *Journal of Plant Nutrition and Soil Science*, 179, 784–798.

Herbrich, M., Gerke, H.H., M. Sommer, 2016. Matric potential and soil water content of differently eroded Luvisols using high precision weighing lysimeters. *Leibniz-Zentrum für Agrarlandschaftsforschung (ZALF) e.V.*, doi: 10.4228/ZALF.2015.291.

Herbrich, M., Gerke, H. H., Bens, O., & Sommer, M, 2017, Water balance and leaching of dissolved organic and inorganic carbon of eroded Luvisols using high precision weighing lysimeters. *Soil and Tillage Research*, 165, 144-160.

Herbrich, M. and Gerke, H. H., 2017, Scales of water retention dynamics observed in eroded Luvisols from arable postglacial soil landscape, *Vadose Zone Journal*, Online First.

Herbrich, M., Gerke, H. H. and Sommer, M, 2017, Root development of winter wheat in erosion-affected soils depending on the position in a hummocky ground moraine soil landscape. *Journal of Plant Nutrition and Soil Science*, under Review.

Hoffmann, M., Jurisch, N., Alba, J. G., Borraz, E. A., Schmidt, M., Huth, V. & Augustin, J., 2017, Detecting small-scale spatial heterogeneity and temporal dynamics of soil organic carbon (SOC) stocks: a comparison between automatic chamber-derived C budgets and repeated soil inventories. *Biogeosciences*, 14, 1003.

Horn, R., Richards, B. G., Grasse W., Baumgartl, T., and Wiermann, C., 1998, Theoretical principles for modelling soil strength and wheeling effects - A review: *Zeitschrift Für Pflanzenernährung Und Bodenkunde*, 161, 333-346.

IPCC, 2013, *Climate Change 2013: The Physical Science Basis. Contribution of Working Group I to the Fifth Assessment Report of the Intergovernmental Panel on Climate Change* [Stocker, T.F., D. Qin, G.-K. Plattner, M. Tignor, S.K. Allen, J. Boschung, A. Nauels, Y. Xia, V. Bex and P.M. Midgley (eds.)]. Cambridge University Press, Cambridge, United Kingdom and New York, NY, USA, 1535 pp,

IUSS Working Group WRB, 2015, *World Reference Base for Soil Resources 2014, update 2015, International soil classification system for naming soils and creating legends for soil maps. World Soil Resources Reports No. 103.* FAO, Rome.

- Jenny, H., 1961, Derivation of state factor equations of soils and ecosystems: *Soil Sci Soc Amer Proc*, 25, 385-388.
- Kalettkka, T., and Rudat, C., 2006, Hydrogeomorphic types of glacially created kettle holes in North-East Germany: *Limnologica-Ecology and Management of Inland Waters*, 36, 54-64.
- Kalettkka, T., Rudat, C., and Quast, J., 2001, 18 "Potholes" in Northeast German agro-landscapes: functions, land use impacts, and protection strategies: *Ecosystem approaches to landscape management in central Europe, ecological studies*, 147, 291-298.
- Kindler, R., Siemens, J. A. N., Kaiser, K., Walmsley, D. C., Bernhofer, C., Buchmann, N., Cellier, P., Eugster, W., Gleixner, G., Grünwald, T., Heim, A., Ibrom, A., Jones, S. K., Jones, M., Klumpp, K., Kutsch, W., Larsen, K. S., Lehuger, S., Loubet, B., McKenzie, R., Moors, E., Osborne, B., Pilegaard, K. I. M., Rebmann, C., Saunders, M., Schmidt, M. W. I., Schruppf, M., Seyfferth, J. Skiba, U. T. E., Soussana, J.-F., Sutton, M. A., Tefs, C. Vowinckel, B. Zeeman, M. J., and Kaupenjohann, M., 2011, Dissolved carbon leaching from soil is a crucial component of the net ecosystem carbon balance: *Global Change Biology*, 17, 1167-1185.
- Kohyama, T., Kubo, T., and Macklin, E., 2005, Effect of temporal autocorrelation on apparent growth rate variation in forest tree census data and an alternative distribution function of tree growth rate: *Ecological Research*, 20, 11-15.
- Kosmas, C., Gerontidis, S., Marathianou, M., Detsis, B., Zafiriou, T., Muysen, W. N. Govers, G., Quine, T., and Vanoost, K., 2001, The effects of tillage displaced soil on soil properties and wheat biomass: *Soil and Tillage Research*, 58, 31-44.
- Lal, R. (2001). Soil degradation by erosion. *Land degradation & development*, 12(6), 519-539.
- Lin, H., 2010, Earth's Critical Zone and hydrogeology: concepts, characteristics, advances: *Hydrology and Earth System Science* 14, 25–45.
- Lin, H., 2011, Three principles of soil change and pedogenesis in time and space: *Soil Science Society of America Journal* 75, 2049–2070.
- Marek, G. W., Evett, S. R., Gowda, P. H., Howell, T. A., Copeland, K. S., and Baumhardt, R. L., 2014, Post-processing techniques for reducing errors in weighing lysimeter evapotranspiration (ET) datasets: *Transactions of the ASABE*, 57, 499-515.
- McCaig, M., 1985, Soil properties and subsurface hydrology: In K.S. Richards, R.R. Arnet and S. Ellis (eds): *Geomorphology and soils*, 121-140.
- Meißner, R., Prasad, M. N. V., Du Laing, G., and Rinklebe, J., 2010, lysimeter application for measuring the water and solute fluxes with high precision: *Curr. Sci. India.*, 99, 601.

- Meißner, R., Seeger, J., Rupp, H., Seyfarth, M., and Borg, H., 2007, Measurement of dew, fog, and rime with a high-precision gravitation lysimeter: *J. Plant Nutr. Soil Sci.*, 170, 335-344.
- Ministerium für Wirtschaft, Arbeit und Tourismus Mecklenburg-Vorpommern, 2010, Studie: Folgen des Klimawandels in Mecklenburg-Vorpommern 2010.
- Morgan, R. P. C., 2009, *Soil erosion and conservation*, Third Edition, Wiley-Blackwell.
- Mullan, D., 2013, Soil erosion under the impacts of future climate change: Assessing the statistical significance of future changes and the potential on-site and off-site problems. *Catena*, 109, 234-246.
- Nearing, M. A., Pruski, F. F., and O'neal, M. R., 2004, Expected climate change impacts on soil erosion rates: a review. *Journal of soil and water conservation*, 59, 43-50.
- Nolz, R., Kammerer, G., and Cepuder, P., 2013, Interpretation of lysimeter weighing data affected by wind: *J. Plant Nutr. Soil Sci.*, 176, 200-208.
- Pachepsky, Y., Rawls, W. J., and Gimenez, D., 2001, Comparison of soil water retention at field and laboratory scales: *Soil Science Society of America Journal*, 65, 460-462.
- Pennock, D. J., 2003, Terrain attributes, landform segmentation, and soil redistribution: *Soil & Tillage Research*, 69, 15-26.
- Peters, A. Nehls, T., Schonsky, H., and Wessolek, G., 2014, Separating precipitation and evapotranspiration from noise - a new filter routine for high resolution lysimeter data: *Hydrol. Earth Syst. Sci. Discuss.*, 18, 1189 -1198.
- Potchter, O., Goldman, D., Kadish, D., & Iluz, D., 2008, The oasis effect in an extremely hot and arid climate: the case of southern Israel. *Journal of Arid Environments*, 72(9), 1721-1733.
- Pütz, T., Kiese, R. Wollschläger, U., Groh, J., Rupp, H., Zacharias, S., Priesack, E., Gerke, H. H., Papen, H., Borg, E., Bens, O., Kaiser, K., Herbrich, M., Munch, J.-C., Sommer, M., Vanderborght, J., and Vereecken, H., 2016, TERENO-SOILCan a Lysimeter-Network in Germany Observing Soil Functions Influenced by Climate Change: *Environ. Earth Sci.*; in press.
- Raab, T., and Völkel, J., 2003, Late Pleistocene glaciation of the Kleiner Arbersee area in the Bavarian Forest, south Germany: *Quaternary Science Reviews*, 22, 581-593.
- Rieckh, H., Gerke, H. H., Glæsner, N., and Kjaergaard, C., 2015, Tracer, Dissolved Organic Carbon, and Colloid Leaching from Erosion-Affected Arable Hillslope Soils: *Vadose Zone Journal*, 14.

- Rieckh, H., Gerke, H. H., and Sommer, M., 2012, Hydraulic properties of characteristic horizons depending on relief position and structure in a hummocky glacial soil landscape: *Soil and Tillage Research*, 125, 123-131.
- Rieckh, H., Gerke, H. H., and Sommer, M., 2014, Water and Dissolved Carbon Fluxes in an Eroding Soil Landscape Depending on Terrain Position *Vadose Zone J.*, 13.
- Schrader, F., Durner, W., Fank, J., Gebler, S., Pütz, T., Hannes, M., and Wollschläger, U., 2013, Estimating precipitation and actual evapotranspiration from precision lysimeter measurements: *Procedia Environ. Sci.*, 19, 543-552.
- Simunek, J., Van Genuchten, M. T., & Sejna, M., 2005, The HYDRUS-1D software package for simulating the one-dimensional movement of water, heat, and multiple solutes in variably-saturated media. *University of California-Riverside Research Reports*, 3, 1-240.
- Sommer, M., Fiedler, S., Glatzel, S., and Kleber, M., 2004, First estimates of regional (Allgau, Germany) and global CH<sub>4</sub> fluxes from wet colluvial margins of closed depressions in glacial drift areas: *Agriculture Ecosystems & Environment*, 103, 251-257.
- Sommer, M., Gerke, H. H., and Deumlich, D., 2008, Modelling soil landscape genesis - A "time split" approach for hummocky agricultural landscapes: *Geoderma*, 145, 480-493.
- Titus, B. D., and Mahendrappa, M. K., 1996, Lysimeter system designs used in soils research: a review (Vol. 301). *Canadian Forest Service*.
- Unold, G., and Fank, J., 2008, Modular Design of Field Lysimeters for Specific Application Needs: *Water Air Soil Pollut.*, 8, 233-242.
- Van Oost, K., Govers, G., De Alba, S., and Quine, T., 2006, Tillage erosion: a review of controlling factors and implications for soil quality: *Progress in Physical Geography*, 30, 443-466.
- Vaughan, P. J., and Ayars, J. E., 2009, Noise Reduction Methods for Weighing Lysimeters: *J. Irrig. Drain. Eng.*, 135, 235-240.
- Vaughan, P. J., Trout, T. J., and Ayars, J. E., 2007, A processing method for weighing lysimeter data and comparison to micrometeorological ETo predictions: *Agric. Water Manage.*, 88, 141-146.
- Wegehenkel, M., and Gerke, H. H. (2013). Comparison of real evapotranspiration measured by weighing lysimeters with simulations based on the Penman formula and a crop growth model. *Journal of Hydrology and Hydromechanics*, 61(2), 161-172.
- West, L. T., Abreu, M. A., and Bishop, J. P., 2008, Saturated hydraulic conductivity of soils in the Southern Piedmont of Georgia, USA: Field evaluation and relation to horizon and landscape properties: *Catena*, 73, 174-179.

Woods, S. A., Dyck, M. F., and Kachanoski, R. G., 2013, Spatial and temporal variability of soil horizons and long-term solute transport under semi-arid conditions: *Canadian Journal of Soil Science*, 93, 173-191.

Young, M. H., Wierenga, P. J., and Mancino, C. F., 1996, Large Weighing Lysimeters for Water Use and Deep Percolation Studies: *Soil Science* 7, 491-501.

Yue, S., Pilon, P., Phinney, B., and Cavadias, G., 2002, The influence of autocorrelation on the ability to detect trend in hydrological series: *Hydrol. Process.*, 16, 1807-1829.



## Acknowledgments

First of all, I want to thank my supervisors Michael Sommer and especially Horst H. Gerke for their help and support during the PhD-period at the Institute of Soil Landscape Research, Leibniz Centre for Agricultural Landscape Research ZALF. This thesis would not have been possible without their feedback, quick responses to questions, manuscripts revisions and many other factors.

My thanks also go to the technical and scientific staff at the Institute of Soil Landscape Research and research station Dedelow. In particular Wilfried Hierold (soil classification), Norbert Wipler (technical support), Ute Moritz (data preparation), Ingrid Onasch (technical support), Lidia Völker (GIS applications), Jörg Haase (lysimeter maintenance) and Gernot Verch (crop cultivation) are worthy of mention. Thanks to all my colleagues at the Institute and ZALF for open ears and open minds during this period in Müncheberg.

Finally, I would like to thank my family for all the support during and before the PhD time – this work would not have been achieved without your encouragements!

## Curriculum vitae and publications

### Die Seite 182 (Curriculum vitae) enthalten persönliche Daten. Sie sind deshalb nicht Bestandteil der Online-Veröffentlichung ###

In the period of the PhD, the following scientific publications were published in peer-reviewed journals:

**Herbrich, M.**, Zönnchen, C., Schaaf, W. (2015). Short-term effects of plant litter addition on mineral surface characteristics of young sandy soils. *Geoderma*, 239, 206-212.

**Herbrich, M.** and H. H. Gerke (2016). Autocorrelation analysis of high resolution weighing lysimeter time series as a basis for determination of precipitation. *Journal of Plant Nutrition and Soil Science*, 179, 784–798.

**Herbrich, M.**, Gerke, H. H., Bens, O., & Sommer, M. (2017a). Water balance and leaching of dissolved organic and inorganic carbon of eroded Luvisols using high precision weighing lysimeters. *Soil and Tillage Research*, 165, 144-160.

**Herbrich, M.** and H. H. Gerke (2017). Scales of water retention dynamics observed in eroded Luvisols from arable postglacial soil landscape, *Vadose Zone Journal*, Online First.

**Herbrich, M.**, Gerke, H. H. & Sommer, M. (2017b). Root development of winter wheat in erosion-affected soils depending on the position in a hummocky ground moraine soil landscape. *Journal of Plant Nutrition and Soil Science*, under Review.

Th. Pütz, Kiese, R., Wollschläger, U., Groh, J., Rupp, H., Zacharias, S., Priesack, E., Gerke, H.H., Gasche, R., Bens, O., Borg, E., Baessler, C., Kaiser, K., **Herbrich, M.**, Munch, J.-C., Sommer, M., Vogel, H.-J., Vanderborght, J., Vereecken, H. (2016). TERENO-SOILCan: a lysimeter-network in Germany observing soil processes and plant diversity influenced by climate change. *Environmental Earth Sciences*, 75(18), 1242.

## Conference contributions

**M. Herbrich**, H.H. Gerke, M. Sommer (2017) Root development of winter wheat in erosion-affected soils depending on the position in a hummocky ground moraine soil landscape, EGU General Assembly 2017-15623, 2017.

H.H. Gerke, **M. Herbrich** (2017) Scales of water retention dynamics observed in eroded Luvisols , EGU General Assembly 2017-15043, 2017.

**M. Herbrich**, H.H. Gerke, M. Sommer (2015) Einfluss erosionsbedingter Pedogenese auf die Wasser- und Stoffbilanzen ackerbaulich genutzter Parabraunerden mittels wägbarer Lysimeter, Jahrestagung der Deutschen Bodenkundlichen Gesellschaft 2015, V135.

**M. Herbrich**, H.H. Gerke, M. Sommer (2015) Soil water retention dynamics in Luvisols at contrasting slope positions in lysimeter monoliths from an eroded soil landscape, EGU General Assembly 2015, Vol. 17, EGU2015-9571, 2015.

**M. Herbrich**, H.H. Gerke, M. Sommer (2015): Erosion effects on water and DOC/DIC fluxes in soils from a hummocky ground moraine landscape, EGU General Assembly 2015, Vol. 17, EGU2015-12746, 2015.

K. Kaiser, O. Bens, P. Fiener, H.H. Gerke, **M. Herbrich**, W. Hierold, R.F. Hützl, C. Kappler, T. Raab, M. Sommer, F. Wilken (2015): Monitoring, reconstruction and effects of soil redistributions in small agricultural catchments (Uckermark area, TERENO-NE), German Aerospace Center (DLR), Oberpfaffenhofen, Annual TERENO Workshop 2015.

**M. Herbrich**, H.H. Gerke, M. Sommer (2014): Water and solute balances of erosion-affected Haplic Luvisols using high precision weighing lysimeter data, EGU General Assembly 2014, Vol. 16, EGU2014-10756, 2014.

**M. Herbrich**, H.H. Gerke (2014): Autocorrelation analysis of high resolution weighing lysimeter time series for determining precipitation, EGU General Assembly 2014, Vol. 16, EGU2014-10924-1, 2014.

# Erklärung

Sehr geehrte Damen und Herren,

hiermit erkläre ich, dass ich die beigefügten Dissertationsinhalte eigenständig verfasst und alle wörtlich oder inhaltlich übernommenen Stellen als solche gekennzeichnet habe. Darüber hinaus versichere ich, dass die beigefügte Dissertation ausschließlich in diesem Promotionsverfahren eingereicht wurde sowie keine gescheiterten Promotionsverfahren vorausgegangen sind.

---

Marcus Herbrich

Potsdam, 16.08.2017

## Erklärung des Eigenanteils

Sehr geehrte Damen und Herren,

hiermit wird bestätigt, dass die beigefügten Angaben über den Eigenanteil der kumulativen Dissertationseinhalte (Publikationen), wie beschrieben, eingegangen sind:

---

Marcus Herbrich

Potsdam, 16.08.2017